

Reconstruction of the Late and Mid-Pleistocene climate and landscape history in SE-Central Europe

**A paleopedological and geochemical multi-proxy approach in
loess-paleosol studies.**

Dissertation
zur Erlangung des Grades
Doktor der Naturwissenschaften
(Dr. rer. nat.)
an der Fakultät für Biologie / Chemie / Geowissenschaften
der Universität Bayreuth

vorgelegt von

Björn Buggle (Dipl.-Geoökologe)
geb. am 10.11.1981 in Kempten

Erstgutachter: Prof. Dr. Bruno Glaser

Bayreuth, Februar 2011

Dedicated to my parents and Soschi

- in love and gratefulness-

*“Look back, lest you fail to mark
the path ahead”*

Lovejoy (2007)

Contents

| | |
|---|--------------|
| Contents | I |
| List of Tables | VI |
| List of Figures | IX |
| List of Abbreviations | XIX |
| Summary | XXV |
| Zusammenfassung | XXVII |
| Extended Summary | 1 |
| 1 Introduction | 2 |
| 1.1 Rationale | 2 |
| 1.2 Objectives | 4 |
| 2 Regional setting | 6 |
| 3 Methods | 7 |
| 3.1 Nomenclature and sample material | 7 |
| 3.2 Analyses, data exploration and applied proxies | 9 |
| 3.2.1 Inorganic geochemistry | 9 |
| 3.2.2 Rock magnetic measurements and parameters | 10 |
| 3.2.3 Soil color measurements and diffuse reflectance spectroscopy | 11 |
| 3.2.4 Grain size and micromorphological analyses | 12 |
| 3.2.5 Micromorphological analyses | 12 |
| 3.2.6 n-Alkane analyses and δD measurements | 12 |
| 4 Results/Discussion | 13 |
| 4.1 Geochemical characterization and origin of the Southeastern and Eastern European loess | 13 |
| 4.1.1 The “Dnieper loess” | 14 |
| 4.1.2 The “Danube loess” | 14 |
| 4.2 Stratigraphy | 15 |
| 4.3 Evaluating rock-magnetic and geochemical proxies of pedogenesis and paleoclimate: the magnetic susceptibility and element ratios | 16 |
| 4.4 Paleoenvironmental reconstruction | 17 |
| 4.5 n-Alkane biomarkers and their δD isotopic signature as novel paleoenvironmental proxies in loess-paleosol studies – an evaluation | 20 |
| 5 Conclusion | 22 |
| 6 Contributions to the manuscripts | 25 |
| References | 28 |

| | |
|--|-----------|
| Study 1: Geochemical characterization and origin of Southeastern and Eastern European loesses (Serbia, Romania, Ukraine) | 36 |
| Abstract | 37 |
| 1 Introduction | 39 |
| 2 Regional setting | 40 |
| 3 Methods | 44 |
| 3.1 Sampling and laboratory analyses | 44 |
| 3.2 Data processing | 45 |
| 3.2.1 Discriminant analysis | 46 |
| 3.2.2 Element ratios | 47 |
| 3.3 Literature data | 48 |
| 4 Results | 51 |
| 4.1 Discriminant analysis | 52 |
| 4.2 Si-Zr-Hf-association | 53 |
| 4.3 Major elements ratios | 54 |
| 4.4 Element fingerprint | 57 |
| 4.5 Background magnetic susceptibility | 59 |
| 5 Discussion | 60 |
| 5.1 Origin and geochemical characteristics | 60 |
| 5.1.1 Stary Kaydaky section | 60 |
| 5.1.1.1 Glaciofluvial sediments – a loess source for the Stary Kaydaky site | 60 |
| 5.1.1.2 Origin of the glaciofluvial sediments | 63 |
| 5.1.2 Batajnica/Stari Slankamen section | 64 |
| 5.1.2.1 The Danube alluvium – the major source for Danube Basin loess. | 64 |
| 5.1.2.2 Sources of alluvial silt | 65 |
| 5.1.3 Mircea Voda section | 67 |
| 5.1.3.1 Geochemical evidence | 67 |
| 5.1.3.2 Magnetic susceptibility evidence | 69 |
| 5.2 Southeastern/Eastern European loess – representative samples of the upper continental crust | 70 |
| 6 Conclusions | 73 |
| Acknowledgements | 74 |
| References | 75 |
| Appendix | 81 |
| | |
| Study 2: Stratigraphy and spatial and temporal paleoclimatic trends in Southeastern/Eastern European loess-paleosol sequences | 88 |
| Abstract | 89 |
| 1 Introduction | 90 |
| 2 Principles of susceptibility enhancement in (paleo-)soils | 92 |
| 3 Regional setting | 94 |

| | | |
|----------|--|------------|
| 3.1 | Batajnica / Stari Slankamen (Serbia) | 94 |
| 3.2 | Mircea Voda (Romania) | 95 |
| 3.3 | Sary Kaydaky (Ukraine) | 96 |
| 4 | Methods | 97 |
| 5 | Results | 101 |
| 5.1 | Magnetic susceptibility variations | 101 |
| 5.2 | Stratigraphy | 104 |
| 5.2.1 | Stratigraphy of Batajnica/Stari Slankamen (Serbia) and Mircea Voda (Romania) | 105 |
| 5.2.2 | Stratigraphy of Sary Kaydaky | 108 |
| 5.3 | Sedimentation rates | 112 |
| 6 | Discussion | 116 |
| 6.1 | Sedimentation rates | 116 |
| 6.2 | Chronostratigraphic revisions | 119 |
| 6.2.1 | The S2S1-unit, stratigraphic setting and implications on orbital tuning | 120 |
| 6.2.2 | Division of pedocomplexes S6 and S7 | 122 |
| 6.2.3 | The local Ukrainian stratigraphy | 123 |
| 6.3 | Evaluation of the susceptibility-rainfall relationship | 124 |
| 6.4 | Paleoclimatic conclusions | 127 |
| 7 | Conclusions | 128 |
| | Acknowledgements | 130 |
| | References | 130 |
| | | |
| | <u>Study 3: An evaluation of geochemical weathering indices in loess-paleosol studies</u> | 135 |
| | Abstract | 136 |
| 1 | Introduction | 137 |
| 2 | Material and Methods | 138 |
| 3 | Chemical weathering indices | 140 |
| 3.1 | Choosing a chemical proxy of alteration for LPSS? – Principal considerations and hypotheses | 140 |
| 3.2 | Overview on widely used indices of feldspar weathering | 145 |
| 4 | Results | 146 |
| 5 | Discussion | 151 |
| 5.1 | Evaluation of the geochemical weathering indices | 151 |
| 5.1.1 | Sr type vs. Na type indices | 151 |
| 5.1.2 | The "classical" Na-type weathering indices – uncertainties due to calcium carbonate | 153 |
| 5.1.3 | The chemical proxy of alteration (CPA) - an evaluation | 154 |
| 6 | Conclusions | 161 |
| | Acknowledgements | 161 |
| | References | 162 |

| | |
|---|------------|
| <u>Study 4: 0.7-Million years of progressive aridization recorded in SE-European loess sequences</u> | 166 |
| Abstract | 167 |
| Study | 168 |
| References and Notes | 177 |
| Supporting Material | 180 |
| | |
| <u>Study 5: Iron mineralogical proxies and Quaternary climate change in SE-European loess-paleosol sequences</u> | 191 |
| Abstract | 192 |
| 1 Introduction | 194 |
| 2 Material and methods | 197 |
| 2.1 The sites and sampling | 197 |
| 2.2 Rock magnetic proxies: measurement and background | 198 |
| 2.3 Soil color proxies | 201 |
| 2.4 Diffuse reflectance spectroscopy, background, measurements and calculations | 202 |
| 3 Results/Discussion | 204 |
| 3.1 Concentration related magnetic parameters | 204 |
| 3.2 Magnetic grain size and mineralogy | 210 |
| 3.3 Diffuse reflectance spectroscopy and soil color proxies for hematite and goethite | 216 |
| 3.4 Proxies of iron mineralogy vs. silicate weathering – an integrative perspective on Quaternary climate change | 220 |
| 3.4.1 Interglacial climate change | 222 |
| 3.4.2 Glacial climate change | 232 |
| 4 Conclusion | 233 |
| Acknowledgements | 235 |
| References | 236 |
| | |
| <u>Study 6: Is there a possibility to correct fossil n-alkane data for postsedimentary alteration effects?</u> | 242 |
| Abstract | 243 |
| 1 Introduction | 245 |
| 2 Material and Methods | 250 |
| 2.1 Sampling, sample preparation and analytical methods | 250 |
| 2.2 The approach to correct n-alkane patterns for alteration effects | 251 |
| 2.2.1 Principles and assumptions | 251 |
| 2.2.2 The mathematical procedure | 254 |
| 3 Results and discussion | 255 |

| | | |
|----------|--|------------|
| 3.1 | The alteration lines of $C_{27}/(C_{31} + C_{27})$, $C_{27}/(C_{29} + C_{27})$, $C_{31}/(C_{27} + C_{31})$ for the profile Mircea Voda | 255 |
| 3.2 | Corrected vs. uncorrected values | 257 |
| 3.3 | Discussing the assumptions – limits and potential of the correction approach | 261 |
| 4 | Conclusion | 265 |
| | Acknowledgements | 268 |
| | References | 269 |
| | Appendix | 273 |
| | | |
| | Study 7: Effect of leaf litter degradation and seasonality on D/H isotope ratios of n-alkane biomarkers? | 275 |
| | Abstract | 276 |
| 1 | Introduction | 278 |
| 2 | Material and methods | 280 |
| 2.1 | Litterbag experiment and samples | 280 |
| 2.2 | Analytical procedures | 281 |
| 2.2.1 | n-Alkane quantification | 281 |
| 2.2.2 | Compound-specific δD analysis | 282 |
| 2.2.3 | Bulk δD analysis | 283 |
| 3 | Results | 283 |
| 3.1 | <i>n</i> -Alkane concentrations, absolute <i>n</i> -alkane masses and <i>n</i> -alkane patterns | 283 |
| 3.2 | Compound-specific δD values of individual <i>n</i> -alkanes | 288 |
| 4 | Discussion | 289 |
| 4.1 | Absence of D/H exchange reaction and negligible fractionation during biodegradation | 289 |
| 4.2 | Possible sources of the new long-chain <i>n</i> -alkanes | 289 |
| 4.3 | Modelling leaf litter <i>n</i> -alkane decay and built-up of a microbial <i>n</i> -alkane pool – explaining the seasonality of the <i>n</i> -alkane δD results | 291 |
| 4.4 | Implications for turnover-times, origin of long-chain <i>n</i> -alkanes in soils/sediments and δD values of <i>n</i> -alkanes as paleoclimate proxy. | 293 |
| 5 | Conclusions | 294 |
| | Acknowledgements | 295 |
| | References | 296 |
| | | |
| | List of Publications | 301 |
| | Acknowledgements/Danksagung | 305 |
| | Declaration/Erklärung | 309 |

List of Tables

| | |
|--|-----|
| Table 1-1. Factor structure matrix: The factor structure coefficients – equivalent to factor loadings – give the strength of correlation between the variables and the discriminant functions. | 53 |
| Table 1-S1. Floodplain sediment samples of the “FOREGS”-dataset (Salminen et al., 2005), assigned to respective source areas. | 81 |
| Table 2-1. Overview on the different timescales for Mid-Pleistocene LPSS and major isotope stages, respectively, applied for sensitivity analyses of sedimentation rates. | 100 |
| Table 2-2. Compilation of different stratigraphic schemes for the Ukraine. The present study favors the scheme of Gerasimenko (2004, 2006). | 109 |
| Table 2-3. Paleoprecipitation for the profiles Batajnica/Stari Slankamen, Mircea Voda, Stary Kaydaky, Koriten, Mostistea. Values were calculated from the magnetic susceptibility using Eq. 1, presented by Maher et al. (1994). | 126 |
| Table 3-1. Weathering indices (molecular proportions). | 145 |
| Table 3-2. Sensitivity analysis for the CIW, PIA, CIA and Index B (see Table 3-1) and the obtained error due to the estimation of silicate bound Ca (CaO*) following the procedure of McLennan (1993). | 155 |

| | |
|---|-----|
| Table 4-S1. Groundmass characteristics of soil thin sections and their ranking following increasing groundmass development intensity with soil formation (carbonate leaching, clay formation, clay translocation). | 187 |
| Table 4-S2. Summary of paleopedologic characteristics of the pedocomplexes at the Mircea Voda site and soil typological interpretation. | 188 |
| Table 6-1. Slopes of LAR - OEP regression lines for the calcic Chernozem of the Mircea Voda site (this study), a dystric Cambisol in the Steigerwald forest (Germany) developed under beech vegetation (this study and Rumpel et al., 2004) and an acid brown earth under grassland pasture (U.K., Huang et al., 1996). | 265 |
| Table 6-A1. Concentration of n-alkane homologues in the modern soil of the Mircea Voda site. | 273 |
| Table 6-A2. Concentration of n-alkane homologues in the loess-paleosol units S4 – S6 of the Mircea Voda site. | 274 |
| Table 7-1. Mass loss of different leaf litter species (Acer, Fagus and Sorbus), relative depletion of cellulose and total cellulose decomposition, relative enrichment of lignin and total lignin decomposition (from Kalbitz et al. (2006)) and relative depletion of total n-alkanes ($\sum(n-C_{20}$ to $n-C_{35}$) and total n-alkane decomposition after 27 months of leaf litter degradation. | 281 |

Table 7-2. Rates of decomposition, coefficients of correlation for a first order decay and turnover times for mid- and long-chain n-alkanes of three leaf litter species (Acer, Fagus and Sorbus) during 27 months of leaf litter degradation.

List of Figures

- Fig. 1-1. Location of the studied loess-paleosol sequences in a schematic map. Limits of the continental ice sheet were taken from Eissmann (2002). 43
- Fig. 1-2. Scatterplot of the canonical scores. Data points, representing individual samples of the loess-paleosol profiles Batajnica/Stari Slankamen (B-SS), Mircea Voda (MV) and Stary Kaydaky (SK) are plotted on the two discriminant functions root 1 and root 2. 53
- Fig. 1-3. Average SiO₂, Zr and Hf content of the profiles Batajnica/Stari Slankamen (B-SS), Mircea Voda (MV) and Stary Kaydaky (SK). 54
- Fig. 1-4. A-CN-K diagram. Values of bulk samples are plotted for the studied sections (left diagram). Samples of the Dnieper and Kaydaky units (MIS 6, MIS 5e) of Stary Kaydaky are highlighted in blue. The composition of several possible source materials is given. 55
- Fig. 1-5. Fe₂O₃/TiO₂ vs. Al₂O₃/TiO₂ diagram. Left plot: loess and soil samples; middle and right plot: only “pure loess” samples. Values of floodplain sediments of selected source areas, rock types as well as average values for the UCC are given. 57
- Fig. 1-6. Element fingerprint normalized to UCC composition (indicated by the number sign) for the “pure loess” of the sections Batajnica/Stari Slankamen, Mircea Voda and Stary Kaydaky, as well as for various loess regions and for the average composition of worldwide loess. 58

- Fig. 1-7. Background magnetic susceptibility of loess-paleosol sections in the Northern Black Sea area and the Ukraine. See Fig. 1-8 for the locations. 59
- Fig. 1-8. Distribution of sand and sandy loam soils (yellow) in the Ukraine, sand and sandy soil texture in Moldova and sand dunes in Romania. The locations of loess-paleosol sites, with published magnetic susceptibility records are given. Arrows indicate proposed paleowind directions during cold stages, according to the distribution of the sandy areas with respect to river valleys. 62
- Fig. 1-S1. Major element composition of Batajnica/Stari Slankamen section. 82
- Fig. 1-S2. Major element composition of Mircea Voda section 83
- Fig. 1-S3. Major element composition of the Stary Kaydaky section. 84
- Fig. 1-S4. Trace element composition of Batajnica/Stari Slankamen section. 85
- Fig. 1-S5. Trace element composition of the Mircea Voda section. 86
- Fig. 1-S6. Trace element composition of the Stary Kaydaky section. 87
- Fig. 2-1. Location of the investigated loess-paleosol sequences; map of current potential vegetation for Southeastern Europe (Frey and Lösch, 1998, modified). 95

Fig. 2-2. Climate diagrams of a) Belgrade (Serbia), b) Constanta (Romania) and c) Dnepropetrovsk (Ukraine). The heavily dotted area marks months with average precipitation being less than twice the value of the average temperature. This indicates periods of drought according to Walter (1974). The slightly dotted areas show months with average precipitation being less than three times the value of average temperature. This characterizes periods of dryness. 96

Fig. 2-3. Variations of magnetic susceptibility (χ) with profile depth and sampling site. The lithology is sketched. 102

Fig. 2-4. Comparison of a high resolution magnetic susceptibility record (sampling in 5 cm intervals) and a lower resolved record (sampling in decimeter intervals) for the Batajnica section. 103

Fig. 2-5. Correlation of the magnetic susceptibility records of the profiles Batajnica/Stari Slankamen, Mircea Voda, Stary Kaydaky with the astronomically tuned benthic oxygen isotope record from ODP site 677 (Shackleton et al., 1990); A $\delta^{18}\text{O}$ value of 4.5 ‰ was used for the limitations of major isotope stages, following Vidic et al. (2004); Comparison with the records of Koriten, Mostistea (redrawn after Jordanova and Petersen, 1999; Panaiotu et al., 2001) and the stacked normalized magnetic susceptibility curve of Lingtai and Zhaojiachuan (Chinese Loess Plateau); data and astronomical tuning for the latter sections were provided by Sun, et al., (2006). 107

- Fig. 2-6. Correlation of the magnetic susceptibility record of the Stary Kaydaky section to that of the Vyazivok section (Ukraine, Rousseau et al. 2001) and the benthic $\delta^{18}\text{O}$ record of ODP 677 (Shackleton et al. 1994), for the last climatic cycle. 110
- Fig. 2-7. Sedimentation rates for the sections Batajnica/Stari Slankamen and Mircea Voda. 114
- Fig. 3-1. Classification of the elements according to the ionic potential (IP) 142
- Fig. 3-2. The CPA, CIA, Index B, CIW, PIA, Ba/Sr, Rb/Sr record of a) the Batajnica/Stari Slankamen section in Serbia, b) the Mircea Voda section in Romania, c) the Stary Kaydaky section in Ukraine. 148
- Fig. 3-3. Correlation of the Rb/Sr (a) and Ba/Sr ratio (b) with the CaCO_3 -content for all studied profile sequences. 152
- Fig. 3-4. Molar $\text{Al}_2\text{O}_3/\text{K}_2\text{O}$ and $\text{Al}_2\text{O}_3/\text{Na}_2\text{O}$ ratios of the studied profiles. 156
- Fig. 3-5. The A-CN-K ($\text{Al}_2\text{O}_3\text{-CaO}^*\text{+ Na}_2\text{O-K}_2\text{O}$) - ternary diagram according to Nesbitt and Young (1984). The characteristic position of the upper continental crust, basalt, granite and the minerals plagioclase, K-feldspar, biotite, muscovite, illite, smectite, kaolinite and gibbsite is given for orientation. In Fig. 3-5 a) – d) a typical weathering line is presented. In Fig. 3-5a, it is shown how biases due to a changing composition of the parent material would appear in the A-CN-K diagram. In Fig. 3-5b, the sorting effect is demonstrated. Fig. 3-5c shows the effect of errors in the CaO^* content, for example due to the

estimation procedure of McLennan (1993). In Fig. 3-5d. datapoints for loess and paleosol samples from the Batajnica/Stari Slankamen, Mircea Voda and Stary Kaydaky sections are shown.

159

Fig. 4-1. Peak values for pedogenesis, weathering and wind strength proxies for the last six glacials and interglacials preserved in loess-paleosol sequences of the middle (Batajnica/Stari Slankamen site) and lower Danube Basin (Mircea Voda site): the U-ratio, the Micromorphological Proxy of soil formation Intensity (MPI), the Chemical Proxy of Alteration (CPA) and the $<5\mu$ fraction.

171

Fig. 4-2. Comparison of climate proxy records from mid-latitude Eurasia over the last six interglacial to glacial cycles. All records indicate aridization and/or a decrease of temperature for interglacials partly also glacials over the last 600-800 ka. A and B) Paleosol succession of the middle and lower Danube Basin as preserved in the loess-paleosol sequence (LPSS) Batajnica/Stari Slankamen and Mircea Voda, respectively; C) Mean annual temperature and precipitation of the NW Black Sea area, as reconstructed from paleopedologic and environmental magnetic properties of LPSS using a modern analogue approach; D) Biogenic silica content in Lake Baikal sediments (core BDP 96-2) as proxy of summer temperature; E and F) Chemical Proxy of Alteration (CPA) record of the Chashmanigar LPSS (Tajikistan) and Lingtai LPSS (Chinese Loess Plateau). G) $<2 / >10 \mu$ grain size ratio record of the Baoji LPSS (Chinese loess plateau); H) Dust flux record in the NW Pacific (core V21-146).

172

- Fig. 4-3. Comparison of proxy records for potential long-term triggers on Eurasian climate during the last 17 marine isotope stages. A-D) The daily insolation at 65°N during the summer solstice, the eccentricity of the Earth's orbit, phasing in obliquity and precession of the Earth; E) Atmospheric CO₂ concentration in parts per million by volume (ppmv); F) δ¹⁸O values of benthic foraminifera from ODP site 677 as proxy of global ice volume. G) Uk'37 based mean annual sea surface temperature at the Iberian Margin (cores MD01-2443 and MD01-2444); H and I) Changes of the summer and winter sea surface temperature in the North Atlantic (composite record from ODP site 607 and core V30-97). 174
- Fig. 4-S1. Picture of Stari Slankamen and Batajnica site (middle Danube Basin, Serbia). 189
- Fig. 4-S2. Picture of the Mircea Voda site (lower Danube Basin, Romania). 189
- Fig. 4-S3. The <5 μm, CPA and U-ratio record of the composite loess-paleosol sequence Batajnica/Stari Slankamen (middle Danube Basin, Serbia). 190
- Fig. 4-S4. The <5μm, CPA and U-ratio record of the composite loess-paleosol sequence Batajnica/Stari Slankamen (middle Danube Basin, Serbia) 190
- Fig. 5-1. Climatic data of stations Belgrade (Serbia) and Constanta (Romania). a) temperature and b) precipitation. 197

Fig. 5-2,a), b). Depth profiles of χ , χ_{fd} , ARM, $IRM_{0.35T}$, SIRM and HIRM for the Mircea Voda and Batajnica/ Stari Slankamen section.

207

Fig. 5-3. Depth profiles of the $<5 \mu\text{m}$ grain size fraction as proxy for pedogenic clay formation and of the Chemical Proxy of Alteration (CPA) as proxy for silicate weathering.

208

Fig. 5-4. $\chi_{fd} - \chi$ crossplot for loess and paleosol samples of the Mircea Voda and Batajnica/ Stari Slankamen LPSS. χ_{fd} and χ show a significant correlation with $R^2 > 0.99$ for both sections. The regression function for the Mircea Voda site is $Y = 7.3 \times X + 16.9$ and for the Batajnica/Stari Slankamen site $Y = 7.2 \times X + 19.0$. The intercept denotes the background susceptibility i.e. initial susceptibility of the parent material before pedogenesis.

209

Fig. 5-5. Depth profiles of the concentration-independent magnetic proxies $\chi_{fd}\%$, ARM/χ_{fd} , $SIRM/\chi_{fd}$, $ARM/SIRM$, B_{cr} and S-ratio for a) the Mircea Voda and b) the Batajnica/ Stari Slankamen section.

213

Fig. 5-6. $\chi_{fd}\% - \chi$ crossplot for loess and paleosol samples of the a) Mircea Voda and b) Batajnica/ Stari Slankamen LPSS. $\chi_{fd}\%$ approaches saturation in paleosols at values around 12.

215

Fig. 5-7, a), b). Depth profiles of the RI (Rubification Index according to Harden 1982) and RR (Redness Rating according to Torrent et al., 1980 and Torrent and Barron, 1993) and the Hematite/(Hematite + Goethite) ratio ($Hm/(Hm+Gt)$) for the profiles a) Mircea Voda and b)

Batajnica/Stari Slankamen. The $Hm/(Hm+Gt)$ was determined via diffuse reflectance spectroscopy following the Torrent et al., (2007) approach.

218

Fig. 5-8. Crossplot of the $Hm/(Hm+Gt)$ ratio vs. rock magnetic proxies of the ferrimagnetic grain size distribution: a) the $Hm/(Hm+Gt)$ vs. ARM/SIRM crossplot, b) the $Hm/(Hm+Gt)$ vs. SIRM/ χ_{fd} crossplot, c) $Hm/(Hm+Gt)$ vs. ARM/ χ_{fd} crossplot, d) the $Hm/(Hm+Gt)$ vs. $\chi_{fd}\%$ crossplot.

219

Fig. 5-9. Peak values for selected rock magnetic parameters, the drs-derived $Hm/(Hm+Gt)$ ratio, the CPA and $<5 \mu m$ fraction. For interglacial pedocomplexes the maximum value of each parameter is given and for glacial loess layers the minimum values.

223

Fig. 6-1. Soil depth profiles of OEP and C27/C31, C29/C31, C29/C27 n-alkane ratios a) for an eutric Cambisol under beech forest; b) for a calcareous Regosol under grassland sampled at the Titel loess plateau 25 km east of Novi Sad (Serbia).

249

Fig. 6-2. Schematic sketch illustrating the approach to correct fossil LARs (as for example the $C27/(C27+C31)$ ratio for degradation effects.

253

Fig. 6-3. Depth profile of the OEP and selected LARs for the modern soil of the Mircea Voda site. Section A (about the upper 50 cm) shows a decrease of the OEP and an increase of the LARs with depth. In section B this is vice versa

256

- Fig. 6-4. Cross-plot of selected LARs vs. OEP for the modern soil and the loess-paleosol units S4 to S6 of the Mircea Voda site. The regression function and correlation coefficients for the OEP vs. LAR relationships are given for the upper 50 cm of the modern soil, the whole modern soil (0-100 cm; index B) and the loess-paleosol samples. 257
- Fig. 6-5. OEP and LAR depth profiles for the loess-paleosol units S4 - S6 of the Mircea Voda site. a) Uncorrected LAR ratios, b) LAR ratios corrected for degradation effects 258
- Fig. 6-6. Comparison of the OEP and $\text{Alk}>\text{C25}/\text{Alk}<\text{C25}$ ratio in the depth profiles of the modern soil of the Mircea Voda section and the loess-paleosol units S4 - S6. 260
- Fig. 6-7. Guidelines for the application of the n-alkane correction procedure 268
- Fig. 7-1. Mass losses a) from Kalbitz et al. (2006) and long-chain n-alkane characteristics for three different leaf litter species (Acer, Fagus and Sorbus) during 27 months of leaf litter degradation in a field experiment. b) n-Alkane concentrations, c) n-alkane amounts, d) odd-over-even predominance and e), f) n-alkane ratios. 285
- Fig. 7-2. n-Alkane concentration patterns of three different leaf litter species (Acer, Fagus and Sorbus) before (0 months) and after (27 months) leaf litter degradation in a field experiment. 286
- Fig. 7-3. a) Mid-chain n-alkane concentrations ($\sum(\text{n-C20 to n-C24})$), b) mid-chain n-alkane amounts ($\sum(\text{n-C20 to n-C24})$), c) compound-specific δD -

values of the most abundant individual n-alkanes and d) bulk δD -values for three different leaf litter species (Acer, Fagus and Sorbus) during 27 months of leaf litter degradation in a field experiment. 287

Fig. 7-4. a) and b) Modelled total, plant and microbial n-alkane amounts, c) modelled contribution of newly synthesized microbial n-alkanes versus 'old' ones, d) modelled δD values for source water, newly synthesized and total microbial n-alkanes and e) comparison of modelled total n-alkane δD values with mean measured δD values. 292

List of Abbreviations

| | |
|---|---|
| ^{18}O | Stable oxygen isotope with atomic mass 18 |
| AAR | Amino acid racemization |
| A-CN-K ternary plot | Ternary plot of Al_2O_3 -($\text{CaO}^* + \text{Na}_2\text{O}$)- K_2O according to Nesbitt and Young (1984) |
| $\text{Alk}_{>\text{C}25}/\text{Alk}_{<\text{C}25}$ | Ratio of of long chain n-alkanes ($\geq\text{C}25$) versus short chain n-alkanes ($<\text{C}25$) |
| ARM | Anhyseretic remanent magnetization |
| ASE | Accelerated soxhlet extraction |
| Ba-94 | Timescale for the Marine Isotope Stages derived from Bassinot et al. (1994) |
| B_{cr} | Coercivity of remanence |
| b-fabric | Birefringence fabric |
| B/M boundary | Brunhes – Matuyama boundary |
| CaO^* | CaO corrected for carbonate - Ca |
| c/f | Coarse/fine |
| Cfa | Type of climate system after the Köppen classification |

| | |
|-----------------|--|
| | (see Sträßler, 1998) |
| Cfb | Type of climate system after the Köppen classification (see Sträßler, 1998) |
| CPA | Chemical Proxy of Alteration i.e. molar ratio of $\text{Al}_2\text{O}_3/(\text{Na}_2\text{O} + \text{Al}_2\text{O}_3) \times 100$ |
| CPI | Carbon Preference Index |
| D | Stable hydrogen isotope with atomic mass 2 (Deuterium) |
| Dfb | Type of climate system after the Köppen classification (see Sträßler, 1998) |
| drs | Diffuse reflectance spectroscopy |
| F-AA | Floodplain sediments of the "Austroalpine cover nappes area" |
| F-BM | Floodplain sediments of the "Bohemian Massif area" |
| F-Drava | Floodplain sediments of the "Drava source area" |
| Fe _d | Dithionite-extractable iron fraction |
| FOREGS | Geochemical data derived from the Global Geochemical Baseline Programme of the Forum of European Geological Surveys (FOREGS) (Salminen et al., 2005) |
| F-WC | Floodplain sediments of the "Western Carpathian area" |

| | |
|------------|--|
| GC | Gas chromatograph |
| Gt | Goethite |
| H | Stable hydrogen isotope with atomic mass 1 |
| He-00 | Timescale developed by Heslop et al. (2000) for Chinese loess-paleosol sequences |
| HIRM | $(IRM_{0.35T} + IRM_{2T})/2$ |
| Hm | Hematite |
| Hz | Hertz. Si unit of frequency |
| INQUA | International Union of Quaternary Research |
| IPCC | Intergovernmental Panel on Climate Change |
| IRM | Isothermal remanent magnetization |
| IRM_{xT} | Isothermal remanent magnetization after exposing the sample to a pulsed magnetic field of x T. |
| IRSL | Infrared stimulated luminescence |
| JP-99b | Timescale for the Koriten section (Jordanova and Petersen, 1999) |
| ka | Kiloannum = 1.000 years |

| | |
|------------------|--|
| LAR | Long chain n-alkane ratios |
| L _x | Loess unit, with x being the stratigraphic number |
| LPSS | Loess-paleosol sequence |
| MD | Multidomain |
| md-n-alkanes | Microbially derived n-alkanes |
| MAP | Mean annual precipitation |
| MIS | Marine Isotope Stage |
| MPI | Micromorphological proxy for soil formation intensity |
| MV | Prefix for loess and paleosol units of the Mircea Voda site |
| M _(x) | Molar mass of compound x |
| n-C _x | Unbranched alkane with x carbon atoms |
| ODP | Ocean Drilling Program |
| OEP | Odd over even predominance i.e. amount of n-alkanes with an odd number of carbon atoms vs. amount of n-alkanes with an even number of carbon atoms |
| pd-n-alkanes | plant derived n-alkanes |
| P-E | Difference of precipitation and evaporation |

| | |
|----------|--|
| RI | Rubification Index according to Harden et al (1982) |
| RR | Redness Rating according to Torrent et al (1980) |
| SD | Single-domain |
| Sh-90 | Timescale derived by correlation to the $\delta^{18}\text{O}$ record of benthic foraminifera at ODP site 677 (Shackleton et al., 1990) |
| SIRM | Saturation isothermal remanent magnetization i.e. IRM_{2T} |
| SK | Prefix for loess and paleosol units of the Sary Kaydaky site |
| S.l. | Sensu latu |
| SOM | Soil organic matter |
| SP | Superparamagnetic |
| S- ratio | $\text{IRM}_{2T}/\text{IRM}_{0.35T}$ |
| Su-06 | Timescale derived by correlation to the magnetic susceptibility record of Sun et al. (2006) |
| Sx | Soil unit, with x being the stratigraphic number |
| T | Tesla. Si unit for the magnetic field strength |
| UCC | Upper continental crust |

| | |
|------------------------|--|
| U-ratio | Ratio of the 16-44 μm to 5.5-16 μm grain size fraction (Vandenberghe et al., 1998) |
| V | Prefix for loess and paleosol units of sites in the Vojvodina |
| XRF | X-Ray fluorescence |
| $\delta^{18}\text{O}$ | Natural abundance of oxygen isotope 18 expressed as the deviation of the $^{18}\text{O}/^{16}\text{O}$ isotope ratio of a sample from that of a standard, relative to the isotope ratio of the standard. Values are given in per mill. |
| δD | Natural abundance of D expressed as the deviation of the D/H isotope ratio of a sample from that of a standard, relative to the isotope ratio of the standard. Values are given in per mill |
| χ | Mass specific magnetic susceptibility ($\text{m}^3 \text{kg}^{-1}$) |
| $\chi_{(\text{xkHz})}$ | Mass specific magnetic susceptibility determined at x kilohertz |
| χ_{C} | Background magnetic susceptibility of the parent material |
| χ_{fd} | Frequency dependence of the magnetic susceptibility ($\chi_{\text{fd}} = \chi_{(0.3 \text{ kHz})} - \chi_{(3 \text{ kHz})}$) |
| $\chi_{\text{fd}\%}$ | χ_{fd} normalized to $\chi_{(0.3 \text{ kHz})}$: $\chi_{\text{fd}}/\chi_{(0.3 \text{ kHz})} \times 100$ |

Summary

Loess-paleosol sequences (LPSS) potentially are valuable archives for past environmental conditions. In SE-Central European lowlands thick loess plateaus can be found comprising several glacial-interglacial cycles. This work focuses on key sections in the middle and lower Danube Basin to i) investigate the origin of the loess and archive genesis, ii) to set up a reliable chronostratigraphy and iii) to contribute to the reconstruction of the Mid- and Late Pleistocene climate and landscape history of the region by a paleopedological – geochemical multi-proxy approach. Furthermore, methodological investigations aim to evaluate the validity of various paleoenvironmental proxies especially geochemically based weathering indices, as well as biomarker and stable isotope approaches in LPSS research.

The results from geochemical analyses reveal that alluvial material of the Danube and its tributaries represent major sources for the loess in the middle and lower Danube Basin. From the geochemical point of view the studied loess can be regarded as a representative sample of the upper continental crust altered by at least one sedimentary cycle.

The chronostratigraphy of the studied sections is based on the correlation of characteristic patterns of the magnetic susceptibility to the $\delta^{18}\text{O}$ record of benthic foraminifera from the Ocean Drilling Program site 677, a proxy record for the global ice volume. This is supplemented by correlating magnetic susceptibility fingerprints and pedostratigraphic marker horizons to previously established chronostratigraphies from profiles in the region as well as in China. The results show that the Batajnica/Stari Slankamen LPSS (Serbia) and Mircea Voda LPSS (Romania) comprise at least the last 700.000 years of climate history i.e. the last 17 marine isotope stages.

The multi-proxy approach for paleoenvironmental reconstruction involves micromorphological parameters, silicate weathering intensity as given by element composition, grain size proxies for pedogenic clay formation and wind strength, as well as

determination of sedimentation rates. As most suitable proxy for silicate weathering in calcareous sediments, the molar ratio $\text{Al}_2\text{O}_3/(\text{Na}_2\text{O} + \text{Al}_2\text{O}_3) \times 100$ is introduced as Chemical Proxy of Alteration (CPA) to loess paleosol research. Moreover, diffuse reflectance spectroscopy, soil color proxies and rock magnetic proxies are applied to gain paleoenvironmental information from the concentration and assemblage of iron minerals. Focusing on the warm periods, these proxies reveal a progressive decrease of interglacial weathering and soil formation intensity over the Mid - and Late Pleistocene. Also soil forming milieu was less oxidative as reflected by the iron mineralogical composition. These findings suggest cooling and a decline of rainfall linked to a change in seasonality from a Mediterranean type of climate to a more continental steppe climate. Results from n-alkane biomarkers support that summer dryness limiting the expansion of trees was a persistent feature of interglacial climate in SE-European lowlands.

In the obtained proxy dataset, increase of wind strength, gradual cooling as well as decrease of rainfall since the early Mid-Pleistocene is also evident for glacial periods. After evaluation of potential triggers, this general climatic trend is proposed to be related to Pleistocene uplift of Eurasian mountain ranges. Changes in atmospheric circulation and rain shadow effects due to mountain uplift (Himalaya, Alps, Carpathians) would provide an explanation for the westward expansion of the Eurasian steppe belt into SE-Central Europe.

Future studies on LPSS may also involve highly innovative proxies such as n-alkane biomarker and their D/H isotope signature. However, the methodological investigations on modern soil profiles and samples from litterbag experiments suggest that in a LPSS these proxies might be biased by microbial reworking. Procedures for correcting n-alkane ratios based on the odd over even predominance as reworking indicator have been developed. Hence, these studies highlight the limitations but also the persisting potential of innovative approaches from organic and isotope geochemistry in paleoenvironmental investigations of loess-paleosol sequences.

Zusammenfassung

Löss-Paläoboden-Sequenzen (LPSS) stellen potentiell wertvolle Paläoumweltarchive dar.

Lössplateaus im südost-mitteleuropäischen Tiefland erreichen mehrere Dekameter an Mächtigkeit und dortige LPSS können mehrere Glazial – Interglazial Zyklen umfassen. Die vorliegende Arbeit befasst sich mit Schlüsselprofilen im Becken der mittleren und unteren Donau. Ziel ist es i) die Lössprovenanz zu untersuchen und somit genauere Erkenntnisse über die Archivgenese zu gewinnen, ii) eine verlässliche Chronostratigraphie aufzustellen und iii) einen Beitrag zur Rekonstruktion der regionale Klima- und Landschaftsgeschichte während des Mittel- und Spätpleistozäns zu liefern. Für Letzteres wurde ein paläopedologischer – geochemischer Multiproxy-Ansatzes herangezogen. In methodischen Studien wurden verschiedene Proxies wie geochemisch basierten Verwitterungsindizes, Biomarker und stabilen Isotopen hinsichtlich ihrer Eignung zur Paläoumweltrekonstruktion evaluiert.

Die Ergebnisse der geochemischen Analysen zeigen, dass alluviale Sedimente der Donau bzw. von Donauzuflüssen die Hauptquelle von Löss im mittleren und unteren Donaubecken darstellen. Die geochemische Zusammensetzung des Lösses ähnelt der der oberen kontinentalen Kruste, jedoch nach Veränderung durch mindestens einen sedimentären Zyklus. Die Chronostratigraphie der untersuchten LPSS basiert auf einer magnetischen Suszeptibilitätsstratigraphie und ist gestützt durch pedostratigraphische Marker. Demnach umfassen die Profile Batajnica / Stari Slankamen (Serbien) und Mircea Voda (Rumänien) mindestens die letzten 700.000 Jahre d.h., die letzten 17 Marinen Isotopen Stufen.

Der Multiproxy-Ansatz zur Paläoumweltrekonstruktion umfasst mikromorphologische Parameter, geochemische Untersuchungen zur Silikatverwitterungsintensität, Untersuchungen zur pedogenen Tonbildung, sedimentologische Untersuchungen zur Windstärke und die Bestimmung von Sedimentationsraten. Als Proxy für Silikatverwitterung wird das molare Verhältnis $\text{Al}_2\text{O}_3/(\text{Na}_2\text{O} + \text{Al}_2\text{O}_3) \times 100$ als Chemical Proxy of Alteration (CPA) für die Löss-

Paläoboden-Forschung eingeführt. Darüber hinaus geben bodenfarb-basierte Proxies, diffuse Reflektionsspektroskopie und Umweltmagnetik Informationen über die eisenmineralogische Zusammensetzung, was ebenfalls Rückschlüsse auf Paläoumweltbedingungen erlaubt. Hinsichtlich der Interglaziale weisen die Multiproxy-Daten auf eine progressive Abnahme der warmzeitlichen Verwitterungs-, und Bodenbildungsintensität während des Mittel – und Spätpleistozäns hin. Auch war das Bodenmilieu während der jüngeren Warmzeiten weniger stark oxidativ, wie die eisenmineralogischen Ergebnisse zeigen. Diese Befunde deuten auf einen Abkühlungstrend und eine Abnahme der warmzeitlichen Niederschlagsmengen während des Mittelpleistozäns hin. Anhand der Daten lässt sich zudem eine Veränderung in der Saisonalität von Mittelmeerklima zu kontinental geprägten Klima (Steppenklima) ableiten. Die Biomarkerbefunde, deuten nur eine geringe Baumverbreitung während der Interglaziale an und bestätigen somit Sommertrockenheit als charakteristisches Merkmal des warmzeitlichen Klimas im mittleren und unteren Donaubecken.

Eine Zunahme der Windstärke, graduelle Abkühlung sowie eine Abnahme der Niederschlagsmenge seit dem unteren Mittelpleistozän zeigt sich auch für die Kaltzeiten. Nach Evaluierung möglicher Ursachen für diesen klimatischen Trend erscheint die Hebung eurasischer Gebirgsketten während des Pleistozäns als mögliche Hypothese. Diese könnte die Ausdehnung des eurasischen Steppengürtels bis ins südöstliche Mitteleuropa erklären.

Für zukünftige Löss-Paläobodenstudien bieten sich n-Alkan Biomarker oder ihre D/H Isotopie als hoch innovative Proxies an. Die methodischen Untersuchungen an verschiedenen Bodenprofilen und an Proben aus einem Streuabbauexperiment weisen jedoch darauf hin, dass Abbau und Kontamination durch mikrobiell-bürtige Alkane deren ursprüngliches Paläoumweltsignal überprägen können. Ein Verfahren zur Korrektur von n-Alkan Verhältnissen kann jedoch aufgezeigt werden. Diese Ergebnisse stellen somit einen Beitrag dar zur Bewertung von Potential als auch Grenzen dieser innovativen organisch- und isotopen-geochemischen Ansätze in der zukünftigen Lösspaläobodenforschung.

**Reconstruction of the Mid- and Late Pleistocene climate and
landscape history in SE-Central Europe.**

**A paleopedological and geochemical multi-proxy approach in loess-paleosol
studies.**

**(Rekonstruktion der Mittel – und Spätpleistozänen Klima und Landschaftsgeschichte in
SO-Mitteleuropa**

Untersuchung von Löss-Paläobodensequenzen mittels eines paleopedologischen und
geochemischen Multiproxy - Ansatzes

Extended Summary

1 Introduction

1.1 Rationale

The scientific consensus expressed in the fourth assessment report of the Intergovernmental Panel on Climate Change (IPCC; 2007) pinpoints that human activity affects climate on earth in an unprecedented way. To give projections on future environmental conditions it is essential to discern and predict their natural baseline fluctuations and validate the predictive models. Therefore, from 1990 to 2007, paleoclimate research got more and more in focus of the IPCC reports (Caseldine et al., 2010). However, there are still ample white patches on the picture of past environmental conditions in space as well as in time. Up to now in Europe only few (quasi-) continuous terrestrial climate records are available, which comprise several glacial-interglacial cycles and have the potential to capture long-term pattern of climate change. These are essentially the pollen sequences from peat profiles in France (Beaulieu et al., 2001; Reille et al., 2000) and Greece (Tzedakis and Bennett 1995; Tzedakis et al., 2006). Recently, after the fall of the Iron Curtain, the lowlands of the middle and lower Danube Basin (Hungary, Serbia, Romania, Bulgaria) as well as the region north of the Black Sea Coast in the Ukraine increasingly attracts paleoenvironmental research. This area represents the westernmost extension of the Eurasian steppe belt, separating the temperate climate zone of central Europe from the Mediterranean climate zone in the S and W Balkan Peninsula. Loess-paleosol sequences (LPSS) of several decameters thickness are widely distributed in this region with loess formation characterizing glacial or stadial intervals and soil formation prevailing in interglacials and interstadials. Hence, this is not only an area potentially sensitive for (past) climate change, but it also gives the opportunity to reconstruct the Mid - and Late Pleistocene environmental conditions from valuable archives. However, most of the existing studies either focus on a single LPSS-section, deal with paleoclimatic records of only

the last few glacial cycles, are lacking a reliable stratigraphic model or focus only on a single proxy approach (e.g. Jordanova and Petersen, 1999; Kostic and Protic, 2000; Tsatskin et al., 2001; Panaiotu et al., 2001, Perederji, 2001; Bronger, 2003; Avramov et al., 2006; Marković et al., 2006; Jordanova et al., 2007; Antoine et al., 2009; Bokhorst and Vandenberghe, 2009).

The environmental conditions under which a loess-paleosol sequence developed can be derived from the identification and (semi-)quantification of characteristic soil forming processes provided their dependency to climate parameters is known. Various methods are used such as micromorphological investigations (Tsatskin et al., 1998; Kemp, 1999; Mestdagh et al., 1999), grain size analyses (Fang et al., 2003; Antoine et al., 2009; Bokhorst et al., 2009) or study of mineralogical (Kalm et al., 1996; Kostic and Protic, 2000; Marković et al., 2004) and geochemical parameters (Schellenberger and Veit, 2006; Bokhorst et al., 2009). Besides the type and intensity of soil forming processes also microfossils and direct proxies of the paleovegetation such as pollen (Rousseau et al., 2001; Wu et al., 2007), phytoliths (Lu et al., 2007; Osterrieth et al., 2009) or the isotopic signature of organic carbon (Hatté et al., 1999; Zech et al., 2009) provide information on past environmental conditions. In recent years, also the lipid biomarker approach was implemented in loess-paleosol research and appeared to be promising for discerning different types of vegetation (e.g. forest vs. grassland) (Bai et al., 2009; Zech et al., 2009; Zech et al., 2010). Meanwhile, also the hydrogen isotopic composition of paleoprecipitation preserved in fossil lipids has been recognized as valuable tool for assessing changes in paleotemperature and/or precipitation from LPSS (Liu and Huang, 2005). Each approach or proxy has a different sensitivity for certain environmental parameters and a different susceptibility for posterior alteration of the original signal. Hence, multi-proxy approaches enable cross-validation of the individual proxies and allow the most comprehensive reconstruction of past environmental conditions (Dodonov and Baguizina, 1995; Derbyshire et al., 1997; Zech et al., 2009).

1.2 Objectives

This dissertation aims to gain information on the Quaternary climate and landscape history of the SE-Central European lowlands, involving multi-proxy investigations of LPSS. The focus is especially on climatic conditions during past interglacials as preserved in the LPSS sites Batajnica/ Stari Slankamen (Serbia), Mircea Voda (Romania) and Stary Kaydaky (Ukraine). These sites comprise more than five major loess-paleosol pairs, hence representing potential key sections for the Late and Mid-Pleistocene of this area. As climatic conditions differ in the middle and lower Danube Basin as well as at the Ukrainian location in terms of aridity and continentality, the chosen sections give not only the possibility to detect paleoenvironmental change in time, but also in space. However, before playing the music on the tape it is necessary to know the peculiarities of the tape i.e. how it was made, how the music was recorded and in which velocity it is to play. That means before any paleoclimatic conclusion can be derived from the LPSS it is essential to understand the process of archive formation, to acquire a reliable chronostratigraphy and to evaluate potential and limits of the applied proxies. Hence, the objective of Study 1 is to investigate the origin of the loess building up the LPSS and to proof their vertical sedimentary homogeneity. This involves a geochemical characterization of the loess and of potential source areas, as well as a reconstruction of prevailing wind directions during loess formation. Subsequently, Study 2 is addressed to the setup of a chronostratigraphy for the Batajnica, Stari Slankamen, Mircea Voda and Stary Kaydaky LPSS. A combined approach will be used based on pedostratigraphy, characteristic magnetic susceptibility fingerprints of the pedocomplexes and their correlation to the $\delta^{18}\text{O}$ record of benthic foraminifera from the Ocean Drilling Program (ODP) site 677 as proxy of the global ice volume (Shackleton et al., 1990). Study 3 aims towards an evaluation of geochemical proxies for silicate weathering in loess as prerequisite for a paleoclimatic interpretation of the silicate weathering record in Study 4 and 5. The goal of Study 4 is to identify soil forming processes and to give a semi-quantitative measure of their intensity

using micromorphology, the elemental composition and grain size distribution. This does not only allow a typification of the paleosols, but also to infer changes in paleoclimatic conditions from proxies of silicate weathering (geochemically based weathering index) and clay formation (clay content, c/f related distribution pattern and b-fabric) as weathering and transformation of silicates to clay minerals are sensitive to precipitation and temperature (Brady and Carroll, 1994; White and Blum, 1995). The assemblage and concentration of iron minerals and their grain size fractions is not only sensitive for the intensity of weathering and pedogenesis (e.g. Maher and Thompson, 1995; Cornell and Schwertmann, 2003) but also reflects periods of excess soil moisture as well as strongly oxidizing conditions (e.g. Thompson and Oldfield, 1986; Yaalon 1997; Cornell and Schwertmann, 2003). Hence, Study 5 focuses on a characterization of the iron mineralogy by various approaches (rock magnetic measurements, soil color proxies, diffuse reflectance spectroscopy). The aim is an integrated interpretation of the iron mineralogical proxy records, the records of silicate weathering and clay formation as well as paleosol typology in order to address changes in seasonal pattern of precipitation. In addition to these investigations of past soil forming conditions, it is intended to identify changes in the eolian activity and wind strength based on sedimentation rates (Study 2) and grain size analyses (Vandenberghe et al., 1998; Vandenberghe et al., 2004) (Study 4). Finally, information on past vegetation changes would substantially contribute to the picture of paleoenvironmental history. While the value of pollen analyses in loess is limited by far distance transport and selective preservation of palynomorphs (Faegri and Iversen, 1989), changes of the on-site vegetation (tree vs. grasses) can be possibly derived from n-alkane biomarkers (Zhong et al., 2007; Zech et al., 2009). Long-chain n-alkanes with a strong predominance of odd over even homologues are essential components of plant-cuticular lipids, herewith a dominance of n-C27 and n-C29 is indicative for woody taxa, whereas n-C31 and n-C33 prevail in most grass taxa (e.g. Maffei 1996; Zech et al., 2009). Due to the relative recalcitrance of long chain n-alkanes, ratios build from these homologues

are used to infer tree vs. grass vegetation changes (e.g. Zhang et al., 2006; Bai et al., 2009). Furthermore, studying the δD signature of these compounds represents an opportunity to infer past climate change rather independent from pedoclimatic conditions (Liu and Huang, 2005). The D/H composition of n-alkanes allows to track changes in the δD signature of past rainfall or soil water, with higher temperatures, less precipitation and higher evaporation leading to less negative δD -values (Gat, 1996; Sachse et al., 2006). Hence, the objective of studies 6 and 7 is to evaluate potential and limits of these innovative approaches, when applied to LPSS. In the former study the applicability of the n-alkane biomarker approach is tested on loess-paleosol samples of the Mircea Voda site, specifically addressing postsedimentary alteration of n-alkane fingerprints. The intention of this study is to evaluate possible ways to recognize such effects and to account for them, when interpreting n-alkane records in terms of paleovegetation. This is supplemented by Study 7 using a litterbag experiment to track alteration of the plant-derived alkane pattern and their δD signature in course of degradation/early diagenesis.

2 Regional setting

The LPSS Batajnica (44° 55' 29'' N, 20° 19' 11'' E) and Stari Slankamen (45° 7' 58'' N, 20° 18' 44'' E) are located in the Vojvodina loess region i.e. in the Serbian part of the Pannonian (middle Danube) Basin (Fig. 1-1, Fig. 2-1, Fig. 4-S1). The climatic data of the station Belgrade (Fig. 2-2, Fig. 5-1; WMO, 1996), show one period of dryness but no period of drought, according to the definition of Walter (1974) and indicate climatic conditions characteristic for forest steppe environment. Forest steppe is also described as potential natural vegetation of this area by Frey and Lössch (1998). The loess-paleosol record of the Vojvodina loess area is a stacked one from the Batajnica section and the Stari Slankamen

section, since there is influence of water-logging in the basal part of the former site. Both sections are situated at the banks of the Danube River.

The Mircea Voda site (44° 19' 15'' N, 28° 11' 21'' E; Fig. 1-1, Fig. 4-S2) is situated at about 13 km distance from the Danube on the Dobrudja loess plateau (Romania). This loess plateau reaches from the Danube River to the Black Sea coast. The potential natural vegetation of this area is feather-grass steppe (Fig. 2-1, Frey and Lösch, 1998). Steppe type conditions were also confirmed by the climate station of Constanta, showing a clear period of drought and dryness (Fig. 2-2, Walter, 1974; WMO, 1996) and also mean annual precipitation of this area is substantially lower than at the Serbian sites (~ 400 vs. ~ 680 mm) (Fig. 2-2, Fig. 5-1). In both the Serbian and Romanian LPSS, more than six major loess-paleosol pairs are outcropped.

The Stary Kaydaky site (48° 22' 42'' N, 35° 07' 30'' E) is located in the Dnieper loess area, next to Dniepropetrovsk at the Dnieper River (Fig. 1-1). The vegetation of this area is described as a wet variant of the feather-grass-steppe (Fig. 2-1; Walter, 1974). The limit of the southernmost extend of the Fennoscandinavian ices sheet (Fig. 1-1), is about 50 km north of the section. In contrast to the Romanian and Serbian sections, which represent LPSS in plateau situation, the outcrops of the Stary Kaydaky site are situated in slope position within a system of gullies. The sequence comprises five major loess-paleosol couples.

3 Methods

3.1 Nomenclature and sample material

The nomenclature of the soil and loess units is in accordance with the nomenclative systematic widely used for the Chinese loess-paleosol sequences (e.g. Derbyshire et al. 1997, Chen et al. 2002). Main paleosols/pedocomplexes are designated with 'Sx' and main loess layers with 'Lx'', with 'x' being the stratigraphic number of soil or loess, starting from the recent soil at x=0. Subunits of the individual pedocomplexes are named SxSy for a paleosol

and SxLy for an intercalated loess layer starting with y=1 for the uppermost soil of a pedocomplex. Weak paleosols, intercalated in a main loess unit, were marked with LxSz, starting with z=1 for the youngest paleosol of a loess unit. Prefixes designate the locality of the section with SK for Sary Kaydaky, MV for Mircea Voda and V for the Vojvodinian loess sites. Having established the chronostratigraphy of these LPSS in Study 2, loess-paleosol units are regarded as correlatives to Chinese stratotype sections and the prefix for locality is not applied in the following studies.

For mineralogical analyses, grain size analyses, organic and anorganic geochemistry, the pedocomplexes were sampled continuously in 10 to 50 cm intervals depending on horizontation and thickness. At least three representative samples were collected from each intercalated loess units. For micromorphological investigations one representative, undisturbed and oriented block was taken from each pedomember horizon. The profiles Batajnica and Stari Slankamen were not sampled for micromorphology, as detailed micromorphological investigations and paleopedological descriptions of these sites are already available (Bronger, 1976; Marković et al., 2009).

For Study 6, modern forest and grassland soils have been sampled for n-alkane analyses. Litterbag samples for Study 7 were provided by Prof. K. Kalbitz (University of Amsterdam, Netherlands). The litterbag experiment was conducted in the Fichtelgebirge using litter of five different species (*Acer pseudoplatanus.*, *Fagus sylvatica*, *Sorbus aucuparia*, *Picea abies* and *Pinus sylvestris*), which has been exposed in the field for up to 27 months. Details on site and experiment design are described in Gerstberger et al. (2004) and Kalbitz et al. (2005). After drying and grinding of the collected litter samples, all replicates were combined for further n-alkane and δD analyses.

3.2 Analyses, data exploration and applied proxies

After drying, all soil samples were finely ground for the further analyses, except the aliquots for rock magnetic measurements, n-alkane analyses and of course the samples for micromorphological investigations. Litter samples (Study 7) were also finely ground for n-alkane analyses to make also internal lipids accessible for the extraction solvent.

3.2.1 Inorganic geochemistry (Study 1 and 3)

The samples were analyzed for their element composition by J. Eidam (University of Greifswald) using a Philips 2404 X-Ray Fluorescence Spectrometer. The sulfur contents were measured separately via thermal conductivity detection on a Vario EL elemental analyzer (Elementar, Hanau, Germany) and carbonate contents were determined according to the procedure of Hedges and Stern (1984) by calculating the difference in C content of the sample material with and without HCl fumigation. The measurements were also carried out on a Vario EL elemental analyzer.

For a geochemical characterization of the loess-paleosol sections (Study 1), a discriminant analysis was carried out. Furthermore, element ratios (Al/Ti, Fe/Ti, Fe/Al) and the A-CN-K diagram (ternary diagram of $K_2O-CaO^* + Na_2O-Al_2O_3$, with CaO^* referring to silicatic bound Ca) according to Nesbitt and Young (1984) were applied allowing to assess provenance, as well as selective enrichment or depletion of grain size and mineral fractions of silicates. The origin of the loess was evaluated based on its geochemical characteristics and comparison to the geochemical composition of potential source areas. The latter is derived from published data of floodplain sediments in the Danube catchment (Salminen et al., 2005) and the average composition of the Ukrainian and Baltic shield (Ronov and Yaroshevskiy, 1976). The interpretation of the geochemical composition in terms of provenance (Study 1) is supplemented by an evaluation of the background susceptibilities of the loess and of the

geomorphodynamic setting such as paleowind direction. For the evaluation of different weathering indices (Study 3), all indices were calculated on a molar base.

3.2.2 Rock magnetic measurements and parameters (Study 2 and 5)

All rock magnetic measurements were performed on sample material densely packed into plastic boxes in order to avoid movement of the particles during the analyses. The magnetic susceptibility was determined on a KLY-3 Kappabridge of Agico (Brno, Czech Republic) at 0.875 kHz and 300 A/m and is given as mass specific susceptibility (χ). The frequency dependence of susceptibility ($\chi_{fd} = \chi_{(0.3 \text{ kHz})} - \chi_{(3\text{kHz})}$) was measured with a MAGNON susceptibility bridge (MAGNON, Dassel, Germany). For the determination of the isothermal remanent magnetization (IRM) the sample material was exposed to a pulsed magnetic field of 2000 (IRM_{2T}) and 350 mT (IRM_{0.35T}) (back field) produced by a MAGNON PM II pulse magnetiser. Magnetization was then measured via an AGICO JR-6 spinner magnetometer. Measurements of the anhysteretic remanent magnetization (ARM) were performed via a Magnon AFD 300 demagnetiser using a 50 μ T static and 100 mT alternating field. The coercivity of remanence (B_{cr}) was determined by linear interpolation between the data points (acquired IRM vs. applied pulse field) when stepwise imprinting IRM reversely to a prior acquired IRM_{2T}.

χ generally reflects concentration of ferrimagnetica (i.e. magnetite and maghemite) as well as changes in their grain size distribution (e.g. Tang et al., 2003). In contrast, χ_{fd} and $\chi_{fd\%}$ ($= \chi_{fd}/\chi_{(0.3 \text{ kHz})} \times 100$) is exclusively sensitive to the concentration and relative contribution of ferrimagnetica in the SP-fraction ($\sim <0.03 \mu\text{m}$), respectively (Banerjee, 1994; Liu et al., 2007). IRMs are essentially controlled by the concentration of antiferromagnetica (hematite and goethite) and of ferrimagnetica in the single-domain (SD) and multidomain (MD) range (0.03-10 μm and $>10 \mu\text{m}$, respectively). While the ratio of IRM_{2T}/IRM_{0.35T} (S-ratio) is applied as proxy for the relative abundance of ferrimagnetica vs. antiferromagnetica (Maher,

1986, Wang et al., 2006), the average of both IRMs, the so-called HIRM, is regarded as a measure for the concentration of antiferromagnetica (Geiss et al., 2004). As the ARM is particularly sensitive to the concentration of SD-ferrimagnetica, the ARM/IRM_{2T} ratio is applied as proxy for changes in the ratio of SD vs. SD to MD ferrimagnetica (Van Velzen and Dekkers, 1999). For further characterization of changes in the grain size distribution of ferrimagnetica the SIRM/ χ_{fd} and ARM/ χ_{fd} ratio have been introduced, indicative for the ratio of SD to MD vs. SP - fraction and SD - vs. SP - fraction, respectively (see Study 5, Section 2.2). B_{cr} generally is controlled by changes in magnetic mineralogy and grain size distribution, but also reflects surficial maghemitization of magnetite (van Velzen and Dekkers, 1999; Avramov et al., 2006; Deng et al., 2006; Wang et al., 2006). The essential fundamentals for the paleoenvironmental interpretation of this set of rock magnetic parameters are that in course of pedogenesis especially SP-sized ferrimagnetica are formed. In case of (seasonal) excess soil moisture, however, preferentially this fraction is destroyed (Thompson and Oldfield, 1986). On the other hand, it is the coarse ferrimagnetic fraction, which is more susceptible for hematization in case of strongly oxidizing conditions (Gallagher et al., 1968; Chen et al., 2005).

3.2.3 Soil color measurements and diffuse reflectance spectroscopy (Study 4 and 5)

Hematite/(Hematite + Goethite) ratios (Hm/(Hm+Gt)) were determined via diffuse reflectance spectroscopy (drs) following the Torrent et al. (2007) approach. Spectroscopic measurements were performed relative to a white HALON (sintered polytetrafluorethylene) standard using an AgriSpec spectrometer coupled with a Mug-Light A1221000 detector (ASDInc, Boulder, Colorado, USA). Besides that, Munsell-color based measures for soil reddening (rubification) were applied i.e. the Rubification Index (RI; Harden 1982) and the Redness Rating (RR; Torrent et al. 1980; Torrent and Barrón 1993). Munsell colors were determined on dry and wet soil clods for each loess-paleosol sample.

3.2.4 Grain size and micromorphological analyses (Study 4)

The grain size analyses were performed using a Malvern Mastersizer S analyzer and wet sieving for the >600 μm fraction. Sample pre-treatment followed the procedure proposed by Konert and Vandenberghe (1997) comprising i) removal of carbonates by boiling HCl (10%) treatment and ii) disaggregation using sodium hexametaphosphate. Prior to laser analyses the material was subjected to ultrasonic treatment to ensure complete disaggregation. As proxy for the clay content the <5 μm laser fraction was applied, showing the best correlation to previously published results from pipette analyses for the Stari Slankamen section (Bronger 1976). To detect sedimentologically caused grain size changes (e.g. due to changing wind strength) the ratio of the 16-44 μm to 5.5-16 μm grain size fraction (U-ratio) was calculated (Vandenberghe et al., 1998, Sun et al., 2006).

3.2.5 Micromorphological analyses (Study 4)

Thin sections of > 2.8*4.8 cm^2 size were prepared from undisturbed oriented soil samples according to Beckmann (1997). The description of micromorphological features follows the nomenclature of Stoops (2003). As the type of “b-fabric” and “c/f related distribution pattern” is related to soil forming intensity a micromorphological proxy of soil formation intensity (MPI) was implemented transferring both features into numerical values (Study 4, Table 4-S1).

3.2.6 n-Alkane analyses (Study 6, 7) and δD measurements (Study 7)

The extraction and purification of the n-alkane fraction followed the procedure given in Zech and Glaser (2008) involving the following steps i) addition of an internal standard (5 α -androstane), ii) lipid extraction with a methanol/toluene mixture (7/3) using 24 h of soxhlet extraction for (paleo-)soil and loess samples (Study 6) and accelerated soxhlet extraction

(ASE) for litter samples (Study 7), iii) saponification of esters using 0.5 M KOH in methanol, iv) purification of the n-alkane fraction via column chromatography (Al-oxide and Silica, each 5% deactivated, elution with hexane - toluene mixture 85/15). After concentration and addition of a recovery standard (hexatriacontane) separation and quantification of individual n-alkane homologues (Study 6) was performed on a HP 6890 gas chromatograph coupled to a flame ionization detector (GC-FID).

δD values of n-C27, n-C29, n-C31 alkanes (Study 7) were measured on a Thermo Scientific Delta V Advantage isotope ratio mass spectrometer interfaced to a Thermo Scientific Trace GC Isolink and expressed relative to Vienna Standard Mean Ocean Water (VMSOW). Samples of spruce and pine were not analysed for isotopic composition as lower n-alkane concentration hampered routine δD -measurements.

4 Results/Discussion

4.1 Geochemical characterization and origin of the Southeastern and Eastern European loess (Study 1)

The element fingerprint (Fig. 1-6) of the loess in the middle and lower Danube Basin sites as well as the Ukrainian site, reveal a composition similar to various other loess regions of the world. The element contents are close to values for the upper continental crust (UCC). Relative enrichment or depletion factors mostly range between 2 and 0.5, which can be attributed to weathering or mineral – and grain size sorting effects on element concentration. Further evidence for UCC-like composition of the loess parent material is provided by element ratios such as Fe/Ti (Fig. 1-5) and the A-CN-K plot (Fig. 1-4). The A-CN-K plot reveals also a high pre-weathering of the loess indicating at least one sedimentary recycling phase of the loess source material. Hence, the weathering signal is most likely inherited

already from sedimentary source rocks, which is also in agreement with findings from other loess regions (Gallet et al., 1998; Jahn et al., 2001).

4.1.1 The “Dnieper loess”

According to discriminant analyses, the loess of the Stary Kaydaky site can be distinguished from the loess at the Danube Basin sites by higher contents of Si and Zr (Fig. 1-2). Also Hf contents are elevated (Fig. 1-3). As glaciofluvial deposits of the Fennoscandinavian ice sheet in the Ukraine are characteristically enriched in these elements (Batista et al., 2006; Lis and Pasieczna, 2006), this may represent a major potential source for the loess material. Additional evidence is given by the A-CN-K plot (Fig. 1-4), indicating grain size - and mineral sorting, typical for glaciofluvially reworked material. The high pre-weathering of the loess and the UCC-like composition of its parent material points to sedimentary rocks of the Russian platform as primary source for these glaciofluvial deposits.

4.1.2 The “Danube loess”

Regarding the geochemical composition, the loess from the lower and middle Danube basin is very similar to each other and to Danube floodplain sediments (Fig. 1-2, Fig. 1-4, Fig. 1-5, Fig. 1-6). This confirms that the loess from both regions derives predominantly from Danube alluvium, as proposed by Smalley and Leach (1978). At the Mircea Voda site, however, distinctly higher Zr, Hf and especially Si contents suggests a minor but geochemically significant contribution of an additional dust source area (Fig. 1-3). Distribution and orientation of sand (dune) fields indicate at least periodically prevailing N to NE paleowind direction in the Eastern part of the lower Danube basin during periods of high eolian activity (Fig. 1-8). Hence, material deriving from the Ukrainian glaciofluvial sediments likely contributes to the loess of the Mircea Voda site. This is also corroborated by a trend in background magnetic susceptibilities recorded in loess sites from the Black Sea coast

northwards (Fig. 1-7). This trend can be explained by an increasing dilution of the magnetic signal due to higher quartz contents. From the geochemical point of view, in all of the studied loess sites, no prominent down-profile change in dust provenance could be detected.

4.2 Stratigraphy (Study 2)

Like in the Chinese loess, the magnetic susceptibility of the LPSS in the Danube and Dnieper loess area is elevated in the paleosols compared to the loess (Fig. 2-3) and thus indicates pedogenesis. Characteristic magnetic susceptibility pattern match changes in the global ice volume as indicated by the $\delta^{18}\text{O}$ signature of benthic foraminifera at ODP site 677. Besides characteristic susceptibility pattern also pedostratigraphic marker horizons have been detected. Both allowed the correlation to LPSS with already established chronostratigraphies in the region as well as on the Chinese loess plateau. At the Danube Basin sections, such a characteristic feature in the magnetic susceptibility record is for example a bend at the top of the S1-peak, possibly representing MIS 5a-c and the twin or triple peak of the S2 pedocomplex, correlating with MIS 7. The S3 pedocomplex typically is the unit with the highest magnetic susceptibility values of the South-Eastern European LPSS and formed during MIS 9. The underlying S4, S5 and S6 pedocomplexes were attributed to MIS 11, MIS 13 – MIS 15 and MIS 17, respectively. The strongly developed S5 can be regarded as kind of marker horizon, since it is the youngest pedocomplex of the Brunhes-chron with remarkable rubification and clay illuviation.

At the Stary Kaydaky section, the magnetic susceptibility record is biased by pedogenic overprint of the loess and several hiatus, especially in the older part of the section. Yet, pedostratigraphic markers could be well identified allowing correlation to the stratigraphic system of the Ukraine. However, there are essentially two main contrasting stratigraphic models proposed for loess-paleosol successions of the Ukraine (Table 2-2). The crucial point for these regional stratigraphic systems is the chronological placement of the so-called

Pryluky and Kaydaky pedocomplexes. Yet, the good concordance of the magnetic susceptibility curve with changes in the marine $\delta^{18}\text{O}$ signal during the last interglacial, provides a strong evidence for correlating the S1 (Pryluky/Kaydaky complex) at Stary Kaydaky to MIS 5 (Fig. 2-6). This supports the stratigraphic model of Gerasimenko (2004, 2006). Accordingly, the time scale for the older units of the Stary Kaydaky section could be developed. As a result, the lowermost sampled paleosol is attributed to MIS 13 – 15. Hence, the time span captured by the studied LPSSs comprise the last 600.000 to 700.000 years (Fig. 2-5).

4.3 Evaluating rock-magnetic and geochemical proxies of pedogenesis and paleoclimate: the magnetic susceptibility and element ratios (studies 2, 3, 5)

In loess-paleosol research, magnetic susceptibility is widely applied as pedogenesis proxy, as data sets can be obtained with little effort. Furthermore, studying surface soils on the Chinese Loess Plateau, Maher et al. (1994) developed a transfer function between magnetic susceptibility and mean annual precipitation (MAP). We evaluated the applicability of this approach to SE-European loess profiles and found that MAP values calculated for the modern soils do not correspond to actual climatological data (Study 2, Table 2-3). Also, neither for modern soils nor for paleosols, relative trends between the profiles are reproduced by the calculated MAP values. Moreover, the attenuation of the magnetic susceptibility from S4 to S6 contrasts intensity of soil development. Several possible explanations for these observations are presented in Study 2. Further evaluation with a more extensive rock magnetic dataset (Study 5) could relate the attenuation of the bulk magnetic susceptibility in the older pedocomplexes to a complex interplay of hematization of MD-ferrimagnetica and preferential destruction of SP-ferrimagnetica. Hence, a straight forward interpretation of magnetic susceptibility in terms of pedogenesis intensity and precipitation is not possible.

As proxies for silicate weathering and also leaching intensity, a variety of element ratios are applied in paleopedology. By evaluating different types of geochemical weathering indices (Study 3) it could be shown that indices involving Si, Zr or Ti as weathering resistant element can be more easily biased by changing parent material composition than those using Al. Furthermore, regarding the choice of the mobile element, proxies relying on Ca or Mg are likely to be influenced by postpedogenic dynamics of secondary carbonate. This is also true for Sr. The case examples from the Mircea Voda, Batajnica/Stari Slankamen and Stary Kaydaky site show a significant correlations between Rb/Sr and Ba/Sr ratios and the carbonate content (Fig. 3-3). The Index B of Kronberg (Kronberg and Nesbitt, 1981), the Chemical Index of Weathering (Harnois, 1988), the Plagioglas Index of Alteration (Fedo et al., 1995) and the Chemical Index of Alteration (Nesbitt and Young, 1982) involve silicatic-bound Ca. Applying to calcium carbonate containing material, sensitivity analyses revealed that these indices can significantly suffer from uncertainties in the determination of the silicatic Ca fraction (Table 3-2). Moreover, ratios relying on K as mobile element can be biased by K-fixation (illitization). Hence, with respect to suitability for loess-paleosol samples, the molar ratio of $Al_2O_3/(Na_2O + Al_2O_3)$ is introduced as Chemical Proxy of Alteration (CPA). The CPA is regarded as proxy of silicate weathering and applied as such in the following studies.

4.4 Paleoenvironmental reconstruction (2, 4, 5, 6)

As the CPA confirmed a multiple pedogenic overprint (soil welding) of major parts of the Stary Kaydaky section, and due to several hiatus, the LPSS of this site turned out to be not suitable for a paleoclimatic transect study. A detailed second field work moreover questioned the plateau-character of the paleorelief. Hence, further paleoclimatic investigations focused only on the Serbian and Romanian LPSS. Being plateau-sites, a similar relief position and

exposition is given for these sequences, allowing spatial comparison of paleopedologic characteristics and climate proxies.

Reconstructing pedogenic processes essentially by means of field observations, micromorphology, calcium carbonate measurements, soil color and grain size analysis, allowed a tentative typological characterization of the paleosols. For the Mircea Voda site a change in typology of interglacial paleosol has been identified (Study 4, Table 4-S2). During younger interglacials (MIS 5, MIS 7) soil development peaked in steppe soils as indicated for example by a microstructure typical for fossil A horizons. Rubified Cambisols were formed in the older warm periods (MIS 13-15, MIS 17) and transitional soils in MIS 9 and 11. A similar change in paleosol typology from fossil rubified Luvisols and rubified Cambisols to steppe soils during the Pleistocene has been previously described also for the Batajnica and Stari Slankamen section (Bronger, 1976; Marković et al., 2009).

Furthermore, as semi-quantitative measures of soil forming processes the MPI, CPA and $<5 \mu\text{m}$ fraction have been applied (Study 4). These proxies reveal a significant decrease of soil formation intensity, silicate weathering intensity and clay formation intensity over the last 700.000 years for the middle and lower Danube Basin sites (Fig. 4-1, Fig. 4-S3, Fig. 4-S4). In light of present day steppic conditions higher intensity of silicate weathering and clay formation in Mid-Pleistocene interglacials likely relate to higher rainfall. The regional climate trend between the Vojvodina and the lower Danube Basin appears to have persisted also during most of the past interglacials, with higher values of the CPA and the $<5 \mu\text{m}$ fraction reflecting the more humid conditions at the Serbian site.

A more differentiated view on changing paleoenvironmental conditions can be achieved by investigating changes of the Fe-mineralogical composition (Study 5). The results show an increase in rubification and drs-determined $\text{Hm}/(\text{Hm}+\text{Gt})$ ratios from Late to early Mid-Pleistocene paleosols (Fig. 5-7). Furthermore, intensified hematization of maghemite is indicated by increasing ARM/SIRM values (Fig. 5-5, Fig. 5-9). Altogether, these parameters

point to more oxidizing conditions during older interglacials being indicative for warmer and/or dryer summers than at present day.

According to n-alkane results (corrected for diagenetic alteration) from Mircea Voda (Study 6, Fig. 6-5), tree abundance was not higher during formation of the fossil Cambisols than in the Holocene. Therefore, also the biomarker analyses provide evidence for summer dryness as a persistent feature in the Danube Basin, during the warm periods of the last 700.000 years. For these reasons, higher rainfall deduced from MPI, CPA and the <5 μm fraction, relates not to an increase in summer precipitation, but mainly to higher rainfall in the winter half-year. This suggests also a rise of winter temperatures so that winter precipitation becomes hydrological active. Hence, regarding the interglacials, the synthesis (Study 5) of the paleopedologic multi-proxy dataset reveals a decrease of rainfall and cooling over the last 700.000 years, which was linked to a shift in seasonality from Mediterranean like conditions to a steppe like climate.

The aridization and cooling trend is accompanied by an increase in dust sedimentation rate (Fig. 2-7), as derived from the depth-age relationship of the Mircea Voda site (Study 2). From the composite Batajnica / Stari Slankamen section no sedimentation rates were calculated to avoid site specific effects of dust deposition. Nevertheless, from applying the U-ratio (Study 4) for both the lower and the middle Danube Basin sections, an increase of wind strength during the Mid- and Late Pleistocene is indicated (Fig. 4-1, Fig. 4-S3, Fig. 4-S4). Hence, climate evolution of the SE-European lowlands during the last 700.000 years' interglacials is also characterized by an enforcement of the aeolian dynamics.

Trends of Pleistocene aridization, cooling and increase of wind strength were detected not only regarding the interglacials, but also the glacial periods (Fig. 4-1, Fig. 5-9). This emphasizes a general climate trend. As similar climate trends can be traced to the East across Eurasia in various types of archives and proxies (Fig. 4-2), the aridization and cooling of SE-European lowlands during the last 700.000 years can be regarded as regional expression of a

Eurasian-wide climate feature. Several mechanisms are discussed as potential triggers (Study 4 and 5), such as changes in solar insolation, atmospheric CO₂, global ice volume, and sea surface conditions. However, these factors fail to explain a gradual cooling and aridization of Eurasian midlatitudes, as none of the relevant proxies exhibit a similar trend (Fig. 4-3). Nevertheless, they likely caused some deviations from the general climatic trend as discussed in Study 5. Yet, Quaternary uplift of Eurasian mountain ranges is proposed as potential trigger, giving the best explanation for the observed gradual climatic shifts in SE-Europe and Eurasia, respectively.

4.5 n-Alkane biomarkers and their δ D isotopic signature as novel paleoenvironmental proxies in loess-paleosol studies – an evaluation (studies 6, 7)

n-Alkane ratios and their δ D isotopic signature have been recently implemented in loess-paleosol studies as novel proxies for paleovegetation and paleoclimate (e.g. Xie et al., 2002; Liu and Huang, 2005). As an outlook for future paleoenvironmental investigations on SE-European loess profiles, studies 6 and 7 are addressed to evaluate the applicability of these novel proxies to LPSS research.

Applying the n-alkane approach to the Mircea Voda site (Study 6), a significant correlation of the long chain n-alkane ratios (LARs) C₂₇/C₃₁ and C₂₇/C₂₉ with the odd over even predominance (OEP) is found in loess-paleosol samples. The results show a decrease of any predominance (e.g. C₃₁ over C₂₇, C₂₉ over C₂₇) in the depth profile of the fossil soils going along with a decrease in OEP (Fig. 6-5). Low OEP values indicate n-alkanes derived from microbial reworking. Microbial derived n-alkanes are furthermore characterized by a low ratio of long-chain n-alkanes (\geq C-25) versus short chain n-alkanes (<C-25) (i.e. Alk_{>C₂₅}/Alk_{<C₂₅} ratio). This ratio is covarying with the OEP in paleosol depth profiles (Fig. 6-5). Therefore, the decrease of long chain n-alkane predominances is likely related to increasing dilution of the original plant derived n-alkane signal by microbial derived n-

alkanes. Investigations on modern soils under various types of vegetation reveal similar pattern (Fig. 6-1, Fig. 6-3, Fig. 6-4, Fig. 6-6), indicating a decrease of long chain n-alkane predominances with depth resulting from increasing degradation of the plant derived alkanes and increasing dilution by microbial derived alkanes. These results highlight postsedimentary alteration of the biomarker signal as an important issue to cope with in paleoenvironmental research. However, based on OEP - LAR regression functions from modern top soils, a correction procedure is proposed (Fig. 6-2, Fig. 6-7) to account for this effect in future n-alkane studies of loess-paleosol sequences.

The findings from soil depth profiles are corroborated by the litterbag study (Study 7). Also this experiment shows a decrease of initially high OEP values and a convergence of LARs to 1 with progressive degradation (Fig. 7-1). Mid-chain n-alkanes become enriched relatively to long chain n-alkanes. During spring and summer times, when plant derived long chain n-alkanes are decomposed fastest, mid-chain n-alkanes exhibit the strongest absolute increase (Fig. 7-3), indicating the microbial production of n-alkanes. Hence, in course of decomposition the long chain plant derived n-alkane pool becomes an increasingly mixed pool of microbial derived and plant derived n-alkanes (Fig. 7-4).

The increase of microbial derived mid-chain n-alkanes in the summer period is furthermore accompanied by δD -enrichment of long-chain homologues (Fig. 7-3). In line with the previous observations, this suggests that long-chain n-alkanes of (fossil) organic matter do not explicitly derive from the degrading leaf-litter, but also from a microbial source, sensitive to seasonal δD variations of the precipitation. Thus, the performed degradation studies advise caution, when applying the n-alkane biomarker and δD approach in loess-paleosol studies. Though these proxies represent potential novel paleoclimatic tools, effects of decomposition/early diagenesis have to be considered.

5 Conclusion

Loess deposits in the middle and lower Danube basin represent valuable archives for the Late and Mid-Pleistocene climate evolution. According to their geochemical composition they also represent an average sample from the UCC, altered by at least one sedimentary cycle. They formed from dust, blown out from alluvial sediments of the Danube and its tributaries and can be geochemically distinguished from the loess in the Dnieper region. For the eastern part of the lower Danube Basin, glaciofluvial sediments of the Fennoscandinavian ice sheet in the Ukraine represent an additional loess source, supplying material via northerly katabatic winds. Chronostratigraphic investigations based on correlation of magnetic susceptibility pattern and pedostratigraphic marker of the Batajnica/Stari Slankamen and Mircea Voda LPSS revealed that these sequences comprise at least the last 700.000 years of climate history in SE-Europe. A chronostratigraphy could be also developed for the Stary Kaydaky site (Ukraine). At this site, the magnetic susceptibility record could give strong evidences for the chronological placement of the Kaydaky soil, a heavily discussed key unit in the Ukrainian pedostratigraphy. However, due to hiati, soil welding and the slope position of the paleosols, this site turned out to be unsuitable for a paleoclimatic transect study. Hence, paleoclimatic investigations focused on the Plateau sites of the lower and middle Danube Basin (Mircea Voda, Batajnica/Stari Slankamen). Yet, our findings showed that a straight forward interpretation of the magnetic susceptibility in terms of paleorainfall and pedogenesis intensity is not applicable at these profiles. Detailed rock magnetic analyses revealed biases due to various factors such as hematization as well as reductive dissolution of ferrimagnetica. Also geochemical based weathering indices should be evaluated carefully, when applied to LPSS. According to sensitivity analyses and the case examples from Mircea Voda, Batajnica/Stari Slankamen and Stary Kaydaky, many indices essentially suffer from postpedogenic alteration due to dynamics of secondary carbonate, uncertainties in quantifying silicatic Ca, illitization in course of diagenesis and changes in parent material composition.

The molar ratio of $\text{Al}_2\text{O}_3 / (\text{Na}_2\text{O} + \text{Al}_2\text{O}_3)$ is introduced as Chemical Proxy of Alteration (CPA), representing the most suitable indicator for silicate weathering intensity in LPSS.

The CPA is one out of several parameters in the applied paleopedological multi-proxy approach. For the studied LPSS in the middle and lower Danube Basin, a decrease of rainfall from the interglacials of the early Mid-Pleistocene to the Late Pleistocene and Holocene is evidenced not only by the silicate weathering intensity but also by micromorphological parameters of soil development intensity, as well as a decrease in clay formation intensity. Furthermore, soil types changed from fossil Luvisol and Cambisols to fossil steppe soils. At the same time, soil color indices, diffuse reflectance spectroscopy as well as rock magnetic parameter suggest less oxidative soil environment, reflected in decreasing intensity of hematite formation. Therefore, based on the presented multi-proxy dataset, it is to conclude that interglacial climate in the lower and middle Danube Basin considerably changed over the Pleistocene. A Mediterranean like climate with high summer temperatures and a pronounced estival dry period and mild and wet winters prevailed in interglacials of the early and middle Mid-Pleistocene. Soil development on loess plateaus peaked in (chromic) Luvisols and Cambisols during these interglacials. In subsequent warm periods, (winter-) temperatures as well as precipitation decreased, resulting in higher continentality and a steppe-type climate. Hence, steppe soils developed on top of loess plateaus. Aeolian activity increased over the Pleistocene as evidenced by the U-ratio and sedimentation rates. According to the relative intensity of pedogenic proxies, today's regional trends in aridity between the middle and lower Danube Basin were persisting also in most of the Mid-Pleistocene interglacials. From the presented findings it is to conclude that summer dryness was a persistent feature of interglacial climate in the middle and lower Danube Basin, at least during the last 700.000 years. This is additionally supported by biomarker results suggesting only a limited expansion of trees during the interglacials on the loess plateaus.

Also regarding the cold stages our results suggest a progressive cooling, increasing dryness and wind strength over the Mid- and Late Pleistocene. These gradual changes of glacial and interglacial climate conditions cannot be explained by orbital forcing, changes in global ice volume or sea surface conditions of the North Atlantic. Having excluded these factors, Quaternary uplift of Eurasian mountain ranges appears as potential trigger for the observed climatic trends in SE-Central European lowlands. Following this hypothesis, especially rain shadow effects and changes in atmospheric circulation induced by uplift of the Alps and Carpathians could be mechanisms explaining the expansion of the Eurasian steppe belt as far west as to SE-Europe over the last 700.000 years. Climate changes on shorter scale and deviations from this gradual climate trend can be related to triggers such as orbital parameters, changes in global ice volume or sea surface hydrography of the North Atlantic.

To conclude, the present study highlights the potential of a paleopedological – geochemical multi-proxy approach to derive information on the natural baseline of environmental change in the past, even with respect to changes in seasonality of climate variables.

The methodological investigations on the n-alkane and D/H isotope approach reveal early diagenesis (microbial reworking) as major drawback of these methods. However, an approach to account for postsedimentary alteration of n-alkane biomarker ratios is proposed. Therefore, ongoing work involves more detailed biomarker and stable isotope (D/H and $\delta^{13}\text{C}$) analyses in multi-proxy studies of LPSS in the middle and lower Danube Basin. Furthermore, microfossil analyses (pollen, phytoliths) will complement the paleoenvironmental reconstruction, representing independent proxies for paleovegetation and paleoclimate. Moreover, modelling studies are currently conducted to test the sensitivity of SE-European climate to elevation changes of surrounding mountain ranges.

6 Contributions to the manuscripts

This cumulative dissertation includes 7 studies. My contributions comprise the preparation of 6 manuscripts as first author including the scientific discussion of the results and preparation of all illustrations. I contributed as co-author in the scientific discussion of Study 7 and preparation of the manuscript. All micromorphological analyses, grain size analyses, diffuse reflectance spectroscopic measurements and n-alkane analyses were done in own work. Approximate contributions to each study are given as follow:

General

Sampling: B. Buggle (45%), B. Glaser, (45 %), I. Glaser (5%), Tivadar Gaudenyi und Mladjen Jovanović (5%).

Sample preparation (drying, milling): 50% (B. Buggle), 50% (Ana Malagodi).

Study 1

Sulfur-Analyses (Vario EL elemental analyzer): B. Buggle (70%, measurement, sample preparation), A. Malagodi (30 %, sample preparation).

Other major and trace elements (XRF-analysis): J. Eidam (100%).

Statistical analysis/discussion of the results: B. Buggle (100%).

Manuscript preparation: B. Buggle (100%).

Comments to improve the manuscript: B. Glaser (30%), U. Hambach (30%), L. Zöller (30%), M. Zech (7%), S. Marković (3%).

Study 2

Environmental magnetic analysis: (Agico KLY-3 Kappabridge): B. Buggle (80 %), U. Hambach (20%).

Discussion of the results: B. Buggle (70%), U. Hambach (20%), N. Gerasimenko (10%).

Manuscript preparation: B. Buggle (100%).

Comments to improve the manuscript: U. Hambach (60%), B. Glaser (30%), N. Gerasimenko (7%), S. Marković (3%).

Study 3

Determination of carbonate content (Vario El elemental analyzer): B. Buggle (70 %, sample preparation, measurement), A. Malagodi (30%, sample preparation).

Major and trace elements (XRF-analysis): see Study 1.

Discussion of the results: B. Buggle (100%).

Manuscript preparation: B. Buggle (100%).

Comments to improve the manuscript: U. Hambach (31%), B. Glaser (23%), N. Gerasimenko (23%), S. Marković (23%).

Study 4

Preparation of thin sections: Th. Beckmann (100 %).

Interpretation of micromorphological features: B. Buggle (75%), M. Kehl (25%).

Grain size analyses (sample preparation and measurement on Malvern Mastersizer S):

B. Buggle (100%).

Determination of total organic carbon (Vario El elemental analyzer): B. Buggle (70%, sample preparation, measurement), A. Malagodi (30 %, sample preparation).

Discussion of the results: B. Buggle (75%), U. Hambach (15%) M. Kehl (7%) N. Gerasimenko (1%), S. Marković (1%), L. Zöllner (1%).

Manuscript preparation: B. Buggle (100%).

Comments to improve the manuscript: U. Hambach (40%), M. Kehl (40%), B. Glaser (15%), S. Marković (5%).

Study 5

Determination of soil color proxies: B. Buggle (75%), A. Malagodi (25%).

Diffuse reflectance spectroscopy (AgriSpec spectrometer): B. Buggle (80% measurement, data analyses), K. Müller (20%, measurement).

Rock magnetic analysis: U. Hambach and co-workers (80%), B. Buggle (20%).

Discussion of the results: B. Buggle (70%), U. Hambach (27%), S. Marković (3%).

Manuscript preparation: B. Buggle (100%).

Comments to improve the manuscript: U. Hambach (45%), B. Glaser (30%), S. Marković (25%).

Study 6

n-Alkane analyses (sample preparation, GC-FID measurements): B. Buggle (100%).

Discussion of the results: B. Buggle (70%), G. Wiesenberg (15%), M. Zech (15%).

Manuscript preparation: B. Buggle (100%).

Comments to improve the manuscript: B. Glaser (50 %), G. Wiesenberg (50%).

Study 7

n-Alkane analyses (sample preparation, GC-FID measurements): B. Buggle (100 %).

Compound specific δD analysis: N. Pedentchouk (100 %).

Bulk δD analysis of leaf litter: Laboratory of Isotope Biogeochemistry, University of Bayreuth (Prof. Gebauer and co-workers) (100%).

Discussion of the results: M. Zech (32%), B. Buggle (28%), N. Pedentchouk (28%), B. Glaser (6%), K. Leiber (6%).

Manuscript preparation: M. Zech (100%).

Comments to improve the manuscript: B. Buggle (39%), N. Pedentchouk (39%), B. Glaser (7%), K. Leiber (7%), K. Kalbitz, (7%), S. Marković (1%).

References

- Antoine, P., Rousseau, D.-D., Fuchs, M., Hatté, C., Gauthier, C., Marković, S.B., Jovanovic, M., Gaudenyi, T., Moine, O., Rossignol, J., 2009. High-resolution record of the last climatic cycle in the southern Carpathian Basin (Surduk, Vojvodina, Serbia). 198, 19-36.
- Avramov, V.I., Jordanova, D., Hoffmann, V., Roesler, W., 2006. The role of dust source area and pedogenesis in three loess-paleosol sections from North Bulgaria: A mineral magnetic study. *Studia Geophysica et Geodaetica* 50 (2), 259-282.
- Bai, Y., Fang, X., Nie, J., Wang, Y., Wu, F., 2009. A preliminary reconstruction of the paleoecological and paleoclimatic history of the Chinese Loess Plateau from the application of biomarkers. *Palaeogeography, Palaeoclimatology, Palaeoecology* 271, 161-169.
- Banerjee, S.K., 1994. Contributions of fine-particle magnetism to reading the global paleoclimate record. *Journal of Applied Physics* 75 (10), 5925-5930.
- Bassiot, F.C., Labeyrie, L.D., Vincent, E., Quidelleur, X., Shackleton, N.J., Lancelot, Y., 1994. The astronomical theory of climate and the age of the Brunhes-Matuyama magnetic reversal. *Earth and Planetary Science Letters* 126, 91-108.
- Batista, M.J., Demetriades, A., Pirc, S., De Vos, W., Bidovec, M., Martins, L., 2006. Factor analysis interpretation of European soil, stream and floodplain sediment data. In: Tarvainen, T., De Vos, W. (Eds.), *Geochemical Atlas of Europe. Part 2. Interpretation of geochemical maps, additional tables, figures, maps, and related publications*. Geological Survey of Finland, Espoo, 567-618.
- Beckmann, T., 1997. Präparation bodenkundlicher Dünnschliffe für mikroskopische Untersuchungen. *Hohenheimer Bodenkundliche Hefte* 40, 89-103.
- Bokhorst, M.P., Vandenberghe, J., 2009. Validation of wiggle matching using a multi-proxy approach and its palaeoclimatic significance. *Journal of Quaternary Science* 24 (8), 937-947.
- Bokhorst, M.P., Beets, C.J., Marković, S.B., Gerasimenko, N.P., Matviishina, Z.N., Frechen, M., 2009. Pedo-chemical climate proxies in Late Pleistocene Serbian-Ukrainian loess sequences. *Quaternary International* 198, 113-123.
- Brady, P.V., Carroll, S.A., 1994. Direct effects of CO₂ and temperature on silicate weathering: Possible implications for climate control. *Geochimica et Cosmochimica Acta* 58 (8), 1853-1856.
- Bronger A., 1976. Zur quartären Klima – und Landschaftsentwicklung des Karpatenbeckens auf paläopedologischer und bodengeographischer Grundlage. *Kieler Geographische Schriften* 45.
- Bronger A., 2003. Correlation of loess-paleosol sequences in East and Central Asia with SE Central Europe - Towards a continental Quaternary pedostratigraphy and paleoclimatic history. *Quaternary International* 106-107, 11-31.
- Caseldine, C.J., Turney, C., Long, A.J., 2010. IPCC and palaeoclimate – an evolving story? *Journal of Quaternary Science* 25 (1), 1–4.
- Chen, J., Junfeng, J., Balsam, W., Chen, Y., Liu, L., An, Z., 2002. Characterization of the Chinese loess-paleosol stratigraphy by whiteness measurement. *Palaeogeography, Palaeoclimatology, Palaeoecology* 183, 287-297.
- Chen, T., Xu, H., Xie, Q., Chen, J., Ji, J., Lu, H., 2005. Characteristics and genesis of maghemite in Chinese loess and paleosols: Mechanism for magnetic susceptibility enhancement in paleosols. *Earth and Planetary Science Letters* 240, 790-802.
- Cornell R.M., Schwertmann U. 2003. *The iron oxides*. Wiley-VCH, Weinheim.
- de Beaulieu, J.-L., Andrieu-Ponel, V., Reille, M., Grüger, E., Tzedakis, C., Svobodova, H., 2001. An attempt at correlation between the Velay pollen sequence and the Middle

- Pleistocene stratigraphy from central Europe. *Quaternary Science Reviews* 20, 1593-1602.
- Deng, C., Shaw, J., Liu, Q., Pan, Y., Zhu, R., 2006. Mineral magnetic variation of the Jingbian loess/paleosol sequence in the northern Loess Plateau of China: Implications for Quaternary development of Asian aridification and cooling. *Earth and Planetary Science Letters* 241, 248-259.
- Derbyshire, E., Kemp, R.A., Meng, X., 1997. Climate change, loess and palaeosols: proxy measures and resolution in North China. *Journal of the Geological Society, London* 154, 793-805.
- Dodonov, A.E., Baiguzina, L.L., 1995. Loess stratigraphy of Central Asia: Palaeoclimatic and paleoenvironmental aspects. *Quaternary Science Reviews* 14, 707-720.
- Eissmann, L., 2002. Quaternary geology of eastern Germany (Saxony, Saxon-Anhalt, South Brandenburg, Thuringia), type area of the Elsterian and Saalian Stages in Europe. *Quaternary Science Reviews* 21, 1275-1346.
- Faegri, K., Iversen, J., 1989. Textbook of pollen analysis. Faegri, K., Kaland, P.E., Krzywinski, K., (Eds.), The Blackburn Press, Caldwell, USA.
- Fang, X., Lü, L., Mason, J.A., Yang, S., An, Z., Li, J., Zhilong, G., 2003. Pedogenic response to millennial summer monsoon enhancements on the Tibetan Plateau. *Quaternary International* 106-107, 79-88.
- Fedo C.M., Nesbitt H.W., Young G.M., 1995. Unraveling the effects of potassium metasomatism in sedimentary rocks and paleosols, with implications for paleoweathering conditions and provenance. *Geology* 23 (10), 921-924.
- Frey, W., Lösch, R., 1998. *Lehrbuch der Geobotanik*. Gustav Fischer, Stuttgart.
- Gallagher, K.J., Feitknecht, W., Mannweiler, U., 1968. Mechanism of oxidation of magnetite to γ - Fe_2O_3 . *Nature* 217, 1118-1121.
- Gallet, S., Jahn, B., Van Vliet Lanoë, B., Dia, A., Rossello E., 1998. Loess geochemistry and its implications for the particle origin and composition of the upper continental crust. *Earth and Planetary Science Letters* 156, 157-172.
- Gat, J.R., 1996. Oxygen and hydrogen isotopes in the hydrologic cycle. *Annual Review of Earth and Planetary Sciences* 24, 225 – 262.
- Geiss, C.E., Zanner, C.W., Banerjee, S.K., Joanna, M., 2004. Signature of magnetic enhancement in a loessic soil in Nebraska, United States of America. *Earth and Planetary Science Letters* 228, 355-367.
- Gerasimenko, N.P., 2004. Quaternary evolution of zonal paleoecosystems in Ukraine. Geophysical Institute of National Ukrainian Academy of Sciences, Kyiv, (in Ukrainian).
- Gerasimenko, N.P., 2006. Upper Pleistocene loess-paleosol and vegetational successions in the Middle Dnieper Area, Ukraine. *Quaternary International* 149, 55-66.
- Gerstberger P., Foken T., and Kalbitz K., 2004. The Lehstenbach and Steinkreuz catchments in NE Bavaria, Germany. In: Matzner, E. (Ed.), *Biogeochemistry of Forested Catchments in a Changing Environment: a German Case Study Ecological Studies* 172, Springer, Berlin.
- Harden J.W., 1982. A quantitative index of soil development from field descriptions: Examples from a chronosequence in central California. *Geoderma* 28, 1-28.
- Harnois L., 1988. The CIW index: A new chemical index of weathering. *Sedimentary Geology* 55, 319-322.
- Hatté, C., Antoine, P., Fontugne, M., Rousseau, D.-D., Tisnérat-Laborde, N., Zöller, L., 1999. New chronology and organic matter $\delta^{13}\text{C}$ paleoclimatic significance of Nußloch loess sequence (Rhine Valley, Germany). *Quaternary International* 62, 85-91.
- Hedges J.I., Stern J.H., 1984. Carbon and nitrogen determinations of carbonate-containing solids. *Limnology and Oceanography* 29 (3), 657-663.

-
- Heslop, D., Langereis, C.G., Dekkers, M.J., 2000. A new astronomical timescale for the loess deposits of Northern China. *Earth and Planetary Science Letters* 184, 125-139.
- Huang, Y., Bol, R., Harkness, D.D., Ineson, P., Eglinton, G., 1996. Post-glacial variations in distributions, ¹³C and ¹⁴C contents of aliphatic hydrocarbons and bulk organic matter in three types of British acid upland soils. *Org. Geochem.* 24, 273-287.
- IPCC, 2007. *Climate Change 2007: The physical science basis. Contribution of working group I to the Fourth Assessment Report of the Intergovernmental Panel on Climate Change.* Solomon, S., Qin, D., Manning, M., Chen, Z., Marquis, M., Averyt, K.B., Tignor, M., Miller, H.L., (Eds.), Cambridge University Press : Cambridge UK.
- Jahn, B., Gallet, S., Han, J., 2001. Geochemistry of the Xining, Xifeng and Jixian sections, loess plateau of China: eolian dust provenance and paleosol evolution during the last 140 ka. *Chemical Geology* 178, 71-94.
- Jordanova, D., Petersen, N., 1999. Palaeoclimatic record from a loess-soil profile in northeastern Bulgaria – II. Correlation with global climatic events during the Pleistocene. *Geophysical Journal International* 138, 533-540.
- Jordanova, D., Hus, J., Geeraerts, R., 2007. Palaeoclimatic implications of the magnetic record from loess/palaeosol sequence Viatovo (NE Bulgaria). *Geophysical Journal International* 171, 1036-1047.
- Kalbitz K., Kaiser K., Bargholz J., Dardenne P., 2006. Lignin degradation controls the production of dissolved organic matter in decomposing foliar litter. *European Journal of Soil Science* 57, 504-516.
- Kalm, V.E., Rutter, N.W., Rokosh, C.D., 1996. Clay minerals and their paleoenvironmental interpretation in the Baoji loess section, Southern Loess Plateau, China. *Catena* 27, 49-61.
- Kemp, R.A., 1999. Micromorphology of loess-paleosol sequences: a record of paleoenvironmental change. *Catena* 35, 179-196.
- Konert, M., Vandenberghe, J., 1997. Comparison of laser grain size analysis with pipette and sieve analysis: a solution for the underestimation of the clay fraction. *Sedimentology* 44, 523-535.
- Kostić N., Protić N., 2000. Pedology and mineralogy of loess profiles at Kapela-Batajnica and Stalać, Serbia. *Catena* 41, 217-227.
- Kronberg B.I., Nesbitt H.W., 1981. Quantification of weathering, soil geochemistry and soil fertility. *Journal of Soil Science* 32, 453-459.
- Liu, W., Huang, Y., 2005. Compound specific D/H ratios and molecular distributions of higher plant leaf waxes as novel paleoenvironmental indicators in the Chinese Loess Plateau 36, 851-860.
- Liu, Q., Deng, C., Torrent, J., Zhu, R., 2007. Review of recent developments in mineral magnetism of the Chinese loess. *Quaternary Science Reviews* 26, 368-385.
- Lis, J., Pasieczna, A., 2006. Geochemical characteristics of soil and stream sediment in the area of glacial deposits in Europe. In: Tarvainen, T., De Vos, W. (Eds.), *Geochemical Atlas of Europe. Part 2. Interpretation of geochemical maps, additional tables, figures, maps, and related publications.* Geological Survey of Finland, Espoo, 519-540.
- Lu, H.-Y., Wu, N.-Q., Liu, K.-B., Jiang, H., Liu, T.-S., 2007. Phytoliths as quantitative indicators for the reconstruction of past environmental conditions in China II: palaeoenvironmental reconstruction in the Loess Plateau. *Quaternary Science Reviews* 26, 759-772.
- Maffei, M., 1996. Chemotaxonomic significance of leaf wax alkanes in the gramineae. *Biochemical Systematics and Ecology* 24 (1), 53-64.
- Maher, B.A., 1986. Characterisation of soils by mineral magnetic measurements. *Physics of the Earth and Planetary Interiors* 42, 76-92.

-
- Maher, B.A., Thompson, R., 1995. Paleorainfall reconstructions from pedogenic magnetic susceptibility variations in the Chinese loess and paleosols. *Quaternary Research* 44, 383-391.
- Maher, B.A., Thompson, R., Zhou, L.P., 1994. Spatial and temporal reconstructions of changes in the Asian palaeomonsoon: A new mineral magnetic approach. *Earth and Planetary Science Letters* 1235, 461-471.
- Marković, S.B., Kostic, K.S., Oches, E.A., 2004. Paleosols in the Ruma loess section (Vojvodina, Serbia). *Revista Mexicana de Ciencias Geológicas* 21(1), 79-87.
- Marković, S.B., Oches, E., Sümegi, P., Jovanović, M., Gaudenyi, T., 2006. An introduction to the Middle and Upper Pleistocene loess-paleosol sequence at Ruma brickyard, Vojvodina, Serbia. *Quaternary International* 149, 80-86.
- Marković S.B., Hambach U., Catto N., Jovanović M., Buggle B., Machalet B., Zöller L., Glaser B., Frechen M., 2009. Middle and Late Pleistocene loess sequences at Batajnica, Vojvodina, Serbia. *Quaternary International* 198, 255-266.
- Mestdagh, H., Haesaerts, P., Dodonov, A., Hus, J., 1999. Pedosedimentary and climatic reconstruction of the last interglacial and early glacial loess-paleosol sequence in South Tadjikistan. *Catena* 35, 197-218.
- McLennan, S.M., 1993. Weathering and global denudation. *The Journal of Geology* 101, 295-303.
- Nesbitt H.W., Young G.M., 1982. Early Proterozoic climates and plate motions inferred from major element chemistry of lutites. *Nature* 299, 715-717.
- Nesbitt H.W., Young G.M., 1984. Prediction of some weathering trends of plutonic and volcanic rocks based on thermodynamic and kinetic considerations. *Geochimica et Cosmochimica Acta* 48, 1523-1534.
- Osterrieth, M., Madella, M., Zurro, D., Alvarez, M.F., 2009. Taphonomical aspects of silica phytoliths in the loess sediments of the Argentinean Pampas. *Quaternary International* 193, 70 – 79.
- Panaiotu, C. G., Panaiotu, E. C., Grama, A., Necula, C., 2001. Paleoclimatic record from a loess-paleosol profile in Southeastern Romania. *Physics and Chemistry of the Earth (A)* 26, 893-898.
- Perederij, V.I., 2001. Clay mineral composition and palaeoclimatic interpretation of the Pleistocene deposits of the Ukraine. *Quaternary International* 76/77, 113-121.
- Reille, M., de Beaulieu, J.-L., Svobodova, H., Andrieu-Ponel, V., Goeur, C., 2000. Pollen analytical biostratigraphy of the last five climatic cycles from a long continental sequence from the Velay region (Massif Central, France). *Journal of Quaternary Science* 15 (7), 665-685.
- Ronov, A.B., Yaroshevskiy, A.A., 1976. A new model for the chemical structure of the earth's crust. *Geochemical International* 13, 89-120.
- Rousseau, D.-D., Gerasimenko, N., Matviischina, Z., Kukla, G., 2001. Late Pleistocene environments of the Central Ukraine. *Quaternary Research* 56, 349-356.
- Rumpel, C., Seraphin, A., Goebel, M.-O., Wiesenberg, G., Gonzales-Vila, F., Bachmann, J., Schwark, L., Michaelis, W., Mariotti, A., Kögel-Knabner, I., 2004. Alkyl C and hydrophobicity in B and C horizons of an acid forest soil. *J. Plant Nutr. Soil Sci.* 167, 685-693.
- Sachse, D., Radke, J., Gleixner, G., 2006. δD values of individual n-alkanes from terrestrial plants along a climatic gradient – Implications for the sedimentary biomarker record. *Organic Geochemistry* 37, 469-483.
- Salminen, R., Batista, M. J., Bidovec, M., Demetriades, A., De Vivo, B., De Vos, W., Duris, M., Gilucis, A., Gregorauskiene, V., Halamic, J., Heitzmann, P., Lima, A., Jordan, G., Klaver, G., Klein, P., Lis, J., Locutura, J., Marsina, K., Mazreku, A., O'Connor, P. J., Olsson, S.Å., Ottesen, R.-T., Petersell, V., Plant, J.A., Reeder, S., Salpeteur, I.,

-
- Sandström, H., Siewers, U., Steenfelt, A., Tarvainen, T., 2005. Geochemical Atlas of Europe. Part 1: Background Information, Methodology and Maps. Geological Survey of Finland, Espoo. (<http://www.gtk.fi/publ/foregsatlas>), downloaded at 24.02.2007.
- Schellenberger A., Veit H., 2006. Pedostratigraphy and pedological and geochemical characterization of Las Carreras loess-paleosol sequence, Valle de Tafi, NW-Argentina. *Quaternary Science Reviews* 25, 811-831.
- Shackleton, N.J., Berger, A., Peltier, W.R., 1990. An alternative astronomical calibration of the lower Pleistocene timescale based on ODP Site 677. *Transactions of the Royal Society of Edinburgh: Earth Sciences* 81, 251-261.
- Smalley I., Leach J.A., 1978. The origin and distribution of the loess in the Danube Basin and associated regions of East-Central Europe- A review. *Sedimentary Geology* 21, 1-26.
- Stoops, G., 2003. Guidelines for analysis and description of soil and regolith thin sections. Soil Science Society of America, Madison, USA.
- Sträßler, M., 1998. Klimadiagramme zur Köppenschen Klimaklassifikation. Klett-Perthes, Gotha.
- Sun, Y., Lu, H., An, Z., 2006. Grain size of loess, palaeosol and Red Clay deposits on the Chinese Loess Plateau: Significance for understanding pedogenic alteration and palaeomonsoon evolution. *Palaeogeography, Palaeoclimatology, Palaeoecology* 241, 129-138.
- Tang, Y., Jia, J., Xie, X., 2003. Records of magnetic properties in Quaternary loess and its paleoclimatic significance: a brief review. *Quaternary International* 108, 33-50.
- Thompson, R., Oldfield, F., 1986. *Environmental Magnetism*. Allen & Unwin Ltd., London.
- Torrent, J., Barrón, V. 1993. Laboratory measurement of soil color: theory and practice. In: Bigham, J.M., Ciolkosz, E.J., Luxmoore, R.J., (Eds.), *Soil Science Society of America Special Publications*. 31, 21-34.
- Torrent, J., Schwertmann, U., Schulze, D.G., 1980. Iron oxide mineralogy of some soils of two river terrace sequences in Spain. *Geoderma* 23, 191-208.
- Torrent, J., Liu, Q., Bloemendal, J., Barrón, V., 2007. Magnetic enhancement and iron oxides in the upper Luochuan loess-paleosol sequence, Chinese Loess Plateau. *Soil Science Society of America Journal* 71, 1570-1578.
- Tsatskin, A., Heller, F., Hailwood, E.A., Gendler, T.S., Hus, J., Montgomery, P., Sartori, M., Virina, E.I., 1998. Pedosedimentary division, rock magnetism and chronology of the loess/paleosol sequence at Roxolany (Ukraine). *Palaeogeography, Palaeoclimatology, Palaeoecology* 143, 111-133.
- Tsatskin, A., Heller, F., Gendler, T.S., Virina, E.I., Spassov, S., Du Pasquier, J., Hus, J., Hailwood, E.A., Bagin, V.I., Faustov, S.S., 2001. A new scheme of terrestrial paleoclimate evolution during the last 1.5 Ma in the Western Black Sea Region: Integration of soil studies and loess magnetism. *Physics and Chemistry of the Earth (A)* 26 (11-12), 911-916.
- Tzedakis, P.C., Bennett, K.D., 1995. Interglacial vegetation succession: A view from southern Europe. *Quaternary Science Reviews* 14, 967-982.
- Tzedakis, P.C, Hooghiemstra, H., Pälike, H., 2006. The last 1.35 million years at Tenaghi Philippon: revised chronostratigraphy and long-term vegetation trends. *Quaternary Science Reviews* 25, 3416-3430.
- Vandenbergh, J., Huijzer, B.S., Múcher, H., Laan, W., 1998. Short climatic oscillations in a western European loess sequence (Kesselt, Belgium). *Journal of Quaternary Science* 13 (5), 471-485.
- Vandenbergh, J., Lu, H., Sun, D., van Huissteden, J., Konert, M., 2004. The late Miocene and Pliocene climate in East Asia as recorded by grain size and magnetic susceptibility of the Red Clay deposits (Chinese Loess Plateau). *Palaeogeography, Palaeoclimatology, Palaeoecology*.

-
- Van Velzen, A.J., Dekkers, M.J., 1999. Low-temperature oxidation of magnetite in loess-paleosol sequences: A correction of rock magnetic parameters. *Studia Geophysica et Geodaetica* 43, 357-375.
- Vidic N.J., Singer M.J., Verosub K.L., 2004. Duration dependence of magnetic susceptibility enhancement in the Chinese loess-palaeosols of the past 620 ky. *Palaeogeography, Palaeoclimatology, Palaeoecology* 211, 271-288.
- Walter, H., 1974. *Die Vegetation Osteuropas, Nord- und Zentralasien*. Gustav Fischer Verlag, Stuttgart.
- Wang, X., Lu, H., Xu, H., Deng, C., Cheng, T., Wang, X., 2006. Magnetic properties of loess deposits on the northeastern Qinghai-Tibetan Plateau: palaeoclimatic implications for the Late Pleistocene. *Geophysical Journal International* 167, 1138-1147.
- White, A.F., Blum, A.E., 1995. Effects of climate on chemical weathering in watersheds. *Geochimica et Cosmochimica Acta* 59 (9), 1729-1747.
- WMO, World Meteorological Organization, 1996. *Climatological normals (CLINO) for the period 1961 - 1990*. Secretariat of the World Meteorological Organization, Geneva.
- Wu, F., Fang, X., Ma, Y., Herrmann, M., Mosbrugger, V., An, Z., Miao, Y., 2007. Plio – Quaternary stepwise drying of the Asia: Evidence from a 3-Ma pollen record from the Chinese Loess Plateau. *Earth and Planetary Science Letters* 257 160-169.
- Xie, S., Wang, Z., Wang, H., Chen, F., An, C., 2002. The occurrence of a grassy vegetation over the Chinese Loess Plateau since the last interglacial: the molecular fossil record. *Science in China Series D*, 45 (1), 53-62.
- Yaalon, D.H., 1997. Soils in the Mediterranean region: what makes them different? *Catena* 28, 157-159.
- Zech, M., Glaser, B., 2008. Improved compound-specific delta C-13 analysis of n-alkanes for application in palaeoenvironmental studies. *Rapid Communication in Mass Spectrometry* 22 (2), 125-142.
- Zech, M., Zech, R., Morrás, H., Moretti, L., Glaser, B., Zech, W., 2009. Late Quaternary environmental changes in Misiones, subtropical NE Argentina, deduced from multi-proxy geochemical analyses in a palaeosol-sediment sequence. *Quaternary International* 196, 121-136.
- Zech, M., Andreev, A., Zech, R., Müller, S., Hambach, U., Frechen, M., Zech, W., 2010. Quaternary vegetation changes derived from a loess-like permafrost palaeosol sequence in northeast Siberia using alkane biomarker and pollen analyses. *Boreas* 39, 540-550.
- Zhang, Z., Zhao, M., Eglinton, G., Lu, H., Huang, C.-Y., 2006. Leaf wax lipids as paleovegetational and paleoenvironmental proxies for the Chinese Loess Plateau over the last 170 ka. *Quaternary Science Reviews* 25, 575-594.
- Zhong, Y., Chen, F., An, C., Xie, S., Huang, X., 2007. Holocene vegetation cover in Qin'an area of western Chinese Loess Plateau revealed by n-alkane. *Chinese Science Bulletin* 52 (12), 1692-1698.

**Reconstruction of the Mid- and Late Pleistocene climate and
landscape history in SE-Central Europe.**

**A paleopedological and geochemical multi-proxy approach in loess-paleosol
studies.**

**(Rekonstruktion der Mittel – und Spätpleistozänen Klima und Landschaftsgeschichte in
SO-Mitteleuropa**

Untersuchung von Löss-Paläobodensequenzen mittels eines paleopedologischen und
geochemischen Multiproxy - Ansatzes

A cumulative study

Study 1

Geochemical characterization and origin of Southeastern and Eastern European loesses (Serbia, Romania, Ukraine)

Björn Buggle^{1*}, Bruno Glaser¹, Ludwig Zöller², Ulrich Hambach², Slobodan Marković³, Irina Glaser² and Natalia Gerasimenko⁴

¹ Soil Physics Department, University of Bayreuth, D-95440 Bayreuth, Germany.

² Chair of Geomorphology, University of Bayreuth, D-95440 Bayreuth, Germany.

³Chair of Physical Geography, Faculty of Sciences, University of Novi Sad, Trg Dositeja Obradovića 3, 21000 Novi Sad, Serbia.

⁴Earth Science and Geomorphology Department, Tarasa Shevchenko National University of Kyiv, Ukraine.

Published in

Quaternary Science Reviews 28 (9-10), 1058-1075.

2008

*Corresponding author: Björn Buggle, Phone:+49(0)921-552174

E-mail:URSBB@gmx.de

Abstract

The loess/paleosol sections of Batajnica/Stari Slankamen (Serbia), Mircea Voda (Romania) and Stary Kaydaky (Ukraine) were geochemically characterized based on discriminant analysis of major and trace elements, the ratios of Al/Ti, Fe/Ti and Al/Fe, the A-CN-K ternary plot and element enrichment/depletion relative to the average composition of the upper continental crust. The origin of the loess material in the southern Pannonian Basin (Vojvodina), the lower Danube Basin/Dobrudja and the Dnieper area was evaluated by comparison with the representative element composition of possible source areas and by considering the geomorphodynamic setting. Also the background values of initial magnetic susceptibility of the loesses were taken into account. For the lower Danube Basin, Dobrudja and the Ukraine, paleowind direction was reconstructed based on the geographic distribution of sandy soil texture and dunes related to river systems. Finally, loesses were evaluated as possible samples of the average upper continental crust. Our results show that Danube and Dnieper loess areas can be clearly distinguished. The former reveal higher Al and Fe contents, the latter higher Si, Zr, Hf content and indications of effective mineral and grain size sorting. We can confirm that Vojvodina loess originated from Danube alluvial material and loess of the Dnieper area from glaciofluvial sediments of the Fennoscandinavian ice sheet. The Dobrudja loess derived also predominantly from Danube alluvium, but shows significant contribution of a second loess source, probably the glaciofluvial sediments of the Ukraine. This was forced by northerly katabatic winds from the Fennoscandinavian ice sheet, whereas WNW winds prevailed in the Western Walachian plain. The studied loesses reflect the average composition of the upper continental crust. Yet, biases exist due to selective mineral/element enrichment and depletion in the course of previous sedimentary recycling phases, respectively. Material of all studied loess deposits seems to derive originally from sedimentary rocks.

Keywords: Loess, origin, geochemistry, upper continental crust, Danube, Dnieper, Serbia, Romania, Ukraine.

1 Introduction

“Loess is not just the accumulation of dust” (Pécsi, 1990). This phrasal originally referred to the diagenetic processes involved in the transformation of dust into loess. Beyond this, we like to reformulate it to “Loess is not just accumulated dust” emphasizing the multiple importance of loess for geosciences. First and foremost to mention is the relevance of loess deposits with intercalated paleosols, so-called loess–paleosol sequences, as potential climate archives (e.g. Kukla, 1977; Catt, 1991; Derbyshire et al., 1997). Furthermore, distribution and origin of loess can give important information about paleowind direction (Pye, 1995; Muhs and Budahn, 2006). Even paleowind strength can be reconstructed by grain size distribution (Xiao et al., 1995). Loess is also considered as an average sample of wide areas of the earth’s surface and thus may be suitable for reconstructing the element composition of the upper continental crust (Taylor and McLennan, 1985). However, the origin of loess is seen as important for understanding the mechanisms connected with the forenamed multiple archive functions of this sediment in a region (Pye, 1995). During the last 15 years, geochemically based provenance studies gained increasing attendance (e.g. Muhs et al., 1990; Schnetger, 1992; Jahn et al., 2001; Muhs and Benedict, 2006). Element fingerprints proved to be a powerful tool in evaluating the contributions of different dust source areas, even in a (semi)-quantitative way (Muhs and Budahn, 2006). Meanwhile, many loess regions of the world are geochemically well characterized (e.g. Taylor, et al., 1983; Schnetger, 1992; Gallet et al., 1996, 1998; Muhs et al., 2001; Smykatz-Kloss, 2003; Muhs and Budahn, 2006). However, this is not the case for the Vojvodina loess in the southern Pannonian Basin, the Romanian loess in the lower Danube Basin and at the Dobrudja loess plateau and the loess of the Dnieper area, though loess deposits of these areas represent extensive, several decameters thick and far back reaching sediments of the Quaternary in Europe (Bronger, 1976, 2003; Marković et al., 2003, 2006, 2007, 2008; Fuchs, et al., 2008; Buggle et al, 2009). Even the

most profound study on the origin of these loesses, given by Smalley and Leach (1978), is based mainly on a review of the geomorphodynamic system of the region. We therefore see the need for a basic geochemical characterization of these European loesses with respect to provenance. Therefore, the objectives of this study are

- 1) To establish a geochemical discrimination and characterization of loess deposits in the southern Pannonian Basin (Vojvodina, Serbia), in the lower Danube Basin/Dobrudja (Romania) and in the Dnieper area. Possible source areas will be evaluated using a promising combination of a geochemical and geomorphodynamic approach. Since the loesses of the Vojvodina and the lower Danube Basin/Dobrudja should originate predominantly from Danube alluvium (Smalley and Leach, 1978), we expect these two areas to have a similar geochemical composition. Due to the proximity of the glaciofluvial deposits of the Fennoscandinavian ice-sheet, representing a likely dust source, the loess of the Dnieper area should show a distinctly different element fingerprint. These hypotheses will be tested.
- 2) To check whether Taylor and McLennan's (1985) proposal that loess deposits should provide information about the average element composition of the upper continental crust, is also valid for the Danube and Dnieper loess areas.

2 Regional setting

The Quaternary landscape evolution of the Pannonian (i.e. middle Danube) basin and lower Danube basin (including the Walachian Plain), and the adjacent Dobrudja Plateau, respectively, was strongly controlled by tectonic processes as well as by the geomorphodynamic response to the paleoclimatic settings. Basin inversion with NW–SE and N–S compression was the dominant endogenic triggering mechanism, causing uplift of the mountains at the basin margin and areas of uplift as well as accelerated subsidence in the interior basin (Nádor et al., 2003; Gábris and Nádor, 2007; Ruszkiczay-Rüdiger 2007). In

these subsiding areas thick sequences of fluvial sediments transported by the Danube and Tisza River accumulated. During cold periods of the Quaternary these rivers behaved as braided river systems, which changed several times their position within the Great Hungarian Plain due to tectonic activity. However, the Danube river channel remained relatively stable in the southern Serbian part of the Pannonian basin (south of the present day Danube-Tisza interflow; Gábris and Nádor, 2007; Ruszkiczay-Rüdiger, 2007). This is also true for the lower Danube basin upstream of Cernavoda City. Near to this location, the Karasu valley crosses the Dobrudja plateau – an upheaval zone between the Walachian Plain and the Black Sea coast. This valley is regarded as an ancient channel of the Danube reaching the Black Sea near Constanta (Pfannenstiel, 1950). Up to now it is neither clear, when the Danube used this channel, nor if the Danube bifurcated at Cernavoda so that a river channel followed the Dobrudja – Walachian Plain line further northwards to form a second mouth into the Black Sea in the area of the present day Danube delta (Pfannenstiel, 1950).

Glacial melt waters are an important hydrographic factor controlling the sediment transport and the general sedimentary architecture of fluvial systems (e.g. Vandenberghe, 1995; Vandenberghe and Woo, 2002) During cold periods of the Quaternary, glaciers within the Danube catchment area were extensively developed in the Alps and alpine foreland. In the Carpathians, however, they developed only in the highest mountain ranges (Reuther et al., 2007; Ruszkiczay-Rüdiger, 2007) and probably more widespread in the Late Pleistocene, considering the recent high surface uplift rates (Reuther et al., 2007). Through the Moravian depression, there was some additional temporary input of glacial melt water, deriving from the Fennoscandinavian ice sheet during the southernmost extension of the Saalian and eventually also Elsterian glaciation (Smalley and Leach; 1978; Macoun and Králík, 1995; Tyráček, 2006). Extensive loess sheets and loess plateaus of several meters thickness accumulated in the Pannonian Basin, especially in its southern part, and in the lower Danube basin/Dobrudja (Smalley and Leach, 1978; Haase, et al., 2007; Marković et al., 2008). These

loesses are intercalated with paleosols, formed during interglacial and interstadial periods, and reflect the Quaternary climate evolution of the region (e.g. Bronger 1976; Marković et al., 2008).

In the Ukraine, the channel of the middle and lower Dnieper river was already established in the Neogene by incision into the rocks of the East European platform. Hence, its position did not change substantially during the Quaternary (Matoshko, 2002). Since the early Pleistocene, the area of the middle and upper Dnieper valley in the Ukraine and neighboring Belarus was several times covered by the Fennoscandinavian ice-sheet, which modulated the land surface by erosional and depositional processes (e.g. Chugunny and Matoshko, 1995; Gozhik, 1995; Matoshko, 1995a, b). The southernmost advance of the ice sheet into Ukraine occurred during the Dnieper (i.e. Saalian) glaciation, approaching the Stary Kaydaky site up to about 50 km (Fig. 1-1). During cold periods of the Quaternary, an extensive and several meters thick loess cover formed in the Ukraine south of about 50 °N. in the western part and south of the Desna river in the eastern part, respectively. The Ukrainian loess is connected with the lower Danube basin loess in the Southeast and with the loess cover in the Russian part of the East European platform (Haase et al., 2007). The loess–paleosol sequences of the Ukraine represent a valuable archive for the environmental evolution during the Quaternary (Veklich, 1982; Sirenko and Turlo, 1986; Velichko, 1990; Gerasimenko, 2004; Lindner et al., 2004; Bolikhovskaya and Molodkov, 2006)

The today's climate of the study areas, is characterized by increasing aridity towards the Black Sea coast. Depending on the dryness and drought periods, different kinds of steppe vegetation have developed (Buggle et al., 2009).

As representative sections for the loess regions of Vojvodina (part of the Pannonian and middle Danube Basin, respectively), the lower Danube Basin/Dobrudja and the Dnieper area, we selected the Batajnica/Stari Slankamen site (Serbia), the Mircea Voda site (Romania) and the Stary Kaydaky site (Ukraine, Fig. 1-1).

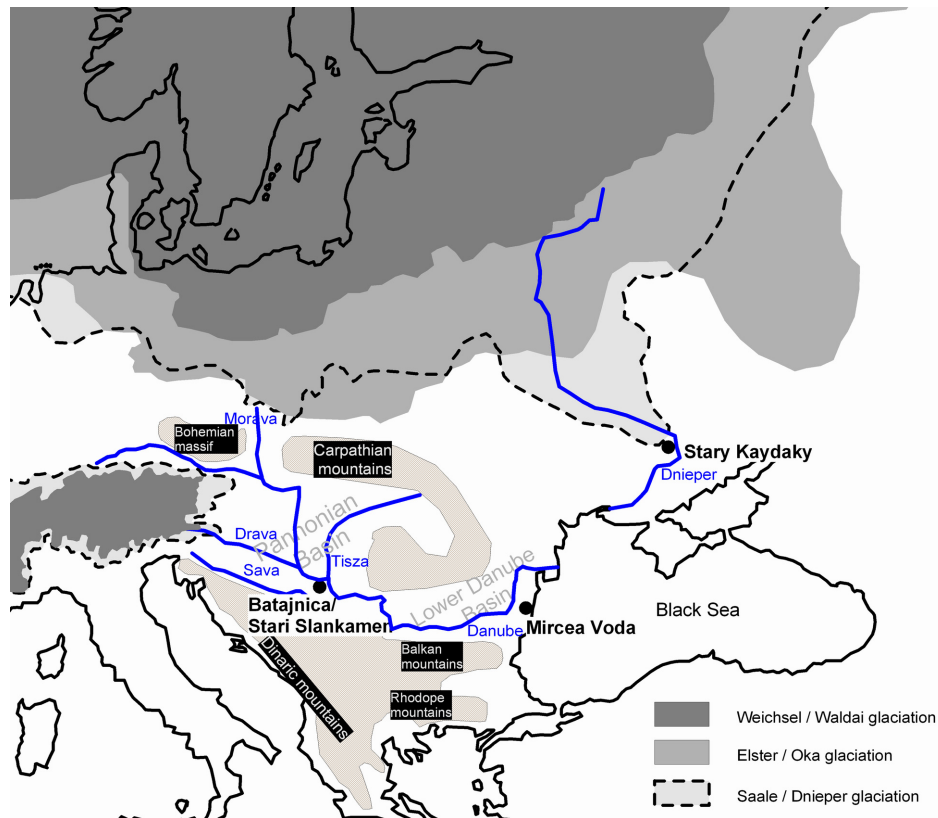


Fig. 1-1. Location of the studied loess-paleosol sequences in a schematic map. Limits of the continental ice sheet were taken from Eissmann (2002).

The two Serbian loess-paleosol sections Stari Slankamen ($45^{\circ} 7' 58''$ N, $20^{\circ} 18' 44''$ E) and Batajnica ($44^{\circ} 55' 29''$ N, $20^{\circ} 19' 11''$ E, Fig. 1-1) are located in about 30 km distance to each other at the right bank of the Danube River between Belgrade in the south and the Danube-Tisza confluence in the north. Both sections are situated in the Vojvodina province (Serbia) – the southeastern part of the Pannonian (Carpathian) Basin. Eight interglacial pedocomplexes were identified in the stacked record of Batajnica/Stari Slankamen, reflecting more than 800,000 years of Quaternary climate variability (Kostić and Protić, 2000; Marković et al., 2003; Buggle et al., 2009). Six loess-paleosol cycles were sampled in the present study. The studied Romanian section at Mircea Voda ($44^{\circ} 19' 15''$ N, $28^{\circ} 11' 21''$ E, Fig. 1-1) is situated on the Dobrudja plateau, at about 13 km distance to the Danube, 40 km distance to

the Black Sea coast and about 2 km north of the Karasu valley. This loess-paleosol sequence comprises probably more than 17 Marine Isotope Stages (MIS) (Bugge et al., 2009).

The outcrops of the Stary Kaydaky section (48° 22' 42'' N, 35° 07' 30'' E, Ukraine) can be found in a system of gullies near the Dnieper River and about 2 km south of Dniepropetrovsk City. According to the stratigraphic frame of Bugge et al. (2009), the section includes pedocomplexes reaching back to MIS 13–15.

3 Methods

3.1 Sampling and laboratory analyses

Before sampling, the first decimeters of material were removed from the front face of the sampling site and the section was cleaned carefully. Then, depending on the horizontation and thickness, each pedocomplex was sampled in 10 – 50 cm intervals by at least 10 samples for the pedocomplexes younger than MIS 11. As our further paleopedological investigations will be mainly focused on this younger part, older pedocomplexes were sampled with lower spatial resolution by at least three representative samples. For each intercalated loess layer about three representative samples were collected, since these are more uniform both macroscopically and according to magnetic susceptibility (Bugge et al., 2009). At the Serbian sections, the units supposed to be younger than MIS 10 were sampled from the Batajnica site. In order to avoid the obvious overprint caused by water logging, we switched for sampling of the older units to the Stari Slankamen site. Therefore, our loess - paleosol sample set of the Serbian section is a composite of the units younger than MIS 10 derived from Batajnica and the older ones from Stari Slankamen. Altogether 64, 73 and 68 samples from the Batajnica/Stari Slankamen section, Mircea Voda section and Stary Kaydaky section, respectively, were collected and stored in air-tight plastic bags. In the following, the whole set of samples i.e. soil and loess samples of the sections, are regarded as “bulk samples”. Those

samples, which did not show indications of pedogenic alteration macroscopically as well as by magnetic susceptibility, are regarded as “pure loess” samples. Thus, 13, 21 and 4 samples were taken as representative for “pure loess” of the Serbian, Romanian and Ukrainian section, respectively. The low number of such samples for Sary Kaydaky is caused by the occurrence of several hiatus as well as an initial soil development in some loess units. Since the Chinese Loess-Paleosol sequences represent potential stratotype sections of the Quaternary (Kukla and An, 1989), also the nomenclature of the lithological units in the presently studied sections follows the Chinese system using “S” for paleosols/pedocomplexes, and “L” for loess layers. Numbers indicate the respective correlatives of the units in the Chinese stratigraphic framework, as derived from pedostratigraphy and fingerprint matching of the magnetic susceptibility record by Buggle et al (2009). The main stratigraphic units with the location of the samples are also presented in the Appendix (Fig. 1-S1, Fig. 1-S2, Fig. 1-S3).

For geochemical analyses, the whole sample material i.e. about 400 g/sample was dried at 40 °C in the laboratory and then finely ground. For each sample, a 2 ccm Eppendorf cup was filled with an aliquot of material and sent for X-ray fluorescence (XRF) analyses to J. Eidam (University of Greifswald, Germany), who provided the element composition using a Philips 2404 XRF Spectrometer. Only sulfur content was determined separately by thermal conductivity detection on a Vario EL element analyzer (Elementar, Hanau, Germany) at the University of Bayreuth, using aliquots of 20 mg.

3.2 Data processing

The geochemical data were corrected for secondary dilution effects by the minerals calcite (CaCO_3), dolomite (MgCO_3) and gypsum ($\text{CaSO}_4 \times 2\text{H}_2\text{O}$) as follows.

$$[X]_{(corrected)} = [X]_{(measured)} * \left(\frac{100}{100 - \%CaCO_3 - \%MgCO_3 - \%CaSO_4 * 2H_2O} \right) \quad 1$$

where [X] is the: element content in % or ppm.

Except for CaO, MgO and S, only the corrected data were used for further calculations and element indices. The contents of gypsum, dolomite and calcite were calculated as follows:

$$\%CaSO_4 * 2H_2O = \frac{\%S}{M_{(S)}} * M_{(CaSO_4 * 2H_2O)} \quad 2$$

$$\%MgCO_3 = \frac{\%MgO}{M_{(MgO)}} * M_{(MgCO_3)} \quad 3$$

$$\%CaCO_3 = \left(\frac{\%CaO}{M_{(CaO)}} - 1 * \frac{\%S}{M_{(S)}} - \frac{5 * 2}{3} * \frac{\%P_2O_5}{M_{(P_2O_5)}} \right) * M_{(CaCO_3)} \quad 4$$

where $M_{(X)}$ is the molar mass of compound X.

Calcite–Ca contents were corrected for Ca in gypsum and apatite ($Ca_5(PO_4)_3(F,Cl,OH)$) (Eq. 4). Samples, which derived from the upper 40 cm below the top of the profiles, were not included in the further data exploration in order to avoid artifacts of anthropogenic pollution.

3.2.1 Discriminant analysis

All statistical analyses were conducted using Statistica 6 software package (Statsoft Inc., 2001). To investigate differences and similarities in element composition of the sections Batajnica/Stari Slankamen, Mircea Voda and Stary Kaydaky, we first conducted a discriminant analyses for the bulk samples. Discriminant analyses require normally distributed data. Since trace elements in geologic systems are often distributed logarithmically (Batista et al., 2006), we tested natural as well as log-transformed data for normal distribution by using the Shapiro-Wilks W test (Statsoft Inc., 2001). Finally, for each element either

natural or log-transformed data, depending on optimum satisfaction of normality distribution, were compiled in a worksheet and used for further calculation. In order to include as many samples as possible for the discriminant analysis, elements with missing data due to the detection limit, were excluded (Co, Hf, La, Nd, Ni, Sc and U).

3.2.2 Element ratios

The comparison of absolute element contents of sediments can be biased by systematic enrichment or dilution effects due to variable amounts of carbonate minerals and quartz. On the contrary, element ratios and ternary diagrams were applied successfully in the geochemical characterization of sediments and in studies concerning their provenance, respectively (e.g. Gallet et al., 1998; Kutterolf, 2001; Muhs and Budahn, 2006).

For discrimination of the loess sites with respect to the macroelement composition, we choose a $\text{Fe}_2\text{O}_3/\text{TiO}_2$ vs. $\text{Al}_2\text{O}_3/\text{TiO}_2$ plot and the $\text{Al}_2\text{O}_3-(\text{CaO}^* + \text{Na}_2\text{O})-\text{K}_2\text{O}$ ternary diagram, with CaO^* referring to CaO in silicate minerals. The $\text{Al}_2\text{O}_3/\text{TiO}_2$ ratio was proposed to reflect the clay content (Muhs et al., 2001) and the $\text{Fe}_2\text{O}_3/\text{TiO}_2$ ratio should indicate iron-enriched material and clay content variations, as well (Muhs, et al., 2001; Smykatz-Kloss, 2003). Due to the intermediate ionic potential of Ti^{4+} , Ti is a low mobility element during weathering processes. Thus, it is a suitable denominator in element ratios (Kabata-Pendias and Pendias, 2001; Kutterolf, 2001; Muhs et al., 1990). Also Fe and Al are hardly mobile in oxidizing environments and at pH values above 4.5, respectively. Hence, the ratio of these elements should not be significantly affected by selective element removal during weathering.

The $\text{Al}_2\text{O}_3-(\text{CaO}^* + \text{Na}_2\text{O})-\text{K}_2\text{O}$ diagram – also known as A–CN–K diagram – was introduced by Nesbitt and Young (1984) and successfully applied for the geochemical characterization of sediments and weathering profiles (e.g. Nesbitt and Young, 1989; Nesbitt et al., 1996). The advantage of this form of presentation is that it displays weathering and sorting effects on aluminosilicates. Also information with respect to the initial composition of

these elements can be provided (McLennan et al., 1993; Nesbitt et al., 1996). CaO* was obtained from measured CaO according to the procedure, described by McLennan (1993), which is based on the assumption that the molar CaO/Na₂O ratio of silicates is not higher than one. In the case of the molar CaO content (corrected for apatite) being less than the molar Na₂O content, this value was taken as CaO*. In the other case, the CaO content of silicates was assumed to be equivalent to the molar Na₂O content (McLennan, 1993). The A–CN–K diagram was plotted for “bulk samples” i.e. also including paleosol material.

Further geochemical fingerprinting also including trace elements was carried out by comparison of the enrichment/depletion of elements related to the average composition of the upper continental crust (UCC). To minimize weathering effects on high and medium mobility elements, only “pure loess” samples were used for the UCC normalized element plot.

3.3 Literature data

For the average composition of the UCC and of granite and basalt, we took the values given by the “map model” of Condie (1993). The position of various minerals, used for orientation purposes in the A–CN–K diagram, is in accordance to Nesbitt and Young (1989) and McLennan et al. (1993).

For evaluating the loess origin, representative geochemical datasets of source rocks were not available. Thus, we decided to compare the element composition of loess with that of floodplain sediments of the Danube catchment, an approach already successfully applied by Muhs and Budahn (2006) for Alaskan loesses. This appeared to be promising, since on the one hand floodplain sediments were proposed to be an important source of silt sized material for the Danube loess province and other loess areas associated to big rivers (Smalley and Leach, 1978; Smalley, 1995; Minkov, 1968; Evlogiev, 1993; The references Minkov (1968) and Evlogiev (1993) are cited in Jordanova and Petersen, 1999). On the other hand, samples of floodplain sediments should, unlike soil samples, represent a mean sample of the

catchment basin. Geochemical data of floodplain sediments were taken from the dataset of the Geochemical Atlas of Europe (Salminen et al., 2005). In this atlas, the European results of the “Global Geochemical Baseline Programme” are published. Since the European part of the program was under the auspices of the former Forum of European Geological Surveys (FOREGS), the data will be regarded as “FOREGS” data in the following. Floodplain samples of the “FOREGS” dataset represent the element composition of large catchment Basins (500 – 6000 km²). For further information on sampling, sample preparation and analyses, the reader is referred to Salminen et al. (2005). We selected floodplain samples of the “FOREGS”-dataset according to following procedure. First, samples of non-Danube tributaries were removed from the dataset. Then, several source areas were defined based on geographic and lithological aspects. The final sample set comprises only floodplain sediment data that are situated within these areas and/or are predominantly composed of material derived from these areas. In detail, we defined the following source areas.

- The “Austroalpine cover nappes area”. This area is characterized by sediments derived from the Austroalpine cover nappes. Selected samples comprise floodplain sediments of Danube tributaries located either in the area of the Austroalpine cover nappes or in the northern Alpine foreland, if the catchment Basin is dominated by glaciofluvial sediments. Floodplain sediments of the Inn River are not included, since the Inn also contributes material from crystalline central Alpine areas. The floodplain samples of the “Austroalpine cover nappes area” are regarded as “F-AA”.
- The “Drava source area”. This area is characterized by metamorphic rocks of the Austrian penninic nappes and crystalline rocks of the Austroalpine basement nappes. Selected sample sites are located in floodplain sediments of the Drava River and tributaries predominantly draining these areas. Floodplain sediments of the Gail River and tributaries, affected by calcareous sediments of the Southern Alpine sedimentary rocks are not included. Drava tributaries in Croatia and southern Hungary were taken

into account, if they are draining catchments dominated by loess sediments probably derived from Drava alluvium. Floodplain samples related to the “Drava source area” are regarded as “F-Drava”.

- The “Bohemian Massif area”. These samples comprise floodplain sediments of Danube tributaries (Regen River, Thaya River, Jihlava River) draining the crystalline and metamorphic rocks of the Bohemian Massif. The samples are regarded as “F-BM”.
- The “Western Carpathian area”. Here, we included floodplain sediments of Danube and Tisza tributaries, predominantly derived from the area of the Beskide Mountains, high Tatra Mountains, and Slovak Ore Mountains. This source is characterized by a high lithological diversity. Samples are regarded as “F-WC”. Unfortunately no data from the Romanian part of the Carpathians were available. However, according to the distribution of rock types, the floodplain samples deriving from the Western Carpathian Mountains are supposed to be geochemically representative for those of the East- and South-Carpathian Mountains.

A compilation of the selected FOREGS-samples is given in the Appendix (Table 1-S1).

For the Dnieper catchment, no representative floodplain data were available. Thus, we were constrained to the major element composition of the Ukrainian and Baltic shield (Ronov and Yaroshevskiy, 1976).

The geochemical compositions of other loess areas are shown for comparison. Data of the Kaiserstuhl area (Rhine Valley, Germany), of Kansas/Iowa and the Bank Peninsula (New Zealand) were taken from Taylor et al. (1983). For the composition of French and Chinese loess areas, the data of various sections given by Gallet et al. (1996), Gallet et al. (1998) and Jahn et al. (2001) were averaged. The average composition of worldwide loess derives from Schnetger (1992). Loess data were corrected for calcite and dolomite. Note that there might

be some bias of the literature data due to different analytical methods for trace elements determination.

Apart from direct geochemical data, we also compiled magnetic susceptibility data of the studied loess sections and adjacent sites. The magnetic susceptibility reflects mainly the content of the ferrimagnetic minerals magnetite and maghemite, and to a lesser extent the content of the antiferromagnetic minerals hematite and goethite (Thompson and Oldfield, 1986). Susceptibility enhancement is commonly interpreted as pedogenesis proxy (Heller and Liu, 1984), see also Buggle et al. (2009) for a basic review about the principles of magnetic susceptibility enhancement. Thus, the background magnetic susceptibility, defined by us as the minimum magnetic susceptibility of the “pure loess” units, should be a proxy for the content of the mentioned minerals in the loess and reflect initial weathering of the source material. Background susceptibilities for the sections Batajnica/Stari Slankamen, Mircea Voda and Stary Kaydaky (Buggle et al., 2009) and for other loess-paleosol profiles of the lower Danube Basin/Dobrudja and other loess areas near the Black Sea coast were taken from the literature (Tsatskin et al., 1998; Jordanova and Petersen, 1999; Nawrocki, et al., 1999; Panaiotu et al., 2001; Rousseau et al., 2001; Tsatskin et al., 2001; Avramov et al., 2005; Dodonov et al., 2006). To ensure the comparability of the data, we gathered profile background susceptibilities by reading off the lowest value of each magnetic susceptibility record. We estimate a standard error of $2.5 \cdot 10^{-8} \text{ m}^3 \text{ kg}^{-1}$ for the procedure.

4 Results

Major and trace element composition of the profiles are given in the Appendix (Fig. 1-S1-Fig. 1-S6). The data are corrected for calcite, dolomite and gypsum, except those of MgO, CaO, S, H₂O and the loss on ignition at 1000 °C (LOI). The magnetic susceptibility curve was redrawn from Buggle et al. (2009).

4.1 Discriminant analysis

The discriminant analysis reveals a clear separation of the three profiles by two discriminant functions. Both discriminant functions are statistically significant, according to the “ χ^2 -test of successive roots”, with $p < 0.01$ (level of significance) for roots 1 + 2 and root 2. Root 1 explains about 74 % of the observed variance (eigenvalue of 74.31) and root 2 about 4 % (eigenvalue of 4.29). So the latter accounts only for a minor part (5.5 %) of all discriminatory power. Plotting the canonical scores of the data points for root 1 vs. root 2 (Fig. 1-2), a clear separation of the three sampling locations is revealed. The clearest discrimination was obtained by root 1 between the Sary Kaydaky samples and the near Danube profiles. Root 1 is in particular positively correlated with the variables Al_2O_3 , Ga, Rb, Fe_2O_3 , MnO and Zn and negatively with SiO_2 and Zr (Table 1-1). Thus, elements of the former group show higher contents in the Serbian and Romanian samples, which occur at the positive side of root 1, whereas Sary Kaydaky samples are placed at the SiO_2 and Zr rich (negative) side of root 1. The near Danube sections were only weakly discriminated by root 1, with Batajnica/Stari Slankamen samples scoring more to the right of the Mircea Voda samples. Root 2 reveals a better separation of the near Danube profiles with the samples of the Serbian sections scoring on positive values. This indicates particularly higher Rb and K contents. The samples of the Romanian section score inversely on root 2 i.e. towards higher Sr, CaO, MgO, and SiO_2 values. The Sary Kaydaky samples are placed between the two groups of the near Danube sites, overlapping with both of them.

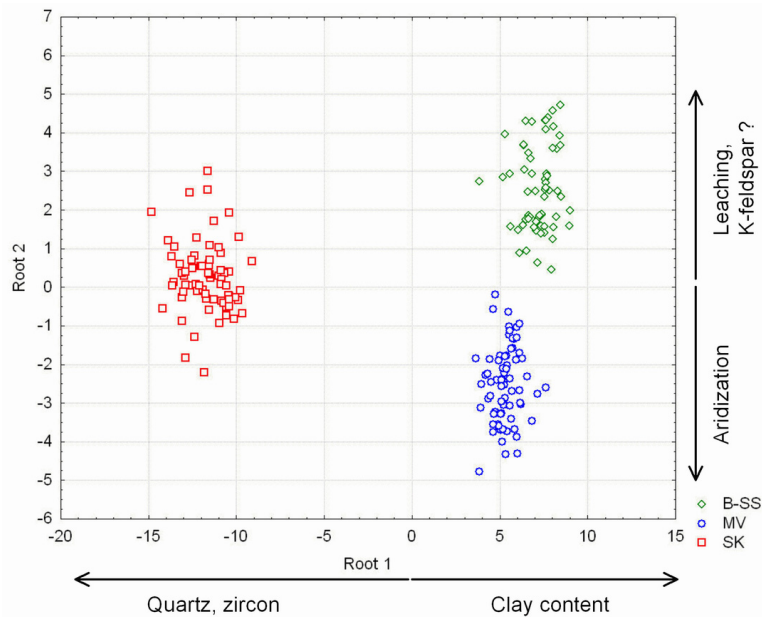


Fig. 1-2. Scatterplot of the canonical scores. Data points, representing individual samples of the loess-paleosol profiles Batajnica/Stari Slankamen (B-SS), Mircea Voda (MV) and Stary Kaydaky (SK) are plotted on the two discriminant functions root 1 and root 2. For the interpretation of the discriminant function we refer to Section 5.1.

Table 1-1. Factor structure matrix: The factor structure coefficients – equivalent to factor loadings – give the strength of correlation between the variables and the discriminant functions. Asterisks mark variables, which were log-transformed for discriminant analyses.

| | root1 | root 2 |
|----------------------------------|-----------|-----------|
| S* | 0.041022 | 0.063932 |
| SiO ₂ | -0.316924 | -0.091605 |
| TiO ₂ * | 0.247594 | -0.022334 |
| Al ₂ O ₃ | 0.417530 | 0.065249 |
| Fe ₂ O ₃ * | 0.284713 | -0.006703 |
| MnO | 0.301205 | 0.019990 |
| MgO* | 0.260079 | -0.135905 |
| CaO* | 0.104654 | -0.114797 |
| Na ₂ O | 0.185791 | -0.036397 |
| K ₂ O | 0.150180 | 0.200528 |
| P ₂ O ₅ | 0.193633 | 0.154288 |
| Ba* | 0.139960 | -0.001266 |
| Ce | 0.228513 | 0.034586 |
| Cr* | 0.234408 | -0.011543 |
| Ga | 0.354239 | 0.138509 |
| Nb | 0.218658 | 0.035784 |
| Pb | 0.218319 | 0.084593 |
| Rb | 0.350517 | 0.288552 |
| Sr* | 0.121018 | -0.217149 |
| Th* | 0.134385 | 0.118295 |
| V* | 0.236090 | -0.045103 |
| Y* | 0.143478 | 0.035368 |
| Zn* | 0.294909 | -0.029768 |
| Zr | -0.156547 | 0.013417 |

4.2 Si-Zr-Hf-association

For our sections, SiO₂ and also Zr are revealed as discriminating variables (Table 1-1). A similar factor group, additionally containing Hf, was identified by Batista et al. (2006) in European topsoil, subsoil, stream sediment and floodplain sediment samples, which among others showed high scores in the areas of glaciofluvial deposits of the Fennoscandinavian ice sheet. Therefore, we took a closer look at the contents of SiO₂, Zr and Hf, the latter being strongly associated with Zr in the mineral zircon (Reeder, et al., 2006). According to the “Scheffé test” and “Tukey HSD test for unequal sample numbers” (Statsoft, 2001), all three profiles can be significantly distinguished with respect to the SiO₂ content of the bulk samples. Highest average SiO₂ contents are obtained for Stary Kaydaky and lowest values for Batajnica/Stari Slankamen (Fig. 1-3). Also Zr and Hf contents are significantly elevated at

Sary Kaydaky. Within the near Danube sections, Mircea Voda tends to have higher contents of SiO₂, Zr and Hf (Fig. 1-3).

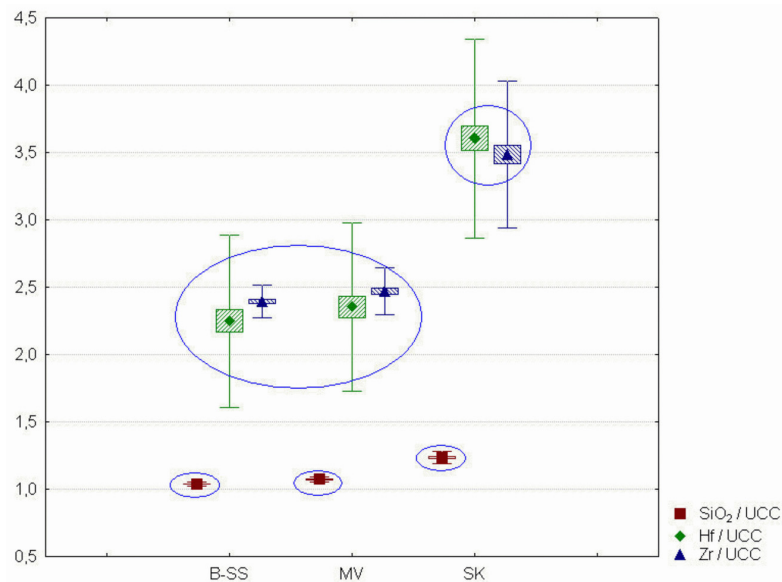


Fig. 1-3. Average SiO₂, Zr and Hf content of the profiles Batajnica/Stari Slankamen (B-SS), Mircea Voda (MV) and Sary Kaydaky (SK). Values are normalized to the respective mean element content of the upper continental crust (Condie, 1993) for better comparability. The boxes represent standard error, whiskers show standard deviation. Significantly different groups are marked by circles.

4.3 Major elements ratios

In the A-CN-K diagram, samples of Batajnica/Stari Slankamen and Mircea Voda plot closely together, at a line parallel to the A-CN join (Fig. 1-4). This is a typical distribution for material with different extend of chemical weathering, resulting in a predominant removal of silicatic Ca and Na due to the destruction of plagioclase. If plagioclase weathering would be in saturation, the weathering line would approach the K-A join, and then be redirected towards the A-CN apex, as a result of predominant loss of K by the weathering of potassic phases such as K-feldspar, mica or illite (Nesbitt and Young, 1989; Nesbitt et al. 1996). This feature was not observed for our profiles. The weathering line for the near Danube sections is very similar and can be drawn back to average UCC composition, showing a UCC-like $K_2O/(CaO^* + Na_2O)$ ratio of the unweathered sediment. For Mircea Voda, there may be some

contribution of material with a lower $K_2O/(CaO^* + Na_2O)$ ratio. The distribution of floodplain sediment data for selected source areas resembles that of the near Danube loess samples, with a greater variability, however. Also here unweathered source material mostly can be characterized by average UCC composition.

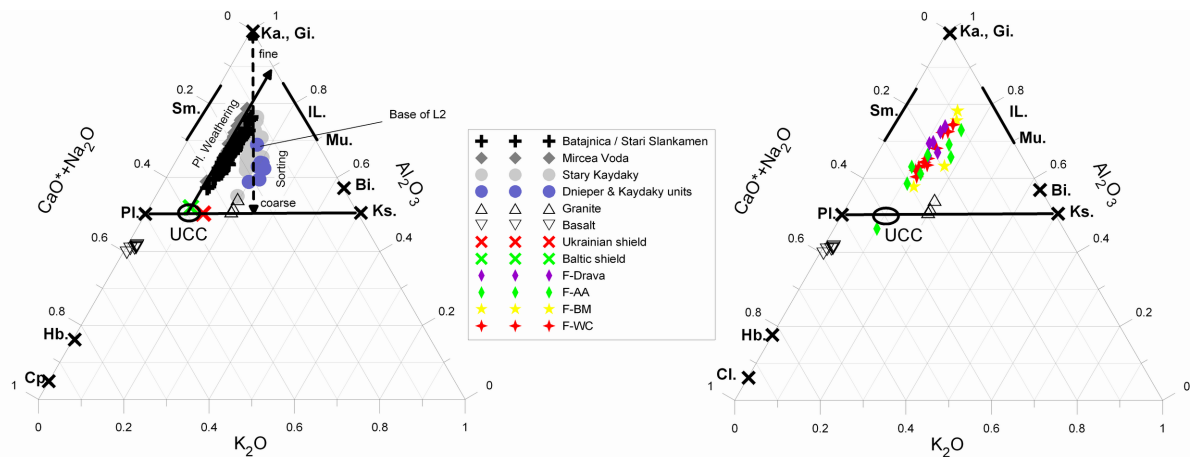


Fig. 1-4 A-CN-K diagram. Values of bulk samples are plotted for the studied sections (left diagram). Samples of the Dnieper and Kaydaky units (MIS 6, MIS 5e) of Stary Kaydaky are highlighted in blue. The composition of several possible source materials is given i.e. of the Ukrainian shield and Baltic shield (left diagram) for Stary Kaydaky, floodplain sediments of the “Austroalpine cover nappes area” (F-AA), the “Drava source area” (F-Drava), the “Bohemian Massif area” (F-BM) and the “Western Carpathian area” (F-WC) for the Danube Basin loess sections (right diagram). See Section 3.3 for a description of the selected source areas. Characteristic values for the upper continental crust (UCC), basalt, granite and the minerals clinopyroxene (Cp.), hornblende (Hb.), plagioclase (Pl.) K-feldspar (Ks.), biotite (Bi.), muscovite (Mu.), illite (IL.), smectite (Sm.), kaolinite (Ka.) and gibbsite (Gi.) are shown for orientation.

The Stary Kaydaky samples plot at a line between the CN-K junction and the Al_2O_3 apex, being characteristic for sorting (Fig. 1-4). According to Nesbitt et al. (1996), finer material is placed closer to the Al_2O_3 apex due to abundant aluminous clay minerals, coarser material vice versa. Therefore, the distribution of Stary Kaydaky samples in the A-CN-K diagram shows clear grain size/ mineral sorting effects. As expected, material that is supposed to be deposited during the most proximal glacier advance i.e. that of the so-called Dnieper stage (penultimate glaciation) is located mostly at the coarse, feldsparic end of distribution. The very base of the Dnieper loess (L2) indicates finer, aluminous material, possibly due to sedimentation before maximum glacier advance. Some data points of other units, however,

are also placed close to the material of the Dnieper loess and the last interglacial soil (the so-called Kaydaky complex), that developed in the underlying loess. Since scattering of the data is not parallel to the A-CN join, no definite initial composition could be deduced. Possible $K_2O/(CaO^* + Na_2O)$ ratios may range from typical granitoid to average UCC composition. Thus, neither the Ukrainian nor the Baltic shield could be ruled out as source material.

The Fe_2O_3/TiO_2 vs. Al_2O_3/TiO_2 plot shows a distinct separation of the near Danube profiles and the Sary Kaydaky section at the Dnieper River (Fig. 1-5). Aluminum and iron contents of bulk samples may be influenced by pedogenesis i.e. clay enrichment and iron migration under reducing conditions. Yet, also the “pure loess samples” confirm a lower Al_2O_3/TiO_2 and Fe_2O_3/TiO_2 ratio at Sary Kaydaky. The Fe_2O_3/Al_2O_3 ratio is between 0.3 and 0.4 for the samples of all three profiles, being consistent with UCC values and also shale values, which are regarded as average sample of the UCC (Taylor and McLennan, 1985). Thus, this ratio does not seem to be significantly influenced by sorting and weathering effects. Hence, for all three profiles a source composition similar to that of the UCC is indicated. Looking at specific source materials, the Fe_2O_3/Al_2O_3 ratio of Sary Kaydaky is close to that of the Baltic shield, whereas the Fe_2O_3/Al_2O_3 ratio of the Ukrainian shield is distinctly higher. Floodplain sediments of possible source areas for the near Danube loess show no distinct difference to the Fe/Al ratio of the loess samples. Yet, the Fe_2O_3/TiO_2 ratios of the “Austroalpine cover nappes” source (“F-AA”) are remarkably higher.

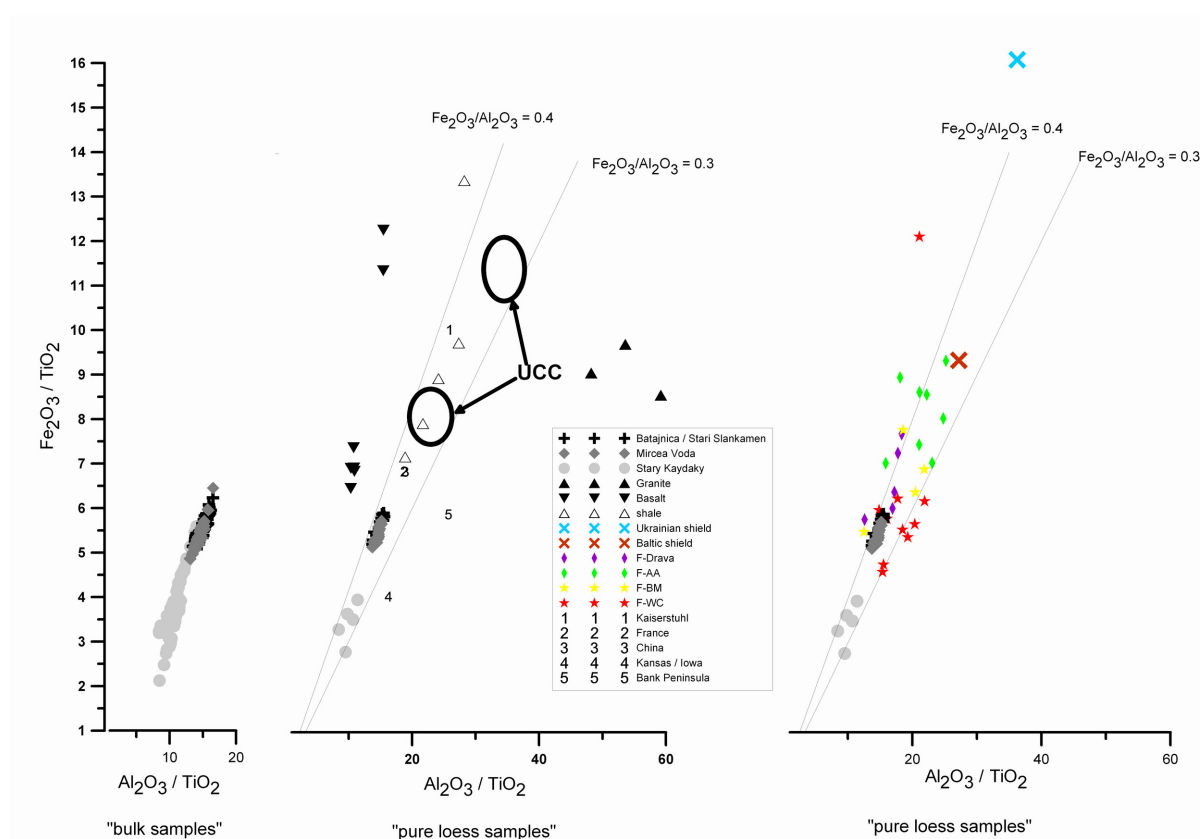


Fig. 1-5. $\text{Fe}_2\text{O}_3/\text{TiO}_2$ vs. $\text{Al}_2\text{O}_3/\text{TiO}_2$ diagram. Left plot: loess and soil samples; middle and right plot: only “pure loess” samples. Values of floodplain sediments of selected source areas, rock types as well as average values for the UCC are given. See Fig. 1-4 and Section 3. for the abbreviations and further explanations. Note, the two distinct groups within the dataset for the UCC and basalt can be attributed to Archean- and post-Archean formation. Ratios of several loess regions of the world are given for comparison.

4.4 Element fingerprint

The fingerprints of UCC-normalized elements show a very similar patterns for the studied sections, also resembling those of other loess areas (Fig. 1-6). Nevertheless, differences in absolute enrichment with respect to the UCC composition and some minor deviations in the patterns are obvious. Generally, the elements Si, Ti (not at Kaiserstuhl), Hf, La, Nb, Nd and Zr are enriched in loess or at least not remarkably depleted with respect to average UCC composition. Note that some deviations in pattern and absolute values of the trace element compositions compiled from literature may be attributed to different analytic methods.

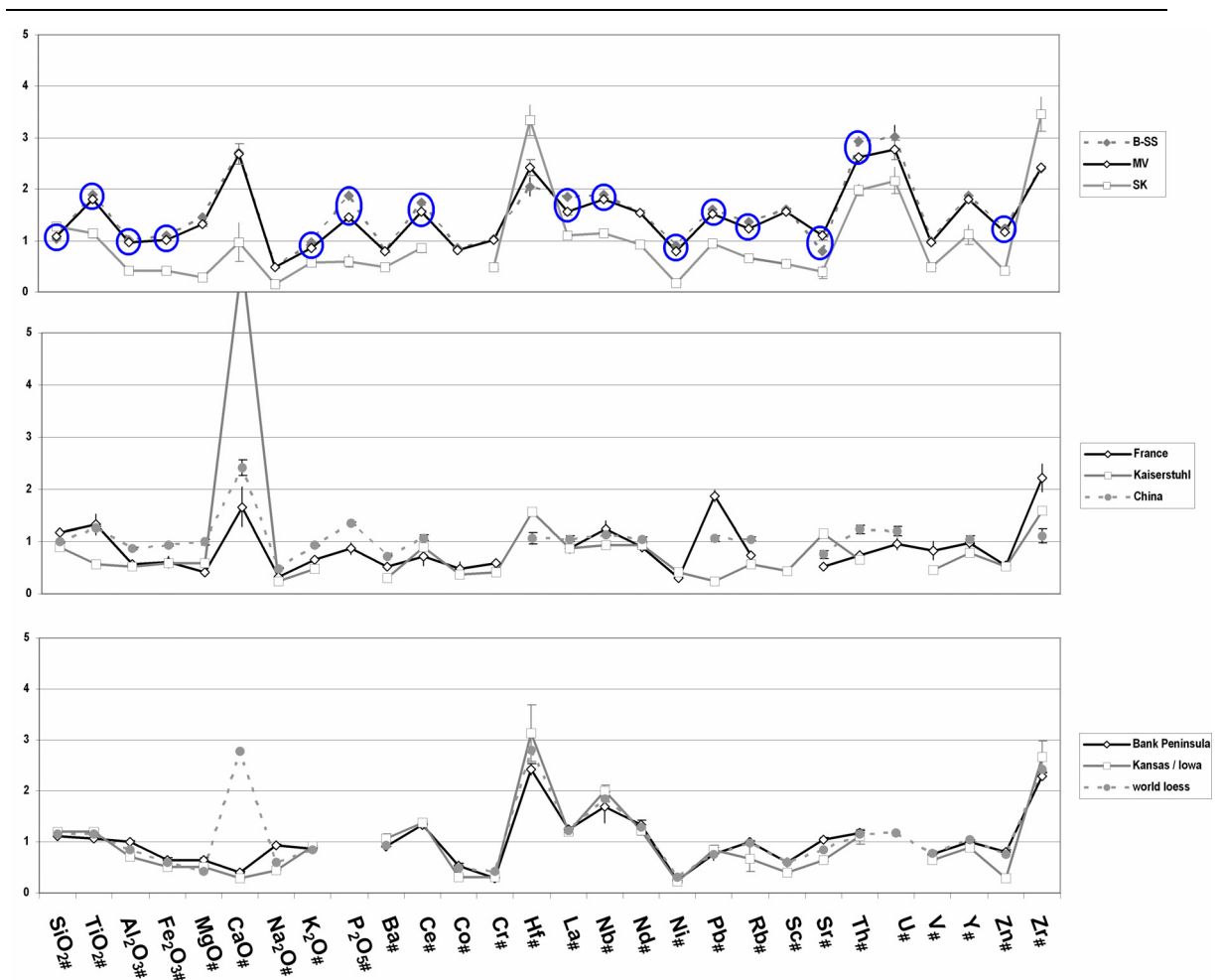


Fig. 1-6. Element fingerprint normalized to UCC composition (indicated by the number sign) for the "pure loess" of the sections Batajnica/Stari Slankamen (B-SS), Mircea Voda (MV) and Stary Kaydaky (SK), as well as for various loess regions and for the average composition of worldwide loess. See Section 3.3 for literature sources. Whiskers indicate standard errors. Significant differences between the fingerprint curve of Mircea Voda section and Batajnica / Stari Slankamen section are highlighted by circles.

The geochemical composition of the Stary Kaydaky section shows mostly an element depletion relative to the UCC, except for the Si, Ti, Hf, La, Nb, Nd, Zr – as mentioned before – and additionally for Ca, Pb, Th, U and Y. The elements of the near Danube loess are enriched with respect to the UCC and the loess of the Stary Kaydaky section. The UCC normalized Zr, Hf, Si contents, however, are higher in the Ukrainian section. Minor differences between the Batajnica/Stari Slankamen and Mircea Voda site are tested for significance. Since neither the natural nor the log-transformed data of the "pure loess" samples are normally distributed for all variables, significance was tested using the non-parametric Mann-Whitney U test (Statsoft Inc, 2001). The results show that loess of the

Mircea Voda section is slightly depleted in some elements (see Fig. 1-6), just for Si and Sr a significant enrichment relative to the Serbian sections is revealed. Note that not all differences in the element concentrations obtained for the “pure loess” are also confirmed by the discriminant analysis, since the latter used “bulk material” i.e. also including paleosols. Thus, weathering induced-redistribution of elements may bias results.

4.5 Background magnetic susceptibility

The background susceptibilities of the Mircea Voda and Batajnica/Stari Slankamen section are both in the range of 21×10^{-8} to $22 \times 10^{-8} \text{ m}^3 \text{ kg}^{-1}$, which is two times higher than at Stary Kaydaky ($7 \times 10^{-8} \text{ m}^3 \text{ kg}^{-1}$, Buggle et al., 2009). The loess deposits of the Black Sea coastal area show considerable variations from site to site. However, one can recognize distinctly lower values of magnetic background susceptibility in the northern sites near the Dniestr and Dniepr (Fig. 1-7).

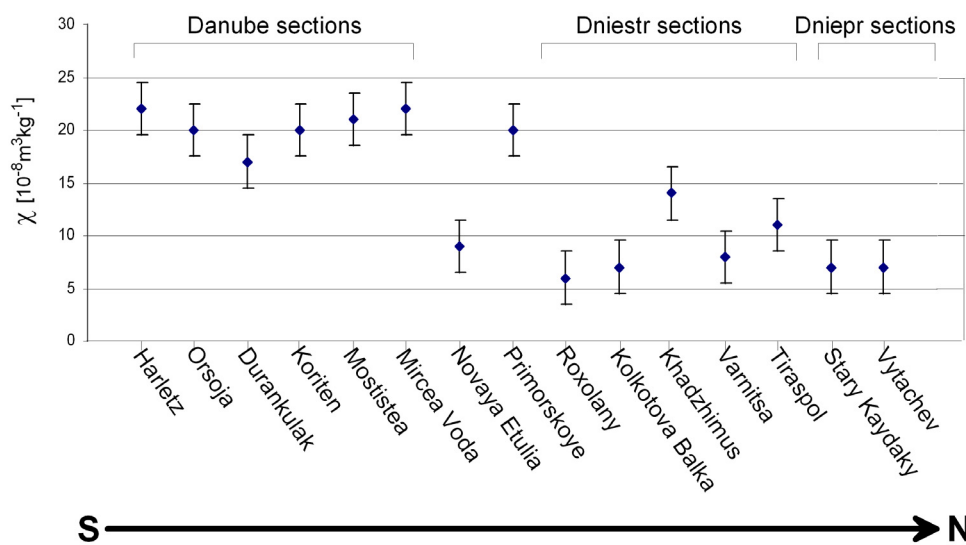


Fig. 1-7. Background magnetic susceptibility of loess-paleosol sections in the Northern Black Sea area and the Ukraine. See Fig. 1-8 for the locations. Standard error was estimated to $2.5 \cdot 10^{-8} \text{ m}^3 \text{ kg}^{-1}$.

5 Discussion

5.1 Origin and geochemical characteristics

Before considering dust sources, we want to outline the general constraints of the applied method. The geochemical signature of a sediment can give strong evidence for or against a potential source, if the following aspects are taken into account. First, element parameters should be evaluated for biasing effects of weathering and sorting. So done, striking similarities in the parameter between the sediment and a potential source may confirm the origin of the material. Yet, this approach requires that the composition of all other major potential source areas is known and also are distinctly different. If not, sources can only be ruled out, rather than confirmed in a positive way. A mixture of several end members can even complicate the interpretation. Additional information about the geomorphological settings may help in such ambiguous situations. Finally, it is very important to stress that this geochemical approach cannot detect minor sediment sources, unless they have a very characteristic composition.

5.1.1 Stary Kaydaky section

5.1.1.1 Glaciofluvial sediments – a loess source for the Stary Kaydaky site

In the Ukraine and nearby in Belarus, respectively, glaciofluvial sediments are continuously present since the Early Pleistocene that means over the whole considered time of loess accumulation (Gozhik, 1995). These areas are drained by the Dnieper River, which is close to the Stary Kaydaky site. Thus the river alluvium and the glaciofluvial sediments in the periglacial desert, at the edge of the ice, are considered as the main dust sources. A confirmation for this assumption is given by the discriminant analysis (Fig. 1-2, Table 1-1) and the element enrichment relative to the UCC (Fig. 1-6). Accordingly, the eolian sediments at Stary Kaydaky are characterized by high contents of the elements Si, Zr and Hf compared

to the near Danube loesses, generally reflecting the contents of the minerals quartz and zircon (Reeder et al., 2006). A similar factor group was identified by Batista et al., (2006) on the FOREGS dataset of European stream sediment, floodplain sediment and soil samples, with high factor scores in the area of the Fennoscandinavian ice sheet. The selective enrichment of these elements in glaciofluvial deposits can be best attributed to the removal of less weathering-resistant minerals during the processes of crumbling and leaching in the sub- and proglacial environment (Lis and Pasieczna, 2006). Whether this mineral sorting is also accompanied with grain size sorting has finally to be proved by texture analyses. However, zirconium and silicon in aeolian sediments are found to be preferentially associated with coarser grain size fractions i.e. coarse silt and sand, respectively (Muhs and Bettis, 2000; Yang et al., 2006). Further evidence for mineral sorting is given by the A-CN-K plot (Fig. 1-4) and a low Al/Ti ratio (Fig. 1-5), indicating selective enrichment of coarser, more feldsparic material over more clayey, aluminous material (Eissmann, 2002; Lindner et al., 2002). Deposits of the Dnieper stage (MIS 6), when the distance to the glacier was most proximal, are not distinctly the coarsest in the A-CN-K plot. This contradicts the expectations, if sorting would be controlled by the eolian transport distance. Differences in wind strength due to ice topography could be more important than the absolute distance from the ice margin. Furthermore, we have to regard the possibility that the mineral sorting is already inherited in the glaciofluvial sediments.

The distribution of sandy and sandy loam soils in the Ukraine (Fig. 1-8) reveals sandy deposits, on the one hand locally distributed close to Stary Kaydaky, on the other hand extensively distributed in about 300 km distance. These may denote both, possible source areas and paleowind direction. The local sand deposits related to rivers are most probably blow outs from the river banks during dry and cold periods of the Quaternary, indicating northerly, katabatic winds from the ice sheet.

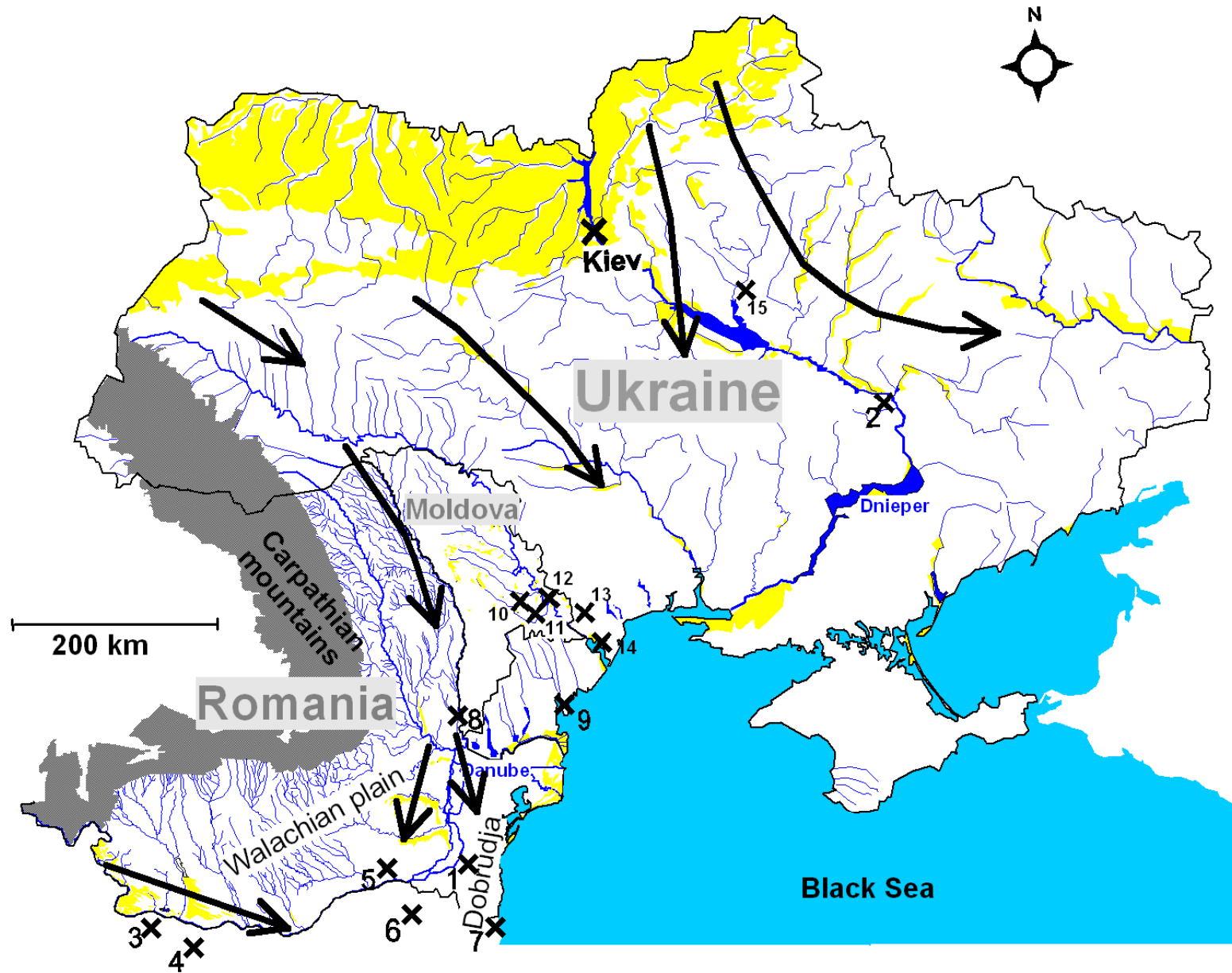


Fig. 1-8. Distribution of sand and sandy loam soils (yellow) in the Ukraine, sand and sandy soil texture in Moldova and sand dunes in Romania. The map is based on the soil map of the Ukraine, (<http://eusoils.jrc.it>, 2006), the geomorphologic map of Romania (<http://eusoils.jrc.it>, 2006 b) and the map of surface sediments of Moldova (Академия Наук Молдавской ССР, 1978). The locations of loess-paleosol sites, with published magnetic susceptibility records are given: 1. Mircea Voda (Buggle et al., 2009; this study), 2. Stary Kaydaky (Buggle et al., 2009; this study), 3./ 4. Orsoja/Harletz (Avramov et al., 2005), 5. Mostistea (Panaiotu et al., 2001), 6. Koriten (Jordanova and Petersen, 1999), 7. Durankulak (Avramov et al., 2005), 8. Novaya Etuliya (Tsatskin et al., 2001), 9. Primorskoje (Nawrocki et al., 1999), 10./11./12. Varnitsa/Khadzhimus/Tiraspol (Dodonov et al., 2006), 13. Kolkotova Balka (Tsatskin et al., 2001), 14. Roxolany (Tsatskin et al., 1998), 15. Vyazivok (Rousseau et al., 2001). Arrows indicate proposed paleowind directions during cold stages, according to the distribution of the sandy areas with respect to river valleys. For the Western Ukraine and East Romania, where such deposits are absent, paleowind directions are based on the orientation of gredas according to Rozycki (1967).

In the western Ukraine, these winds were deflected by the Carpathian mountains towards ESE, changing to SE and then to southerly directions at the eastern backside of the Carpathians, as can be deduced from the orientation of gredas (Rozycki, 1967). For the large sand area in the north of the Ukraine, it is not possible to distinguish Quaternary sands and possible autochthonous Paleogene sands. The striking similarity in the zirconium and silicon enrichment of the loess south of it and of Northern European glaciofluvial sediments, however gives reason to favor predominant Quaternary origin. Both, the Dnieper River and the northerly katabatic winds from the ice sheet are seen as responsible for the southward transport of glaciofluvially derived material, in the Ukraine.

5.1.1.2 Origin of the glaciofluvial sediments

Having confirmed that glaciofluvial deposits of the Fennoscandinavian ice sheet with characteristic mineral and grain size sorting are the major loess source, the potential origin of this material is to be evaluated. According to petrographic studies (Dorofeev, 1969; Gaigalas, 1978, 1982; all cited in Matoshko, 1995), far transported material provided by the ice sheet originates from the southern part of the Baltic shield i.e. southern Finland and Gulf of Finland. However, there are also contributions from sedimentary rocks of the Russian platform and locally of crystalline rocks of the Ukrainian shield.

We firstly focused to rule out one of the remaining crystalline areas, but the separation of the potential source areas in the A-CN-K plot was not satisfying. Yet, the Ukrainian shield could

be ruled out as a relevant source due to a low Al/Fe ratio. This ratio is believed to be not affected by weathering or sorting effects, since it is constant for the Dnieper as well as the near Danube loess sections and equal to ratio of the average UCC. The Baltic shield composition fits well with Al/Fe ratio of the loess. This would strongly suggest far-transported material as a major component of the glaciofluvial sediments. Unfortunately, the contribution of the mentioned sedimentary rocks could not be directly evaluated, because suitable data are lacking. However, due to the high extend of initial weathering of the material, we propose that in fact preweathered sediments of the Russian platform account for the major proportion of the glaciofluvial-loess source material. This is not necessarily a contradiction to the observed geochemical similarity between the loess in the Dnieper area and the Baltic shield, showing average UCC like composition, since Taylor and McLennan (1985) observed various terrigenous sediments to be good samples for average UCC. See Section 5.2 for more detailed explanations.

5.1.2 Batajnica/Stari Slankamen section

5.1.2.1 The Danube alluvium – the major source for Danube Basin loess.

For the Danube Basin, Smalley and Leach (1978) considered the Danube alluvium as the important source of loess. This is also supported by the paleowind direction reconstructed by Rozycki (1967) and Marković et al. (2008). According to their results based on orientation of gredas and loess isopach mapping, respectively, northwesterly and northerly winds prevailed in the Pannonian Basin during the periods of loess formation, except for the region southeast of the present day Danube-Tisza confluence, for which Marković et al. (2008) reported southeasterlies. Silty material potentially could have been uptaken by these winds, and after a certain distance of transport deposited to form thick loess plateaus, as they can be found in the Vojvodina region (Smalley and Leach, 1978). Lacking any other possible major dust sources in the area, we follow this idea. The strong similarities between the element composition of

the Serbian and Romanian section are an additional confirmation. Whereas the loess of the Dnieper area is characterized by higher Zr, Hf and Si content and mineral sorting, due to glaciofluvial reworking of the source material, the near Danube loess show higher contents of Al, Fe, Ti, Rb and associated elements, as revealed by discriminant analysis and the UCC normalized element fingerprint. In other loess deposits, aluminum content is generally found to be enriched with decreasing grain size, especially in the clay fraction. The same holds true for Fe, Ti and Rb (Chapman and Horn, 1968; Reeder et al., 2006; Yang et al., 2006). Thus, discriminant function 1 can also be interpreted as negative grain size function. Additionally, the Fe/Ti and Al/Ti ratios point to a higher clay content (Muhs and Bettis, 2000; Muhs et al., 2001) of the near Danube loess compared to the Dnieper loess. This fits to the supposed alluvial origin (Stoilov, 1984, cited in Jordanova and Petersen, 1999). However, grain size analyses would be required to confirm our conclusion. Nevertheless, with the Danube alluvium representing the source of the loess material, the exceptional thickness of the Vojvodina loess deposits can be explained. In the Vojvodina region, the Danube river turned from South to East, during the considered time period of loess formation, as it is today (Gábris and Nádor, 2007; Ruszkiczay-Rüdiger, 2007). Exactly here is the transition zone between the northerly and southeasterly winds in the southern Pannonian Basin, where material of the Danube alluvium potentially could be blown together from two directions.

5.1.2.2 Sources of alluvial silt

In their profound work, Smalley and Leach (1978) evaluated the relative contribution of different source areas of alluvial silt by considering the settings and processes of the geomorphodynamic system of the Danube Basin.

Our geochemical approach to identify the areas of the Danube catchment that are most important for the Pleistocene delivery of silt sized alluvial sediments was partially successful. The comparison of the Serbian loess with floodplain sediments could not reveal a dominating source area. The major element composition (Fig. 1-4, Fig. 1-5) of the Drava floodplain

sediments, originating in the metamorphic, crystalline Eastern Alps (“F-Drava”), showed no clear differences to alluvial material of the Bohemian Massif (“F-BM”), the Western Carpathians (“F-WC”) and to the Vojvodina loess. With respect to geochemistry, none of these source areas could be ruled out as major supplier of sediments into the southern Pannonian Basin. However, Danube tributaries, draining predominantly the Eastern Alpine cover nappes area and glaciated alpine foreland (“F-AA”), revealed relatively high Fe/Ti ratios in the floodplain sediments compared to the Serbian loess. True iron enrichment should increase both, the Fe/Ti and the Fe/Al ratio (Smykatz-Kloss, 2003), whereas increasing clay content should rise the Fe/Ti as well as the Al/ Ti ratio (Muhs and Bettis, 2000; Muhs et al., 2001). Since none of both can be observed, a combination of the two effects probably causes the Fe/Ti offset of the “F-AA” floodplain samples. Note that the Fe/Al ratio of loess and floodplain sediments is mostly in the range of the UCC. Thus, we suppose that reductive element removal during fluvial transport did not alter noteworthy the element ratios. To conclude, elevated Fe/Ti ratios indicate only a minor contribution of material from the Austroalpine cover nappes and deposits of the northern alpine foreland glaciation (not including the Inn area) to the Vojvodina loess.

From the geochemical point of view, the Bohemian Massif may be a possible significant source area, supplying silty material produced by frost shattering and thermal weathering. Yet, due to the extent of this area and the lack of major melt water streams, we consider its relative importance even smaller than that of the “F-AA” source area. The Moravian melt water channel situated between the Bohemian Massif and the Carpathian Mountains was proposed by Smalley and Leach (1978) as possible source of glaciofluvial material for the Pannonian Basin. This melt water channel was active during the Saalian and eventually Elsterian glaciation maximum (Macoun and Králík, 1963; Tyráček, 2006). In this case one should expect elevated Si, Zr and Hf values – as in Stary Kaydaky and as it is typical for glaciofluvial sediments of the Fennoscandinavian shield- in the samples representing Saalian

and eventually also Elsterian loess. However, the respective material didn't stand out against the other Serbian samples, regarding the discriminant analyses. Thus, we conclude that glaciofluvial material, transported through the Moravian melt water channel into the Danube drainage area, did not significantly contribute to the alluvial loess source material, at least not in the southern Pannonian basin. For the Tisza River, draining the Romanian part of the Carpathian Basin, no floodplain data were available. However, we assume that the element composition of the Western Carpathian floodplain sediments is a representative for this major Danube tributary. From the geochemical point of view and also because of their regional extension and tectonically accelerated erosion during the Quaternary the Carpathian Mountains are a likely source area for contributing silt sized weathering products. Smalley and Leach (1978) draw the same conclusion. As further important silt source, we consider also the Drava River, supplying glaciofluvial sediments of the Eastern Alps. The geochemistry of Inn tributaries was not evaluated, since they are expected to cluster partly with the Austroalpine cover nappes ("F-AA") and partly with the Austroalpine basement nappes ("F-Drava"). Smalley and Leach (1978) suggested the Inn River to be a significant sediment supplier to the Pannonian Basin, since it is the second largest Danube tributary upstream of the Vojvodina and fed by glacial melt water.

5.1.3 Mircea Voda section

5.1.3.1 Geochemical evidence

The loess of the Mircea Voda section reveals a very similar geochemical fingerprint (Fig. 1-6) and major element ratios (Fig. 1-4, Fig. 1-5) as the Serbian loess. Therefore, we conclude that also for this site the prevailing loess sources were Danube alluvial sediments. Yet, the statistical analyses of bulk material show a weakly expressed, but still significant discrimination between these two near Danube loess-paleosol sites by discriminant function 2 (Fig. 1-2). This function has highest negative correlation with CaO, MgO and Sr, implicating

higher carbonate content (Reeder et al., 2006) in the Mircea Voda section compared to the Serbian one. This probably reflects the aridity trend between the sites (Bugge et al., 2009). The Serbian samples load positively on discriminant function 2, which is correlated with K and Rb, possibly indicating higher K-feldspar or mica content (Reeder et al., 2006). Enrichment of K and Rb in course of pedogenic clay enrichment seems unlikely, since this should be also reflected in a higher Al content, which is not observed (Table 1-1).

Besides K and Rb, small but significant differences in the enrichment of some other trace and macroelements over average UCC-composition for the “pure loess”, indicate minor contributions of at least one additional dust source for the Mircea Voda site. More specifically, the aeolian sediments at the Mircea Voda site have significantly higher Si contents and a trend to higher Zr and Hf contents compared to the Serbian sections (Table 1-1, Fig. 1-3), whereas most other elements (except those related to carbonates) are depleted. Thus, we can conclude a dilution effect due to a higher quartz content for this Romanian section and also selective zircon enrichment similar to the Ukrainian section. However, its extent is much weaker expressed as in Sary Kaydaky.

Considering the origin of this quartz and zircon rich loess contribution, we have to evaluate additional loess source areas for the lower Danube Basin/Dobrudja. Here, one may suggest the Sava River, the largest river entering the Danube River downstream of Belgrade, to change the composition of the Danube alluvial sediments. Smalley and Leach (1978) stated that, lacking major glaciation and silt deposits, a significant contribution from the Sava catchment is not probable. Thus, evaluating sources and transport vectors of quartz rich material, we focus on the distribution and orientation of sand dunes and gredas in the lower Danube basin and Dobrudja, respectively (Fig. 1-8). These indicate prevailing WNW paleowinds in the western part and NNW – NNE paleowinds in the eastern and northern part of the plain. The transition zone is west of Mircea Voda between the Mostistea Lake and the Olt River. Therefore, a contribution of silt sized material from the glaciofluvial deposits of the

Ukraine is likely, but also an input from local sand dune fields is possible. Finally we also want to point out that several authors favor additional dust contributions from the Black Sea shelf (Conea et al., 1972, cited in Smalley and Leach, 1978) or the Aral and Caspian Sea arid lands (Stephens et al., 2003; Avramov et al., 2006). We cannot prove or disprove this by geochemistry.

The obtained results concerning the provenance of the loess in the Dobrudja may also shed new light onto the drainage history of the lower Danube during the Pleistocene. With the loess of the Dobrudja originating from Danube alluvium, the Danube River should have been situated north of the site, considering the paleowind direction. However, the Karasu valley is situated south of the loess-paleosol section Mircea Voda and other Mid-, and Late Pleistocene loesses of the Dobrudja (Conea 1969; Haase, et al., 2007). Therefore, the Karasu valley is unlikely to be the major Danube channel for a long period of the Mid-, or Late Pleistocene. Thus, either the Danube bifurcated at Cernavoda in two arms, one using the Karasu-valley and the other passing the Dobrudja at its Western and Northern flank (Pfannenstiel, 1950), as the present day Danube, or the Karasu channel was already inactive before the deposition of the studied loesses started i.e. before MIS 17. Up to now there is no reliable dating of the loess deposits within the Karasu valley.

5.1.3.2 Magnetic susceptibility evidence

Besides direct geochemical measurements, the magnetic susceptibility of the loess can provide further evidences to identify and characterize source areas with respect to magnetite and maghemite content and initial weathering, respectively. The available data reveal differences in background magnetic susceptibility between the Batajnica/Stari Slankamen, Mircea Voda section (22×10^{-8} and $21 \times 10^{-8} \text{ m}^3 \text{ kg}^{-1}$, respectively) and the Stary Kaydaky section ($7 \times 10^{-8} \text{ m}^3 \text{ kg}^{-1}$). The significant lower values of background magnetic susceptibility in the north of the Black Sea coastal area indicate a contribution from an alternative dust source. It seems likely that this is the area of glaciofluvial sediments in the middle and

northern Ukraine. Dilution by quartz may account for the low magnetic susceptibility in the Dnieper and Dniester loess region. The substantial variations within the sites of a region are attributed to local effects. As to this, we are generally aware of three possibilities: (1) a different degree of initial pedogenetic alteration of the source material available for eolian transport leads to different secondary mineralogical composition and/or grain size distribution, depending on source locality; (2) a different extend of initial pedogenetic alteration of the dust after its accumulation i.e. during loessification; and (3) different local sources may provide dust with different primary mineralogical composition and/or grain size distribution of magnetic minerals. Also here dilution of iron minerals by quartz can play an important role – with locally variable degree – controlled by presence and distribution of nearby sand dunes. At Mircea Voda, the additional quartz contribution is probably too weak to influence the magnetic susceptibility significantly.

5.2 Southeastern/Eastern European loess – representative samples of the upper continental crust

As the A–CN–K plot shows, near Danube loess is derived from material with UCC-like composition. Though, due to grain size/mineral sorting no clear source composition is revealed by this diagram for Stary Kaydaky, initial UCC-like composition is evident by the $\text{Fe}_2\text{O}_3/\text{Al}_2\text{O}_3$ ratio, also for this site. Hence, loess deposits of the Danube Basin/Drobrudja and the Dnieper area represent average samples of the upper continental crust. This result is conform with studies from other loess regions of the world (Taylor et al., 1983; Gallet et al., 1996, 1998). For the loess material at the Dnieper River, originating from glaciofluvial sediments of the Fennoscandinavian ice-sheet, the most effective sampling process was probably glacial grinding of bedrocks with subsequent mixing of the different rock end-members. For the lower Danube Basin/Drobrudja loess, source material is proposed to be provided by river transport of the Danube River and its tributaries, draining the Eastern Alps

and the Carpathian Basin. Since already floodplain sediments of the Danube catchment mostly show a UCC-like initial composition, of the unweathered material (Fig. 1-5, Fig. 1-6), sampling and mixing occurs by fluvial processes. In both cases, loess is not the primary sample of the UCC, however, loess deposits act as archives for UCC samples provided by glaciofluvial and fluvial systems, respectively. Yet, the information about UCC composition, derived by loess geochemistry, can be biased by several effects such as mineral weathering, grain size and mineral sorting and dilution effects by minerals such as quartz (Taylor and McLennan, 1985). The A–CN–K plot indicates that the samples of the loess-paleosol-sequences, also including “pure loess” samples, are substantially altered by weathering with respect to UCC composition. So at least one cycle of erosion/transport (activity phase) and sedimentation/weathering (stability phase) has to be proposed for the source material, before it is entrained and transported by the wind as dust and finally deposited and archived as loess. For the lower Danube Basin loess, this previous recycling phase may either have occurred during the material is retained in the fluvial system or already during the formation of the various types of clastic sedimentary rocks in the drainage basin. Since for the material of Stary Kaydaky the intersect of the sorting trend with the weathering trend of the UCC is clearly situated towards lower $\text{CaO}^* + \text{NaO}$ contents (Fig. 1-4), also here at least one phase of recycling has to be proposed. For comparison, the composition of a probably prevailing original source itself i.e. the Baltic shield, does not reveal remarkable changes with respect to the UCC (Fig. 1-4, Fig. 1-5). This was expected, since the Precambrian shields are commonly taken as representatives of the average upper continental crust (Ronov and Yaroshevskiy, 1976; Taylor and McLennan, 1985; Condie, 1993). However, question arises about the timing of this weathering phase in the loess material of the Dnieper area. There is no simple answer for this, especially with respect to the high extent of weathering, compared to the aeolian sediments of the Danube Basin. Following the evolution history of the loess in the Dnieper area, we have to start with the uptake of the relatively unweathered bedrock of the Baltic shield

into the ice shield. During the phase of the glaciofluvial transport in sub- and proglacial streams, material gets further crushed and grinded. Generally, chemical weathering in the subglacial environment is thought to be low, according to the Arrhenius relationship between temperature and reaction rate. We are aware that significant silicate weathering in subglacial systems was observed e.g. by Tranter et al. (2002) and Anderson (2005). The latter regarded glaciers even as “flow-through reactors”. In spite of the long transport distance and residence time in the subglacial system of the Fennoscandinavian ice sheet, for us subglacial weathering does not appear likely to explain such strong initial weathering of loess. Also proglacial weathering and alteration during loessification are not expected to act sufficiently strong. Therefore, only a combination of all three weathering phases may account for a relatively high initial weathering of the Stary Kaydaky loess. Yet, this should then be still reduced compared to loess with an alluvial source. Thus, it is to conclude that sedimentary rocks (of the Russian platform) with an inherited weathering signal, entering the glaciofluvial system, have to be the dominant source of the material and not the Baltic shield. This corresponds also to the findings of Gallet et al. (1998) that loess deposits from various parts of the world show evidences of previous sedimentary recycling. As to this, also Jahn et al. (2001) emphasized the general importance of sedimentary rocks as dust sources.

Generally, the deviations from the UCC element composition of the “pure loess” mostly reflect selective mineral enrichment and depletion, respectively, according to the weathering resistance (Schnetger, 1992). In the studied Southeastern/Eastern European loesses, low mobility elements such as Si, Ti and some trace elements (e.g. Zr, Hf) (Fig. 1-6), which are commonly associated with weathering-resistant minerals such as quartz, rutil and zircon, are enriched compared to UCC composition. Conversely, quartz accumulation leads to a dilution effect, affecting the concentrations of the other elements, as is well indicated for the Stary Kaydaky loess. The enrichment of the relatively mobile elements Ca and Mg compared to

UCC is explained by the accumulation of secondary carbonates, leached from the paleosols in the underlying loess units.

6 Conclusions

- 1) As already proofed for several other loess regions such as the Chinese loess plateau (Gallet et al., 1996, 1998), Western Europe (Gallet et al., 1998) and the Midwest of the USA (Taylor et al., 1983), loess of the Danube Basin/Dobrudja and the Dnieper areas represent a representative sample of the upper continental crust.
- 2) Compared to the upper continental crustal composition, loess shows general evidence of at least one previous recycling phase, which probably is an inherited signal from sedimentary source rocks. This is particularly obvious from the depletion of some elements, reflecting weathering resistance of their host minerals and element mobility. Further bias of initial average UCC composition is due to mineral dilution effects especially by quartz and – if not corrected for – by secondary carbonates, as well as mineral and grain size sorting.
- 3) Loess of the Stary Kaydaky site (Dnieper loess area) is most likely derived from glaciofluvial sediments of the Fennoscandinavian ice sheet in the Ukraine and adjacent areas. Initial source rocks are proposed to be sedimentites of the Russian platform. Prevailing cold stage paleowind direction in the Ukraine was WNW to N due to katabatic winds descending from the ice sheet.
- 4) .In the southern Pannonian Basin (Vojvodina, Serbia), where the course of the Danube river turns from South to East, thick loess plateaus build up by dust supply from two wind systems: N/NW winds, as they prevail in the main part of the Pannonian Basin and SE winds in the Southeastern part of the basin. This loess is confirmed by our geochemical results to originate from alluvial sediments of the Danube river. Due to the element composition, the area of the northern Alpine cover nappes and foreland

glaciations (not including the Inn area), does not seem to be the dominant initial source. Weathering products of the Carpathian mountain range, drained by the Tisza River and several smaller Danube tributaries, and of the Austroalpine base nappes, drained by the Drava River, appear to be more likely source areas with respect to element composition. Though not evaluated geochemically, the Inn River is also considered as significant sediment supplier into the Pannonian Basin (Smalley and Leach, 1978).

- 5) As in Serbia, the loess of the Dobrudja plateau (Romania) is predominantly derived from Danube alluvium. However, a minor but geochemically significant contribution of one or several additional source areas is evident. The prevailing paleowind direction was WNW in the Western Walachian plain and N to NE in the Dobrudja and eastern Walachian plain. Thus, the additional material input is supposed to be derived from the Ukrainian glaciofluvial deposits, probably with strongly variable contributions from local sand dune fields.
- 6) Further research is needed for a better differentiation between the possible source areas of the Southeastern/Eastern European loesses. Isotope studies ($^{87}\text{Sr}/^{86}\text{Sr}$, $^{143}\text{Nd}/^{144}\text{Nd}$, $^{187}\text{Os}/^{188}\text{Os}$, $^{187}\text{Re}/^{188}\text{Os}$, $\delta^{18}\text{O}$ of quartz) and element composition of different grain size fractions may be promising with this respect (Mizota and Matsuhisa, 1995; Hattori et al., 2003; Honda et al., 2004; Nakano et al., 2004).

Acknowledgements

We thank Tivadar Gaudenyi and Mladjen Jovanović for assistance during fieldwork in Serbia, J. Eidam (University of Greifswald) for XRF analyses and Dr Michael Zech for comments on the manuscript. Financial support was provided by the German Research Foundation DFG (GL 327/8-2).

References

- Академия Наук Молдавской ССР, 1978. Почвообразующие Породы (Surface sediments) In: Главное Управление Геодезии и Картографии при Совете Министров СССР, Атлас Молдавской ССР (Atlas of the Moldavian SSR), Moscow (In Russian).
- Anderson, S.P., 2005. Glaciers show direct linkage between erosion rate and chemical weathering fluxes. *Geomorphology* 67, 147-157.
- Avramov, V.I., Jordanova, D., Hoffmann, V., Roesler, W., 2006. The role of dust source area and pedogenesis in three loess-paleosol sections from North Bulgaria: a mineral magnetic study. *Studia Geophysica et Geodaetica* 50 (2), 259-282.
- Batista, M.J., Demetriades, A., Pirc, S., De Vos, W., Bidovec, M., Martins, L., 2006. Factor analysis interpretation of European soil, stream and floodplain sediment data. In: Tarvainen, T., De Vos, W. (Eds.), *Geochemical Atlas of Europe. Part 2. Interpretation of geochemical maps, additional tables, figures, maps, and related publications.* Geological Survey of Finland, Espoo, 567-618.
- Bolikhovskaya, N.S., Molodkov A.N., 2006. East European loess-palaeosol sequences: palynology, stratigraphy and correlation. *Quaternary International* 149, 24-36.
- Bronger, A., 1976. Zur quartären Klima – und Landschaftsentwicklung des Karpatenbeckens auf paläopedologischer und bodengeographischer Grundlage. *Kieler Geographische Schriften* 45.
- Bronger A. 2003. Correlation of loess–paleosol sequences in East and Central Asia with SE Central Europe – Towards a continental Quaternary pedostratigraphy and paleoclimatic history. *Quaternary International* 106-107, 11-31.
- Buggle, B., Hambach, U., Glaser, B., Gerasimenko, N., Marković, S., Glaser, I., Zöller, L., 2009. Stratigraphy, and spatial and temporal paleoclimatic trends in Southeastern/Eastern European loess–paleosol sequences. *Quaternary International* 196, 86-106.
- Catt, J.A., 1991. Soils as indicators of Quaternary climatic change in mid-latitude regions. *Geoderma* 51, 167-187.
- Chapman, S.L., Horn, M.E., 1968. Parent material uniformity and origin of silty soils in Northwest Arkansas based on zirconium – titanium contents. *Soil Science Society American Journal* 32, 265-271.
- Chugunny, Y.G., Matoshko, A.V., 1995. Dnieper glaciation – till deposits of ice-marginal zones. In: Ehlers, J., Kozarski, S., Gibbard, P. (Eds.), *Glacial Deposits in North-East Europe.* Balkema, Rotterdam, 249-256.
- Condie, K.C., 1993. Chemical composition and evolution of the upper continental crust: Contrasting results from surface samples and shales. *Chemical Geology* 104, 1-37.
- Conea, A., 1969. Profils de Loess en Roumanie. *Supplément au Bulletin de l'Association française pour l'étude du Quaternaire*, 127-134.
- Conea, A., Balley, R., Canarache, A., 1972. Guidebook to excursions of the INQUA loess symposium in Romania. *Guidebooks for excursions* 10, 54pp.
- Derbyshire, E., Kemp, R.A., Meng, X., 1997. Climate change, loess and paleosols: proxy measures and resolution in North China. *Journal of the Geological Society, London* 154, 793-805.
- Dodonov, A.E., Zhou, L.P., Markova, A.K., Tchepalyga, A.L., Trubikhin, V.M., Akesandrovski, A.L, Simakova, A.N., 2006. Middle-Upper Pleistocene bio-climatic and magnetic records of the Northern Black Sea Coastal Area. *Quaternary International* 149, 44-54.

- Dorofeev, L.M., 1969. Liiodovikovi ta vodno-liiodovikovi vidkladi. In: Bondarchuk V.G. (Ed.), *Stratigrafiya URSR. Vol. XI. Antrophogen*. Kiev, 145-170 (In Ukrainian).
- Eissmann, L., 2002. Quaternary geology of eastern Germany (Saxony, Saxon-Anhalt, South Brandenburg, Thüringia), type area of the Elsterian and Saalian Stages in Europe. *Quaternary Science Reviews* 21, 1275-1346.
- Evlogiev, J., 1993. Paleogeography and stratigraphy of the Early Pleistocene in near Danube Northeastern Bulgaria. Dissertation, Bulgarian Academy of Science, Sofia. (in Bulgarian).
- Fuchs, M., Rousseau, D. D., Antoine, P., Hatté, C., Gauthier, C., Marković, S., Zöller, L., 2008. Chronology of the Last Climatic Cycle (Upper Pleistocene) of the Surduk loess sequence, Vojvodina, Serbia. *Boreas* 37, 66-73.
- Gábris, G., Nádor, A., 2007. Long-term fluvial archives in Hungary: response of the Danube and Tisza rivers to tectonic movements and climatic changes during the Quaternary: a review and new synthesis. *Quaternary Science Reviews* 26 (22-24), 2758-2882.
- Gaigalas, A., 1978. Zakonomernosty rasprostraneniya kristallicheskich rukovodyazhich valunov v kraevykh lednikovykh obrazovaniyakh zapadnoi chasty SSSR. In: Bondarchuk V.G. (Eds.), *Kraevye obrazovaniya materikovykh oledeney*. Materialy V Vsesouznogo sovezhaniya, Naukova Dumka, Kiev, 56-62 (In Ukrainian).
- Gaigalas, A., 1982. The possibilities of moraine correlation according to their debris composition. In: Goretskiy G.I., Chebatoreva, N.S., Shick, S.M. (Eds.), *Moskovskiy lednikovyi pokrov Vostochnoi Evropy (Moscow ice sheet in Eastern Europe)*. Nauka, Moscow, 42-43 (In Russian).
- Gallet, S., Jahn, B., Torii, M., 1996. Geochemical characterization of the Luochuan loess-paleosol sequence, China, and paleoclimatic implications. *Chemical Geology* 133, 67-88.
- Gallet, S., Jahn, B., Van Vliet Lanoë, Dia, A., Rossello, E., 1998. Loess geochemistry and its implications for the particle origin and composition of the upper continental crust. *Earth and Planetary Science Letters* 156, 157-172.
- Gerasimenko, N. P., 2004. Quaternary evolution of zonal paleoecosystems in Ukraine. Habilitation thesis, Geographical Institute of National Ukrainian Academy of Sciences, Kyiv (in Ukrainian).
- Gozhik, P.F., 1995. Glacial history of the Ukraine. In: Ehlers, J., Kozarski, S., Gibbard, P. (Eds.), *Glacial Deposits in North-East Europe*. Balkema, Rotterdam.
- Haase, D., Fink, J., Haase, G., Ruske, R., Pécsi, M., Richter, H., Altermann, M., Jäger, K.-D., 2007. Loess in Europe-its spatial distribution based on a European Loess Map, scale 1:2,500,000, *Quaternary Science Reviews* 26, 1301-1312.
- Hattori, Y., Suzuki, K., Honda, M., Shimizu, H., 2003. *Geochimica et Cosmochimica Acta* 67. 1195-1205.
- Heller, F., Liu, T., 1984. Magnetism of Chinese loess deposits. *Geophysical Journal Royal Astronomical Society* 77. 125-141.
- Honda, M., Yabuki, S., Shimizu, H., 2004. Geochemical and isotopic studies of aeolian sediments in China. *Sedimentology* 51, 211-230.
- <http://eussoils.jrc.it>, 2006a. Downloaded at 14.12.2006. Почвенная карта Украинской ССР (Soil map of the Ukraine), In: Главное управление геодезии и картографии при Совете Министров СССР (Ed.), 1977. Moscow.
- <http://eussoils.jrc.it>, 2006b. Downloaded at 14.12.2006. Harta geomorfologică (geomorphological map), In: Atlasul Republicii Socialiste România, 1976.
- Jahn, B., Gallet, S., Han, J., 2001. Geochemistry of the Xining, Xifeng and Jixian sections, loess plateau of China: eolian dust provenance and paleosol evolution during the last 140 ka. *Chemical Geology* 178, 71-94.

- Jordanova, D., Petersen, N., 1999. Palaeoclimatic record from a loess-soil profile in northeastern Bulgaria—I. Rock magnetic properties. *Geophysical Journal International* 138, 520-532.
- Kabata-Pendias, A., Pendias, H., 2001. Trace elements in soils and plants. CRC Press, Boca Raton.
- Kostić, N., Protic, N., 2000. Pedology and mineralogy of loess profiles at Kapela-Batajnica and Stalac, Serbia. *Catena* 41, 217-227.
- Kukla, G.J., 1977. Pleistocene land–sea correlation I. Europe. *Earth Science Reviews* 13, 307-374.
- Kukla, G., An, Z., 1989. Loess stratigraphy in Central China. *Palaeogeography, Palaeoclimatology, Palaeoecology* 72, 203-225.
- Kutterolf, S., 2001. Die klastischen Sedimente der karbonen Hochwipfel– und Auernig Formation der Ostkarawanken (Österreich/Slowenien). Dissertation, University of Stuttgart, URL: <http://elib.uni-stuttgart.de/opus/volltexte/2002/994/>, URN: urn:nbn:de:bsz:93-opus-9948.
- Lindner, L., Bogutsky, A., Gozhik, P., Marciniak, B., Marks, L., Łancont, M., Wojtanowicz, J., 2002. Correlation of main climatic glacial-interglacial and loess–paleosol cycles in the Pleistocene of Poland and Ukraine. *Acta Geologica Polonica* 4, 450-469.
- Lindner, L., Gozhik, P., Marciniak, B., Marks, L., Yelovicheva, Y., 2004. *Geological Quaterly* 48 (2), 97-114.
- Lis, J., Pasieczna, A., 2006. Geochemical characteristics of soil and stream sediment in the area of glacial deposits in Europe. In: Tarvainen, T., De Vos, W. (Eds.), *Geochemical Atlas of Europe. Part 2. Interpretation of geochemical maps, additional tables, figures, maps, and related publications*. Geological Survey of Finland, Espoo, 519-540.
- Macoun, J., Králík, F., 1995. Glacial history of the Czech Republic. In: Ehlers, J., Kozarski, S., Gibbard, P. (Eds.), *Glacial Deposits in North-East Europe*. Balkema, Rotterdam, 389-405.
- Marković, S.B., Heller, F., Kukla, G.J., Gaudenyi, T., Jovanović, M., Miljković, L.J., 2003. Magnetostratigraphy of Stari Slankamen loess section. *Zbornik Radova Instituta za Geografiju* 32, 20-28 (in Serbian with English summary).
- Marković, S.B., Oches, E.A., Sümegi, P., Jovanović, M., Gaudenyi, T., 2006. An introduction to the Upper and Middle Pleistocene loess-paleosol sequences of Ruma section (Vojvodina, Serbia). *Quaternary International* 149, 80-86.
- Marković, S. B., Oches E. A., McCoy W. D., Frechen, M., Gaudenyi T., 2007. Malacological and sedimentological evidence for “warm” glacial climate from the Irig loess sequence, Vojvodina, Serbia, *Geochemistry, Geophysics, Geosystems* 8, Q09008.
- Marković, S.B., Bokhorst, M, Vandenberghe, J., McCoy, W.D., Oches, E.A., Hambach, U., Gaudenyi, T., Jovanović, M., Zöller, L., Stevens, T., Machalett, B., 2008. Late Pleistocene loess-paleosol sequences in the Vojvodina region, North Serbia. *Journal of Quaternary Science* 23 (1), 73-84.
- Matoshko, A.V., 1995. Dnieper glaciation - basal till deposits. In: Ehlers, J., Kozarski, S., Gibbard, P. (Eds.), *Glacial Deposits in North-East Europe*. Balkema, Rotterdam, 231-239.
- Matoshko, A.V., 1995a. The Dnieper Glaciation: bedrock dislocations and glacial erosional landscapes. In: Ehlers, J., Kozarski, S., Gibbard, P. (Eds.), *Glacial Deposits in North-East Europe*. Balkema, Rotterdam, 241-248.
- Matoshko, A.V., 1995b. Dnieper Glaciation – meltwater deposits. In: Ehlers, J., Kozarski, S., Gibbard, P. (Eds.), *Glacial Deposits in North-East Europe*. Balkema, Rotterdam, 257-263
- McLennan, S.M., 1993. Weathering and global denudation. *The Journal of Geology* 101, 295-303.

- McLennan, S.M., Hemming, S., McDaniel, D.K., Hanson, G.N., 1993. Geochemical approaches to sedimentation, provenance, and tectonics. Geological Society of America, Special Paper 284, 21-39.
- Minkov, M., 1968. Loess in North Bulgaria. Bulgarian Academy of Science, Sofia. (in Bulgarian).
- Mizota, C., Matsuhisa, Y., 1995. Isotopic evidence for the eolian origin of quartz and mica in soils developed on volcanic material in the Canary Archipelago. *Geoderma* 66, 313-320.
- Muhs, D.R., Bettis, E.A., 2000. Geochemical variations in Peoria loess of Western Iowa indicate paleowinds of midcontinental North America during last glaciation. *Quaternary Research* 53, 49-61.
- Muhs, D.R., Benedict, J.B., 2006. Eolian additions to late Quaternary alpine soils, Indian Peaks Wilderness area, Colorado Front Range. *Arctic, Antarctic, and Alpine Research* 38, 120-130.
- Muhs, D. R., Budahn, J.R., 2006. Geochemical evidence for the origin of late Quaternary loess in central Alaska. *Canadian Journal of Earth Sciences* 43, 323-337.
- Muhs, D.R., Bush, C.A., Stewart, K.C., 1990. Geochemical evidence of Saharan dust parent material for soils developed on Quaternary limestones of Caribbean and Western Atlantic islands. *Quaternary Research* 33, 157-177.
- Muhs, D.R., Bettis, E.A., Been, J., McGreehin, J.P., 2001. Impact of Climate and Parent Material on Chemical Weathering in Loess-derived Soils of the Mississippi River Valley. *Soil Science Society of America Journal* 65, 1761-1777.
- Nádor, A., Lantos, M., Toth-Makk, A., Thamó-Bozsó, E., 2003. Milankovitch-scale multi-proxy records from fluvial sediments of the east 2.6 MA, Pannonian Basin, Hungary. *Quaternary Science Reviews* 22 (10), 2157-2175.
- Nakano, T., Yokoo, Y., Nishikawa, M., Koyanagi, H., 2004. Regional Sr-Nd isotopic ratios of soil minerals in northern China as Asian dust fingerprints. *Atmospheric Environment* 38, 3061-3067.
- Nawrocki, J., Bakhmutov, V., Bogucki, A., Dolecki, L., 1999. The paleo- and petromagnetic record in the Polish and Ukrainian loess-paleosol sequences. *Physics and Chemistry of the Earth, Part A: Solid Earth and Geodesy* 24, 773-777.
- Nesbitt, H.W., Young, G.M., 1984. Prediction of some weathering trends of plutonic and volcanic rocks based on thermodynamic and kinetic considerations. *Geochimica et Cosmochimica Acta* 48, 1523-1534.
- Nesbitt, H.W., Young, G.M., 1989. Formation and diagenesis of weathering profiles. *The Journal of Geology* 97, 129-147.
- Nesbitt, H.W., Young, G.M., McLennan, S.M., Keays, R.R., 1996. Effects of chemical weathering and sorting on the petrogenesis of siliciclastic sediments, with implications for provenance studies. *The Journal of Geology* 104, 525-542.
- Panaiotu, C. G., Panaiotu, E. C., Grama, A., Necula, C., 2001. Paleoclimatic record from a loess-paleosol profile in Southeastern Romania. *Physics and Chemistry of the Earth (A)* 26, 893-898.
- Pfannenstiel, M., 1950. Die Quartärgeschichte des Donaudeltas. *Bonner Geographische Abhandlungen* 6.
- Pécsi, M., 1990. Loess is not just the accumulation of dust. *Quaternary International* 7/8, 1-21.
- Pye, K., 1995. The nature, origin and accumulation of loess. *Quaternary Science Reviews* 14, 653-667.
- Reeder, S., Taylor, H., Shaw, R.A., Demetriades, A., 2006. Introduction to the chemistry and geochemistry of the elements. In: Tarvainen, T., De Vos, W. (Eds.), *Geochemical*

- Atlas of Europe. Part 2. Interpretation of geochemical maps, additional tables, figures, maps, and related publications. Geological Survey of Finland, Espoo, 48-429.
- Reuther, A.U., Urdea, P., Geiger, C., Ivy-Ochs, S., Niller, H.-P., Kubik, P.W., Heiner, K., 2007. Late Pleistocene glacial chronology of the Pietrele Valley, Rezetat Mountains, Southern Carpathians constrained by ^{10}Be exposure ages and pedological investigations. *Quaternary International* 164-165, 151-169.
- Ronov, A.B., Yaroshevskiy, A.A., 1976. A new model for the chemical structure of the earth's crust. *Geochemistry International* 13, 89-120.
- Rousseau, D.D., Gerasimenko, N.P., Matviischina, Z., Kukla, G.J., 2001. Late Pleistocene environments of the Central Ukraine. *Quaternary Research* 56, 349-356.
- Rozycki, St. Zb., 1967. Le sens des vents portent la poussière de loess à la lumière de l'analyse des formes d'accumulation du loess en Bulgarie et en Europe Centrale. *Revue de Géomorphologie Dynamique* 1, 1-9.
- Ruszkiczay-Rüdiger, Zs., 2007. Tectonic and climatic forcing in Quaternary landscape evolution in the central Pannonian Basin: A quantitative, geomorphological, geochronological and structural analysis. Dissertation, VU University Amsterdam, URL: <http://hdl.handle.net/1871/10689>, downloaded at 08.10.07.
- Salminen, R., Batista, M. J., Bidovec, M., Demetriades, A., De Vivo, B., De Vos, W., Duris, M., Gilucis, A., Gregorauskiene, V., Halamic, J., Heitzmann, P., Lima, A., Jordan, G., Klaver, G., Klein, P., Lis, J., Locutura, J., Marsina, K., Mazreku, A., O'Connor, P. J., Olsson, S.Å., Ottesen, R.-T., Petersell, V., Plant, J.A., Reeder, S., Salpeteur, I., Sandström, H., Siewers, U., Steenfelt, A., Tarvainen, T., 2005. *Geochemical Atlas of Europe. Part 1: Background Information, Methodology and Maps*. Geological Survey of Finland, Espoo. (<http://www.gtk.fi/publ/foregsatlas>), downloaded at 17.12.2006.
- Schnetger, B., 1992. Chemical composition of loess from a local and worldwide view. *Neues Jahrbuch Mineralogische Abhandlungen, Monatshefte* 1, 29-47.
- Sirenko N.A., Turlo, S.I., 1986. Evolution of soils and vegetation of Ukraine in the Pliocene and Pleistocene. *Naukova Dumka, Kiev* (in Russian).
- Smalley, I., 1995. Making the material: The formation of silt-sized primary mineral particles for loess deposits. *Quaternary Science Reviews* 14, 645-651.
- Smalley, I., Leach, J.A., 1978. The origin and distribution of the loess in the Danube Basin and associated regions of East-Central Europe- a review. *Sedimentary Geology*, 21, 1-26.
- Smykatz-Kloss, B., 2003. Die Lößvorkommen des Pleiser Hügellandes bei Bonn und von Neustadt/Wied sowie der Picardie: Mineralogisch-geochemische und geomorphologische Charakterisierung, Verwitterungs-Beeinflussung und Herkunft der Löss. URL: http://hss.ulb.uni-bonn.de/diss_online/math_nat_fak/2003/smykatz-kloss_bettina, URN: urn:nbn:de:hbz:5n-03082.
- StatSoft Inc., 2001. STATISTICA für Windows [Software-System für Datenanalyse] Version 6. (<http://www.statsoft.com>).
- Stephens, M., Krzyszkowski, D., Ivchenko, A., Majewski, M., 2003. Palaeoclimate and pedosedimentary reconstruction of a Middle to Late Pleistocene loess-palaeosol sequence. Prymorske, SW Ukraine, *Studia Quaternaria* 19, 3-17.
- Stoilov, K., 1984. *Loess Formation in Bulgaria*. Bulgarian Academy of Science, Sofia.
- Taylor, S.R., McLennan, S.M., 1985. *The continental crust: its composition and evolution*. Blackwell, London.
- Taylor, S.R., McLennan, S.M., McCulloch, M.T., 1983. Geochemistry of loess, continental crustal composition and crustal model ages. *Geochimica et Cosmochimica Acta* 47, 1897-1905.
- Thompson, R., Oldfield, F., 1986. *Environmental Magnetism*. Allen & Unwin Ltd., London.

-
- Tranter, M., Sharp, M.J., Lamb, H.R., Brown, G.H., Hubbard, B.P., Willis, I.C., 2002. Geochemical weathering at the bed of Haut Glacier d'Arolla Switzerland – a new model. *Hydrological Processes* 16, 959-993.
- Tsatskin, A., Heller, F., Hailwood, E.A., Gendler, T.S., Hus, J., Montgomery, P., Sartori, M., Virina, E.I., 1998. Pedosedimentary division, rock magnetism and chronology of the loess / paleosol sequences at Roxolany (Ukraine). *Palaeogeography, Palaeoclimatology, Palaeoecology* 143, 111-133.
- Tsatskin, A., Heller, F., Virina, E.I., Spassov, S., Du Pasquier, J., Hus, J., Hailwood, E.A., Bagin, V.I., Faustov, S.S., 2001. A new scheme of terrestrial paleoclimate evolution during the last 1.5 Ma in the western Black Sea region: Integration of soil studies and loess magnetism. *Physics and Chemistry of the Earth (A)* 26 (11-12), 911-916.
- Tyráček, J., 2006. Okraj Skandinávského Zalednění v Moravské Bráně (Margin of the Scandinavian glaciation in the Moravian Gate). In: Česká geologická služba (Eds.), *Zprávy o geologických výzkumech v roce 2006*, 97-101 (in Czech with English summary).
- Vandenberghe, J., 1995. Timescales, climate and river development. *Quaternary Science Reviews* 14, 631–638.
- Vandenberghe, J., Woo, M.-k., 2002. Modern and ancient periglacial river types. *Progress in Physical Geography* 26, 479-506.
- Veklitch M.F., 1982. Paleogeographical stages and stratotypes of the Upper Cenozoic soil formations in Ukraine. *Naukova Dumka, Kiev* (in Russian).
- Velichko, A.A., 1990. Loess-Paleosol formation on the Russian Plain. *Quaternary International* 7/8, 103-114.
- Xiao, J., Porter, S., An, Z., Kumai, H., Yoshikawa, S., 1995. Grain size of quartz as an indicator of winter monsoon strength on the loess plateau of central China during the last 130,000 yr. *Quaternary Research* 43, 22-29.
- Yang, S., Ding, F., Ding, Z., 2006. Pleistocene chemical weathering history of Asian arid and semi-arid regions recorded in loess deposits of China and Tajikistan. *Geochimica et Cosmochimica Acta* 70, 1695-1709.

Appendix

Table 1-S1. Floodplain sediment samples of the “FOREGS”-dataset (Salminen et al., 2005), assigned to respective source areas. F-AA: Floodplain sediments of Danube tributaries originating from the area of the Austroalpine cover nappes. F-Drava: Floodplain sediments of the Drava River and its tributaries, dominated by crystalline or metamorphic material. F- BM: Floodplain sediments of Danube tributaries with source in the Bohemian Massif. F-WC: Floodplain sediments of rivers, draining the Western Carpathian mountains. For more detailed description of the “source areas” see Section 3.

| Sample | Longitude | Latitude | „Source area“ |
|----------|-----------|----------|---------------|
| N32E06F2 | 10.69250 | 47.47028 | F-AA |
| N32E07F1 | 13.73778 | 47.78667 | F-AA |
| N32E07F2 | 12.65806 | 47.74306 | F-AA |
| N32E07F5 | 12.73167 | 47.66278 | F-AA |
| N32E08F2 | 14.76278 | 47.675 | F-AA |
| N33E05F3 | 10.100 | 48.160 | F-AA |
| N33E06F2 | 10.87 | 48.51 | F-AA |
| N33E06F5 | 11.77 | 48.86 | F-AA |
| N31E09F1 | 17.3683 | 45.9850 | F-Drava |
| N31E10F2 | 18.1570 | 45.8072 | F-Drava |
| N32E07F3 | 12.59028 | 46.92778 | F-Drava |
| N32E08F3 | 15.53306 | 46.77333 | F-Drava |
| N32E08F5 | 14.51167 | 46.74694 | F-Drava |
| N32E09F5 | 16.63018 | 46.46813 | F-Drava |
| N33E07F4 | 12.71 | 49.22 | F-BM |
| N33E08F1 | 16.46583 | 48.82389 | F-BM |
| N33E08F2 | 15.99194 | 49.20861 | F-BM |
| N33E08F3 | 15.59806 | 48.85750 | F-BM |
| N33E09F1 | 18.07 | 48.9 | F-WC |
| N33E09F2 | 18.75 | 49.25 | F-WC |
| N33E10F2 | 18.89 | 48.11 | F-WC |
| N33E10F3 | 19.17 | 49.14 | F-WC |
| N33E10F4 | 20.20 | 48.29 | F-WC |
| N33E10F5 | 19.56 | 48.80 | F-WC |
| N33E11F1 | 21.92 | 48.93 | F-WC |
| N33E11F2 | 20.99 | 48.87 | F-WC |
| N33E11F3 | 21.35 | 48.60 | F-WC |
| N33E11F5 | 21.75 | 48.76 | F-WC |

Batajnica / Stari Slankamen

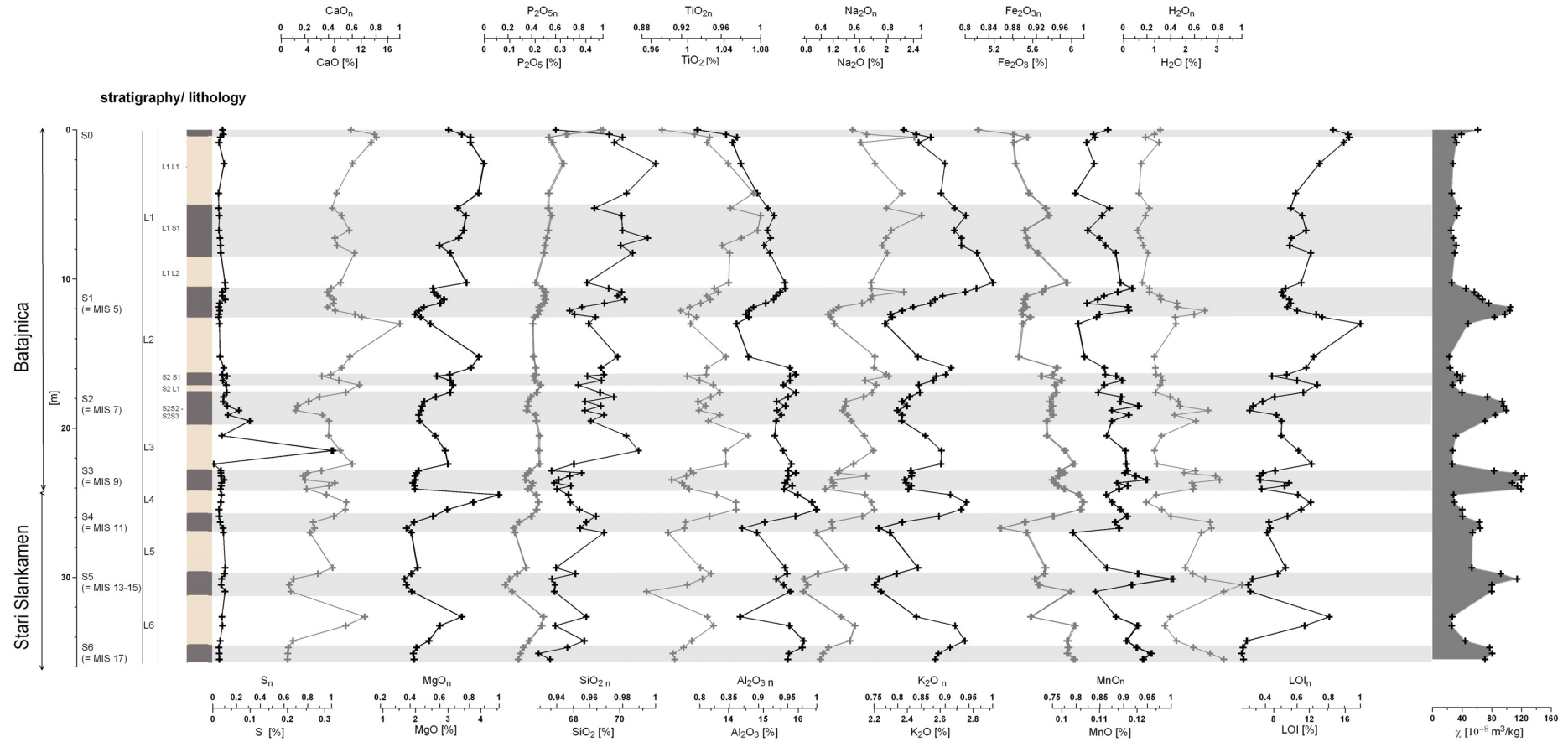


Fig. 1-S1. Major element composition of Batajnica/Stari Slankamen section. Data are corrected for calcite, dolomite and gypsum according to 1, except for MgO, CaO H₂O, and LOI (loss on ignition at 1000 °C). Second x-axes (index: n) show normalization of the data on profile maximum value of the respective variable. Magnetic susceptibility (χ) data are redrawn from Buggle et al. (2009).

Mircea Voda

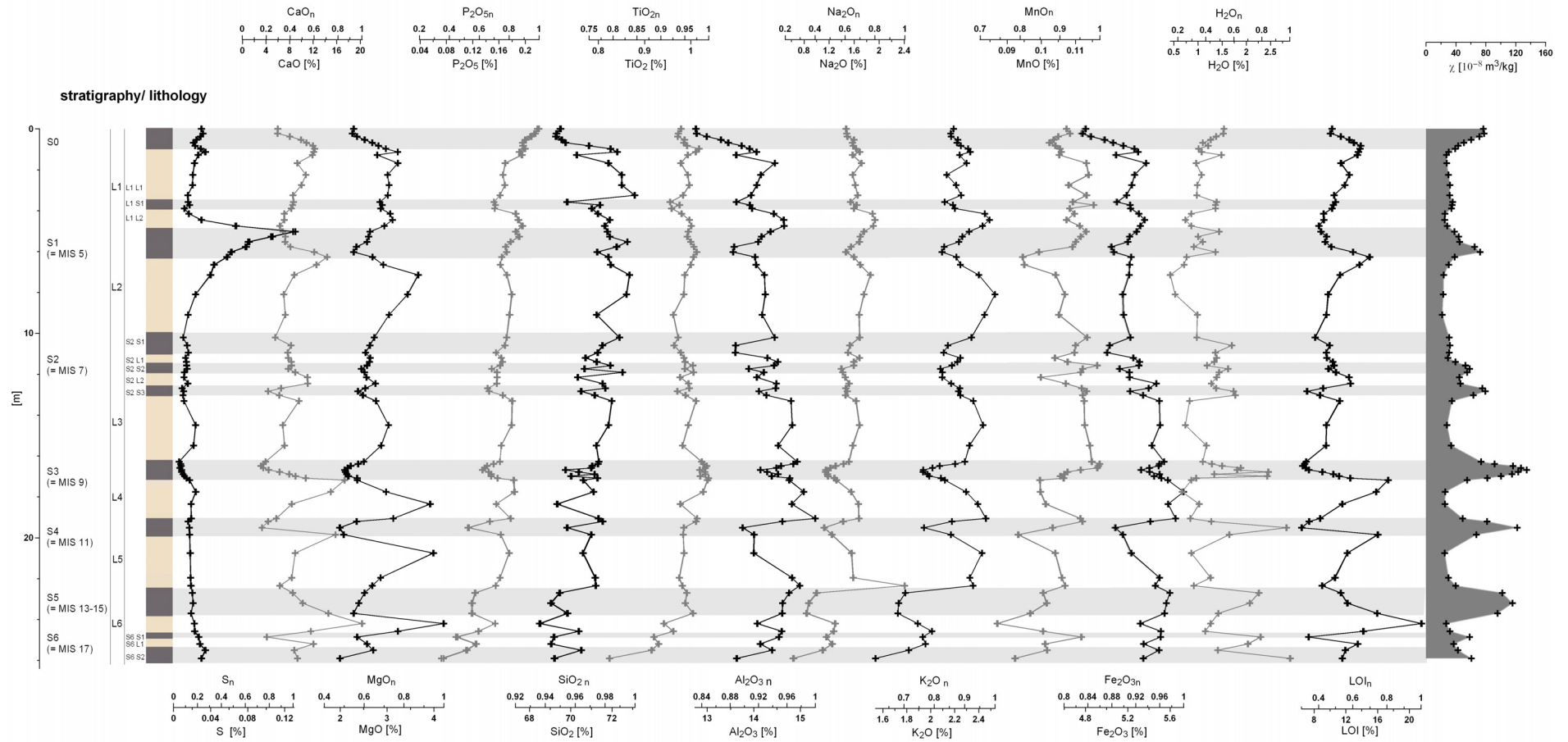


Fig. 1-S2. Major element composition of the Mircea Voda section. Data are corrected for calcite, dolomite and gypsum according to 1, except for MgO, CaO H₂O, and LOI (loss on ignition at 1000 °C). Second x-axes (index: n) show normalization of the data on profile maximum value of the respective variable. Magnetic susceptibility (χ) data are redrawn from Bugge et al. (2009).

Stary Kaydaky

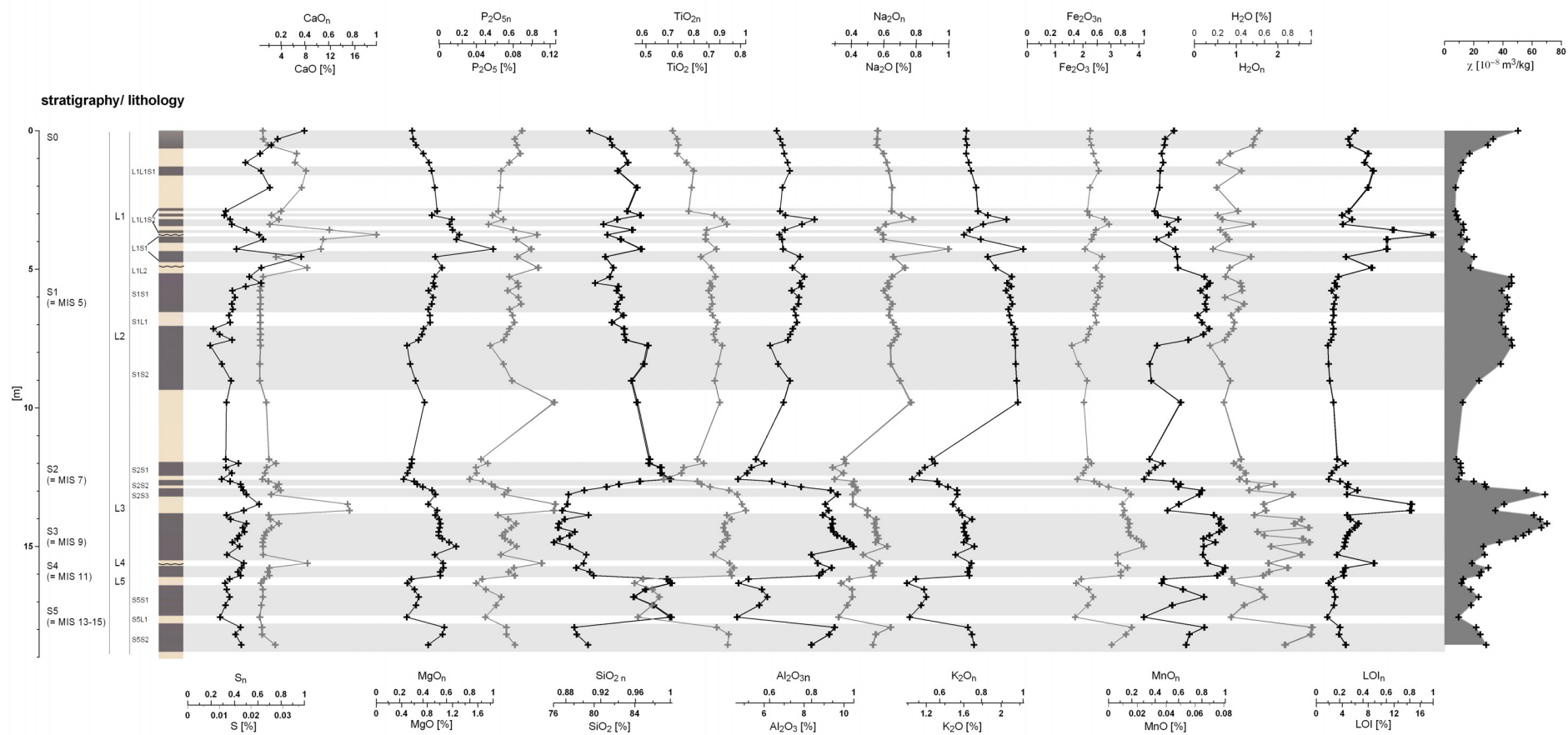


Fig. 1-S3. Major element composition of the Stary Kaydaky section. Data are corrected for calcite, dolomite and gypsum according to 1, except for MgO, CaO H₂O, and LOI (loss on ignition at 1000 °C). Second x-axes (index: n) show normalization of the data on profile maximum value of the respective variable. Magnetic susceptibility (χ) data are redrawn from Buggle et al. (2009).

Batajnica / Stari Slankamen

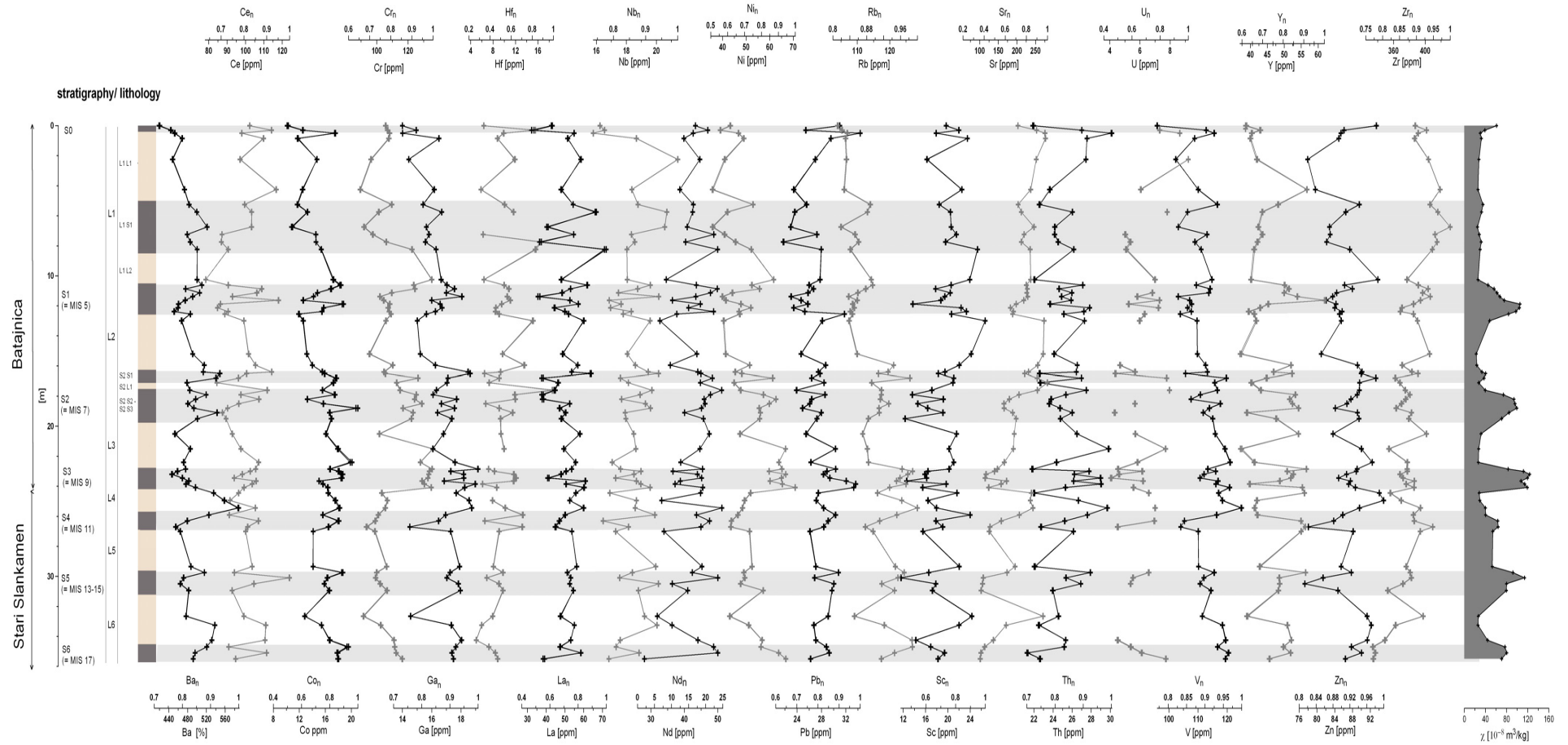


Fig. 1-S4. Trace element composition of Batajnica/Stari Slankamen section. Data are corrected for calcite, dolomite and gypsum according to 1. Second x –axes (index: n) show normalization of the data on profile maximum value of the respective variable. Magnetic susceptibility (χ) data are redrawn from Buggle et al. (2009).

Mircea Voda

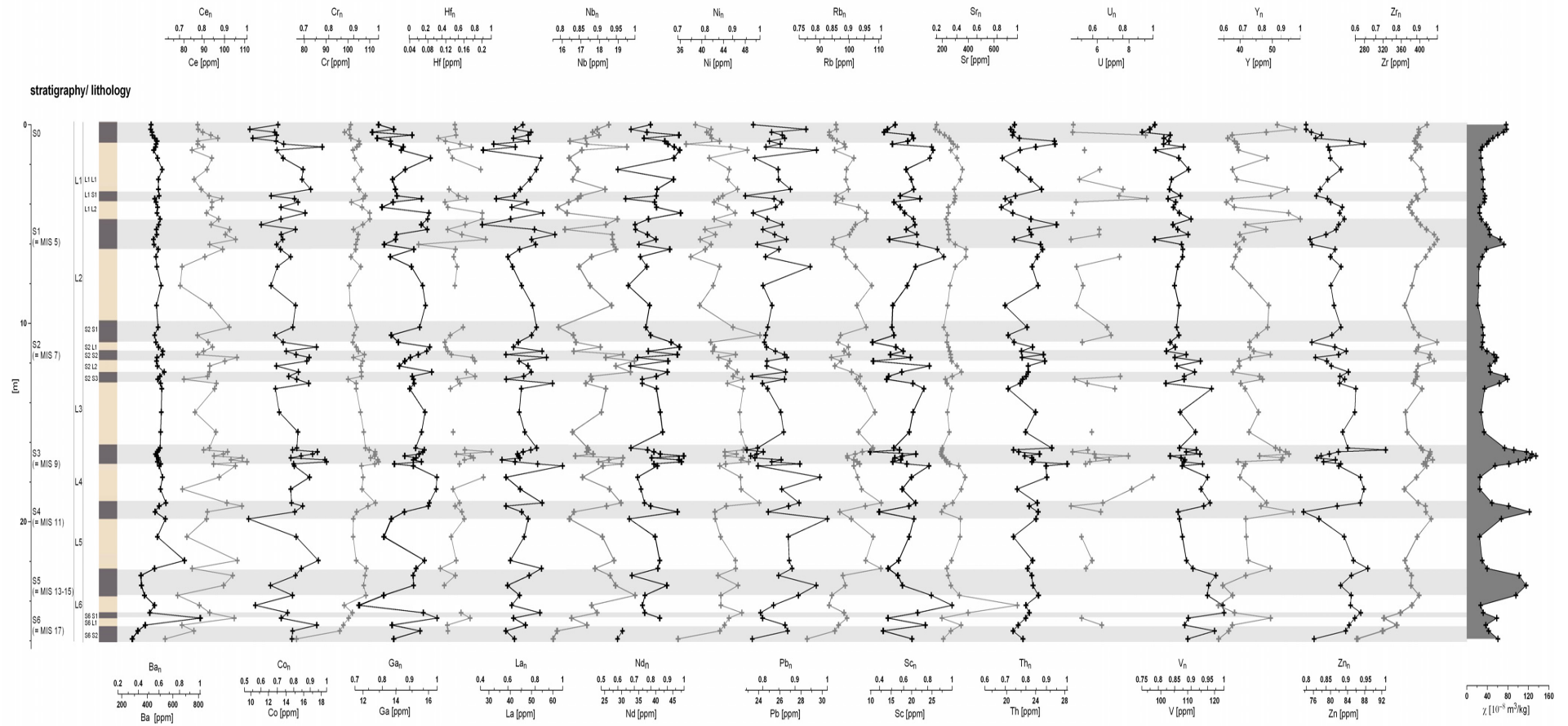


Fig. 1-S5. Trace element composition of the Mircea Voda section. Data are corrected for calcite, dolomite and gypsum according to 1. Second x-axes (index: n) show normalization of the data on profile maximum value of the respective variable. Magnetic susceptibility (χ) data are redrawn from Bugge et al. (2009).

Stary Kaydaky

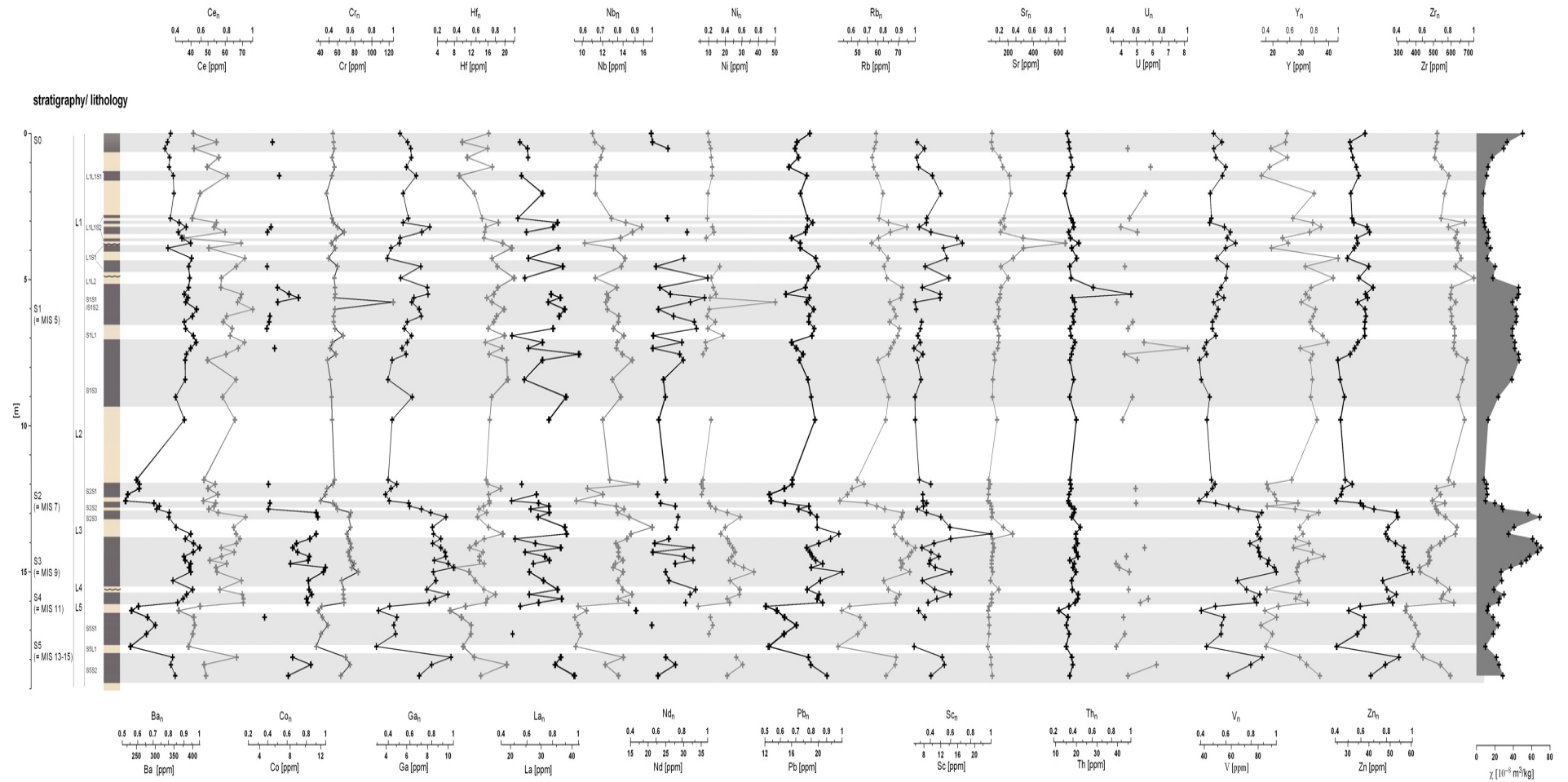


Fig. 1-S6. Trace element composition of the Stary Kaydaky section. Data are corrected for calcite, dolomite and gypsum according to 1. Second x-axes (index: n) show normalization of the data on profile maximum value of the respective variable. Magnetic susceptibility (χ) data are redrawn from Buggle et al. (2009).

Study 2

Stratigraphy and spatial and temporal paleoclimatic trends in Southeastern/Eastern European loess-paleosol sequences.

Björn Buggle¹, Ulrich Hambach², Bruno Glaser¹, Natalia Gerasimenko³, Slobodan Marković⁴,
Irina Glaser² and Ludwig Zöller²

¹ Soil Physics Department, University of Bayreuth, D-95440 Bayreuth, Germany.

² Chair of Geomorphology, University of Bayreuth, D-95440 Bayreuth, Germany.

³ Earth Science and Geomorphology Department, Tarasa Shevchenko National University of Kyiv, Ukraine.

⁴ Quaternary Research Center, University of Novi Sad, Faculty of Sciences, Trg Dositeja Obradovića 3, Serbia.

Published in

Quaternary International 196, 86-106.

2009

Corresponding author: Björn Buggle, Phone:+49(0)921 552174
E-mail: Bjoern.Buggle@uni-bayreuth.de

Abstract

The loess-paleosol sections Batajnica/Stari Slankamen (Serbia), Mircea Voda (Romania) and Stary Kaydaky (Ukraine) are presently located in areas of different types of steppe, being highly sensitive for recording climatic changes. In this paper, we present a stratigraphy for these three Southeastern/Eastern European sections, based on pedostratigraphy and correlation of recently obtained susceptibility records with susceptibility data of other sections of the area (Koriten, Mostistea, Vyazivok), of the Chinese Loess Plateau and with the benthic $\delta^{18}\text{O}$ record of ODP 677. Six pedocomplexes were studied at the Serbian and Romanian section and five at the Ukrainian section. The oldest one being investigated is related to Marine Isotope Stage (MIS) 17 to 18 and MIS 13-15 for Stary Kaydaky, respectively. Some points of discussion, concerning existing chronostratigraphies of Bulgaria, Ukraine and China are developed.

The comparative study of the profiles allows to trace paleoclimatic and paleoenvironmental changes in Southeastern/Eastern Europe in time and space. Reconstruction of paleoprecipitation based on susceptibility-rainfall relationship and calculations of sedimentation rates are evaluated.

Keywords: Loess, paleosols, stratigraphy, susceptibility, sedimentation rate, paleoprecipitation, Southeastern Europe, Serbia, Romania, Ukraine, Danube, Dnieper.

1 Introduction

Mid-latitude loess originated from silty material blown out of sparsely vegetated areas during dry and cold periods of the Pleistocene. These so-called glacial periods are characterized by extensive glaciations of continental land masses, whereas during the interglacials and mostly also interstadials soil formation prevailed. Thus, the alternation of cold and warm periods throughout the Quaternary led to the formation of loess-paleosol sequences (LPSS), which potentially provide continuous, paleoclimatic and paleoenvironmental information. Therefore, LPSS are one of the most valuable terrestrial archives especially for Southeastern and Eastern Europe, due to their widespread occurrence along the banks of the Danube and Dnieper rivers. Thus, this area was already object of various studies. Origin and distribution of Danube loess was reviewed by Smalley and Leach (1978) already almost 30 years ago and recently new investigated by Bugge et al. (2008) and Újvári et al. (2008). In Serbia, the first description of a LPSS was by Marsigli (1726) (see also Marković et al., 2004a). A milestone in regional loess research was the contribution of Marković-Marjanovic (1968) to the activities of the INQUA loess commission, attracting attention of the post-war scientific community to the Serbian loess sections. Latest works of Kostić and Protić (2000), Marković et al. (2004b, c, 2005, 2006, 2007, 2008, 2009) and Fuchs et al. (2008) put the Serbian loesses in a Eurasian context. The former presented paleoclimatic implications based on mineralogy and grain size analyses of two Serbian sections for a time span of more than 700 ka. The latter gave paleoclimatic reconstructions using malacology and a revision of the chronology of Serbian LPSS based on magnetic susceptibility and amino acid racemization. Also, the various works of Bronger (1976; 2003) have to be highlighted, since he presented a detailed paleopedological investigation and a classification of the paleosols of the Carpathian basin by means of micromorphology. Furthermore, he provided a first attempt of trans-continental stratigraphic correlation between European and Asian loess regions. For the lower Danube,

one can look back to more than 100 years of loess research (Conea, 1969). For this area fundamental descriptions were done by Haase and Richter (1957), Conea (1969) and Minkov (1970). Jordanova and Petersen (1999a, b), Panaiotu et al. (2001) and Jordanova et al. (2007) presented detailed environmental and rock magnetic research and published one of the first stratigraphies for Bulgarian and Romanian sections using magnetic susceptibility. In Ukraine, the first prominent study on loess stratigraphy was carried out by Krokos (1932), later being extensively developed by Veklich (1969, 1993). Paleoenvironments of the Ukrainian Quaternary have also been profoundly investigated (Matviishina, 1982; Veklich and Sirenko, 1982; Sirenko and Turlo, 1986; Gerasimenko, 1988; 2004; 2006; Rousseau et al., 2001). However, most of the existing studies either focused on a single LPSS-section or dealt with paleoclimatic records of only the last few glacial cycles or are lacking of a reliable stratigraphic model.

This study considered LPSS sites in Serbia (Batajnica/Stari Slankamen), Romania (Mircea Voda) and Ukraine (Stary Kaydaky). These sites were thought to bear far back reaching paleoclimatic records. Since the sections are presently located in areas of different kinds of steppe and rather close to the temperate forest and submediterranean types of vegetation (Frey and Lösch, 1998), respectively, they are supposed to be sensitive to climatic changes. On the one hand, the studied sections cover different types of climate zones following a gradient of increasing aridity towards the Black Sea coast. On the other hand, they form a W-E transect across the region, thus, giving the possibility of Late and Mid-Pleistocene climate reconstruction in space and time.

Our purposes are

- 1) to set up a stratigraphy for these prominent Southeastern European paleoclimate archives based on pedostratigraphy and correlations of the magnetic susceptibility records with those of Chinese stratotype sections and with the $\delta^{18}\text{O}$ record of benthic foraminifera of ODP 677 as proxy for the global ice volume. The obtained stratigraphy will be validated

by correlations to other dated sections of the region and, respectively, may give evidences clarifying ambiguous points in existing stratigraphic models of the region. A reliable stratigraphy is required for further paleoclimatic studies in this area.

- 2) to calculate sedimentation rates and to evaluate their informative value.
- 3) to give a tentatively paleoclimatic interpretation of the magnetic susceptibility record and to evaluate the use of the susceptibility-rainfall equation of Maher et al. (1994) for the Danube and Dnieper loess area.

2 Principles of susceptibility enhancement in (paleo-)soils

Generally, the magnetic susceptibility is controlled by the amount and composition of iron-bearing para-, and ferromagnetic (s.l.) minerals and their grain-size distribution. Focusing on iron oxides and oxyhydroxides, as the most common iron-bearing compounds in soils without influence of water-logging, special attention has always to be drawn to the so-called ferrimagnetic minerals (magnetite and maghemite). The susceptibility of these minerals are several magnitudes higher ($4\text{-}5 \cdot 10^{-4} \text{ m}^3 \text{ kg}^{-1}$) than of the so-called antiferromagnetic minerals hematite and goethite ($6\text{-}7 \cdot 10^{-7} \text{ m}^3 \text{ kg}^{-1}$) (Thompson and Oldfield, 1986). Thus, even small amounts of these ferrimagnetics, which are predominantly formed during pedogenesis, significantly influence total magnetic susceptibility.

Besides mineralogy, magnetic susceptibility is also controlled by grain size. Intense research in Eurasian loesses has demonstrated that magnetic grains of superparamagnetic size (SP) ($< \sim 30 \text{ nm}$) are predominant in paleosols, and single-domain (SD) and multidomain-grains (MD) ($> \sim 30 \text{ nm}$) prevail in loesses (Evans and Heller, 2003). The term “single”- or “multidomain” grain means that there exist only one or several regions with parallel coupled atomic magnetic moments, respectively. Below a certain size, no stable domain can exist (superparamagnetism, Thompson and Oldfield, 1986). The susceptibility of a mineral is highest in the SP-fraction, because these particles align instantaneously to any ambient field.

The susceptibility of magnetite grains with 0.023 μm diameter is, for example, about three times higher than that of magnetite grains with 0.5 μm diameter (Tang et al., 2003). Thus, magnetic susceptibility can reflect intensity of pedogenesis, as it has been observed at the Chinese loess sequences (Heller and Liu, 1984). The models dealing with the enhancement processes are essential for understanding the direct mineralogical reasons for magnetic susceptibility enhancement. The formation of ferrimagnetic minerals in the course of pedogenesis is the most important mechanism. Its rate and the equilibrium between the formation of magnetite/maghemite and other Fe-minerals is controlled by conditions in the soil environment such as temperature, moisture (alternating wet and dry periods), pH and content of organic matter (Evans and Heller, 2001). The most widely accepted model (Thompson and Oldfield, 1986; Maher, 1998; Evans and Heller, 2001; Chen et al. 2005;) assumes, as first step, alternating reducing and oxidizing conditions leading to a release of Fe^{2+} from the weathering of Fe minerals and subsequent ferrihydrite ($5\text{Fe}_2\text{O}_3 \times 9\text{H}_2\text{O}$) formation. With excess of Fe^{2+} in solution an intermediate $\text{Fe}^{2+}/\text{Fe}^{3+}$ compound is formed. For this step, the relevance of iron-reducing bacteria is stressed by several authors (Chen et al., 2005; Evans and Heller, 2001; Maher 1998). Prerequisite for this biologically induced mineralization is a sufficient content of organic matter for microbial respiration. As third step, magnetite of predominantly superparamagnetic size is formed by dehydration of the $\text{Fe}^{2+}/\text{Fe}^{3+}$ intermediate at moderately oxidizing conditions. Magnetite is still susceptible for dissolution. Only further oxidation to maghemite results in a more stable ferrimagnetic mineral (Maher, 1998). Other mechanisms contributing to susceptibility enhancement of soils are the fire-induced formation of ferromagnetics, the relative enrichment due to carbonate leaching or biologically induced mineralization by magnetotactic bacteria (Evans and Heller, 2001; Tang et al. 2003).

3 Regional setting

3.1 Batajnica / Stari Slankamen (Serbia)

The Batajnica section (44° 55' 29'' N, 20° 19' 11'' E, Fig. 2-) is situated along the Danube River bank about 12 km north of Belgrade. The sequence is about 40 m thick and contains at least six strongly developed pedocomplexes. The lowermost pedocomplex is already below the Danube level and was only outcropped for a short time in a trench. The three lowermost pedocomplexes are influenced by water logging. Since this lead to changes in mineralogical composition, resulting in a disturbance of the magnetic susceptibility record (Evans and Heller, 2001), we sampled these pedocomplexes at Stari Slankamen, where water logging is absent. The Stari Slankamen section (45° 7' 58'' N, 20° 18' 44'' E, Fig. 2-1) is located about 45 km upstream of Batajnica at the right bank of the Danube river opposite to the confluence of the Tisza and Danube river. Below the pedostratigraphic analog to the sixth pedocomplex of Batajnica, the Stari Slankamen section contains at least four older loess-paleosol couples (Bronger, 1976), which, however, were buried by colluvial deposits and thus only exposed during the sampling period. Tertiary lime-, and sandstones form the base of the Quaternary sequence (Bronger, 1976).

Both, the Batajnica and Stari Slankamen site, are situated in the Vojvodina – the Serbian part of the Pannonian Basin.

The climatic data of the nearby station Belgrade (Fig. 2-2) show a mean annual precipitation of 683 mm. According to the Köppen classification system (Sträbler, 1998), the area has a Cfb climate with strong tendency to Cfa. Despite the absence of a prominent drought period, August can be still regarded as a dry period. According to Walter (1974), this is characteristic of a forest-steppe type of climate. This kind of vegetation is typical for the dry central Pannonian basin. It is replaced by submediterranean and supramediterranean thermophile mixed oak forests (*Quercion pubescenti*) near the Carpathian Mountains (Fig. 2-1).

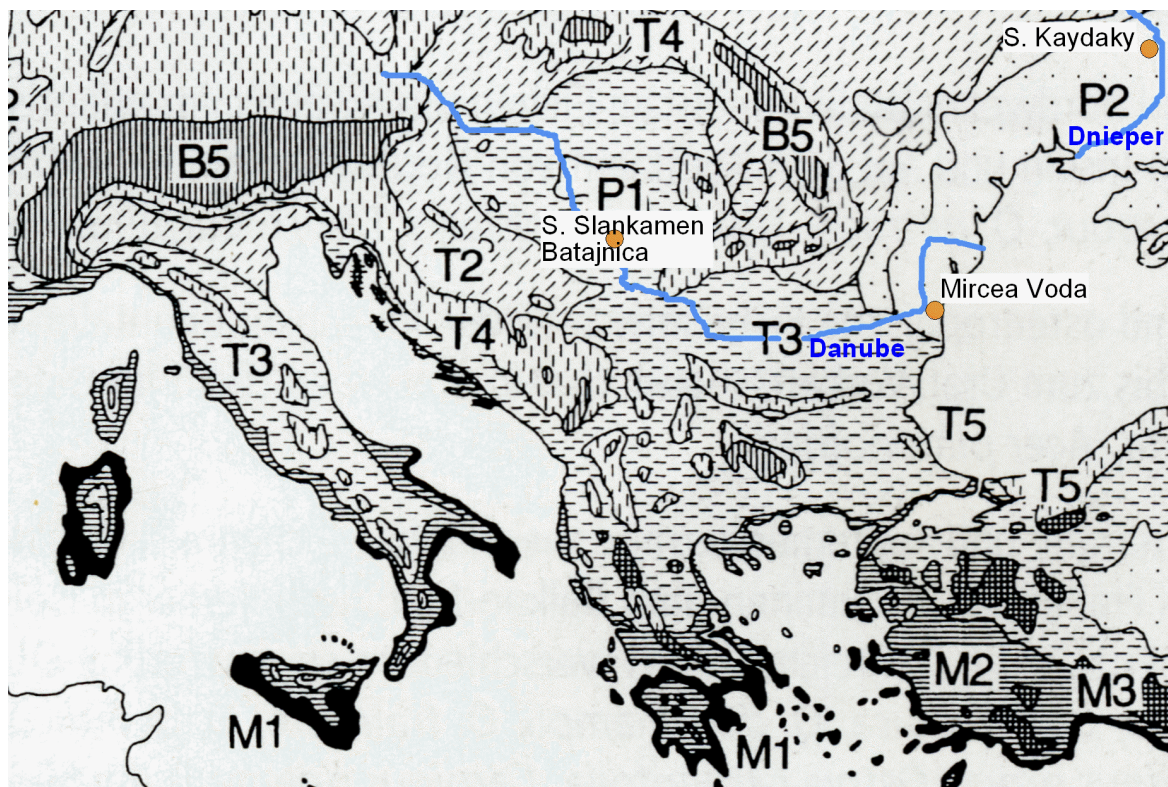


Fig. 2-1. Location of the investigated loess-paleosol sequences; map of current potential vegetation for Southeastern Europe (Frey and Lösch, 1998, modified). B5: Mountainous and subalpine coniferous forest and krummholz-shrubbery, M1: Thermomediterranean oak forest and olive-carob shrub-forest, M2: Mesomediterranean holm- oak forest, M3: Submediterranean and mediterranean xerotherme coniferous forest, P1: Forest steppe, P2: Feather-grass steppe, T2: Middle-, and Eastern-European mixed oak forest, T3: Submediterranean und supramediterranean thermophile mixed oak forest, T4: West-, Middle -, and Southeastern European common beech - and common beech - fir forest, T5: Euxinian orient-oak forest.

3.2 Mircea Voda (Romania)

The section of Mircea Voda ($44^{\circ} 19' 15''$ N, $28^{\circ} 11' 21''$ E, Fig. 2-1) is located in the Dobrudja plateau (Romania) at a distance of about 13 km from the Danube and 40 km from the Black Sea coast. About 30 m of Quaternary aeolian deposits including six strongly developed pedocomplexes can be observed. The loess-paleosol successions overlie limnic sediments of presumably lower Pleistocene age (Domokos et al., 2000) on Tertiary and Mesozoic sediments.

The climatic station of Constanta recorded a mean annual precipitation of 396 mm. Due to strong northerly winds prevailing most of the year (Jordanova and Petersen, 1999a), the

regional climate is characterized by hot and dry summers, i.e. Cfa-climate with six months of dryness and three months of drought (Fig. 2-2). This favors feather-grass steppe vegetation (Fig. 2-1, Walter, 1974). According to Mavrocordat (1971), the actual mean annual temperature for Mircea Voda (station Cernavoda in about 10 km distance from Mircea Voda) was 0.5 °C higher and the mean annual precipitation was 57 mm higher than for Constanta, resulting in only 4 months of dryness (in the observation periods 1896-1915 and 1921-1955).

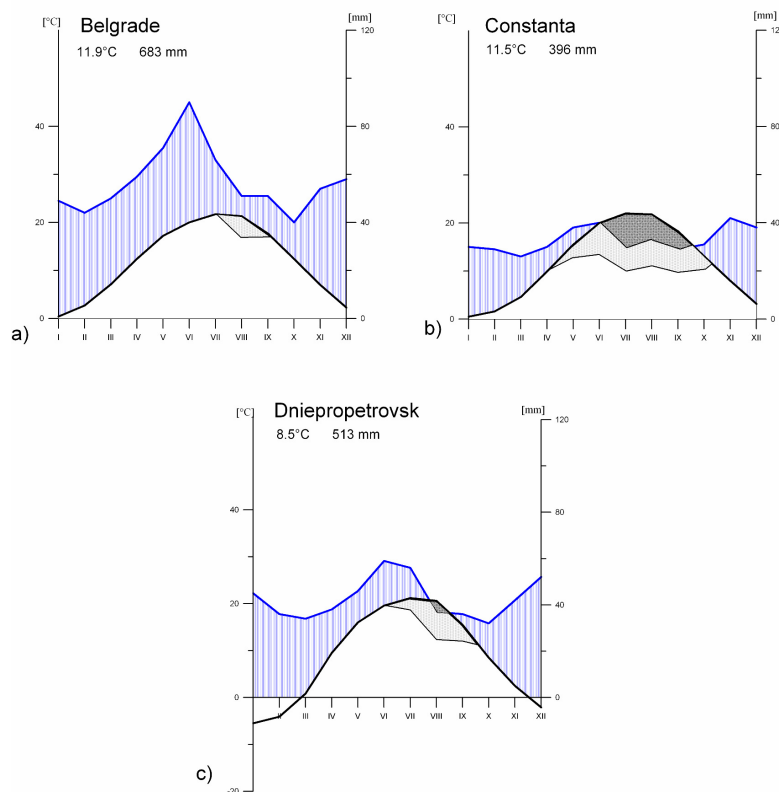


Fig. 2-2. Climate diagrams of a) Belgrade (Serbia), b) Constanta (Romania) and c) Dniepropetrovsk (Ukraine). The diagrams were created on basis of the climatological normals for the period 1961-1990 (WMO, 1996). The heavily dotted area marks months with average precipitation being less than twice the value of the average temperature. This indicates periods of drought according to Walter (1974). The slightly dotted areas show months with average precipitation being less than three times the value of average temperature. This characterizes periods of dryness.

3.3 Stary Kaydaky (Ukraine)

The large “balka” (Russian term for gently sloping gully in loess) with its system of younger ravines, reaching the Dnieper River near the village Stary Kaydaky (48° 22′ 42″ N, 35° 07′

30' E, about 2 km S from Dniepropetrovsk city, Fig. 2-1), has multiple outcrops of at least five different pedocomplexes. Some of the outcrops have been primarily investigated as key sections of the Ukrainian Quaternary (Veklich and Sirenko, 1982). At Stary Kaydaky, special care had to be given to hiatus. For instance, the Vytachiv pedocomplex (MIS 3) was eroded at the main sampling site and, thus, has been sampled separately, few hundred meters aside. The climate of the area can be classified as Dfb-type, with a drought period of one month, and a period of dryness of three months (Fig. 2-2). This site is climatically intermediate between Batajnica/Stari Slankamen and Mircea Voda, which is also reflected by the character of the vegetation. Walter (1974) described the area around Dniepropetrovsk as so-called Northern feather-grass steppe (Hygroherbeto-Stipetum), relatively wet and rich in herbs. About 120 km to the north, the feather-grass steppe is replaced by forest steppe. The aridity gradually increases southwards to the Black Sea coast. Together these three locations cover a range of different steppe conditions (Fig. 2-1), following precipitation gradients towards the Black Sea coast.

4 Methods

As further investigations will focus on paleopedology, pedocomplexes were sampled with higher resolution than the loesses. Samples of the pedocomplexes were taken in 10 to maximum 50 cm intervals, depending on horizontation and thickness of a unit. We took at least ten samples for each of the younger paleosols (i.e. the uppermost three interglacial pedocomplexes) and at least three samples for each of the older ones. The intercalated loesses were sampled by about three representative samples corresponding to individual loess layers. All our samples were stored in air-tight plastic bags and dried at 40 °C in the laboratory. The material was then packed in 6 cm³ plastic boxes and magnetic susceptibility measurement was carried out using a KLY-3 Kappabridge of Agico (Brno, Czech Republic) at 0.875 kHz and 300 A/m. For normalization on density of the packed material and for better comparison with

literature data, the susceptibility values were expressed as mass-specific susceptibility (m^3/kg). The minimum susceptibilities of the pure loess units of each profile were taken as background susceptibilities.

Field and working nomenclature of the stratigraphic units is similar to the Chinese system, using the following abbreviations for the lithological units: Main paleosols/pedocomplexes—‘Sx’, main loess layers—‘Lx’, with ‘x’ being the stratigraphic number of the soil or loess, starting from the youngest soil. For instance, S0 corresponds to the recent soil, S1 to the first main pedocomplex from the top, L1 means the main loess unit above S1 and so on. Subunits of the individual pedocomplexes are abbreviated as SxSy for a paleosol (also regarded as pedomember) and SxLy₊₁ for an intercalated loess layer, with y=1 for the uppermost soil of a pedocomplex. Within main loess units, intercalated weak paleosols are marked with LxSz, with z=1 for the youngest paleosol of a loess unit. However, we also added prefixes designating to the locality of the sections i.e. SK for Stary Kaydaky and MV for Mircea Voda. For Batajnica/Stari Slankamen the prefix V was used, referring to the standard pedostratigraphic framework of the Vojvodina region (Marković et al., 2008; Marković et al., 2009).

To derive a chronostratigraphy for the studied sections, the magnetic susceptibility curve was correlated with the astronomically tuned stacked records of Lingtai and Zhaojiachuan of the Chinese Loess Plateau (Sun et al., 2005), and the benthic $\delta^{18}\text{O}$ values of ODP site 677, situated in the Eastern tropical Pacific ($1^{\circ}12'\text{N}$, $83^{\circ}44'\text{W}$, Shackleton et al., 1990). Wherever no clear bench marks in the ODP-record were found for correlating our susceptibility record, a $\delta^{18}\text{O}$ value of 4.5 ‰ was used to determine age boundaries between major warm and cold stages, following Vidic et al. (2004). The obtained chronostratigraphy was validated against existing chronostratigraphic models of other LPSS in the region such as Ruma (Serbia, Marković et al., 2006), Koriten (NE Bulgaria, Jordanova and Petersen, 1999b), Mostistea (SE

Romania, 44.16° N, 26.83° E; Panaiotu et al, 2001) and Vyazivok (Dnieper plain, 49° 198' N, 32° 58.8' E; Rousseau et al., 2001

For paleoclimatic deductions, paleorainfall we calculated by using Eq. (1) according to Maher et al. (1994).

$$\text{MAP (mm/yr)} = 222 + 199 \log_{10}[(\chi_B \cdot \chi_C) 10^{-8} \text{ m}^3 \text{ kg}^{-1}] \quad (1)$$

where χ_B is the susceptibility of the subsoil and χ_C the background susceptibility of the loess.

Sedimentation rates were only calculated for the Mircea Voda section due to several hiatus in the Stary Kaydaky LPSS and due to the Serbian LPSS, being composed from LPSS of two sites with possibly different rates of dust deposition. Calculating sedimentation rates, one is generally confronted with the problem that the lower boundary of a soil does not reflect the upper boundary of the sediments deposited during the preceding cold and dry period. Hence, we calculated sedimentation rates, assuming two different worst case scenarios. Variant A took into account the fact that dust accumulation may still exist during soil development (synpedogenetic sedimentation) and the thickness of paleosols was completely attributed to interglacial dust deposition. Variant B assumed dust accumulation being only restricted to cold stages. Consequently, each portion of material comprising both, loess layer and the associated overlying pedocomplex, was fully attributed to a cold stage. For better comparison with literature data, sedimentation rates were first calculated using the timescale of Koriten (JP-99b), developed by Jordanova and Petersen (1999b). To test the sensitivity to uncertainties in the age model, calculated sedimentation rates were based on

- 1) correlation to the benthic $\delta^{18}\text{O}$ record of ODP site 677 (Sh-90; Shackleton et al., 1990);
- 2) correlation to the susceptibility record of Sun et al. (2006; Su-06);
- 3) the timescale of Jordanova and Petersen (1999b) for the Koriten site (lower Danube basin, Bulgaria);
- 4) the timescale of Heslop et al. (2000) (He-00), derived from the astronomical tuning of the Baoji (China) grain size record and the Luochuan susceptibility record; and

- 5) an age model of the marine isotope events, developed at the planktonic $\delta^{18}\text{O}$ record of core MD900963 (Maldives area, Indian Ocean; Bassinot et al., 1994; Ba-94).

These different timescales represent studies in various regions of the earth with different well established methods for setting up a Quaternary climate- and chronostratigraphy. However, each of the studied regions and applied methods differs in its sensitivity for recording climatic changes. Only for the last glacial cycle a supposedly more reasonable and accurate timescale for Europe was available in Guiter et al. (2003). In all calculations, age boundaries for MIS 2 - 5 were taken from this review of various West and Central European terrestrial records. The lower boundary of the recent soil was set to 11.5 ka according to the Younger Dryas - Preboreal boundary, given by Litt et al. (2001) for Central Europe. Although these compiled datasets from more proximal terrestrial records were used, some minor uncertainties cannot be excluded, since age boundaries of climatic stages are probably not synchronous within all parts of Europe. Furthermore, ages derived from dating of the lower boundaries of paleosols are probably overestimating the duration of warm periods as emphasized before. For the purpose of clarity no further sensitivity analyses with respect to these aspects was carried out. An overview of the applied timescales is given in Table 2-1.

Table 2-1. Overview on the different timescales for Mid-Pleistocene LPSS and major isotope stages, respectively, applied for sensitivity analyses of sedimentation rates.

| Base of / lower boundary of | Timescale based on Jordanova and Petersen (1999b) [ka] | Duration [ka] | Timescale based on correlation to Sun et al. (2006) [ka] | Duration [ka] | Timescale based on correlation to Shackleton et al. (1990) [ka] | Duration [ka] | Timescale based on Heslop et al. (2000) [ka] | Duration [ka] | Timescale based on Bassinot et al. 1994 [ka] | Duration [ka] |
|-----------------------------|--|---------------|--|---------------|---|---------------|--|---------------|--|---------------|
| L2 / MIS 6 | 180 | 54 | 162 | 33 | 188 | 62 | 196 | 70 | 186 | 60 |
| S2 / MIS 7 | 245 | 65 | 258 | 70 | 247.5 | 59.5 | 250 | 54 | 242 | 56 |
| L3 / MIS 8 | 280 | 35 | 275 | 17 | 280 | 32.5 | 290 | 40 | 301 | 59 |
| S3 / MIS 9 | 331 | 51 | 340 | 65 | 333.5 | 53.5 | 342 | 52 | 334 | 33 |
| L4 / MIS 10 | 357 | 26 | 388 | 48 | 373 | 39.5 | 386 | 44 | 364 | 30 |
| S4 / MIS 11 | 410 | 53 | 427 | 39 | 416 | 43 | 417 | 31 | 427 | 63 |
| L5 / MIS 12 | 470 | 60 | 474 | 47 | 453 | 37 | 503 | 86 | 474 | 47 |
| S5 / MIS 13-15 | 620 | 150 | 623 | 149 | 623 | 170 | 625 | 122 | 621 | 147 |
| L6 / MIS 16 | 671 | 51 | 683.5 | 60.5 | 668.5 | 45.5 | 693 | 68 | 659 | 38 |

5 Results

5.1 Magnetic susceptibility variations

For all three profiles, the magnetic susceptibility record follows generally the lithology (Fig. 2-3), being enhanced in the paleosols compared to the parent loess. The background susceptibility for Batajnica/Stari Slankamen and Mircea Voda are about two times higher than for the Stary Kaydaky section, in spite the older loesses at Stary Kaydaky (>SK-L2) showing more pedogenic alteration.

The LPSS of Batajnica/Stari Slankamen has a background susceptibility of $22 \cdot 10^{-8} \text{ m}^3 \text{ kg}^{-1}$. Pedogenic alteration may be the reason for a relative high susceptibility at the upper and lower part of the V-L5. The strongest susceptibility enhancement can be observed in the V-S3 and the V-S5, whereas relative weak enhancement can be found in V-S6, V-S4 and V-L1S1 of Batajnica/Stari Slankamen (Fig. 2-3). The susceptibility of the recent soil is measured as $61 \cdot 10^{-8} \text{ m}^3 \text{ kg}^{-1}$. In unit V-L1S1, the susceptibility record shows a double peak. Further distinctive peak structures can be observed for the V-S2 pedocomplex, in which the uppermost pedomember has a relatively low susceptibility enhancement and is clearly offset against the rest of the pedocomplex by a thin loess layer with nearly background susceptibility. In general, the high resolution susceptibility record of Batajnica (Marković et al., 2009) confirms the patterns of the lower resolved record (Fig. 2-4). The only markable difference is a tephra-layer indicated by a sharp peak in unit V-L2, which was not detected with the low resolution sampling (Fig. 2-4). Further distinctive peak structures can be observed for the V-S2 pedocomplex, in which the uppermost pedomember has a relatively low susceptibility enhancement and is clearly offset against the rest of the pedocomplex by a thin loess layer with nearly background susceptibility.

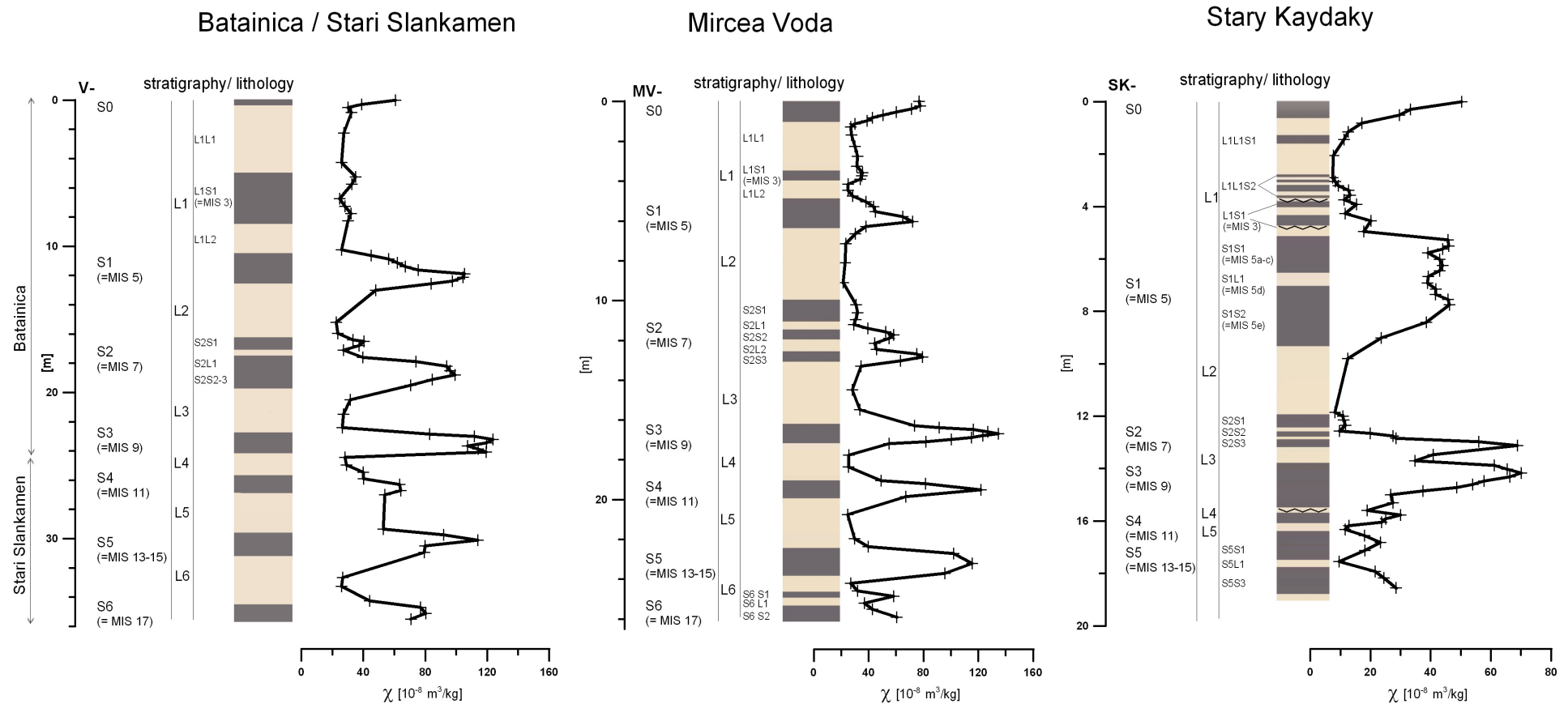


Fig. 2-3. Variations of magnetic susceptibility (χ) with profile depth and sampling site. The lithology is sketched. Dark layers indicate paleosols (= S-units), light layers indicate loess units or weakly (compared to adjacent paleosol units) pedogenetic altered loess (=L-units). Wiggled lines indicate probable hiatus. The assumed chronology, related to marine isotope stages (MIS), resulted from the magnetic susceptibility stratigraphy and for Stary Kaydaky also from pedomatigraphy (see also Fig. 2-5). Note that the Serbian profile is a composite of the Stari Slankamen (bottom) and Batajnica loess-paleosol sequence (top).

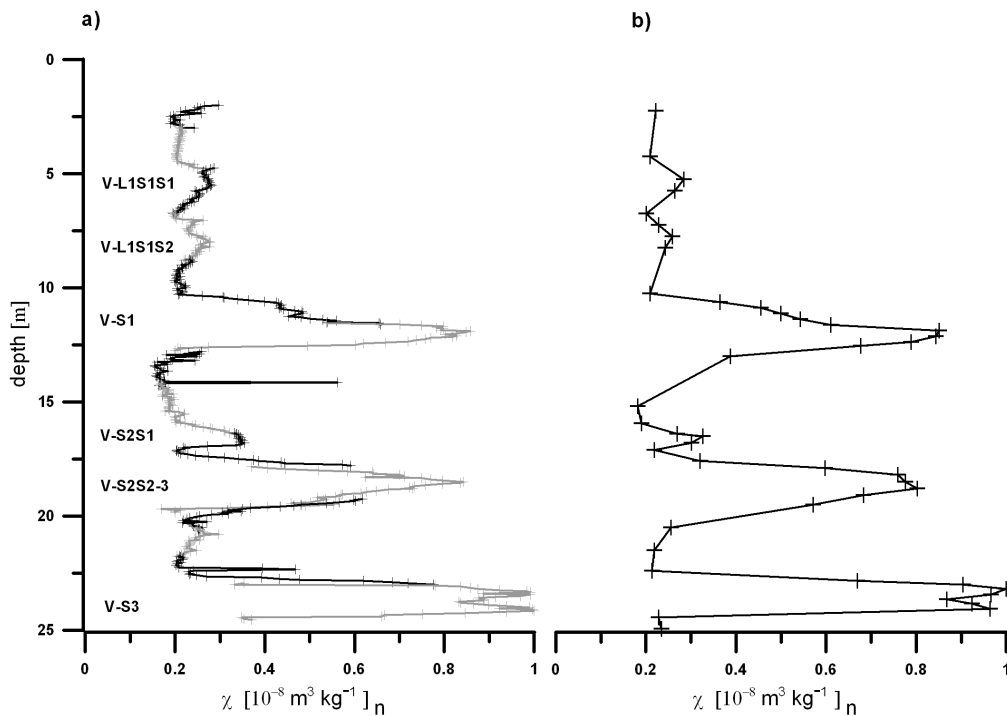


Fig. 2-4. Comparison of a high resolution magnetic susceptibility record (a, sampling in 5 cm intervals, data taken from Marković et al, 2009) and a lower resolved record (b, sampling in decimeter intervals) for the Batajnica section. Note that in graph a there are 14 subcolumns, which are indicated by a change from black to grey and vice versa. Values are normalized to the maximum value.

In general, the high resolution susceptibility record of Batajnica (Marković et al., 2009) confirms the patterns of the lower resolved record (Fig. 2-4). The only markable difference is a tephra-layer indicated by a sharp peak in unit V-L2, which was not detected with the low resolution sampling (Fig. 2-4). The background susceptibility of the Mircea Voda record ($21 \cdot 10^{-8} \text{ m}^3 \text{ kg}^{-1}$) is similar to that of the Serbian sections. Confirming field observations, pedogenic alteration of the intercalated loesses can especially be noted in MV-S2L2 and MV-S6L1 (Fig. 2-3). Consistent with the results from Serbia, the maximum susceptibility enhancement ($134 \cdot 10^{-8} \text{ m}^3 \text{ kg}^{-1}$) occurs in the MV-S3. Also the MV-S5 shows a relatively strong magnetic signal ($116 \cdot 10^{-8} \text{ m}^3 \text{ kg}^{-1}$). However, in contrast to the Stari Slankamen record, the magnetic susceptibility of the MV-S4 ($122 \cdot 10^{-8} \text{ m}^3 \text{ kg}^{-1}$) is almost as high as that of the MV-S3. Only weak enhancement can be found again in the MV-S6 and MV-L1S1. The susceptibility of the recent topsoil is about $77 \cdot 10^{-8} \text{ m}^3 \text{ kg}^{-1}$. Individual paleosols are indicated most expressively by susceptibility patterns in the MV-S6 (two pedomembers) and

in the MV-S2 (three pedomembers). The magnetic susceptibility record of the Stary Kaydaky section shows remarkable differences in pattern as well as in the absolute values (Fig. 2-3). The background susceptibility is $7 \cdot 10^{-8} \text{ m}^3 \text{ kg}^{-1}$. So, it is clearly lower than in the studied sections in Serbia and Romania. However, for most of the loess units (SK-L3 and older, as well as for the loess above unit SK-L1L1S1), pedogenic overprint is indicated by higher susceptibilities. The modern soil is characterized by a magnetic susceptibility of about $50 \cdot 10^{-8} \text{ m}^3 \text{ kg}^{-1}$, which is also lower than in the modern soils of the Serbian and Romanian sections. The maximum susceptibility, found in the Ukrainian S2 and S3, is approximately half that at Batajnica/Stari Slankamen and at Mircea Voda. Only relative weak magnetic susceptibility enhancement compared to background values can be observed in the SK-S4, SK-S5 and SK-L1S1, whereas the incipient soil SK-L1L1S1 does not exhibit enhanced magnetic susceptibility at all. Further interesting patterns are the three-partitioned record of the SK-S1, the typical peak association of the SK-S2, already described for the Batajnica section, and the two susceptibility peaks in the SK-S5 unit. Several peaks of magnetic susceptibility generally point towards a discontinuous soil development, forming a pedocomplex, consisting of individual pedomembers separated by layers of less intensive or different pedogenesis.

5.2 Stratigraphy

The magnetic susceptibility record of our profiles can be used for stratigraphic correlation. Though having a relatively coarse sampling design, characteristic susceptibility patterns are similar to the high resolution records of the area (Fig. 2-4; Rousseau et al., 2001; <http://ns.geo.edu.ro/~paleomag/loess-MV.htm>). A comparison between the magnetic susceptibility record of these profiles and the benthic $\delta^{18}\text{O}$ dataset of ODP site 677 (Shackleton et al., 1990), reflecting the global ice volume, exhibits concordance in the general patterns (Fig. 2-5). The match of paleosols/pedocomplexes with enhanced susceptibility to specific interglacials/interstadials and cold stages with reduced magnetic susceptibility comes

out more clearly in comparison with the stacked susceptibility record of Lingtai and Zhaojiachuan (Chinese Loess Plateau, Sun et al., 2006, Fig. 2-6). The chronology also corresponds well with the records of Koriten (Bulgaria) and Mostistea (Romania) and their correlation to the marine $\delta^{18}\text{O}$ record (Jordanova and Petersen, 1999b; Panaiotu et al., 2001). This similarity can be distinctly traced for our profiles Stary Slankamen/Batajnica and Mircea Voda. However, for the Stary Kaydaky section, a correlation solely based on the magnetic record is in large part ambiguous. Here, the given chronostratigraphy strongly relies on the Ukrainian stratigraphic framework (Veklitch, 1993; Gerasimenko, 2004).

5.2.1 Stratigraphy of Batajnica/Stari Slankamen (Serbia) and Mircea Voda (Romania)

Above the first strong interglacial pedocomplex (V-S1, MV-S1) weak magnetic enhancement within a zone of incipient soil formation points towards an interstadial pedocomplex (V-L1S1, MV-L1S1) of the last glacial cycle, most probably of the MIS 3. This corresponds also to the IRSL dates and amino acid racemization (AAR) chronology of other sections in the Vojvodina (Marković et al., 2008) and the chronostratigraphic interpretation of the Batajnica section given by Marković et al (2009). The pedocomplex S1 of Batajnica and Mircea Voda i.e. F2 according to the older nomenclature of Bronger (1976; see Marković et al., 2008 for the parallelization of the F and the S-L nomenclature) shows a dominating magnetic susceptibility peak in its basal half, probably representing MIS 5e. This resembles the pattern of Koriten, Lingtai/Zhaojiachuan and the trend visible in the ODP record. For the sections Durankulak (Romanian - Bulgarian border at the Black Sea coast, 43°43'N, 28°34'E) and Harlets (43° 42'16'' N, 23° 49'55.2''E). Avramov et al. (2005) reported a weakly expressed susceptibility peak at the top of S1 just above the S1 - susceptibility maximum. This feature is also indicated by a bend in the record of the profiles Batajnica and Mircea Voda, potentially resulting from pedogenesis during MIS 5a and 5c. Additional evidence for assigning the S1 unit to MIS 5 is its stratigraphic position as the first strongly developed pedocomplex below

the surface and above the S2 with its characteristic susceptibility feature of twin or triple peaks. Further support comes from the amino acid dating of the V-S1 in Ruma (Marković et al.; 2006) and IRSL dates of the loess below and above this pedocomplex in Surduk, a section situated in between Batajnica and Stari Slankamen (Fuchs et al., 2008).

As can be seen in the record of Mircea Voda, Koriten and Mostistea (Fig. 2-5), the S2 pedocomplex shows actually three peaks, two well expressed peaks at its base and a weak one at the top. In some cases, as in Batajnica, the two basal peaks are not separated clearly (Fig. 2-4). The characteristic magnetic susceptibility patterns of the Serbian and Romanian S2-unit can be correlated with corresponding patterns in the susceptibility record of Chinese LPSS (Fig. 2-5; Heslop et al., 2000) and with the benthic $\delta^{18}\text{O}$ record of ODP 677 (Fig. 2-6). This pedocomplex is attributed to MIS 7, which is in accordance to the amino acid chronology of Ruma (Marković et al.; 2006). MIS 9 shows also a characteristic double peak in the isotope curve of ODP 677 and in the magnetic susceptibility curve of Lingtai/Zhaojiachuan (Fig. 2-5). For this reason, the Batajnica S3 is correlated to MIS 9. At the Mircea Voda section, this feature is not visible, but the magnetic enhancement of the S3 paleosol in this section is the strongest one of the observed time interval, the same as in Batajnica, Koriten, Mostistea (Fig. 2-5) and Ruma (Marković et al.; 2006). This, together with the similar stratigraphic position of the S3 in all studied sections, clearly indicates the same range of age of this pedocomplex. The obtained chronostratigraphic placement is in accordance to the AAR results of Ruma (Marković et al.; 2006). Further down, the magnetic susceptibility peaks in the V-S4, MV-S4 and V-S5, MV-S5 paleosols are correlated with MIS 11 and MIS 13 - 15, respectively. In the Chinese loess-paleosol sequences, magnetic enhancement is continuously observed through the whole duration of MIS 13 and 15, and its attenuation during MIS 14 is rather weak (Sun et al., 2006; Heslop et al. 2000). The work of Jordanova and Petersen (1999b) on Koriten and the pedostratigraphy confirm the correlation of the Serbian and Romanian S4 and S5 with these MISs

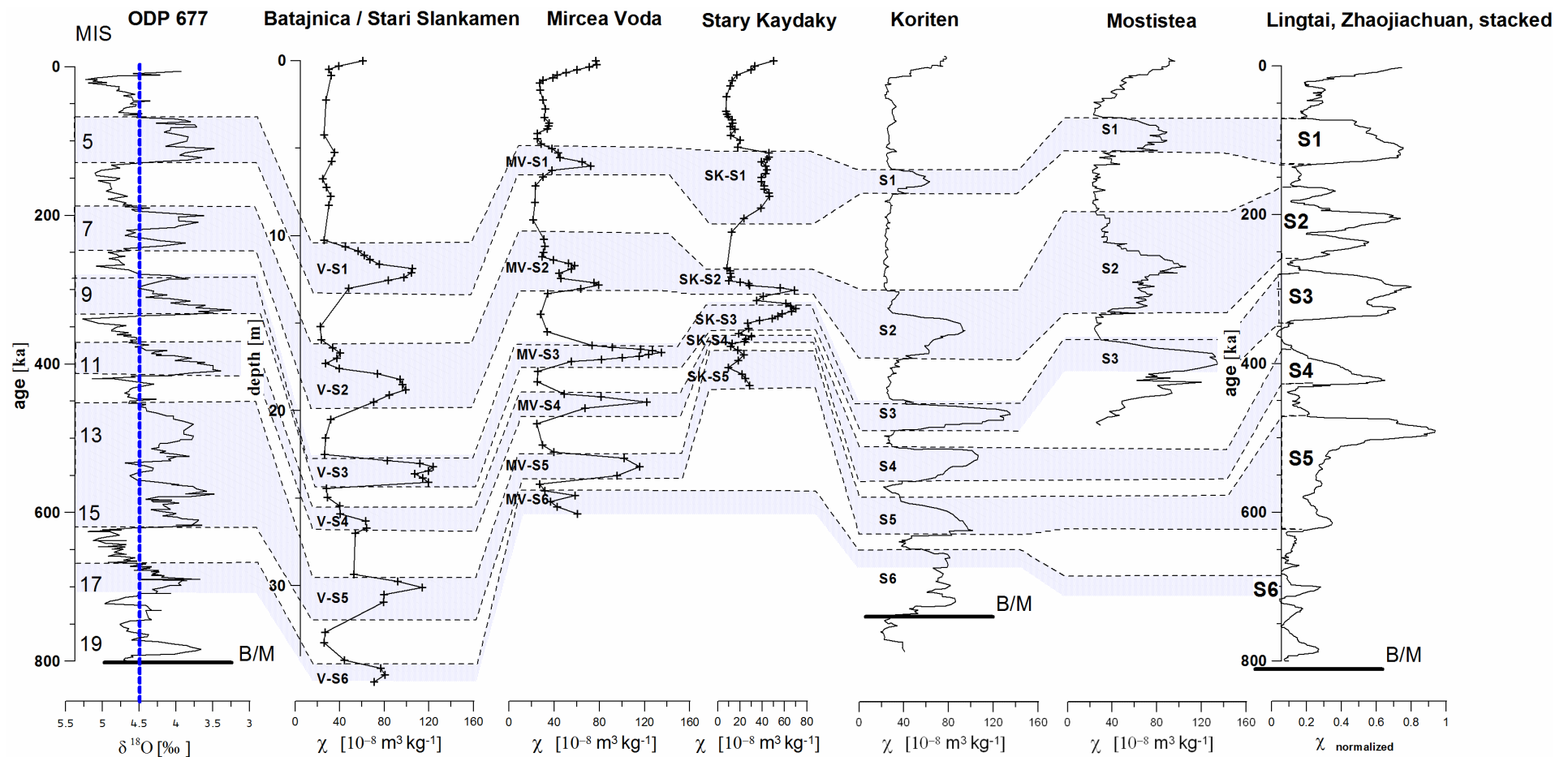


Fig. 2-5. Correlation of the magnetic susceptibility records of the profiles Batajnica/Stari Slankamen, Mircea Voda, Stary Kaydaky with the astronomically tuned benthic oxygen isotope record from ODP site 677 (Shackleton et al., 1990); A $\delta^{18}\text{O}$ value of 4.5 ‰ was used for the limitations of major isotope stages, following Vidic et al. (2004); Comparison with the records of Koriten, Mostistea (redrawn after Jordanova and Petersen, 1999b; Panaiotu et al., 2001) and the stacked normalized magnetic susceptibility curve of Lingtai and Zhaojiachuan (Chinese Loess Plateau); data and astronomical tuning for the latter sections were provided by Sun, et al., (2006).

Being the youngest and best-developed soil of the Brunhes-chron with remarkable rubification and clay illuviation in Stari Slankamen and Mircea Voda, the S5 may serve as a marker horizon for MIS 13-15, in this area. The magnetic susceptibility enhancement in unit S6 of Stari Slankamen is assigned to MIS 17, also supported by the magnetostratigraphy of Marković et al. (2003). At Mircea Voda the magnetic susceptibility record of the MV-S6 revealed two peaks. The first one resulted from MIS 17, but the chronological placement of the second was not clear. A comparison with the magnetic susceptibility records of Koriten and the Chinese loess plateau (Fig. 2-5) may point to a MIS 18 interstadial soil. However, pedogenesis of this lower pedomember seems to be even stronger than that of the upper one. Therefore, at the present state of knowledge, it is attributed to the MIS 17 interglacial (Fig. 2-5) (see for further discussion Section 6.2.2). Preliminary paleomagnetic investigations of Marković et al. (2004c) revealed evidences for the Brunhes-Matuyama (B/M) boundary in the L8 of Stari Slankamen. This represents a further support for the correctness of the chronostratigraphic model. Contrasting TL dates for the S1 to S4 at Stari Slankamen (Singhvi, 1989) suffer probably from age underestimation due to methodological reasons (Fuchs et al., 2008).

5.2.2 Stratigraphy of Stary Kaydaky

A key in the different stratigraphic models, which are proposed for the LPSS of the Ukraine (Gerasimenko, 2004; Gerasimenko, 2006; Lindner et al., 2006; Veklich, 1995, cited in Bolikhovskaya and Molodkov, 2006), is the chronological placement of the Kaydaky pedocomplex (SK-S1S2) and the Dnieper loess (SK-L2). In the Ukraine, especially at its type locality at Stary Kaydaky, the Kaydaky pedocomplex is formed by a dark steppe soil-type paleosol over a forest-soil type paleosol overlying the Dnieper loess (SK-L2). The Dnieper loess is the unit associated with the moraine of the Dnieper glaciation. In the stratigraphic models of the Ukrainian Quaternary, it is generally argued whether this loess and the

respective glaciation occurred during MIS 8 or MIS 6. Therefore, the Kaydaky unit is placed either in MIS 5e or MIS 7. An overview of the stratigraphic schemes for the Ukraine, resulting from the different opinions on the chronological placement of the Dnieper and Kaydaky units, is given in Table 2-2. Clarifying this question allows the development of a chronostratigraphy for the Stary Kaydaky section on the basis of the respective pedo-, and pollen stratigraphic framework of the Ukraine.

Table 2-2. Compilation of different stratigraphic schemes for the Ukraine. The present study favors the scheme of Gerasimenko (2004, 2006).

| Unit (Lindner et al. 2006) | Unit (Veklich, 1995, cited in Bolikhovskaya and Molodkov, 2006) | Unit (Gerasimenko, 2004; Gerasimenko, 2006) | Marine Isotope Stage |
|-------------------------------|--|---|----------------------------|
| Valday | Prychernomorsk | Prychernomorsk | 2 |
| | | Dofinivka | |
| | | Bug | |
| | Dofinivka | Vytachiv | 3 |
| | Bug | Uday | 4 |
| Pryluky | Vytachiv, Uday, Pryluky | Pryluky | 5a-c |
| | | Tyasmyn | 5d |
| Dnieper 2 | Tyasmyn | Dnieper | 6 |
| Kaydaky | Kaydaky | Potagaylivka | 7 |
| Dnieper 1 | Dnieper | Orel | 8 |
| Potagaylivka | | | 9 |
| Orel | Zavadivka | Zavadivka | 10 |
| Zavadivka | | | 11 |
| Tiligul | Tiligul | Tiligul | 12 |
| Lubny | Lubny | | 13 |
| | | Lubny | 14 |
| | | | 15 |

The S1 pedocomplex of Stary Kaydaky contains a forest steppe/steppe-soil type paleosol (=Pryluky complex), which is separated by thin pedogenetically altered loess (= Tyasmyn) from the typical Kaydaky pedocomplex. The three peaked susceptibility record of S1 reflects the pattern of the benthic $\delta^{18}\text{O}$ record of MIS 5 as well as the susceptibility pattern of the S1 pedocomplex in Mostistea and the Pryluky-, Kaydaky complex in Vyazivok (Rousseau et al., 2001, Fig. 2-6). This good correspondence suggests that the magnetic susceptibility record at least of this younger part of the section reflects paleoclimatic variations and is not affected by strong biases as in the older part of the sequence (see below).

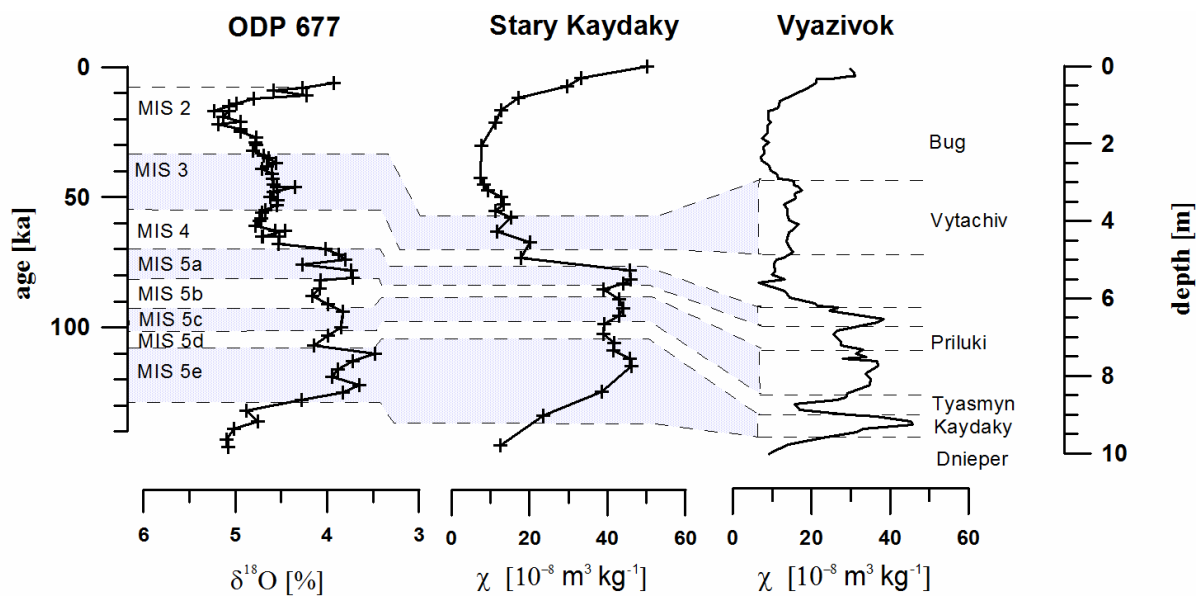


Fig. 2-6. Correlation of the magnetic susceptibility record of the Sary Kaydaky section to that of the Vyazivok section (Ukraine, Rousseau et al. 2001) and the benthic $\delta^{18}\text{O}$ record of ODP 677 (Shackleton et al. 1994), for the last climatic cycle.

With the given susceptibility curve and AAR dates in the range of MIS 6 for the loess below the Kaydaky –complex (i.e. Dnieper) in Vyazivok, it appears most reasonable to correlate the Pryluky complex (SK-S1S1) with MIS 5a to MIS 5c, the Tyasmyn unit (SK-S1L1) with MIS 5d and the Kaydaky complex (at its type locality) with MIS 5e. This correlation supports the stratigraphic scheme of Gerasimenko (2004, 2006). Having clarified the chronological placement of the S1 (Pryluky, Tyasmyn, Kaydaky) allows to develop the chronostratigraphy of the other units of the Sary Kaydaky section, above and below, based on the respective (pedo-)stratigraphic framework of the Ukraine. At the Sary Kaydaky section, the pedocomplex SK-L1S1 (= Vytachiv in the Ukrainian nomenclature) is situated in its characteristic stratigraphic position above the last interglacial pedocomplex being separated from it by the so-called Uday loess (SK-L1L2). The Vytachiv complex is represented by two pedomembers with a layer of weakly pedogenetically altered loess between them. The lowermost pedomember is most expressed in susceptibility (Fig. 2-3, Fig. 2-6). Considering the placement of the Kaydaky-and Priluki-complex, the Vytachiv complex can be best

attributed to MIS 3 (Fig. 2-6, Gerasimenko 2004; Rousseau et al., 2001). This is also in agreement with ESR and ^{14}C ages between 30 and 40 ka BP reported for the Vytachev-complex at other sites in the Ukraine (Gerasimenko, 2006). A line of erosional incision is observed between the Vytachiv pedocomplex and the overlying Bug loess (27-18 ka, Gerasimenko, 2006). Two soil subunits (SK-L1L1S1 and SK-L1L1S2), separated by loess, were found above the erosional incision. In the Kaydaky section, both have been related to the Dofinivka unit (Veklitch et al., 1982), though there are two reasons for doubting this assignment: a significant thickness of loess between the two subunits, and the presence of a set of incipient soils within the lower subunit (SK-L1L1S2). A similar succession of incipient soils is discovered in other sections of the Ukraine at the base of the Bug unit (bg1), whereas the upper Bug (bg2) is represented by pure loess (Veklitch 1993, Gerasimenko, 2000, 2006). Thus, only the uppermost soil (SK-L1L1S1) can be related to the Dofinivka paleosol unit (17-15 ka, Gozhik et al., 2000). A differentiation between the unit SK-L1L1S1 and the loess above does not clearly appear in the susceptibility record of Stary Kaydaky (Fig. 2-3), probably due to the low sesquioxide content (Gerasimenko 2000).

Below the L2 loess (Dnieper, MIS 6), the SK-S2 pedocomplex is formed by a succession of a brownish horizon (incipient soil) on top, a pedomember of steppe-soil type paleosol and a pedomember of forest/forest-steppe soil type at the base. This succession can be related to the Potagaylivka complex i.e. MIS 7 (Gerasimenko, 2004). Thus, the magnetic susceptibility pattern should also correspond to the characteristic twin peak association in the Serbian and Romanian S2. The underlying loess SK-L3 shows cryofeatures, penetrating into the SK-S3 paleosol. Thus, despite its pedogenic overprint from the overlying pedocomplex, SK-L3 can be attributed to glacial conditions i.e. representing the so-called Orel-loess. The SK-S3 appears to be the pedocomplex of a strongly developed steppe-soil type paleosol and forest-soil type paleosol and the SK-S4 is a truncated forest-soil type paleosol. The SK-S3 and SK-S4 are regarded as upper and lower Zavadivka soil, which can be palynologically correlated

with MIS 9 and 11 (Gerasimenko 2004). Similar to the record of Mircea Voda and Batajnica section, the SK-S3 shows relatively high magnetic enhancement (Fig. 2-5). In the pedocomplex units SK-S4 and SK-S5 the magnetic susceptibility is systematically lower. Although currently no explanation is suggested, climatic reasons are excluded, as steppe-soil type and forest-soil type paleosols are affected in a similar way.

The SK-S5 paleosol comprises two pedomembers: the upper one is a dark steppe-soil type paleosol and the lower one a brown-red forest-steppe soil type paleosols. Due to this association, the SK-S5 probably corresponds to the Lubny pedocomplex, correlating with MIS 13-15 (Gerasimenko, 2004). Preliminary investigations by V. Bakhmutov (personal communication, 2006) could not detect the geomagnetic polarity change of the B/M boundary within the studied part of the profile.

5.3 Sedimentation rates

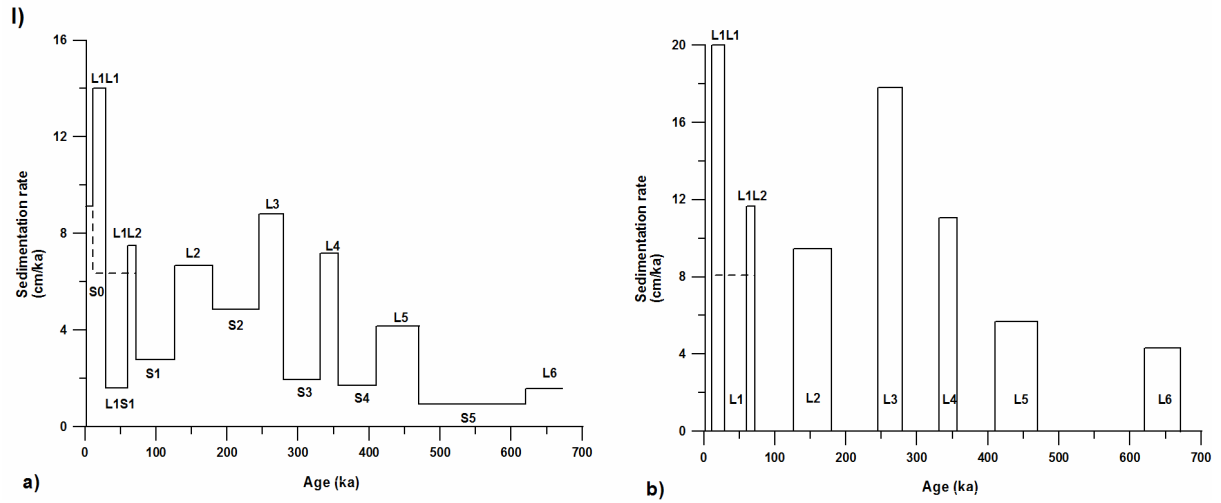
Sedimentation rates were calculated for two worst case models of dust deposition i.e. synpedogenetic sedimentation (variant A) and prepelodogenetic sedimentation (variant B). Furthermore sensitivity analyses concerning the timescale model have been conducted.

Variant A suggested mostly increased sedimentation rates at the loess units of Mircea Voda compared to the adjacent pedocomplexes, regardless of the applied time scale model (Fig. 2-7). An exceptions is the S2 for the timescales of Bassinot et al. (1994) and Heslop et al. (2000). Differences between sedimentation rates of pedocomplexes and loess units are most expressed for the JP-99b timescale and for the Su-06 and Sh-90 age models. Considering the duration of the units, the application of He-00 timescale yields generally lower values for pedocomplex units and higher values for loess units than using the other timescales (Table 2-1). Thus, in this age model, sedimentation rates for loess units tend to be relatively low and for pedocomplex units relative high.

The JP-99b timescale shows a tendency of decreasing sedimentation rates towards the older units of the Mircea Voda section (variant A and B) resembling the pattern of sedimentation rates at Koriten (Jordanova and Petersen, 1999b). Remarkably high values can be found for the younger loesses L1 to L4 and here especially for the L1L1 and L3. Low sedimentation rates are obtained for L5 and L6 (variant A and B). Regarding the paleosols, the pedocomplex S5 exhibits the lowest values and relatively high sedimentation rates were found for the S2, due to the intercalated loess layers S2L1 and S2L2 (variant A). Furthermore, synpedogenetic sedimentation is probably the reason for the high sedimentation rates of the L1L2 using variant B, judging from the magnetic susceptibility pattern of the L1S1 (Fig. 2-7). For the other units, synpedogenetic sedimentation cannot be excluded. Minimum sedimentation rates for the S5 and maximum for either the L1 or the L3 are generally confirmed by the other timescale-models (Fig. 2-7). However, not all models produce the lowest sedimentation rate of the major loess units for the L5 and L6 of Mircea Voda. This feature is only clearly expressed using the JP-99b, timescale (variants A and B), the He-00 timescale (variants A and B) and Su-06- timescale (variants A and B). With the latter timescale, the L4 can be characterized by low and even slightly lower sedimentation rates than the L5. Applying the Sh-90 and Ba-94 age models, the L5 does not exhibit distinctly lower rates of dust deposition than the younger loess units. Here, only the L6 shows a clear offset towards lower values (variant A and B).

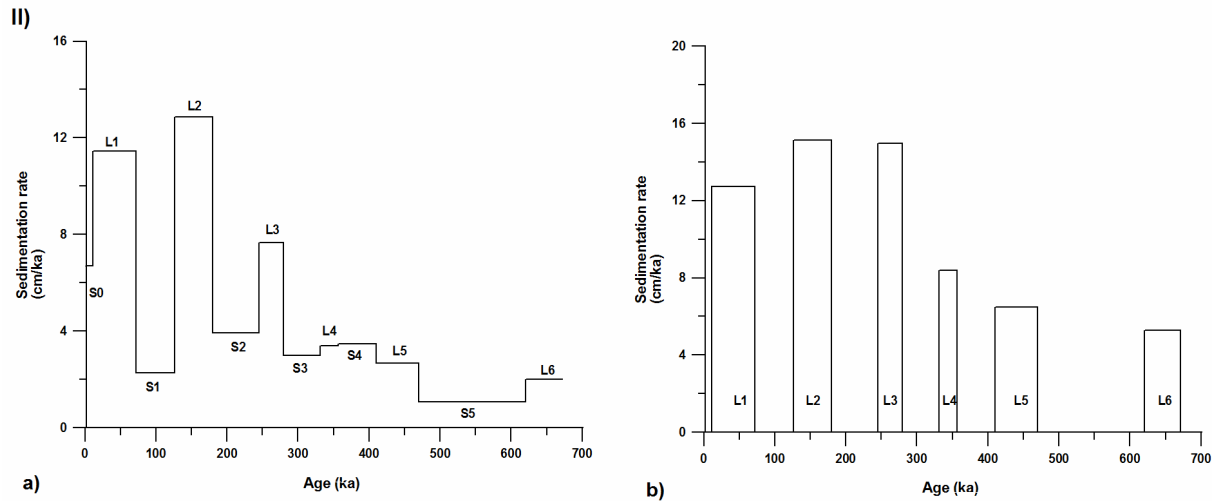
Mircea Voda

timescale according to Jordanova and Petersen (1999b)



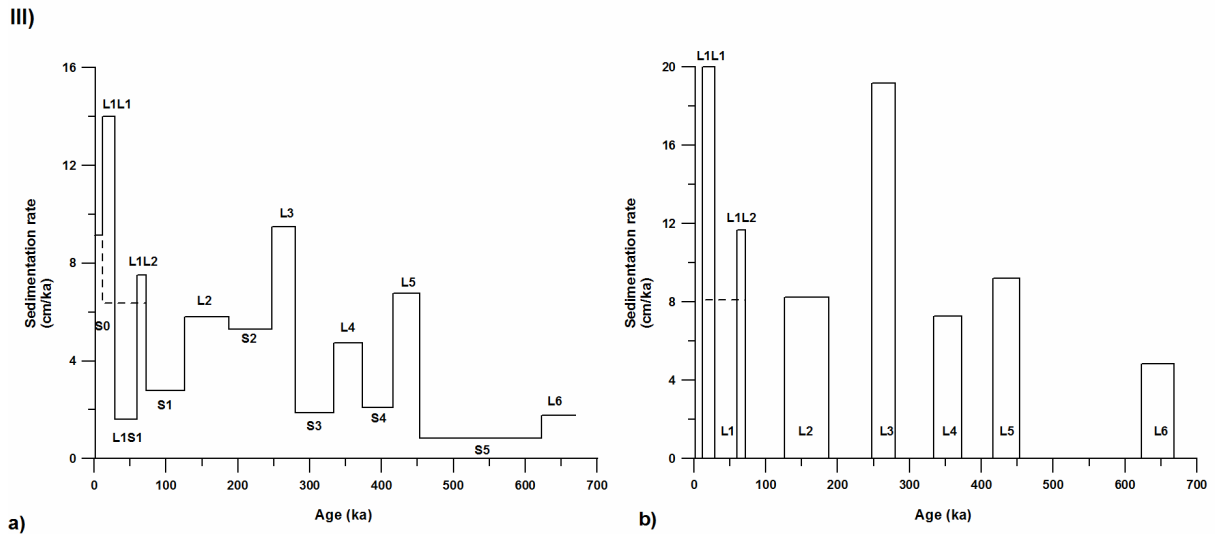
Koriten

timescale according to Jordanova and Petersen (1999b)



Mircea Voda

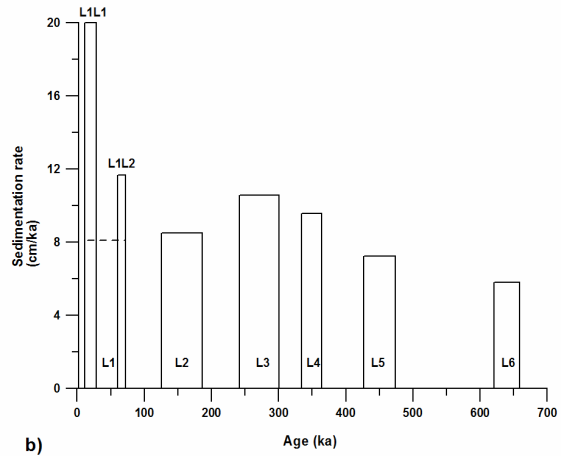
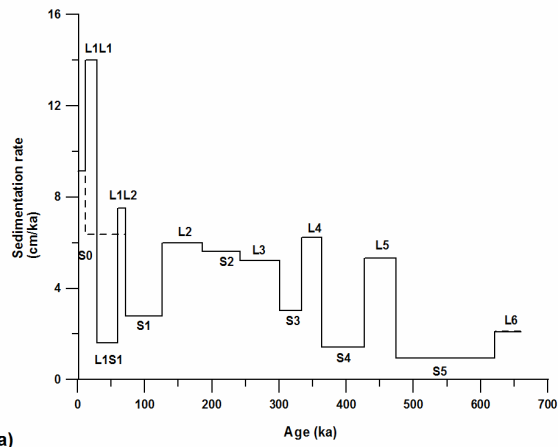
timescale based on correlation to Shackleton et al. (1990)



Mircea Voda

timescale based Bassinot et al (1994)

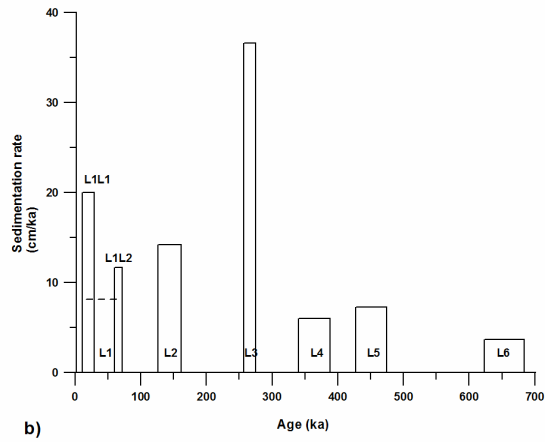
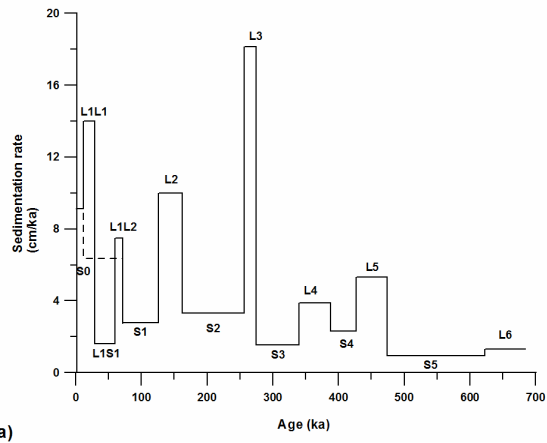
IV)



Mircea Voda

timescale based on correlation to Sun et al. (2006)

V)



Mircea Voda

timescale based on Heslop et al. (2000)

VI)

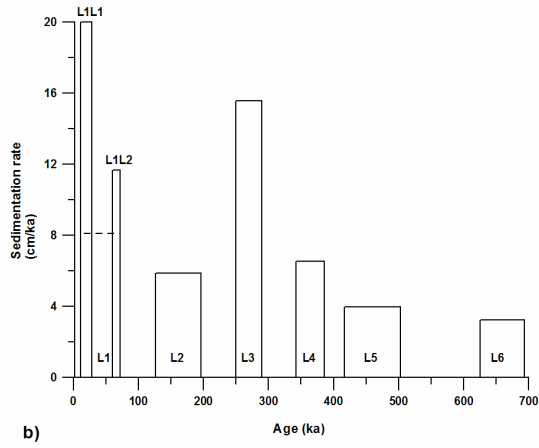
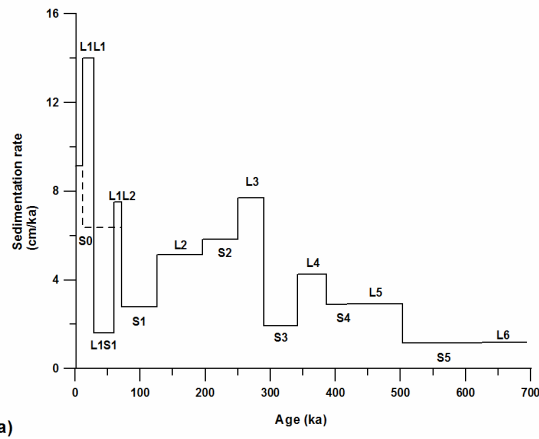


Fig. 2-7. Sedimentation rates for the sections Batajnica/Stari Slankamen and Mircea Voda. (I) Sedimentation rates for the LPSS Mircea Voda, calculated for the timescale used by Jordanova and Petersen (1999b). This timescale was based on correlation of the magnetic susceptibility record of Koriten to the planktonic $\delta^{18}\text{O}$ record of ODP 677. (II) Sedimentation rates for the LPSS Koriten (Jordanova and Petersen (1999b), modified). (III) Sedimentation rates for the LPSS Mircea Voda, calculated for a timescale derived by correlation of the susceptibility records of Fig. 2- to the benthic $\delta^{18}\text{O}$ of ODP 677 (Shackleton et al., 1990). (IV) Sedimentation rates for the LPSS Mircea Voda, calculated for the age boundaries of the isotope events, developed by Bassinot et al., (1994) for planktonic foraminifers of core MD900963 (Indian Ocean). (V) Sedimentation rates for the LPSS Mircea Voda, calculated for a timescale derived from correlating the susceptibility records of Southeastern Europe to the susceptibility record of Lingtai and Zhaojiachuan (Chinese Loess Plateau). The astronomical tuning for these section was done by Sun et al. (2006) using a record of mean grain size of quartz particles (MGSQ). (VI) Sedimentation rates for the LPSS Mircea Voda were calculated using the timescale given by Heslop et al. (2000) for the loess-paleosol units of the Baoji section (China). (a) Sedimentation rates calculated according to variant A (worst case): synpedogenetical sedimentation, the whole thickness of a paleosol is attributed to sedimentation during warm stages. (b) Sedimentation rates calculated according to variant B (worst case): no sedimentation during warm stages (prepedogenetical sedimentation). The dashed line gives the mean sedimentation rate for L1.

6 Discussion

As in the Chinese loess records (e.g. Kukla, 1987; Kukla and An, 1989; Maher et al., 1994), magnetic susceptibility at the studied LPSS of Serbia, Romania and Ukraine is clearly enhanced in paleosols. This is, on the one hand, fundamental for stratigraphic correlations based on this proxy of pedogenesis.. On the other hand, it allowed paleoclimatic deductions. In this context, the use of the susceptibility-rainfall equation (1), presented by Maher et al. (1994), will be discussed. Moreover, the chronostratigraphic model permitted the calculation and evaluation of sedimentation rates. In the following section, the stratigraphic units are regarded as correlatives of the Chinese loess-paleosol sequences, and the use of local stratigraphic names is avoided if possible.

6.1 Sedimentation rates

When calculating the sedimentation rates for LPSS, one is confronted with the following questions: (i) what is the appropriate timescale for the calculation, (ii) are there remarkable hiatus in the profile, and (iii) do soils thicken during their formation (synpedogenetic sedimentation) or were sedimentation and pedogenesis non-simultaneous processes (prepedogenetic sedimentation)? As to the second point, there is no field evidence indicating

remarkable hiatus in the profile of Mircea Voda. Regarding the first point, a sensitivity analysis for the timescale model was conducted. For the third point, sedimentation rates were calculated for the two different models of dust deposition: variant A, i.e. attributing the whole thickness of a paleosol/pedocomplex to interglacial and interstadial dust sedimentation, and variant B, i.e. attributing the total thickness of a paleosol/pedocomplex to sedimentation during the preceding glacial/stadial stage. Both models have their limitations. In the case of low sedimentation rates and/or deep downward pedogenic alteration, variant A would distinctly underestimate the sedimentation rates for the loess units. However, when considering paleosols that clearly grew up or pedocomplexes with intercalated loess layers, variant B would overestimate sedimentation rates of the underlying loess units to a greater extent. This is the case at the L3 and L1L2 of Mircea Voda and L1L2, L3, L4 of Batajnica/Stari Slankamen, (Fig. 2-7). Furthermore, variant B restricts interpretations to the level of couples of loess and pedocomplex/paleosol units. Though both variants are per se probably unrealistic, they represent worst-case scenarios for the model of dust sedimentation with the truth being in between these two extremes. For the Chinese loess plateau, for example, Kohfeld and Harrison (2003) proposed that only a certain fraction (2/3) of the soil material is deposited synpedogenetically. The use of both worst case scenarios, variant A and B, however, provides a tool for the verification of observed patterns and trends in the calculated sedimentation rates by testing the robustness of the observed features. Relative trends that result in variant A and in variant B can be assumed to be reliable with respect to the uncertain extent of synpedogenetic sedimentation. This would be the case for the decrease in dust sedimentation rates (variant A and B) towards the older units, which was obtained for the Mircea Voda section, using the JP-99b, He-00 and Su-06 timescale. The decrease is markedly expressed below the L4 (Jp-99b, He-00) and below L3 (Su-06) (Fig. 2-7). At the Koriten site in the Bulgarian part of the lower Danube basin, Jordanova and Petersen (1999b) obtained the lowest rates of dust deposition for the older loesses L4 to L6 (Fig. 2-7). At this

section there appears to be a trend of decreasing sedimentation rate from one loess unit to the next older one, regarding the units L2 to L6. A similar trend can be observed in Mircea Voda (L3 to L6) only when applying the same time-scale as Jordanova and Petersen (1999b). One may interpret the lower rates of dust deposition in the older loess units L6, L5 and eventually L4 in a paleoclimatic sense. It could indicate a change in atmospheric circulation and/or a decrease in wind force and/or an increase in humidity towards the older units. Jordanova and Petersen (1999b) speculated about a link to the build up of a permanent ice cover of the Arctic Ocean with implications on the atmospheric circulation. However, the observed patterns are less clear, conducting sensitivity analysis for the applied ages by using other timescale models (Table 2-1, Fig. 2-7). Using the Sh-90 and Ba-94 timescale only the L6 shows a distinctly lower sedimentation rate. Differences in the timescales may exist due to the method of astronomical tuning or difficulties in finding benchmarks at the saw tooth pattern of highly resolved marine paleoclimatic records to correlate with less resolved records of terrestrial archives. This may lead to differences of more than 100 % in the duration of a period and consequently to a high uncertainty of the sedimentation rates. Therefore, the sensitivity analysis for the timescale model shows that a trend in sedimentation rates i.e. a gradual increase of dust deposition from L6 to L3 or L2 is questionable, though one might have interpreted the results of Koriten (Jordanova and Petersen, 1999b) and Mircea Voda in this sense, using only the JP-99b timescale. However, at Mircea Voda, the sensitivity analysis confirmed that relatively high rates of sedimentation occurred within the period of MIS 2-4 (=L1), MIS 8 (=L3) and the warm stage MIS 7, whereas the lowest rate of sedimentation in cold stages occurred during MIS 16 (L6), and the lowest rate during warm stages in MIS 13-15 (S5). These findings can be interpreted with respect to paleoclimate or atmospheric circulation.

For the last climatic cycle, no sensitivity analysis with respect to timescale was conducted. The applied age model is based on Guiter et al. (2003) and Litt et al. (2001), who compiled

the results of several West and Central European studies. Uncertainties, reported in these studies, seem to be negligibly small. However, the onsets of climate variations in Southeastern Europe are not necessarily simultaneous to those of Western and Central Europe. Therefore, and due to the rather diffuse lower boundary of the recent soil, sedimentation rates obtained for the Holocene should not be overinterpreted. The short duration of this period makes these results sensitive to uncertainties in the thickness of the corresponding units. High resolution luminescence dating may provide a suitable tool for a more precise determination of the age boundaries of the upper Pleistocene climatic stages in the profiles (Lai and Wintle, 2006).

6.2 Chronostratigraphic revisions

For setting up a timescale of Mid-Pleistocene terrestrial archives, there is a lack of reliable methods of numerical dating. Therefore, relative stratigraphies in combination with astronomical tuning are widely used for working out chronostratigraphies of LPSS. Correlations and tunings are often ambiguous in detail and highly subjective. Continuous validation of existing stratigraphies is crucial for setting up a reliable timescale of the Quaternary. These results can provide a useful contribution to ongoing discussions about the stratigraphy of the region and it may initiate a new discussion concerning the astronomical tuning of Chinese LPSS.

For Batajnica/Stari Slankamen and Mircea Voda, the stratigraphy is well established by correlation of the magnetic susceptibility records to the $\delta^{18}\text{O}$ record of benthic foraminifera of ODP site 677 (Shackleton et al., 1990), to a stacked magnetic susceptibility record of two sections from the Chinese Loess Plateau (Sun et al., 2006) and validated by correlations to other profiles of the study area (e.g. Jordanova and Petersen, 1999b; Panaiotu et al, 2001; Rousseau et al., 2001; Marković et al., 2006; Fig. 2-5, Fig. 2-6). Contrasting TL ages for the Stari Slankamen S1 to S4 (Singhvi et al. 1989, cited in Bronger 2003) are probably due to a

methodological age underestimation (Dodonov et al., 2006a, Fuchs et al., 2008). For the Stary Kaydaky section, the type locality of the Kaydaky pedocomplex, magnetic susceptibility correlations to the dated Vyazivok section (Rousseau et al., 2001) and to the ODP 677 proxy record of the global ice volume gives an important contribution to clarify contrasting stratigraphic frameworks of the Ukraine.

Here, the focus is on some implications of our inter-profile correlations concerning following topics: 1) the S2S1-unit, stratigraphic setting and implications on orbital tuning, 2) the division of the S6 and S7 pedocomplexes, 3) the local Ukrainian stratigraphy.

6.2.1 The S2S1-unit, stratigraphic setting and implications on orbital tuning

One of the most characteristic magnetic susceptibility patterns of loess profiles covering Southeastern-Europe through Tajikistan (Dodonov et al., 2006b) to the Chinese loess plateau (Sun et al., 2006) is an association of three peaks (see for example, the Mircea Voda record, Fig. 2-5), assigned here to the S2 pedocomplex. Probably due to sampling resolution and/or local effects, the two lowermost peaks are not always to distinguish in the profiles (for example, the Batajnica record, Fig. 2-5). The uppermost pedomember (unit S2S1) – having only weak susceptibility enhancement – is clearly visible in the field. We consider this pedocomplex as a formation of MIS 7. Correlating the susceptibility feature of the S2 in Southeastern Europe with the stacked astronomically tuned record of Lingtai/Zhaojiachuan, we conclude that the units S2S3 and S2S2 match to the susceptibility peaks at 236 and 204 ka (hereafter named LZe and LZc+d, Fig. 2-5). The S2S1 is correlated with the benthic $\delta^{18}\text{O}$ peak at 190 ka of ODP 677. There are three possible correspondences of the S2S1 unit in the terrestrial records. The first one is a correlation with the upper part of the slightly splitted major S2 susceptibility peak in Louchuan (Heslop et al., 2000) and Lingtai/Zhaojiachuan (LZc). This does not seem likely, since the susceptibility enhancement in the Southeastern European S2S1, as well as the intensity of pedogenesis observed in the field for this unit is

generally weak and clearly offset from the S2S2. Furthermore, this correlation is not supported by Jordanova and Petersen (1999b) and Panaiotu et al. (2001). The second possibility is a correlation with the bend in the top of the major S2 susceptibility peak in Louchuan and a peak (Lzb) in the susceptibility record of Lingtai/Zhaojiachuan at an age of 192 ka (Sun et al., 2006). This possible correlation would be in accordance with the proposed position of the S2S1 at the top of the S2 pedocomplex, attributed to MIS 7 (Fig. 2-5, Jordanova and Petersen, 1999b; Panaiotu et al., 2001). Here, the third possibility is favored, correlating the susceptibility peak of the S2S1 unit with the susceptibility peak of 167 ka (LZa) in Lingtai/Zhaojiachuan (Sun et al., 2006). This matches best the susceptibility patterns of the Southeastern European sections (Fig. 2-5) and is also in agreement with the correlations of Jordanova and Petersen (1999b) and Panaiotu et al. (2001). However, with an age of 167 ka following Sun et al. (2006), the S2S1 paleosol would then be assigned to MIS 6. Heslop et al. (2000) presented an orbital tuning for the susceptibility record of the Louchuan section, showing an age of about 175 ka for the corresponding peak of LZa and S2S1. Both the timescales of Sun et al. (2006) and Heslop et al. (2000) seem to underestimate the age of this susceptibility peak, when compared to the benthic oxygen isotope record of Shackleton et al. (1990, Fig. 2-5). This record, reflecting the global ice volume, gives an age of 188 ka for the MIS 6 / MIS 7 boundary and of 190 ka for the most likely counterpart of the S2S1-susceptibility peak.

Heslop et al. (2000) present a match of the magnetic susceptibility record of Luochuan, the benthic $\delta^{18}\text{O}$ record of ODP 677 and the insolation curve. This we take as base to suggest an improvement of the orbital tuning of the questionable period. Heslop et al. (2000) associated three insolation peaks (at about 195, 220, 240 ka) with MIS 7. The lowermost is attributed to the counterpart of S2S3 and LZe at Louchuan. The younger two peaks are both correlated with the slightly splitted susceptibility peak S2-1 (Heslop et al. 2000), which is the counterpart of the Southeastern European S2S2 and LZc+d of the Chinese Loess Plateau.

More reasonable, with respect to magnetic susceptibility stratigraphy, seems to be a match of the uppermost MIS 7 insolation peak, shown by Heslop et al. (2000), with the susceptibility peak at 15 m depth in Louchuan, the LZa in Lingtai/Zhaojiachuan and the uppermost benthic $\delta^{18}\text{O}$ peak of MIS 7. The susceptibility pattern of the MIS 7 (= S2 pedocomplex) of Southeastern Europe would then better correspond to the Chinese records. The best Chinese counterpart of the S2S1 paleosol would no more belong to MIS 6, due to a back shift in time by about 20 ka according to the Heslop et al. (2000) timescale and by about 25 ka according to the timescale of Sun et al. (2006). In consequence of this improvement, an overall shift in the astronomical tuning of Heslop et al. (2000) and Sun et al. (2006) would not be necessary, if the timescale is stretched for the Chinese L2. Further research is needed to clarify the questions about the L2/S2 and MIS 6/MIS 7 boundaries.

6.2.2 Division of pedocomplexes S6 and S7

At Koriten, Jordanova and Petersen (1999b) found a single pedocomplex (regarded as S6) spanning from the L6 to the B/M boundary. There are two reasons to doubt that the Koriten-S6, in terms of Jordanova and Petersen (1999b), corresponds to the Chinese S6. First, susceptibility records of Chinese LPSS (Heslop et al., 2000; Sun et al., 2006) exhibit a similar susceptibility pattern, implicating the correlation of the upper part of the Koriten S6 with the Chinese S6 (MIS 17), the middle part of Koriten S6 with MIS 18 (interstadial soil development), the lower part of Koriten S6 with Chinese S7 (MIS 19). Second, the true position of the Brunhes- Matuyama (B/M) boundary is located in the S7, as shown by Zhou and Shackleton (1999). Due to the fact that the acquisition of remanent magnetization in loess is diagenetically delayed, the B/M boundary is often found in the underlying L8 loess or even in the upper part of S8 (Zhou and Shackleton, 1999). Therefore, the B/M boundary in Koriten probably indicates the base of the equivalent to the Chinese S7.

At the Mircea Voda section, the S6 showed two susceptibility peaks (Fig. 2-3). The lower one is most likely to be an interglacial formation, as it is more strongly developed than the upper one. Thus, the S6S2 is most probably a soil formation of either MIS 17 or MIS 19. A preliminary screening on several orientated samples of the underlying loess by the paleomagnetic standard procedure of the laboratory for Paleomagnetism and Environmental Magnetism (University of Bayreuth) did not indicate a geomagnetic reversal. Therefore, at the present state of research, the lowermost susceptibility peak of the Mircea Voda S6 does not seem to represent the Chinese S7, rather the S6 of Mircea Voda is an equivalent of the Chinese S6. However, more detailed systematic investigations for detecting the B/M boundary in Mircea Voda are required.

6.2.3 The local Ukrainian stratigraphy

At the Stary Kaydaky section, erosional capping, pedogenic overprint of loess units and some unknown bias on the susceptibility of the older units, required besides the magnetic susceptibility record, also pollen- and pedostratigraphic information to develop a chronostratigraphy.. However, in the present Ukrainian stratigraphic system, the chronological setting of the Kaydaky and Dnieper units is regarded in two different ways (Table 2-2): 1) as respective correlatives of MIS 7 and MIS 8 (e.g. Veklitch, 1993; Lindner et al., 2006), and 2) as terrestrial equivalents of MIS 5 and MIS 6 (e.g. Rousseau et al., 2001; Gerasimenko, 2004; Gerasimenko, 2006; Bolikhovskaya and Molodkov, 2006). The results of this research (Fig. 2-6) support the latter model. Having cleared the chronological placement of these key-units, it was possible to suggest a chronostratigraphy for the upper and lower part of the Stary Kaydaky section. Accordingly the oldest studied pedocomplex is assigned to MIS 13-15 (see Table 2-2).

Two versions can be considered for the refined stratigraphy of L1. In the sections of the Black Sea coast, the uppermost soil within L1 is dated to Bölling-Alleröd (Gozhik et al., 2000). In

the northern and central Ukraine, Bölling-Alleröd deposits are mainly included in the lower layers of the thicker Holocene soils, and the uppermost soil within the loess of MIS 2 belongs to the Dofinivka unit, dated to 15-17 ka (Gozhik et al. 2000). Furthermore, the underlying Bug loess is thick and includes a set of 2-4 incipient soils in its lower part (Gerasimenko 2006).

At the Sary Kaydaky section, a similar succession of incipient soils in the lower part of L1 favors the second version of L1-stratigraphy.

6.3 Evaluation of the susceptibility-rainfall relationship

Maher et al. (1994) developed a climate function (Eq. 1) calculating mean annual precipitation from the magnetic susceptibility of surface soils of the Chinese Loess Plateau by means of least squares regression. The equation was then successfully used in paleoprecipitation reconstruction. According to Maher et al. (1994, 2002) and Maher and Thompson (1995), this relationship should also be valid for Southeastern and Eastern European LPSS. Indeed, Panaiotu et al. (2001) performed a paleorainfall reconstruction based on this formula for the Mostistea section. Eq. (1) was applied to the profiles and to the susceptibility record of Koriten (Jordanova and Petersen, 1999b). The χ_c value was not strictly determined according to Maher et al. (1994), who used the susceptibility data of the parent material for pedogenesis i.e. of the respective loess unit below a paleosol as background values. However, due to pedogenic alteration of several loess units, in this study the lowest susceptibility value of the loess for each profile was selected as characteristic background for the respective profile, assuming that initial background composition of highly susceptible minerals does not change significantly with depth. Loess units with remarkable pedogenetic overprint from the paleosol in the top, as to field observations and elevated susceptibility values, were excluded from the calculation (see Table 2-3). To test this assumption, rainfall was also calculated by taking the χ_c -values from the loess unit below the respective paleosol

unit, wherever it was possible. In most cases both results are very close (Table 2-3) and lead to the same interpretation: The calculated MAP values for the recent soil do not correspond to the numerical values derived from the climatological dataset (Fig. 2-2). Only for Stary Kaydaky (this study) and for Mostistea (Panaiotu et al., 2001) are the calculated MAP values closer to the true ones. The relative MAP relationship between sections is reflected neither in the calculated present-day values nor in the reconstructed paleoprecipitation (except for the S2 unit). Therefore, Eq. (1) cannot be simply transferred to the study area. However, it might be valuable for the comparison of relative precipitation patterns on small regional scale, since it reflects relatively well the Mostistea-Mircea Voda relationship. Improvement of Eq. (1) by increasing the dataset for the susceptibility-rainfall regression would also not ensure realistic values, since the site with the lowest MAP (Mircea Voda) exhibits the highest susceptibility enhancement for the modern soil and also for some paleosols.

For the observed disagreement, several explanations are possible, which are hard to evaluate with the available dataset. First, the magnetic susceptibility of a subsoil horizon (as suggested by Maher et al., 1994) cannot be used to calculate the present day MAP, since the S0 soils are steppe soils lacking of any B-horizon. Susceptibility enrichment effects due to surface pollution, cannot be discounted, for example by atmospheric deposition of magnetic spherules out of fossil combustion (Thompson and Oldfield, 1986). Also a different fire history may disturb the MAP-susceptibility relationship (Maher and Thompson, 1995). Further, it can be argued whether the susceptibility of a soil is in equilibrium with the climatic conditions during all the time of pedogenesis. Though gleying was not observed, the optimum humidity conditions for the formation and sustainment of ferrimagnetic minerals may be exceeded in some units. Therefore, the regression function of Maher et al. (1994) has to be critically evaluated. Maher et al. (2002) presented a rainfall - susceptibility analysis of several Russian steppe soils, which fit well with data from the Chinese Loess Plateau. However, some data points of the Russian and Ukrainian steppe, having the same pedogenic susceptibility, show

MAP values between about 330 and 510 mm/year. Probably other climatic and/or pedogenic factors such as seasonal distribution of precipitation, temperature and time may be responsible for this scatter (Maher, 1998; Vidic et al. 2004) and may also disturb the MAP-susceptibility relation for these sections. Maher herself found, besides the MAP-susceptibility relation, a significant correlation of temperature and susceptibility (Maher et al., 1994).

Table 2-3. Paleoprecipitation for the profiles Batajnica/Stari Slankamen, Mircea Voda, Stary Kaydaky, Koriten, Mostistea. Values were calculated from the magnetic susceptibility using Eq. 1, presented by Maher et al. (1994). For Mostistea, the results from the calculation by Panaiotu et al. (2001) are shown. Background magnetic susceptibility was taken from a reference loess unit (Ref.) for each section. Wherever it was possible, rainfall calculations were also conducted for background susceptibilities taken from the respective loess unit below a paleosol (results in brackets).

| <i>Batajnica / Stari Slankamen</i> | | <i>Mircea Voda</i> | | <i>Stary Kaydaky</i> | | <i>Koriten (calculation done on values of Jordanova 1999b)</i> | | <i>Mostistea (according to Panaiotu et al. 2001)</i> | |
|--|-------------|------------------------|-------------|--------------------------|-------------|--|-------------|--|-------------|
| Unit | MAP [mm] | Unit | MAP [mm] | Unit | MAP [mm] | Unit | MAP [mm] | Unit | MAP [mm] |
| S0 | 537 | S0 | 570 | S0 | 547 | S0 | 570 | S0 | 587 |
| L1L1 | 328 | L1L1 | 372 | L1L1 | Ref. | | | | |
| L1S1 | 441 | L1S1 | 451 | L1S1 | 442 | | | | |
| L1L2 | 330 | L1L2 | 331 | L1L2 | 424 | | | | |
| S1 | 604 | S1 | 561 | S1 | 538 | S1 | 543 | S1 | 580 |
| L2 | Ref. | L2 | Ref. | L2 | 188 | Ref. | | | |
| S2S1 | 471 | S2S1 | 425 | S2S1 | 348 | S2S1 | 444 | | |
| S2S2-3 | 597 | S2S2 | 533 | S2S2-3 | 578 | S2S2-3 | 593 | S2 | 603 |
| | | S2S3 | 573 | | | | | | |
| L3 | 341 | L3 | 384 | | | | | | |
| S3 | 621 | S3 | 631 | S3 | 580 | S3 | 631 | S3 | 627 |
| L4 | 373 | L4 | 339 | | | | | | |
| S4 | 544 | S4 | 620 | S4 | 491 | S4 | 606 | | |
| | | L5 | 330 | | | | | | |
| S5 | 612 | S5 | 615 | S5 | 485 | S5 | 599 | | |
| L6 | 328 | L6 | 371 | | | | | | |
| S6 | 573 | S6S1 | 534 | | | S6 | 580 | | |
| | | S6S2 | 539 | | | | | | |

Altogether in our study area, the use of magnetic susceptibility as a quantitative MAP proxy does not seem rational for the comparison of absolute MAP values between the sections. However, magnetic susceptibility is sufficiently valid for careful qualitative paleoclimatic deductions within one section due to the general mechanisms of susceptibility enhancement (Section 2).

6.4 Paleoclimatic conclusions

The magnetic susceptibility records of the studied Southeastern/Eastern European sections show high susceptibility values in the paleosols and low values in the loesses (Fig. 2-3), reflecting the sequence of interstadial/interglacial and stadial/glacial periods of the Quaternary (Fig. 2-5). This is in accordance with the susceptibility enhancement model for the Chinese LPSS. Reduction of the magnetic susceptibility of paleosols in comparison to the loess units, due to waterlogged conditions or the wind-vigor model – as described for some sections of Siberia and Alaska (Evans and Heller, 2001) – could not be found. Focusing on the paleosols of Batajnica/Stari Slankamen and Mircea Voda, there is an increase in susceptibility from the S1 - in Batajnica, from the S2 - to the S3. The S3 shows strongest susceptibility enhancement of the whole LPSS. This is interpreted as an indication of a warmer and wetter climate during MIS 9 compared to the younger interglacials/interstadials. This observation corresponds to the susceptibility record of other sections of the Northern Black Sea coastal area (Dodonov et al., 2006a), the lower Danube area (Jordanova and Petersen, 1999b; Panaiotu et al., 2001), as well as to the records of the sections Darai Kalon (Dodonov et al., 2006b) and Chashmanigar (Ding et al., 2002) in Tajikistan, whereas the Karamaidan section (Tajikistan, Forster and Heller, 1994) and the stacked record of Lingtai/Zhaojiachuan (Sun et al., 2006) show different susceptibility behavior. A direct climatic trigger mechanism, responsible for these findings, could not yet be identified. Local climatic factors may explain why there are paleosols in some sections, which do not exhibit the observed trend. Below the S3, there is a trend to lower susceptibility values at least upto S6, also described for Koriten by Jordanova and Petersen (1999b). Field observations at the Serbian and Romanian sections, the observations of Marković et al. (2009), specifically for Batajnica and the study of Bronger on sections of the Carpathian basin (1976), especially the Stari Slankamen site, show a trend from more steppe-soil type paleosols at the top of the LPSS to stronger developed and more reddish (rubificated) paleosols at the bottom, partly with iron and manganese coating. In the

Lingtai/Zhaojiachuan record, the S5 is the one having the strongest susceptibility enhancement among the Brunhes-chron-paleosols. Therefore, the susceptibility enhancement of these older paleosols does not fully reflect the intensity of pedogenesis. At the present state, decrease of susceptibility at the paleosols of MIS 11–17 is tentatively explained by an increase in humidity, so that the optimum conditions for the formation of ferrimagnetic minerals could be exceeded. These results implicate a stronger monsoonal type of climate at the beginning of the Mid-Pleistocene, at least for Southeastern Europe. For Stary Kaydaky, a climatic interpretation of the susceptibility record is difficult, because the signal is significantly diminished in the older units (S4, S5) for some unknown reason. Field observations and the susceptibility record of the younger units do not support a trend as in the Southeastern European sections. Presumably, the (paleo)-climate of this location is controlled by another trigger mechanism.

Further paleoclimatic and rock magnetic research on LPSS of Southeastern and Eastern Europe is necessary to validate these rather preliminary interpretations and to find answers for the open questions revealed by this study.

7 Conclusions

- 1) Loess-paleosol sequences of the sections Batajnica/Stari Slankamen (Serbia) and Mircea Voda (Romania) comprise at least six and at Stary Kaydaky (Ukraine) at least five paleosol/pedocomplexes. Susceptibility enhancement is generally found in paleosols. Similar patterns in the susceptibility record allowed spatial correlation of the stratigraphic units to profiles in the Chinese loess plateau and also with the benthic $\delta^{18}\text{O}$ record of ODP 677. The Mircea Voda and Batajnica/Stari Slankamen sections bear paleoclimatic records at least to MIS 17 and the Stary Kaydaky section probably to MIS 13-15. The Kaydaky pedocomplex is correlated with MIS 5e and the underlying Dnieper loess with MIS 6. The presented chronostratigraphy for the studied sections is additionally

confirmed by pedostratigraphic correlations to other dated loess-paleosol sequences of Southeastern and Eastern Europe. It provides the possibility to regard the stratigraphic units as correlatives of loess-paleosol units in the Chinese stratotype sections of the Quaternary (Kukla and An, 1989) and to avoid the use of (often confusing) local stratigraphic names in future studies.

- 2) The stratigraphic work suggests a rediscussion of the astronomical tuning of the MIS 6 / MIS 7 boundary for the Chinese loess-paleosol sequences.
- 3) For the calculation of sedimentation rates, it is strongly recommend to use sensitivity analyses with respect to the applied timescale and to the degree of synpedogenetic sedimentation in order to interpret reliable results. At Mircea Voda, relatively high sedimentation rates were clearly obtained for the younger loess units, especially the L1 and L3. Lowest rates of dust deposition during a cold stage occurred in MIS 16 (=L6) and during a warm stage in MIS 13-15 (=S5). The marine isotope stage 7 was characterized by relatively high sedimentation rates for an odd numbered marine isotope stage, probably due to intercalated periods of pronounced climate deterioration.
- 4) The mean annual precipitation-susceptibility relation obtained by Maher et al. (1994) is not valid for this study area, at least not for the large regional scale from Serbia and Romania to Ukraine. However, magnetic susceptibility can be used for qualitative interpretations within a single section.
- 5) Qualitative paleoclimatic interpretations of the obtained susceptibility dataset indicate a gradual increase of paleoprecipitation from the younger to the older warm stages in Southeastern Europe. the tentative paleoclimatic interpretation emphasizes the potential and need for further research in the study area.

Acknowledgements

We thank Tivadar Gaudenyi and Mladjen Jovanović for assistance during fieldwork in Serbia and Simo Spassov and Jozef Hus, as well as an anonymous reviewer for their constructive comments on the manuscript. Financial support was provided by the German Research Foundation DFG (GL 327/8-2).

References

- Avramov, V.I., Jordanova, D., Hoffmann, V., Roesler, W., 2006. The role of dust source area and pedogenesis in three loess-paleosol sections from North Bulgaria: A mineral magnetic study. *Studia Geophysica et Geodaetica* 50 (2), 259-282.
- Bassinot, F.C., Labeyrie, L.D., Vincent, E., Quidelleur, X., Shackleton, N.J., Lancelot, Y., 1994. The astronomical theory of climate and the age of the Brunhes-Matuyama magnetic reversal. *Earth and Planetary Science Letters* 126, 91-108.
- Bolikhovskaya, N.S., Molodkov A.N., 2006. East European loess-palaeosol sequences: Palynology, stratigraphy and correlation. *Quaternary International* 149, 24-36.
- Bronger, A., 1976. Zur quartären Klima – und Landschaftsentwicklung des Karpatenbeckens auf paläopedologischer und bodengeographischer Grundlage. *Kieler Geographische Schriften* 45.
- Bronger, A., 2003. Correlation of loess-paleosol sequences in East and Central Asia with SE Central Europe: towards a continental Quaternary pedostratigraphy and paleoclimatic history. *Quaternary International* 106-107, 11-31.
- Buggle, B., Glaser, B., Zöller, L., Hambach, U., Marković, S., Glaser, I., Gerasimenko, N., 2008. Geochemical characterization and origin of Southeastern and Eastern European loesses (Serbia, Romania, Ukraine). *Quaternary Science Reviews* 28 (9-10), 1058-1075.
- Chen, J., Junfeng, J., Balsam, W., Chen, Y., Liu, L., An, Z., 2002. Characterization of the Chinese loess-paleosol stratigraphy by whiteness measurement. *Palaeogeography, Palaeoclimatology, Palaeoecology* 183, 287-297.
- Chen, T., Xu, H., Xie, Q., Chen, J., Ji, J., Lu, H., 2005. Characteristics and genesis of maghemite in Chinese loess and paleosols: Mechanism for magnetic susceptibility enhancement in paleosols. *Earth and Planetary Science Letters* 240, 790-820.
- Conea, A., 1969. Profils de Loess en Roumanie. *Supplément au Bulletin de l'Association française pour l'étude du Quaternaire*, 127-134.
- Derbyshire, E., Kemp, R.A., Meng, X., 1997. Climate change, loess and paleosols: proxy measures and resolution in North China. *Journal of the Geological Society, London* 154, 793-805.
- Ding, Z.L., Ranov, V., Yang, S.L., Finaev, A., Han, J.M., Wang, G.A., 2002. The loess record in southern Tajikistan and correlation with Chinese loess. *Earth and Planetary Science Letters* 200, 387-400.
- Dodonov, A.E., Zhou, L.P., Markova, A.K., Tchepalyga, A.L., Trubikhin, V.M., Akesandrovski, A.L., Simakova, A.N., 2006a. Middle-Upper Pleistocene bio-climatic and magnetic records of the Northern Black Sea Coastal Area. *Quaternary International* 149, 44-54.

-
- Dodonov, A.E., Sadchikova, T.A., Sedov, S.N., Simakova A.N., Zhou, L.P., 2006b. Multidisciplinary approach for paleoenvironmental reconstruction in loess-paleosol studies of the Darai Kalon section. *Quaternary International* 152-153, 59-69.
- Domokos, M., Neppel, F., Somogyi, S., 2000. Paläogeographische Geschichte der Donau und ihres Einzugsgebietes. *Hydrologie und Wasserbewirtschaftung* 44 (4), 172-183.
- Evans, M.E., Heller, F., 2001. Magnetism of loess/palaeosol sequences: recent developments. *Earth-Science Reviews* 54, 129-144.
- Evans, M.E., Heller, F., 2003. Environmental magnetism – principles and applications of Enviromagnetics. Academic Press, Amsterdam.
- Forster, Th., Heller, F., 1994. Loess deposits from the Tajik depression (Central Asia): magnetic properties and paleoclimate. *Earth and Planetary Science Letters* 128, 501-512.
- Frey, W., Lösch, R., 1998. *Lehrbuch der Geobotanik*. Gustav Fischer, Stuttgart.
- Fuchs, M., Rousseau, D. D., Antoine, P., Hatté, C., Gauthier, C., Marković, S., Zöller, L. 2008. Chronology of the Last Climatic Cycle (Upper Pleistocene) of the Surduk loess sequence, Vojvodina, Serbia. *Boreas* 37, 66-73.
- Gerasimenko, N.P., 1988. Pleistocene and Pliocene Vegetational and Soil Evolution at the Kiev Dnieper area, Ukraine. VINITI, Moscow, (in Russian).
- Gerasimenko, N.P., 2000. Late Pleistocene vegetational and soil evolution at the Kiev Loess Plain as recorded in the Stari Bezradychy section, Ukraine. *Studia Quaternaria* 17, 19-28.
- Gerasimenko, N. P., 2004. Quaternary Evolution of Zonal Paleoecosystems in Ukraine. Geophysical Institute of National Ukrainian Academy of Sciences, Kyiv, (in Ukrainian).
- Gerasimenko, N.P., 2006. Upper Pleistocene loess-palaeosol and vegetational successions in the Middle Dnieper Area, Ukraine. *Quaternary International* 149, 55-66.
- Gozhik, P.F., Shelkopyas, V.N., Komar M.S., Matviishina, Zh.N., Perederiy, V.I., 2000. Correlation of Loesses and Glacial Deposits of Poland and Ukraine. X Polish-Ukrainian Seminar, Kyiv, (in Ukrainian).
- Guiter, F., Andrieu-Ponel, V., de Beaulieu, J., Cheddadi, R., Calvez, M., Ponel, P., Reille, M., Keller, T., Goeury, C., 2003. The last climatic cycles in Western Europe: a comparison between long continuous lacustrine sequences from France and other terrestrial records. *Quaternary International* 111, 59-74.
- Haase, G., Richter, H., 1957. Fossile Böden im Löss an der Schwarzmeeküste bei Constanta. *Petermanns Geographische Mitteilungen* 101, 161-173.
- Heller, F., Liu, T., 1984. Magnetism of Chinese loess deposits. *Geophysical Journal Royal Astronomical Society* 77. 125-141.
- Heslop, D., Langereis, C.G., Dekkers, M.J., 2000. A new astronomical timescale for the loess deposits of Northern China. *Earth and Planetary Science Letters* 184, 125-139.
- <http://ns.geo.edu.ro/~paleomag/loess-MV.htm>, downloaded on 23.10.2006. (E.C. Panaiotu, University of Bucharest).
- Jordanova, D., Petersen, N., 1999a. Palaeoclimatic record from a loess-soil profile in northeastern Bulgaria—I. Rock magnetic properties. *Geophysical Journal International* 138, 520-532.
- Jordanova, D., Petersen, N., 1999b. Palaeoclimatic record from a loess-soil profile in northeastern Bulgaria—II. Correlation with global climatic events during the Pleistocene. *Geophysical Journal International* 138, 533-540.
- Jordanova, D., Hus, J., Geeraerts, R., 2007. Palaeoclimatic implications of the magnetic record from loess/palaeosol sequence Viatovo (NE Bulgaria). *Geophysical Journal International* 171, 1036-1047.

- Kohfeld, K.E., Harrison S.P., Glacial-interglacial changes in dust deposition on the Chinese Loess Plateau, *Quaternary Science Reviews*, 22, 1859-1878, 2003.
- Kostić, N., Protic, N., 2000. Pedology and mineralogy of loess profiles at Kapela-Batajnica and Stalac, Serbia. *Catena* 41, 217-227.
- Krokos, V.I., 1932. Directions on studies of Quaternary deposits in Ukraine, *Chetvertynny period* 3, 17-55, (in Ukrainian).
- Kukla, G.J., 1987. Loess Stratigraphy in Central China. *Quaternary Science Reviews* 6, 191-219.
- Kukla, G.J., An, Z., 1989. Loess Stratigraphy in Central China. *Palaeogeography, Palaeoclimatology, Palaeoecology* 72, 203-225.
- Lai, Z-P., Wintle, A.G., 2006. Locating the boundary between the Pleistocene and the Holocene in Chinese loess using luminescence. *Holocene* 16, 893-899.
- Lindner, L., Bogutsky, A., Gozhik, P., Marks, L., Fancont, M., Wojtanowicz, J., 2006. Correlation of Pleistocene deposits in the area between the Baltic and Black Sea, Central Europe. *Geological Quarterly* 50 (1), 195-210.
- Litt, T., Brauer, A., Golsar, T., Merkt, J., Bałaga, K., Müller, H., Ralska-Jasiewiczowa, M., Stebich, M., Negendank, J.F.W., 2001. Correlation and synchronisation of Lateglacial continental sequences in northern central Europe based on annually laminated lacustrine sediments. *Quaternary Science Reviews* 20, 1233-1249.
- Maher, B.A., 1998. Magnetic properties of modern soils and Quaternary loessic paleosols: paleoclimatic implications. *Palaeogeography, Palaeoclimatology, Palaeoecology* 137, 25-54.
- Maher, B.A., Thompson, R., 1995. Paleorainfall reconstructions from pedogenic magnetic susceptibility variations in the Chinese loess and paleosols. *Quaternary Research* 44, 383-391.
- Maher, B.A., Thompson, R., Zhou, L.P., 1994. Spatial and temporal reconstructions of changes in the Asian palaeomonsoon: A new mineral magnetic approach. *Earth and Planetary Science Letters* 125, 461-471.
- Maher, B.A., Alekseev, A., Alekseeva, T., 2002. Variation of soil magnetism across the Russian steppe: its significance for use of soil magnetism as a palaeorainfall proxy. *Quaternary Science Reviews* 21, 1571-1576.
- Marković-Marjanovic, J. 1968. Loess section in the Danube Valley, Yugoslavia, and their importance for the Quaternary stratigraphy of south-eastern Europe. In: Schultz, C.B. and Frye, J.C. (Eds.), *Loess and Related Eolian Deposits of the World*, 7th International Congress on Quaternary (INQUA), Boulder 1965, Report 12, University of Nebraska Press, Lincoln 261-278.
- Marković, S.B., Heller, F., Kukla, G.J., Gaudenyi, T., Jovanović, M., Miljković, L.J., 2003. Magnetostratigraphy of Stari Slankamen loess section. *Zbornik radova Instituta za geografiju* 32, 20-28 (in Serbian with English summary).
- Marković S.B., Kostić, N., Oches, A.E., 2004a. Paleosols in the Ruma loess section. *Revista Mexicana de Ciencias Geológicas* 21, 79-87.
- Marković S.B., Oches EA, Gaudenyi T, Jovanović M, Hambach U, Zöller L, Sümegi P, 2004b. Paleoclimate record in the Late Pleistocene loess-palesol sequence at Miseluk (Vojvodina, Serbia). *Quaternaire* 15, 361-368.
- Marković, S.B., Heller, F., Kukla, J.G., Gaudenyi, T., Jovanović, M., 2004c. The paleoclimatic record of Stari Slankamen loess-palesol sequence during the last 850 ka, In: Marković, S.B., Jovanović, M. and Ercegovac, M.(Eds.), *Field Guide of Milutin Milankovitch Anniversary Symposium*. Serbian Academy of Sciences and Arts, Belgrade, 6-12.
- Marković, S.B., McCoy, W.D., Oches, E.A., Savić, S., Gaudenyi, T., Jovanović, M., Stevens, T., Walther, R., Ivanišević, P., Galović, Z., 2005. Paleoclimate record in the Late

- Pleistocene loess-paleosol sequence at Petrovaradin Brickyard (Vojvodina, Serbia). *Geologica Carpathica* 56, 545-552.
- Marković, S.B., Oches, E.A., Sümegi, P., Jovanović, M., Gaudenyi, T., 2006. An introduction to the Middle and Upper Pleistocene loess-paleosol sequence at Ruma brickyard, Vojvodina, Serbia. *Quaternary International* 149, 80-86.
- Marković, S.B., Oches, E.A., McCoy, W.D., Gaudenyi, T., Frechen, M., 2007. Malacological and sedimentological evidence for “warm” climate from the Irig loess sequence (Vojvodina, Serbia). *Geophysics, Geochemistry and Geosystems* 8. Q09008.
- Marković, S.B., Bokhorst, M.P., Vandenberghe, J., McCoy, W.D., Oches, E.A., Hambach, U., Gaudenyi, T., Jovanović, M., Stevens, T., Zöller, L., Machalet, B., 2008. Late Pleistocene loess-paleosol sequences in the Vojvodina region, North Serbia. *Journal of Quaternary Science* 23 (1), 73-84.
- Marković, S.B., Hambach, U., Catto, N., Jovanović, M., Bugge, B., Machalet, B., Zöller, L., Glaser, B., Frechen, M., 2009. Middle and Late Pleistocene loess sequences at Batajnica, Vojvodina, Serbia. *Quaternary International* 198, 255-266.
- Marsigli, L.F., 1726. *Danubius Pannonico Mysicus; Observationibus Geographicis, Astronomicis, Hydrographicis, Physicis; perlustratus*: Grosse, P., Alberts, Chr., de Hoodt P., Herm. Uytwert and Franc Changuion, The Hague and Amsterdam.
- Matviishina, Zh. N., 1982. Micromorphology of Pleistocene soils of Ukraine. *Naukova Dumka, Kiev*, (in Russian).
- Mavrocordat, G., 1971. Die Böden Rumäniens, *Giessener Abhandlungen zur Agrar-, und Wirtschaftsforschung des Europäischen Ostens* 58.
- Minkov, M., 1970. Über die Lössstratigraphie in Nordbulgarien. *Arbeit der INQUA Lösskommission, Bulgarien* 1970, 3-51.
- Panaiotu, C. G., Panaiotu, E. C., Grama, A., Necula, C., 2001. Paleoclimatic record from a loess-paleosol profile in Southeastern Romania. *Physics and Chemistry of the Earth (A)* 26, 893-898.
- Rousseau, D.D., Gerasimenko, N.P., Matviishina, Z., Kukla, G.J., 2001. Late Pleistocene environments of the Central Ukraine. *Quaternary Research* 56, 349-356.
- Shackleton, N.J., Berger, A., Peltier, W.R., 1990. An alternative astronomical calibration of the lower Pleistocene timescale based on ODP Site 677. *Transactions of the Royal Society of Edinburgh: Earth Sciences* 81, 251-261.
- Sirenko, N.A., Turlo, S.I., 1986. *Evolution of Soils and Vegetation of Ukraine at Pliocene and Pleistocene*. *Naukova Dumka, Kiev*, (in Russian).
- Smalley, I., Leach, J.A., 1978. The origin and distribution of the loess in the Danube basin and associated regions of East-Central Europe- A review. *Sedimentary Geology* 21, 1-26.
- Sträßler, M., 1998. *Klimadiagramme zur Köppenschen Klimaklassifikation*. Klett-Perthes, Gotha.
- Sun, Y., S.C. Clemens, Z. An, Yu, Z., 2006. Astronomical timescale and palaeoclimatic implication of stacked 3.6-Myr monsoon records from the Chinese Loess Plateau. *Quaternary Science Reviews* 25, 33-48.
- Tang, Y., Jia, J., Xie, X., 2003. Records of magnetic properties in Quaternary loess and its paleoclimatic significance: a brief review. *Quaternary International* 108, 33-50.
- Thompson, R., Oldfield, F., 1986. *Environmental Magnetism*. Allen & Unwin Ltd., London.
- Újvári, G., Varga, A., Balogh-Brunstad, Z., 2008. Origin, weathering, and geochemical composition of loess in southwestern Hungary. *Quaternary Research* 69, 421-437.
- Veklitch, M.F., 1969. La stratigraphie des loess d'Ukraine. *Supplément au Bulletin de l'Association française pour l'étude du Quaternaire*, 145-150.
- Veklitch, M.F. (Ed.), 1993. *Stratigraphical framework of the Quaternary of Ukraine*. Gosgeolkom Ukrainy, Kiev. (In Ukrainian).

-
- Veklitch, M.F., Sirenko, N.A., 1972. Geological key sites of the Ukrainian Quaternary, vol. 3. Naukova Dumka, Kiev (in Russian).
- Vidic, N.J., Singer, M.J., Verosub, K.L., 2004. Duration dependence of magnetic susceptibility enhancement in the Chinese loess-palaeosols of the past 620 ky. *Palaeogeography, Palaeoclimatology, Paleoecology* 211, 271-288.
- Walter, H., 1974. *Die Vegetation Osteuropas, Nord- und Zentralasien..* Gustav Fischer Verlag, Stuttgart.
- WMO, World Meteorological Organization, 1996. *Climatological Normals (CLINO) for the Period 1961-1990.* Secretariat of the World Meteorological Organization, Geneva.
- Zhou, L.P., Shackleton, N.J., 1999. Misleading positions of the geomagnetic reversal boundaries in Eurasian loess and implications for the correlation between continental and marine sedimentary sequences. *Earth and Planetary Science Letters* 168, 117-130.

Study 3

An evaluation of geochemical weathering indices in loess-paleosol studies

Björn Buggle^{1*}, Bruno Glaser¹, Ulrich Hambach², Natalia Gerasimenko³ and Slobodan Marković⁴

¹ Soil Physics Department, University of Bayreuth, D-95440 Bayreuth, Germany.

² Chair of Geomorphology, University of Bayreuth, D-95440 Bayreuth, Germany.

³ Earth Science and Geomorphology Department, Tarasa Shevchenko National University of Kyiv, Ukraine.

⁴ Chair of Physical Geography, Faculty of Sciences, University of Novi Sad, Trg Dositeja Obradovića 3, 21000 Novi Sad, Serbia.

Quaternary International

In press

DOI:10.1016/j.quaint.2010.07.019

Corresponding author: Björn Buggle, Phone:+49(0)921 552174

E-mail: Bjoern.Buggle@uni-bayreuth.de

Abstract

Applying geochemical proxies as measure for the weathering intensity of paleosols and sediments such as loess, the Quaternary scientist is confronted with various element ratios that have been proposed in literature. This paper gives an overview on the principle of geochemical weathering indices. Different types of indices are evaluated with respect to the suitability for loess-paleosol sequences, regarding the special characteristics of this type of sediments and paleosols. Case examples in this study are key sections in Southeastern and Eastern Europe: the loess-paleosol sequences Batajnica/Stari Slankamen (Serbia), Mircea Voda (Romania) and Stary Kaydaky (Ukraine), which represent archives of the Late and Mid-Pleistocene climate change of the region. Considering element behavior during weathering or diagenesis, the Chemical Proxy of Alteration (CPA) - i.e. the molar ratio $\text{Al}_2\text{O}_3/(\text{Al}_2\text{O}_3 + \text{Na}_2\text{O}) \times 100$ - is proposed as the most appropriate index for silicate weathering. The CPA was evaluated against commonly used weathering indices including the "Chemical Index of Alteration" (CIA), the "Chemical Index of Weathering" (CIW), the "Plagioclase Index of Alteration" (PIA), the Index B of Kronberg and Nesbitt, and the Ba/Sr and Rb/Sr ratio. Depth profiles of "Sr-type indices" (e.g. Ba/Sr, Rb/Sr) are likely to be influenced by the dynamics of secondary carbonate. On the other hand, common "Na-type indices" (e.g. CIA, PIA, CIW) may suffer from uncertainties in separating carbonate-Ca from silicate-Ca or from biases due to K-fixation (illitization). The CPA is insensitive against such effects. Additionally, using the CPA (as with other Na-type indices) gives the possibility to evaluate the homogeneity of the parent material regarding the relevant host minerals via the A-CN-K diagram.

Keywords: Weathering Index, Chemical Proxy of Alteration, CPA, Paleosols, Loess, Southeastern Europe

1 Introduction

“Loess is a terrestrial clastic sediment, composed predominantly of silt-sized particles, which is formed essentially by the accumulation of wind-blown dust” (Pye, 1995). In Northern- and mid-latitudes, this dust originated mainly from sparsely vegetated foreland areas of the ice sheets and the alluvial plains of large rivers during the Pleistocene cold periods (Smalley and Leach, 1978; Buggle et al., 2008; Újvári et al., 2008; Smalley et al., 2009). Also, desert regions may represent important dust source areas (e.g. Smalley and Krinsley, 1978). It was only during interstadial and interglacial warm periods and more humid periods, respectively, when dust deposition decreased or even ceased, so that environmental conditions allowed extensive mineral weathering and thus soil formation. Therefore, sequences of relatively unaltered loess and more or less well developed paleosols – so-called loess-paleosol sequences (LPSS) – reflect land surface stability and Pleistocene climate development.

Under weathering conditions, the element composition of a given parent material changes. Soluble and mobile elements are depleted and less soluble and immobile elements are enriched. However, pedogenesis does not only mean weathering of minerals and loss of elements, but also mineral transformation and formation of new (secondary) minerals such as clay minerals or iron oxides. Amount and composition of iron oxides for example can be reflected in mineral magnetic properties as well as the color of a soil sample (Schwertmann, 1993, Evans and Heller, 2003). As the type and intensity of such pedogenic features essentially depend on (soil-) environmental conditions, they can be valuable indicators of the (past) climatic characteristics. There are a number of parameters and various proposals by paleopedologists for proxies enabling a quantification of paleoclimatic meaningful pedogenic processes (e.g. Derbyshire et al., 1997). Maher et al. (1994) for example introduced a quantitative relationship between enhancement of the magnetic susceptibility as proxy for the pedogenic formation of ferromagnetics and mean annual precipitation. However, in several situations this approach has shown to be not straightforward (Evans and Heller, 2003, Buggle

et al., 2009). Other widely used measures of pedogenesis intensity are geochemically based weathering indices. Although relying on similar concepts, a variety of such indices have been published in literature (e.g. Ding et al., 2001; Smykatz-Kloss, 2003; Schellenberger and Veit, 2006). Especially, non-geochemically specialized Quaternary scientists are often confronted with the question: “what is the most appropriate index for a certain LPSS and, respectively, LPSS in general?”. From this evolves the motivation to give an overview on the principle of geochemical weathering indices aiming towards an answer for this question. The case examples for this purpose, use geochemical data of the loess-paleosol sequences Batajnica/Stari Slankamen (Serbia), Mircea Voda (Romania) and Stary Kaydaky (Ukraine).

2 Material and Methods

The composite loess-paleosol sequence Batajnica and Stari Slankamen (44° 55' 29'' N, 20° 19' 11'' E and 45° 7' 58'' N, 20° 18' 44'' E) is situated in the Vojvodina, the Serbian part of the Pannonian (Carpathian) Basin. The two individual profiles are about 40 km distant to each other and located along the banks of the Danube River. Each section is about 40 m thick and comprises at least six major interglacial pedocomplexes (Buggle et al., 2009; Marković et al., 2009). Due to a major hiatus in the younger part of the Stari Slankamen site and ground water influence at the older part of the Batajnica site, Buggle et al. (2008, 2009) built a composite rock magnetic and geochemical record from these two sites using the younger (<MIS 9) part from Batajnica and the older (>MIS 9) from Stari Slankamen. The time span represented by the composite record includes the last 17 Marine Isotope Stages (Buggle et al., 2009).

The Mircea Voda loess-paleosol sequence (44° 19' 15'' N, 28° 11' 21'' E) is located in the Dobrudja region (Romania) between the Danube and the Black Sea coast. This site is formed by a similar succession of loess and paleosol units as the Serbian one, comprising also the last 17 MIS.

Both, the Serbian and Romanian sections represent LPSS on loess-plateaus, with thick loess layers separating the major interglacial pedocomplexes. The main climatic difference between both sites is the more pronounced dryness at Mircea Voda (~ 400 – 450 mm mean annual precipitation) than in the Vojvodina region (~ 600 – 680 mm mean annual precipitation).

The outcrops of the Stary Kaydaky site (48° 22' 42'' N, 35° 07' 30'' E) are situated in a system of gullies near to the Dnieper River (Ukraine). The profile comprises the last 15 MIS. However, most loess layers separating the interglacial pedocomplexes are eroded and thin. While the Serbian and Romanian site contain carbonate throughout the profile, parts of the Stary Kaydaky LPSS are completely free of carbonates. Therefore, older loess layers and paleosols are partly influenced by pedogenesis and weathering during subsequent interglacials.

For detailed information on the regional setting, description of the loess-paleosol successions, the chronostratigraphy, sampling strategy and sample preparation for geochemical analyses please refer to Bugge et al., (2008, 2009). Composition of major and trace elements was determined using a Philips 2404 X-Ray Fluorescence (XRF) Spectrophotometer. Determination of the carbonate content followed the procedure of Hedges and Stern (1984) by calculating the difference in C content of the sample material with and without vapor fumigation. The measurement was carried out on a Vario EL element analyzer (Elementar, Hanau, Germany) at the University of Bayreuth. Element ratios are calculated on molar base. The nomenclature of the lithological units follows the Chinese “S-L” system (Bugge et al., 2009).

3 Chemical weathering indices

3.1 Choosing a chemical proxy of alteration for LPSS? – Principal considerations and hypotheses

The concept of geochemical proxies of mineral alteration (i.e. weathering indices) relies on the selective removal of soluble and mobile elements from a weathering profile compared to the relative enrichment of rather immobile and non-soluble elements (e.g. Smykatz-Kloss, 2003; Yang et al., 2004). A number of element indices, based on this principle, have been published as proxies of mineral weathering for various kinds of sediments, including LPSS (e.g. ; Liu et al., 1993; Chen et al., 1999; Ding et al., 2001; Muhs et al., 2001; Yang et al., 2004; Schellenberger and Veit, 2006; Tan et al., 2006; Jeong et al., 2008; Bokhorst et al., 2009). Especially for non-geochemists it is often difficult to decide which index is most appropriate for a given weathering profile. The following Section gives some background information on element behavior under weathering conditions to deduce the answer of this question in the case of LPSS.

More specifically, two questions must be considered: (i) What is the most appropriate soluble and mobile element? And (ii) What is the most appropriate immobile non-soluble element?

A first step in answering both questions is the classification of the elements according to their ionic potential (IP), i.e., the ratio between ionic charge and ionic radius, as shown in . Cations having an IP below 3 form only weak bonds with oxygen. Thus, they are preferentially released from their host minerals during weathering. In solution, they can be regarded as soluble cations, since they are fully hydrated. If the IP is higher (between 3 and 8), the high density of the positive charge enables strong bonds with oxygen. Thus, these elements form weathering resistant oxides. Furthermore, between an IP of 3 and 10 or 12, (depending on the literature source), the density of the positive charge is in the proper range to cause a deprotonation of water molecules in the hydration shell of the cation. As a result, insoluble

hydroxides or oxyhydrates are formed to achieve charge neutrality. Elements of this category, when released during weathering, precipitate quickly as insoluble and immobile hydrolyzates. With a further increase of the IP i.e. charge density of the cation, all protons of the water molecules are repelled and water soluble anionic complexes are formed (Goldschmidt, 1937; Mason and Moore, 1985; Kutterolf, 2001; Railsback, 2003, 2005; Smykatz-Kloss, 2003). There are also other factors that can influence the solubility of ions, such as the activity of further components in solution, pH-value, redox conditions and temperature. Under near neutral and oxidizing conditions, however, the classification according to the IP successfully predicts the behavior of the most common elements of interest for weathering indices (e.g. alkali-, earth-alkali elements, elements of the Al- and Ti-group), at least in a general way (Blumer, 1950; McBride, 1994; Railsback, 2003; Smykatz-Kloss, 2003).

Concerning question one, all alkali- and earth alkali elements, except for Be, can be categorized as soluble cations according to the ionic potential (Fig. 3-1; Wedepohl, 1978; Railsback, 2003, Reeder et al., 2006). However, solubility does not always mean mobility. With increasing radius, the tendency of an ion for being adsorbed on clay minerals is higher and thus, its mobility is reduced (Nesbitt et al., 1980; Smykatz-Kloss, 2003). Therefore, weathering indices relying on the mobility of the elements Cs, Rb, Ba, K such as Cs/K, Ba/K, Rb/K, K/Zr, K/Ti, K/Al (Harriss and Adams, 1966; Nesbitt et al., 1980; Liu et al., 1993; Muhs et al., 2001) can be expected to be less sensitive for weak pedogenic alteration.

The earth alkali elements Ca, Mg and Sr, having a smaller ionic radius, are common in silicate minerals such as plagioclase, pyroxene, amphibole and biotite, which are susceptible to weathering (Nesbitt et al., 1980; Reeder, et al., 2006). As these elements are highly mobile in the weathering environment, they appear in several weathering indices like the Ba/Sr, Rb/Sr, Sr/K, Sr/Zr, Mg/K, Mg/Ti, Ca/K, Ca/Zr and Ca/Ti-ratio (e.g. Nesbitt et al., 1980; Liu et al., 1993; Chen et al., 1999; Muhs et al., 2001; Bokhorst et al., 2009). However, in a parent material containing carbonate - as in most loess deposits - the mobility of Ca and Mg is

predominantly controlled by the behavior of calcite and dolomite. This is also true for Sr, which can substitute Ca in carbonates (Wedepohl, 1978; Reeder et al., 2006). Therefore, indices relying on Ca, Mg or Sr are not expected to reflect the true weathering and leaching intensity of a paleosol, owing to postpedogenetic formation of secondary carbonates. Thus, it is advisable to restrict the use of such indices to carbonate-free parent material to avoid the problem that effects of silicate weathering are masked by the dynamics of carbonates (Smykatz-Kloss, 2003).

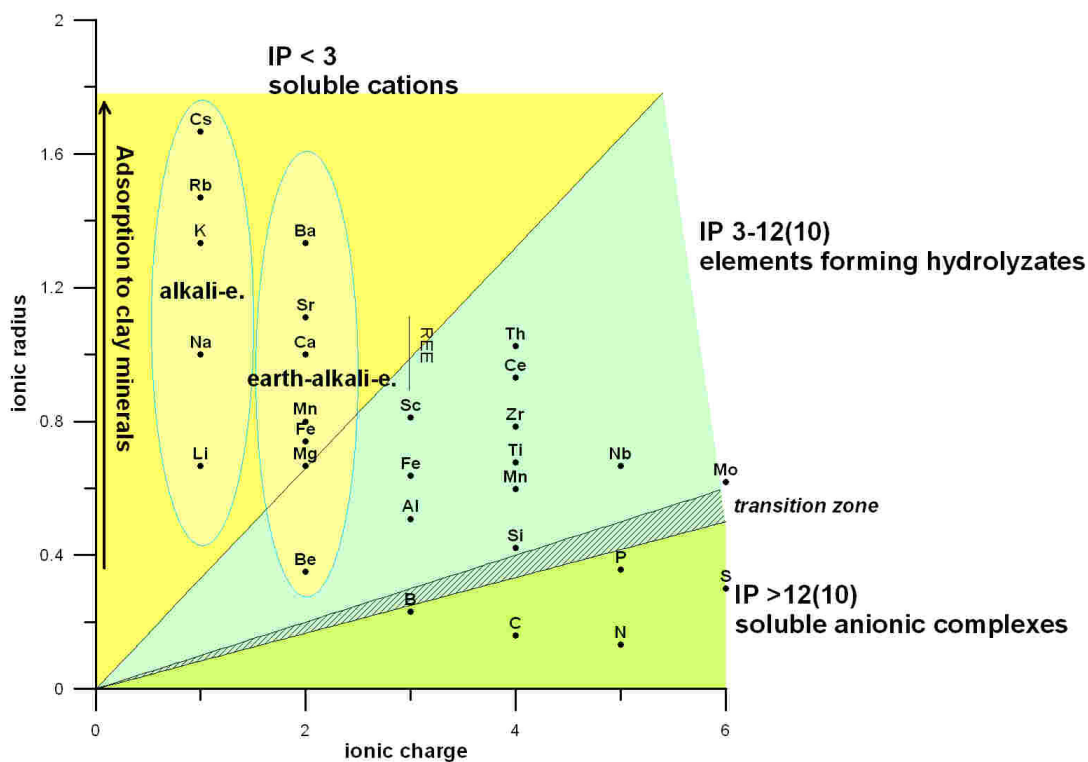


Fig. 3-1. Classification of the elements according to the ionic potential (IP). Values for the ionic potential and ionic radius are taken from Mason and Moore (1985). Cations having an IP below 3 are generally soluble in water, whereas cations with an IP between 3 and 10 (according to Mason and Moore, 1985) or 12, respectively (Goldschmidt, 1937; Kabata-Pendias and Pendias, 2001), form insoluble, immobile hydrolyzates under near neutral-conditions. Elements having a higher IP tend to form soluble anionic complexes. The adsorption to clay minerals tends to increase with the radius of the cation (Nesbitt et al., 1980; Smykatz-Kloss, 2003).

As stated above, the distribution of some elements might be controlled by redox conditions, also after burial of the paleosol. For this reason, the use of the elements Fe and Mn in weathering studies is not recommended.

Having checked all those mentioned criteria, Li^+ and Na^+ appear to be the most suitable mobile cations for weathering indices in loess-paleosol sequences. As the former is seldomly analyzed, the use of Na^+ is proposed.

Regarding the choice of the immobile element, ions of intermediate ionic potential, i.e. ions that tend to form insoluble hydrolyzates (Fig. 3-1) are generally employed. Also Rb, Ba and K i.e. ions that can be immobilized by adsorption on clay minerals due to their large ionic radius, are often used as immobile references, for example in the Rb/Sr, Ba/Sr or Na/K ratio (e.g. Liu et al., 1993; Gallet et al., 1996; Chen et al., 1999; Smykatz-Kloss, 2003; Tan et al., 2006). However, under intense weathering conditions, significant losses of these “large ionic radius elements” can occur during the transformation of micas, feldspars and other host minerals into secondary clay minerals (e.g. Gallet et al., 1996; Muhs et al., 2001). Gallet et al. (1996) for example, observed a significant loss of Rb in the strongly developed Chinese paleosol S5. Thus, the focus should be on elements of the “insoluble hydrolyzate” category, especially on Al, Si, Ti and Zr, which are most frequently used in weathering proxies. As a criterion for a suitable reference element, the mobile and immobile elements should form “a homogeneous mineralogical weathering system”. This means that also the immobile element is hosted by the same, mobile element bearing minerals and their weathering residues. The reason for such a criterion is to minimize possible effects of down-profile variations in the parent material composition. This is especially important in LPSS, where it is not always possible to determine the composition of an unaltered parent material for each pedomember. Thin stadial loess layers for example are often pedogenetically influenced by succeeding periods of soil formation. In that case, the composition of the parent material has to be estimated from thicker unmodified loess layers, assuming a uniform composition of the different loess units. According to the proposed criterion, Na and Al is a suitable pair of elements (in non-saline soils). The main host mineral group of Na and Al in unweathered loess protoliths is the feldspar group. Weathering products of this group are clay minerals and

as end product under extensive weathering conditions kaolinite ($\text{Al}_2\text{Si}_2\text{O}_5(\text{OH}_4)$) or gibbsite ($\text{Al}(\text{OH})_3$), both aluminous residues (Taylor et al., 1983; Taylor and McLennan, 1985; Reeder et al., 2006). In contrast, quartz is an important host mineral for Si. Therefore, a weathering index based on Na and Si would be sensitive for inhomogenities in the quartz content (Smykatz-Kloss, 2003). The same is true for Zr and Ti, which reside in substantial proportions in discrete weathering resistant minerals such as zircon, anatase, rutile, beidellite and ilmenite, respectively. These minerals are possibly present in variable amounts within the profile sequence due to temporally changing heavy mineral enrichment during transport processes (Wedepohl, 1978; Reeder et al., 2006). To conclude, using Na as the mobile element of a weathering index, Al is proposed as the immobile counterpart to minimize biases due to variable mineralogical composition of the loess parent material. Accordingly, simple Al/Na ratios have been used already in earlier studies to characterize the weathering intensity of a material or soil horizon (Gallet et al., 1998; Ding et al., 2001; Smykatz-Kloss, 2003). Instead of a simple Al/Na ratio we suggest the use of molar Al/(Na+Al) ratio times 100 to restrict the index to values between 0 and 100. This avoids out of scale variations and values if Na contents are low. This ratio (Formula 1) was formerly applied by Cullers (2000) for carbonate rich shales, siltstones and sandstones and introduced as Chemical Index of Weathering (CIW'). Cullers used the apostrophe to indicate that his ratio is a modified (Ca-free) version of the classical CIW, published by Harnois (1988, Table 3-1). To the authors' knowledge, the CIW' was never applied to loess deposits previously. However, this index is proposed as the most appropriate geochemically based weathering proxy for most LPSS. Regarding the main host minerals of Na and Al in loess protoliths, it should indicate feldspar, especially plagioclase weathering. In the following, the term **Chemical Proxy of Alteration (CPA)** is used instead of CIW' to avoid any confusion with the classical CIW of Harnois (1988).

$$CPA = 100 \times Al_2O_3 / (Al_2O_3 + Na_2O) \text{ (in molar proportions)} \quad (1)$$

3.2 Overview on widely used indices of feldspar weathering

To test the before mentioned hypotheses, the results derived by the proposed CPA were compared with the Rb/Sr and the Ba/Sr ratios, which are widely employed to characterize weathering intensity in LPSS (e.g. Liu et al., 1993; Gallet et al., 1996; Chen et al., 1999; Ding et al., 2001; Tan et al., 2006; Bokhorst et al., 2009), often notwithstanding the above-mentioned problems concerning these ratios. Furthermore, the CPA was compared to the common established indices for feldspar or plagioclase weathering (Table 3-1): the Chemical Index of Alteration (CIA; Nesbitt and Young, 1982), the Chemical Index of Weathering (CIW; Harnois, 1988), the Plagioclase Index of Alteration (PIA, Fedo, et al., 1995) and Index B of Kronberg and Nesbitt (1981) (see also Guggenberger et al., 1998).

Table 3-1. Weathering indices (molecular proportions). Note, CaO* refers to silicatic Ca.

| |
|--|
| (1) CPA = $[Al_2O_3 / (Al_2O_3 + Na_2O)] \times 100$ |
| (2) CIA = $[Al_2O_3 / (Al_2O_3 + Na_2O + CaO^* + K_2O)] \times 100$ |
| (3) Index B = $(CaO^* + Na_2O + K_2O) / (Al_2O_3 + CaO^* + Na_2O + K_2O)$ |
| (4) CIW = $[Al_2O_3 / (Al_2O_3 + Na_2O + CaO^*)] \times 100$ |
| (5) PIA = $[(Al_2O_3 - K_2O) / (Al_2O_3 + CaO^* + Na_2O - K_2O)] \times 100$ |

- (1) Chemical Proxy of Alteration (this paper)
- (2) Chemical Index of Alteration (Nesbitt and Young, 1982)
- (3) Index B (Kronberg and Nesbitt, 1981)
- (4) Chemical Index of Weathering (Harnois, 1988)
- (5) Plagioclase Index of Alteration (Fedo et al., 1995)

The rationale of the CIA is to give a quantitative measure of feldspar weathering by relating Al, which is enriched in the weathering residues, to Na, Ca and K, which should be removed from a soil profile in the course of plagioclase and K-feldspar weathering (Nesbitt and Young, 1982). Index B of Kronberg and Nesbitt (1981; Guggenberger, et al., 1998) is based on the same considerations. In 1988, Harnois modified the CIA. He emphasized that K should not be used in weathering indices, since it shows no consistent behavior during weathering, being either enriched in the residue, if weathering is weak, or depleted under more intense

weathering conditions. Thus, K was eliminated from the CIA and the resulting index of feldspar weathering was reported as CIW (Harnois, 1988) or K-free CIA (Maynard, 1992). Fedo et al. (1995) introduced a correction of the CIW for the Al content in K-feldspar, otherwise rocks rich in K-feldspar would be characterized by misleadingly high CIW values. This modified version of the CIW is reported as PIA, indicating plagioclase weathering. The CIA, Index B, CIW and PIA index, require all the content of silicatic Ca (=CaO*). This value was obtained from measured CaO according to the procedure described by McLennan (1993), who assumed that the molar CaO/Na₂O ratio of carbonate-free, silicatic material does not exceed 1.

4 Results

Raw data of the geochemical analyses have been already presented in Buggle et al. (2008).

This contribution presents the depth profiles of the applied weathering indices and of the carbonate content (Fig. 3-2). In the following, “Na-type” weathering indices, refer to the CIA, Index B, CIW, PIA, and the CPA, whereas Rb/Sr and Ba/Sr will be regarded as “Sr-type” weathering indices.

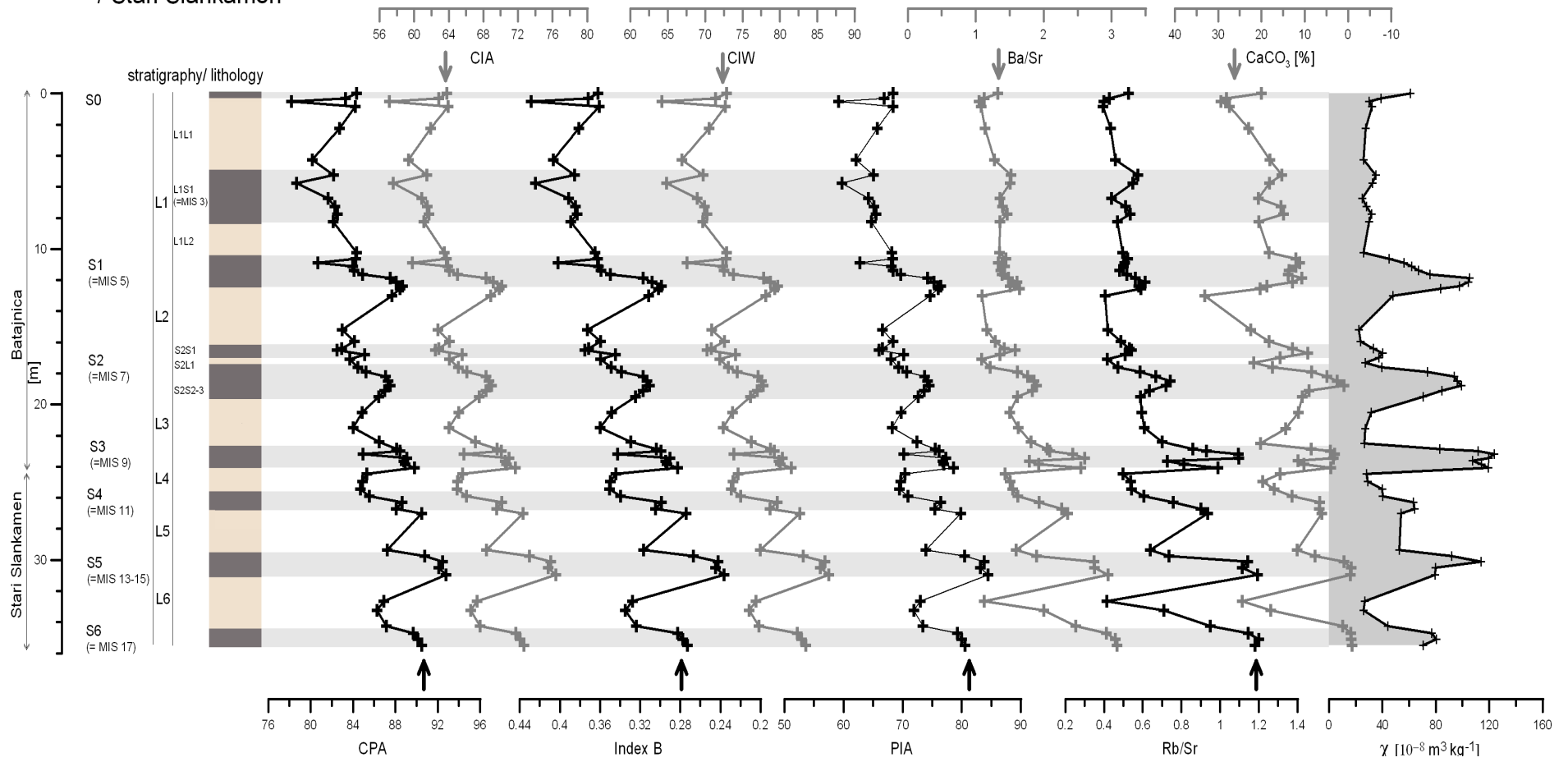
At Batajnica/Stari Slankamen, all indices of the Na-type show a similar trend of more intense weathering in the older loess units. Regarding the pedocomplexes, strongest weathering intensity is recorded in the older units with a maximum in the S5. From the S5 to the recent soil, S0, the peak values of the interglacial pedocomplexes generally decreased, except for the S1, which exhibits again stronger feldspar weathering than the next older interglacial soil formation (S2). The intensity of feldspar weathering in the S6 is lower than in the S5 and comparable to the S4, as shown by all Na-type weathering proxies. Also, with respect to the detailed patterns, the Na-type feldspar weathering indices resemble each other closely and reflect sensitively different phases of pedogenesis within a pedocomplex, mostly consistent with patterns of the magnetic susceptibility record. The depth profile of the Sr-type indices

shows similarities to the magnetic susceptibility record. However, these patterns also strongly follow the calcium carbonate content and exhibit some differences to the “Na-type” indices (Fig. 3-2).

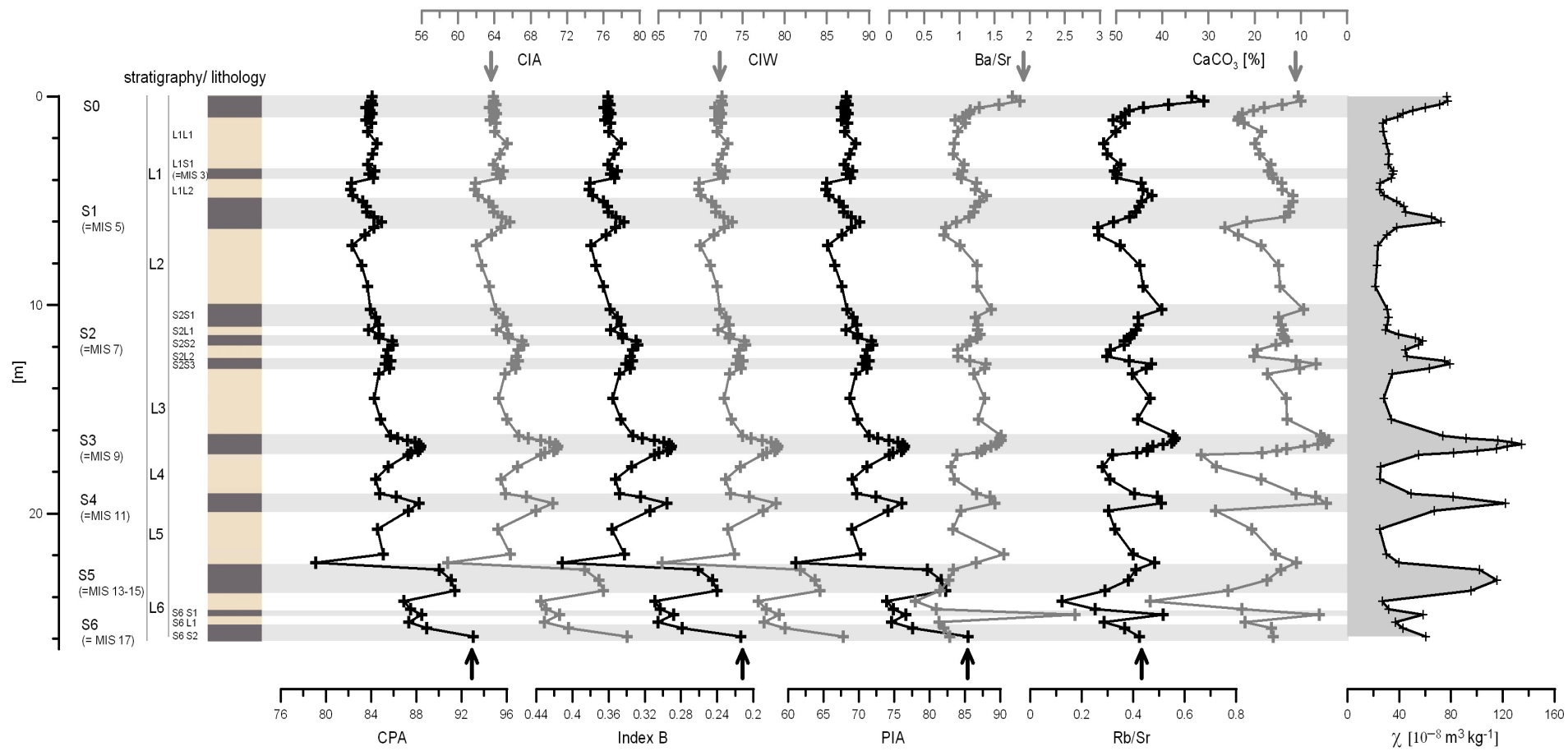
At Mircea Voda, the records of the Na-type indices, on the one hand, are very similar to each other and on the other hand, the Sr-type indices resemble each other closely, showing parallels to the CaCO₃ record (Fig. 3-2). The Na-type indices reveal most intense feldspar weathering in the basal pedocomplexes S6 and S5, with the maximum in the lowermost pedocomplex. The feldspar weathering intensity of the S4 and S3 is less. Nevertheless Na-type indices exhibit still a pronounced enhancement in weathering intensity in this paleosols compared to the loess. An even lower degree of feldspar weathering is revealed for the S2, S1 and the recent soil S0. In contrast to these findings, no comparable trend is shown by the Ba/Sr and Rb/Sr ratios. Comparing loess units, no clear trend can be recognized in the “Na-type” weathering record, disregarding the high values for the thin loess unit L6, which are possibly caused by the influence of pedogenic alteration during the formation of the S5.

At Stary Kaydaky (Fig. 3-2), the succession of loess layers and paleosols is especially in the lower part of the profile (below S2) hardly reflected by the weathering indices. There, loess units are only thin and loess as well as paleosol units show multiply pedogenetic overprinting and exhibit enhanced mineral weathering. In accordance with these findings, the profile sequence is almost carbonate-free, except for some parts of the L1, L3 and L4. These carbonate peaks are also clearly reflected by the Ba/Sr and Rb/Sr record. In the S1, Sr-type indices show an upward decreasing trend, which is neither reflected by the Na-type indices nor by the carbonate content or by the magnetic susceptibility record. This pattern therefore can be best explained by changing composition of the Rb/Sr and Ba/Sr ratio of the parent material. A paleoenvironmental interpretation of the presented weathering records and a discussion of the dataset with respect to loess provenance is beyond the scope of this study and will be given elsewhere.

a) Batajnica
/ Stari Slankamen



Mircea Voda



Stary Kaydaky

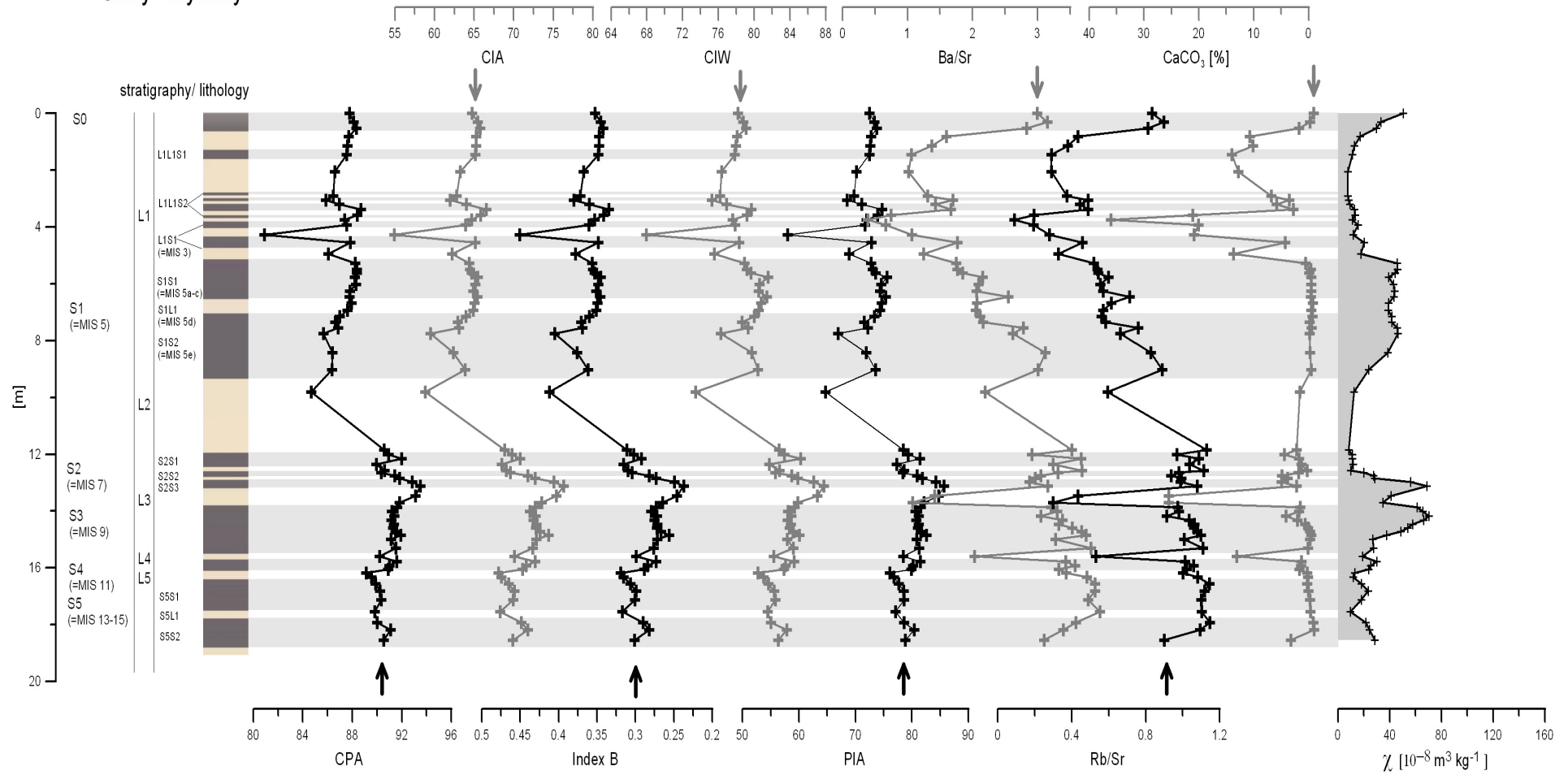


Fig. 3-2. The CPA, CIA, Index B, CIW, PIA, Ba/Sr, Rb/Sr record of a) the Batajnica/Stari Slankamen section in Serbia, b) the Mircea Voda section in Romania, c) the Stary Kaydaky section in Ukraine. See Section 3.2. for a more detailed description of these weathering indices. Note that the carbonate content is given with an inverse scale for better comparison with the weathering proxy records. The magnetic susceptibility record (Bugge et al., 2009) is shown to facilitate correlation to previous studies (Bugge et al., 2008; Bugge et al., 2009; Marković et al., 2009).

5 Discussion

5.1 Evaluation of the geochemical weathering indices

5.1.1 Sr type vs. Na type indices

Within the last 15 years, "Sr-type" indices including Rb/Sr or Ba/Sr gained increasing popularity as weathering proxies, also in LPSS (e.g. Gallet et al., 1996; Chen et al., 1999; Ding et al., 2001; Tan et al., 2006; Bokhorst et al., 2009). The rationale behind this practice is the fact that Sr can substitute for Ca in minerals and also shows an analogous behavior to Ca in the weathering profile. Accordingly, Sr is easily released into solution and mobilized in the course of weathering, whereas Rb or Ba can be regarded as relatively immobile under moderate weathering conditions due to strong adsorption to clay minerals (Dasch, 1969; Nesbitt et al., 1980; Liu et al., 1993; McLennan et al., 1993; Reeder et al., 2006). For the LPSS Mircea Voda, Batajnica/Stari Slankamen and Stary Kaydaky, the depth profiles of „Sr-type“ indices were compared with those of „Na-type“ indices. The latter rely on the principle that Na is easily released from minerals and mobilized during weathering, whereas Al is retained in the profile, forming secondary clay minerals and/or Al-oxides (see Section 3.2.). As revealed by the depth profiles of the applied weathering indices (Fig. 3-2), all "Na-type" indices and all "Sr-type" indices resemble each other closely, but between these two types of weathering indices distinct differences can be observed. A comparison between the depth profiles of the Sr-type indices and the distribution of CaCO₃ suggests that in most cases low and high Ba/Sr and Rb/Sr ratios are connected with high and low carbonate contents, respectively. This observation is confirmed by a significant correlation ($p < 0.05$) between the "Sr-type" indices and the carbonate content (Fig. 3-3) in all sections and gives evidence for a significant substitution of carbonate-Ca by Sr. Therefore, the initial Rb/Sr and Ba/Sr ratios are supposed to be at least partly post-pedogenetically masked by the dynamics of carbonate-

bound Sr. Hence, it is expected that paleosols altered by the precipitation of secondary carbonate, which is leached from overlying loess or paleosols, would exhibit misleadingly low Rb/Sr and Ba/Sr ratios. This would cause an underestimation of the weathering intensity and would also bias the interpretation of these ratios as proxies of the leaching intensity i.e. paleoprecipitation, as also stated by Retallack and Germán-Heins (1994), Retallack (1997) and Tan et al. (2006).

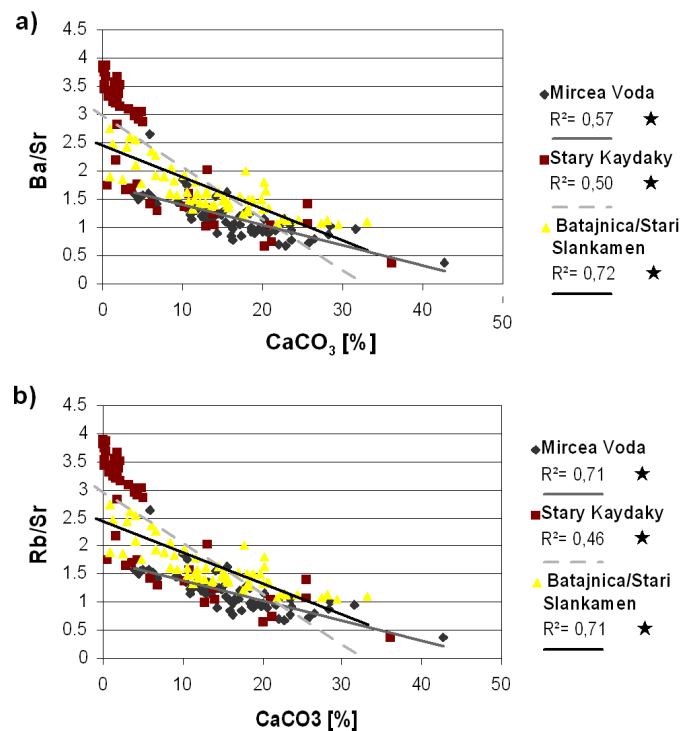


Fig. 3-3. Correlation of the Rb/Sr (a) and Ba/Sr ratio (b) with the CaCO₃-content for all studied profile sequences. The asterisk indicates that the correlation is significant at $p < 0.05$ (t-test, Statistica 6 software package, Statsoft Inc, 2001).

To conclude, it is recommended to restrict the use of "Sr-type" weathering indices such as Rb/Sr and Ba/Sr to carbonate-free material, where they should reflect the intensity of silicate weathering (Dasch, 1969; Nesbitt et al., 1980), keeping in mind that under extreme weathering conditions also Rb and eventually even Ba may undergo mobilization (Nesbitt et al., 1980; Marques et al., 2004; Reeder et al., 2006). For LPSS, mostly characterized by strong carbonate dynamics, it is proposed to employ weathering indices of the „Na-type“, such as the CPA.

5.1.2 The "classical" Na-type weathering indices – uncertainties due to calcium carbonate

The most prominent "Na-type" indices of feldspar weathering are the Index B of Kronberg and Nesbitt (1981), the CIA (Nesbitt and Young, 1982) and especially for plagioclase weathering the CIW (Harnois, 1988) and the PIA (Fedó et al., 1995; see Section 3.2 and Table 3-1). All of these indices employ the molar content of the silicatic bound Ca, given usually as CaO*. For this, one has to know the contribution of the carbonate Ca to the measured CaO, when dealing with calcareous material. The most widely used methods to determine the carbonate content rely on the "selective removal technique", i.e. either on the selective removal of the organic carbon from the inorganic carbon during low temperature combustion or the selective removal of carbonate during acid treatment (Hedges and Stern, 1984; Bisutti et al., 2004, 2007). However, due to an imperfect selectivity of these methods (Froelich, 1980; Hedges and Stern, 1984; Bisutti et al., 2004), one may derive erroneous carbonate contents, which consequently bias also the calculation of CaO* from total CaO and carbonate-bound CaO.

To avoid the time consuming step of carbonate determination, the CaO* is often estimated following the procedure of McLennan (1993), (e.g. Gallet et al., 1998; Yadav and Rajamani, 2004; Schellenberger and Veit, 2006; Lacka et al., 2007). He suggested to first correct the measured molar CaO content for Ca in apatite, as calculated from the P₂O₅ content, and then to compare the resulting value (here termed CaO_{corr}) with the molar Na₂O content. If the latter is smaller than CaO_{corr}, a molar CaO*/Na₂O ratio of one is assumed. In the other case, the molar CaO* is set equal to the molar CaO_{corr}. However, this estimation procedure may cause uncertainties in calculating CaO*-based weathering indices. Table 3-2 exhibits this for a 1/7 mixing ratio of the plagioclase end-members anorthite/albite, which can be a realistic value for loess (Dultz and Graf von Reichenbach, 1995). Three scenarios were calculated. The first one, which assumes a pure mixture of 80 g plagioclase and 20 g calcium carbonate, shows

that the CIW calculated from estimated CaO* values is underestimating the "real" CIW by 11.2 units, i.e. 22.4 % deviation from the real value. This is also the case for the second scenario applying only 10 g CaCO₃. Thus, in both cases the CIW calculated by following the procedure of McLennan (1993) is lower than the theoretical value of the unaltered plagioclase i.e. the „real“ CIW. Also for the other indices an underestimation of the weathering intensity was obtained. Regarding the formula of the CIW, PIA and CIA, the actual error due to CaO* estimation should decrease with increasing Al content. Therefore, the third scenario also accounts for the presence of other aluminous phases in loess such as K-feldspar or secondary clay minerals (see caption of Table 3-2 for a detailed description of this scenario). However, also this variant, regarding a composition more realistic for loess deposits, reveals an underestimation of the weathering intensity by more than 10%. Consequently, the interpreter of these weathering proxy records, would for example overestimate the weathering enhancement of a paleosol compared to the underlying loess parent material, if the paleosol is carbonate-free and the loess is not.

To avoid such uncertainties, it is recommended for LPSS studies to apply a "Na-type" weathering index as CPA, which does not employ Ca. This is in line with Jeong et al. (2008), who proposed to omit CaO from weathering indices in LPSS due to the presence of secondary carbonates.

5.1.3 The chemical proxy of alteration (CPA) - an evaluation

As hypothesized in Section 3.2, the CPA should be a suitable weathering index for LPSS, indicating especially plagioclase weathering. Indeed, the good correspondence to the "classical" Na-type plagioclase weathering indices, i.e. the CIW and the PIA (Fig. 3-2) confirms the proposed interpretation of the CPA as proxy of the plagioclase weathering intensity. However, in contrast to the "classical" indices, the CPA does not involve CaO*. Therefore, it is free of the CaO* related uncertainties. Though these uncertainties are

apparently small in the Serbian, Romanian and Ukrainian sites, they could be remarkable on other loess sites depending on mineralogical composition, as shown in Section 5.1.2.

Table 3-2. Sensitivity analysis for the CIW, PIA, CIA and Index B (see Table 3-1) and the obtained error due to the estimation of silicate bound Ca (CaO*) following the procedure of McLennan (1993). Three scenarios were calculated. Scenarios 1 and 2 assume a mixture of 20 and 10 g calcite, respectively, with 80 g plagioclase. For the plagioclase composition an anorthite/albite mixing ratio of 1/7 is assumed – a realistic value for loess deposits (Dultz and Graf von Reichenbach, 1995). Scenario 3 takes also account of other Al phases, such as K-feldspar and secondary Al minerals. To achieve realistic element ratios we choose a K-feldspar content of 54.3 g and an additional Al₂O₃ content (Al₂O_{3-sec}) of 34.8 g. The Al₂O_{3-sec} can be regarded as Al of secondary clay minerals or Al-oxides. These preset values correspond to an Na₂O/K₂O ([%]/[%]) ratio of 0.9 and an Al₂O₃/Na₂O ([%]/[%]) ratio of 7.5. These values are in between the observed range for most loesses in various parts of the world i.e. 1.3-0.5 for Na₂O/K₂O and 6-9 for Al₂O₃/Na₂O (Taylor et al., 1993; Gallet et al., 1996; Gallet et al., 1998, Buggle et al., 2008; Újvári et al., 2008). The subscript „tot“ refers to the total content of the oxide, as calculated from the preset mineralogical composition. The real content of CaO*, as calculated for each scenario, is given as „CaO*_{real}“, whereas CaO*_{estimated} terms the estimated CaO* following McLennan (1993). Accordingly, the results present „real“ and „estimated“ weathering indices. Difference between both is given in percent of the real value.

| Scenario presetting | Scenario 1 | | | Scenario 2 | Scenario 3 |
|---|---|-------|-------|------------|------------|
| | Anorthite/Albite Mixing ratio [g/g] | 10/70 | 10/70 | 10/70 | 10/70 |
| | CaCO ₃ [g] | 20 | 10 | 10 | 10 |
| | K-feldspar [g] | 0 | 0 | 54.3 | 54.3 |
| | Al ₂ O _{3-sec} [g] | 0 | 0 | 0 | 34.8 |
| Interim values for index calculation | Al ₂ O _{3tot} [mmol] | 169.4 | 169.4 | 169.4 | 608.5 |
| | Na ₂ O _{tot} [mmol] | 133.5 | 133.5 | 133.5 | 133.5 |
| | K ₂ O _{tot} [mmol] | 0 | 0 | 0 | 97.6 |
| | CaO _{tot} [mmol] | 235.8 | 135.9 | 135.9 | 135.9 |
| | CaO* _{estimated} [mmol] | 133.5 | 133.5 | 133.5 | 133.5 |
| | CaO* _{real} [mmol] | 35.9 | 35.9 | 35.9 | 35.9 |
| Results | CIW _{estimated} | 38.8 | 38.8 | 38.8 | 69.5 |
| | CIW _{real} | 50 | 50 | 50 | 78.2 |
| | Difference [%] | 22.4 | 22.4 | 22.4 | 11.1 |
| | PIA _{estimated} | 38.8 | 38.8 | 38.8 | 65.7 |
| | PIA _{real} | 50 | 50 | 50 | 75.1 |
| | Difference [%] | 22.4 | 22.4 | 22.4 | 12.5 |
| | CIA _{estimated} | 38.8 | 38.8 | 38.8 | 62.5 |
| | CIA _{real} | 50 | 50 | 50 | 69.5 |
| | Difference [%] | 22.4 | 22.4 | 22.4 | 10.1 |
| | Index B _{estimated} | 61.2 | 61.2 | 61.2 | 37.5 |
| | Index B _{real} | 50 | 50 | 50 | 30.4 |
| | Difference [%] | 22.4 | 22.4 | 22.4 | 23.4 |

Fig. 3-2 compares the CPA and other plagioclase weathering indices to the CIA and Index B, which have been previously proposed as silicate weathering proxies. The objective of these indices is to quantify also weathering of K-feldspar and mica by employing K. However, these indices show close similarity to the CIA and CIW (Fig. 3-2). Thus, it is to conclude that as long as plagioclase weathering does not reach saturation, K-free indices are also a good proxy for the intensity of silicate weathering in general. This is supported by the $\text{Al}_2\text{O}_3/\text{Na}_2\text{O}$ and $\text{Al}_2\text{O}_3/\text{K}_2\text{O}$ depth profiles of the studied sections, showing that K variations mimic the Na variations, however, with smaller amplitude (Fig. 3-4).

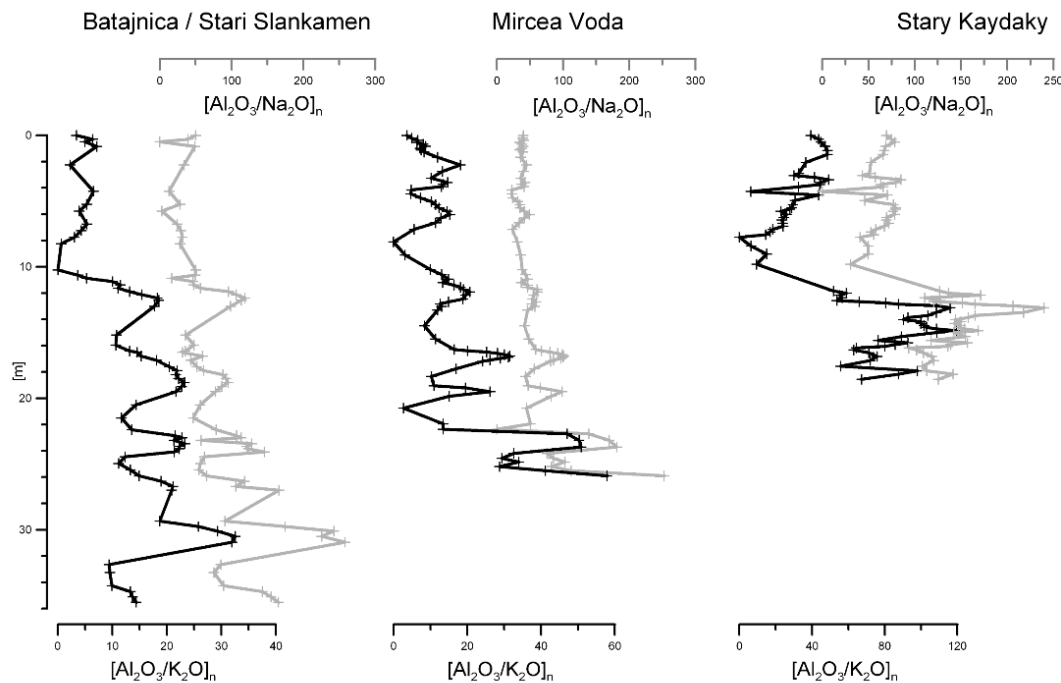


Fig. 3-4. Molar $\text{Al}_2\text{O}_3/\text{K}_2\text{O}$ and $\text{Al}_2\text{O}_3/\text{Na}_2\text{O}$ ratios of the studied profiles. Subscript “n” indicates that the data are normalized to the lowest value of each section in order to compare the relative changes of the ratios.

These results are in accordance with observations in other weathering studies and theoretical considerations of the element behavior, suggesting that K release is small compared to the Na release. This is due to stronger weathering resistance of K phases such as K-feldspar and due to the fixation of K on clay minerals (Nesbitt and Young, 1984, 1989; Blum, 1994; Smykatz-Kloss, 2003; Yang et al., 2004; Reeder et al., 2006).

Though weathering profiles of the proposed CPA and K-free Na-type indices are consistent for the studied sections, this might not be true in other sites with strong K fixation and illitization. Harnois (1988) has pointed out that K-fixation can cause an inconsistent behavior of this element in the weathering environment and thus, he recommended not to use K in weathering indices. The CPA being a K-free index, takes account of this recommendation. Furthermore it avoids uncertainties due to determination of CaO* and thus the CPA can be applied more general on loess-paleosol sequences.

As a conclusion, the CPA seems to be the most promising weathering proxy for LPSS. However, as with other weathering indices, it requires also certain prerequisites to be fulfilled. Dealing with a “Na-type” weathering index, the studied material has to be free of Na salts, which would lead to an underestimation of the weathering intensity. Within mid-latitude loess deposits, significant amounts of these salts are only expected in exceptional settings as near to the seashore or in locations with warm-(semi-)arid climate and groundwater near to surface, either in the past or in the present time. For the studied sections an influence of Na-salts is not likely due to the plateau situation of the loess, the lack of a soil structure characteristic of a natric horizon (IUSS Working Group WRB, 2006), and the geochemical composition (Buggle et al., 2008). The latter does not indicate a relationship of the CPA to the dynamics of other salts such as gypsum, but rather to the magnetic susceptibility as independent pedogenesis proxy (Fig. 3-2). However, it has to be evaluated by further studies, whether the remarkable minimum of the CPA at the lower boundary of the L5 in Mircea Voda indeed reflects low weathering intensity due to cold and/or dry paleoclimatic conditions. A possible connection to the recent gypsum formation at the front face of the exposure wall in the respective depth cannot be excluded. A record of the chlorine content would be useful to clarify such inconclusive situations in future studies.

A second prerequisite for all Na-type indices is the absence of mineral or grain size sorting in the sampled material. This can be tested by using an $\text{Al}_2\text{O}_3\text{-CaO}^*\text{-Na}_2\text{O-K}_2\text{O}$ ternary plot -

also known as A-CN-K diagram (Nesbitt and Young, 1984). This diagram informs about weathering and sorting effects of aluminosilicates, as well as the initial composition of the unweathered material (e.g. Nesbitt and Young, 1989; McLennan et al., 1993; Nesbitt et al., 1996; Fig. 3-5). A sorting effect, i.e. a selective enrichment of coarser (finer), more feldspathic (more clayey and aluminous material), as revealed for the Stary Kaydaky section (Fig. 3-5), would cause a decrease (increase) of the Al/Na ratio and the CPA.

The third prerequisite is common for all types of weathering indices: the homogeneity of the parent material. With respect to the CPA, a relatively homogeneous composition of the unweathered material regarding the most abundant aluminous Na phase, i.e. albite, in relation to the aluminous K phases, i.e. mostly K-feldspar and mica, and to the Ca phase, i.e. anorthite, is important. For example, an increasing K-feldspar/albite ratio of the parent material would cause a higher Al/Na ratio (Fedo et al., 1995). This would result in a misleading increase of the CPA. Also this prerequisite can be tested using the A-CN-K diagram. Variations in the K-feldspar or mica to plagioclase ratio of the unweathered parent material would be revealed by a scatter of the data points parallel to the CN-K – axis (Fig. 3-5). On the other hand, a single weathering line would indicate parent material with an invariable composition of aluminosilicates, as it is the case for the data points of the sections Mircea Voda and Batajnica/Stari Slankamen (Fig. 3-5). The congruence between the CIA, Index B, PIA and K-free indices as the CIW and CPA gives further reason to assume homogeneity of the unweathered loess parent material at the investigated sections, regarding the (K-feldspar + mica)/albite ratio. For the Stary Kaydaky site, it is not possible to exclude variations in the (K-feldspar + mica)/albite ratio due to the scatter along the sorting line being parallel to the CN-K axis (Fig. 3-5).

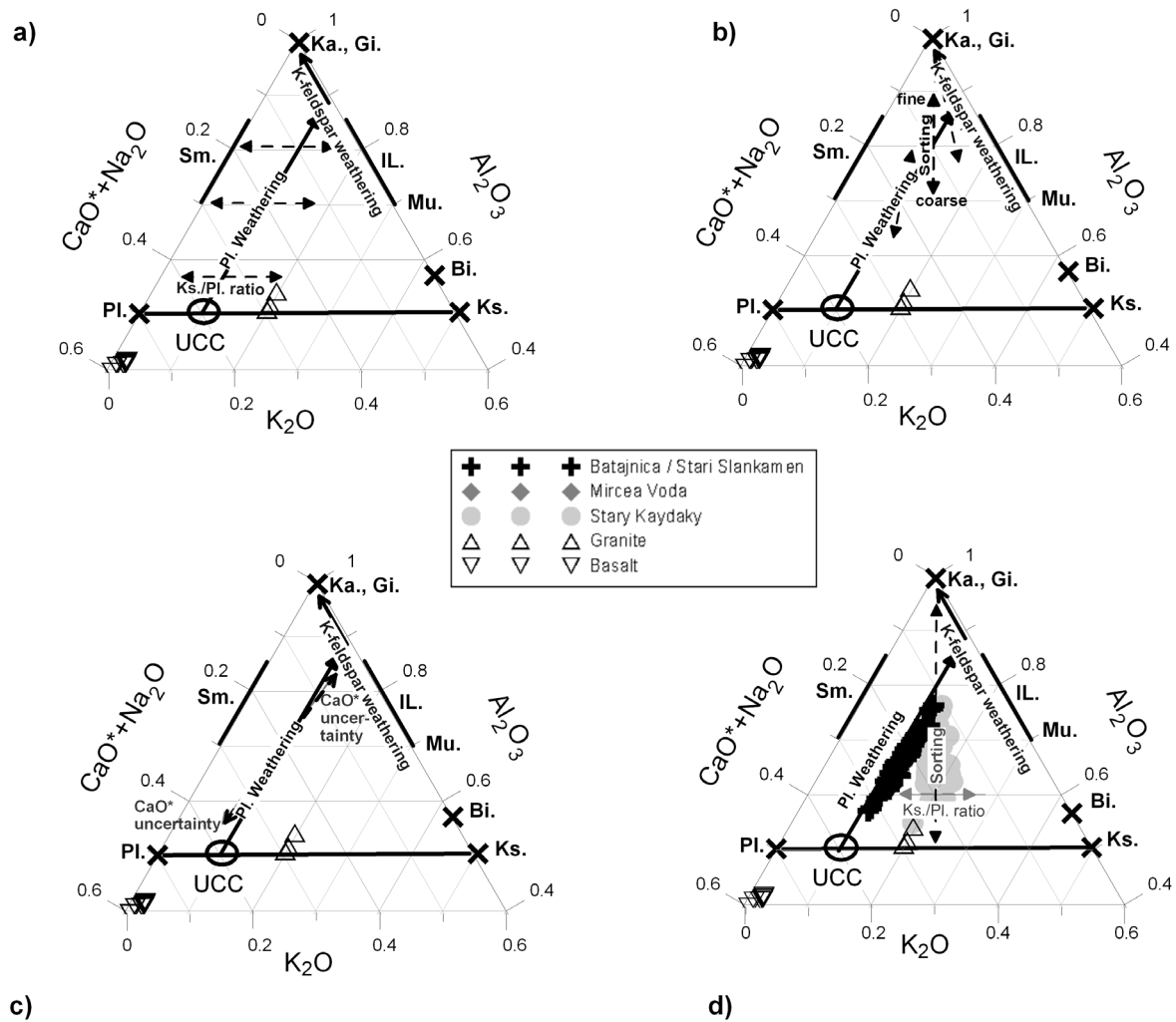


Fig. 3-5. The A-CN-K (Al₂O₃-CaO*+Na₂O-K₂O) - ternary diagram according to Nesbitt and Young (1984). The characteristic position of the upper continental crust (UCC), basalt, granite and the minerals plagioclase (Pl.), K-feldspar (Ks.), biotite (Bi.), muscovite (Mu.), illite (IL.), smectite (Sm.), kaolinite (Ka.), and gibbsite (Gi.) is given for orientation. Note that only the upper part of the ternary diagrams is shown, which is of interest for the present study. In Fig. 3-5 a) – d) a typical weathering line is presented, emerging from loess source material with UCC-like composition, as found to be true for many loess deposits around the world and also the Southeastern European loesses (e.g. Taylor and McLennan, 1985; Gallet et al., 1998; Buggle et al., 2008). The first part of the weathering line is (sub-)parallel to the A-CN join, representing prevailing Ca and Na removal due to plagioclase weathering. With plagioclase weathering being in saturation, i.e. approaching to the A-K join, the second part of the weathering line is redirected to the Al₂O₃-apex as a result of predominantly loss of K by weathering of K-rich phases like K-feldspar (Nesbitt and Young, 1984). In Fig. 3-5a, it is shown how biases due to a changing composition of the parent material would appear in the A-CN-K diagram. Variations in the K-feldspar/plagioclase ratio (Ks./Pl. ratio) of the parent material would cause a shift parallel to the CN-K join and the datapoints would not plot on the same weathering line. In Fig. 3-5b, the sorting effect is demonstrated. A sample enriched in fine and more clayey material due to grain size and mineral sorting plots closer to the Al₂O₃-apex and a sample enriched in coarse and less clayey material plots vice versa. Fig. 3-5c shows the effect of errors in the CaO* content, for example due to the estimation procedure of McLennan (1993). An overestimation of the CaO* would cause a shift from the original weathering line towards the CN apex, an underestimation vice versa. Since this line of “CaO* uncertainty” is close to the original weathering line, an erroneous CaO* would hardly affect the identification of mineral/grain size sorting and of a variable Ks./Pl. ratio of the source material. Fig. 3-5d. Datapoints for loess and paleosol samples from the Batajnica/Stari Slankamen, Mircea Voda and Stary Kaydaky sections are shown (modified after Buggle et al., 2008). The samples from the Batajnica/Stari Slankamen and Mircea Voda sections plot on a plagioclase weathering line originating from the UCC, not indicating a variable Ks./Pl. ratio. Samples from Stary Kaydaky plot on a sorting line, which is possibly modified by variable Ks./Pl. ratios. See Buggle et al. (2008) for a more detailed discussion of these features with respect to loess provenance.

The invariance of the albite/anorthite mixing ratio of plagioclase can be assessed indirectly, assuming that it is controlled by the type and composition of the igneous source rocks of the loess parent material. This assumption seems plausible, since many loess deposits around the world have been identified as recycled sedimentary material (Taylor et al., 1983; Gallet et al., 1998; Buggle et al., 2008), essentially originating from igneous protoliths. Accordingly, an increasing felsic (mafic) character of the idealized protolith would cause higher (lower) albite/anorthite ratios. As K is enriched in felsic rocks, an invariant K/Na ratio of the protolith, as can be inferred for the Batajnica/Stari Slankamen and Mircea Voda sections, should also indicate a relatively stable albite/anorthite ratio of the unweathered protolith.

If the composition of the parent material changes down-profile, the CPA still could be reasonably applied to LPSS using Δ CPA values. Δ CPA values can be obtained by relating CPA values of a weathering horizon or paleosol to the CPA value of the respective parent material ("background CPA), i.e. the loess layer from which each paleosol developed. These Δ CPA values can be interpreted in terms of weathering enhancement.

Therefore, the application of the $Al/(Na + Al) \times 100$ ratio (CPA, CWI' according to Cullers, 2000) is proposed not only for calcareous marine sediments, but also for loess-paleosol sequences as a measure of silicate weathering intensity. As with other weathering indices, a homogeneous parent material (regarding the relevant host minerals) is required to obtain a continuous weathering record. However, using the CPA, this prerequisite can be easily evaluated via the A-CN-K diagram not needing UCC normalized plots of trace elements and REE. Furthermore, diagenetic effects due to dynamics of secondary carbonate or K-fixation (illitization) are no issue in contrast to other indices (Sr-type indices, Na-type indices involving CaO^* and K_2O).

6 Conclusions

Commonly applied weathering indices involving Ti, Zr, and Si are relatively sensitive for changes in parent material composition. Other widely used weathering indices relying on Al as immobile element such as the CIA (Nesbitt and Young, 1982), the CIW (Harnois, 1988), the PIA (Fedo et al., 1995) and the Index B (Kronberg and Nesbitt, 1981) involve uncertainties due to diagenetic effects (illitization). Estimation of silicate Ca in calcareous material, as common in most loesses, may lead to biased weathering records using these indices. Furthermore, carbonate-free element ratios incorporating Sr, such as the Ba/Sr and Rb/Sr ratio (e.g. Liu, et al., 1993; Gallet et al., 1996; Bokhorst et al., 2009), can be problematic due to interferences of the carbonate and Sr dynamics. To overcome such uncertainties, the Chemical Proxy of Alteration CPA (the molar ratio $\text{Al}_2\text{O}_3/(\text{Al}_2\text{O}_3 + \text{Na}_2\text{O}) \times 100$) – also known as CIW' (Cullers, 2000) – is proposed as a more appropriate geochemical proxy of silicate weathering for LPSS. Homogeneity of the parent material can be checked for this index via the A-CN-K diagram.

Acknowledgements

We thank Tivadar Gaudenyi and Mladjen Jovanović for assistance during fieldwork in Serbia, Ana Malagodi for support in sample preparation, and J. Eidam (University of Greifswald) for XRF analyses. This study was financially supported by the German Research Foundation DFG (GL 327/8-2).

References

- Bisutti, I., Hilke, I., Raessler M., 2004. Determination of total organic carbon – an overview of current methods. *Trends in Analytical Chemistry*. 23 (10-11), 716-726.
- Bisutti, I., Hilke I., Schumacher J., Raessler M., 2007. A novel single-run dual temperature combustion (SRDTC) method for the determination of organic, in-organic and total carbon in soil samples. *Talanta* 71, 521-528.
- Blum, A.E., 1994. Feldspars in weathering. In: Parsons, I. (Ed.), *Feldspars and Their Reactions*. NATO ASI Series, Series C: Mathematical and Physical Sciences, vol. 421, Kluwer Academic Publishers, Dordrecht, pp. 595-630.
- Blumer, M., 1950. Die Existenzgrenzen anorganischer Ionen bei der Bildung von Sedimentgesteinen. *Geochemische Untersuchungen IV. Helvetica Chimica Acta* 33 (6), 1468-1581.
- Bokhorst, M.P., Beets, C.J., Marković, S.B., Gerasimenko, N.P., Matviishina, Z.N., Frechen, M., 2009. Pedo-chemical climate proxies in Late Pleistocene Serbian-Ukrainian loess sequences. *Quaternary International* 198, 113-123.
- Buggle, B., Glaser, B., Zöller, L., Hambach, U., Marković, S., Glaser, I., Gerasimenko, N., 2008. Geochemical characterization and origin of Southeastern and Eastern European loesses (Serbia, Romania, Ukraine). *Quaternary Science Reviews* 27, 1058-1075.
- Buggle, B., Hambach, U., Glaser, B., Gerasimenko, N., Marković, S.B, Glaser, I., Zöller, L. 2009. Stratigraphy and spatial and temporal paleoclimatic trends in East European loess paleosol sequences. *Quaternary International* 196, 86-106.
- Chen, J., An, Z., Head, J., 1999. Variation of the Rb/Sr ratios in the loess-paleosol sequences of Central China during the last 130,000 years and their implications for monsoon paleoclimatology. *Quaternary Research* 51, 215-219.
- Cullers, R.L., 2000. The geochemistry of shales, siltstones and sandstones of Pennsylvanian-Permian age, Colorado, USA: implications for provenance and metamorphic studies. *Lithos* 51, 181-203.
- Dasch, E.J., 1969. Strontium isotopes in weathering profiles, deep-sea sediments, and sedimentary rocks. *Geochimica et Cosmochimica Acta* 33 (12), 1521-1552.
- Derbyshire, E., Kemp, R.A., Meng, X., 1997. Climate change, loess and palaeosols: proxy measures and resolution in North China. *Journal of the Geological Society, London* 154, 793-805.
- Ding, Z.L., Sun, J.M., Yang, S.L., Liu, T.S., 2001. Geochemistry of the Pliocene red clay formation in the Chinese Loess Plateau and implications for its origin, source provenance and paleoclimatic change. *Geochimica et Cosmochimica Acta* 65 (6), 901-913.
- Dultz, S., Graf von Reichenbach, H., 1995. Quantitative Mineralbestimmung in der Schlufffraktion von Böden auf der Grundlage der chemischen Analyse und unter Anwendung der Karl-Fischer-Titration. II. Ergebnisse bei Böden aus Geschiebedecksand, Geschiebemergel und Löß. *Journal of Plant Nutrition and Soil Science* 158, 459-464.
- Evans, M.E., Heller, F., 2003. *Environmental Magnetism – Principles and Applications of Enviromagnetics*. Academic Press, Amsterdam.
- Fedo, C.M., Nesbitt, H.W., Young, G.M., 1995. Unraveling the effects of potassium metasomatism in sedimentary rocks and paleosols, with implications for paleoweathering conditions and provenance. *Geology* 23 (10), 921-924.

- Froelich, P.N., 1980. Analysis of organic carbon in marine sediments. *Limnology and Oceanography* 25 (3), 564-572.
- Gallet, S., Jahn, B., Torii, M., 1996. Geochemical characterization of the Luochuan loess paleosol sequence, China, and paleoclimatic implications. *Chemical Geology* 133, 67-88.
- Gallet, S., Jahn, B., Van Vliet Lanoë, B., Dia, A., Rossello, E., 1998. Loess geochemistry and its implications for the particle origin and composition of the upper continental crust. *Earth and Planetary Science Letters* 156, 157-172.
- Goldschmidt, V.M., 1937. The principles of distribution of chemical elements in minerals and rocks. *Journal of the Chemical Society*, 655-673.
- Guggenberger, G., Bäuml, R., Zech, W., 1998. Weathering of soils developed in eolian material overlying glacial deposits in eastern Nepal. *Soil Science* 163 (4), 325-337.
- Harnois L., 1988. The CIW index: a new chemical index of weathering. *Sedimentary Geology* 55, 319-322.
- Harris R.C., Adams J.A.S., 1966. Geochemical and mineralogical studies on the weathering of granitic rocks. *American Journal of Science* 264 (2), 146-178.
- Hedges J.I., Stern J.H., 1984. Carbon and nitrogen determinations of carbonate-containing solids. *Limnology and Oceanography* 29 (3), 657-663.
- IUSS Working Group WRB, 2006. World Reference Base for Soil Resources 2006. In World Soil Resources No. 103, FAO, Rome.
- Jeong, G.Y., Hillier, S., Kemp, R.A., 2008. Quantitative bulk and single particle mineralogy of a thick Chinese loess-paleosol section: implications for loess provenance and weathering. *Quaternary International* 27, 1271-1287.
- Kabata-Pendias, A., Pendias, H., 2001. Trace Elements in Soils and Plants. CRC Press, Boca Raton.
- Kronberg, B.I., Nesbitt, H.W., 1981. Quantification of weathering, soil geochemistry and soil fertility. *Journal of Soil Science* 32, 453-459.
- Kutterolf, S., 2001. Die klastischen Sedimente der karbonen Hochwipfel - und Auernig Formation der Ostkarawanken (Österreich / Slowenien). Dissertation, University of Stuttgart, URL: <http://elib.uni-stuttgart.de/opus/volltexte/2002/994/>, URN: urn:nbn:de:bsz:93-opus-9948; downloaded at 02.06.2010.
- Lacka, B., Lanczont, M., Madeyska, T., Boguckij, A., 2007. Geochemical composition of Vistulian loess and micromorphology of interstadial palaeosols at the Kolodiv site (East Carpathian Foreland, Ukraine). *Geological Quarterly*, 51 (2), 127-146.1.
- Liu, C.-Q., Masuda, A., Okada, A., Yabuki, S., Zhang, J., Fan, Z.L., 1993. A geochemical study of loess and desert sand in northern China: implications for continental crust weathering and composition. *Chemical Geology* 106, 359-374.
- Maher, B.A., Thompson, R., Zhou, L.P., 1994. Spatial and temporal reconstructions of changes in the Asian palaeomonsoon: A new mineral magnetic approach. *Earth and Planetary Science Letters* 125, 461-471.
- Marković, S.B., Hambach, U., Catto, N., Jovanović, M., Buggle, B., Machalett, B., Zöller, L., Glaser, B., Frechen, M., 2009. Middle and Late Pleistocene loess sequences at Batajnica, Vojvodina, Serbia. *Quaternary International* 198, 255-266.
- Marques, J.J., Schulze, D.G., Curi, N., Mertzman, S.A., 2004. Trace element geochemistry in Brazilian Cerrado soil. *Geoderma* 121 (1-2), 31-43.
- Mason, B., Moore, C.B., 1985. Grundzüge der Geochemie. Enke-Verlag, Stuttgart.
- Maynard, J.B., 1992. Chemistry of modern soils as a guide to interpreting Precambrian paleosols. *The Journal of Geology* 100 (3), 279-289.
- McBride, M.B., 1994. Environmental Chemistry of Soils. Oxford University Press, New York.

- McLennan, S.M., 1993. Weathering and global denudation. *The Journal of Geology* 101, 295-303.
- McLennan, S.M., Hemming, S., McDaniel, D.K., Hanson, G.N., 1993. Geochemical approaches to sedimentation, provenance, and tectonics. In: Johnsson, M.J., Basu, A. (Eds.), *Processes Controlling the Composition of Clastic Sediments*, Special Paper.- Geological Society of America vol. 284, pp. 21-40.
- Muhs, D.R., Bettis, E.A., Been, J., McGeehin, J.P., 2001. Impact of climate and parent material on chemical weathering in loess-derived soils of the Mississippi River valley. *Soil Science Society of America Journal*. 65 (6), 1761-1777.
- Nesbitt, H.W., Young, G.M., 1982. Early Proterozoic climates and plate motions inferred from major element chemistry of lutites. *Nature* 299, 715-717.
- Nesbitt, H.W., Young, G.M., 1984. Prediction of some weathering trends of plutonic and volcanic rocks based on thermodynamic and kinetic considerations. *Geochimica et Cosmochimica Acta* 48, 1523-1534.
- Nesbitt, H.W., Young, G.M., 1989. Formation and diagenesis of weathering profiles. *The Journal of Geology* 97, 129-147.
- Nesbitt, H.W., Markovičs, G., Price, R.C., 1980. Chemical processes affecting alkalis and alkaline earths during continental weathering. *Geochimica et Cosmochimica Acta* 44, 1659-1666.
- Nesbitt, H.W., Young, G.M., McLennan, S.M., Keays, R.R., 1996. Effects of chemical weathering and sorting on the petrogenesis of siliciclastic sediments, with implications for provenance studies. *The Journal of Geology* 104, 525-542.
- Pye, K., 1995. The nature, origin and accumulation of loess. *Quaternary Science Reviews* 14, 653-667.
- Railsback, L.B., 2003. An earth scientist's periodic table of the elements and their ions. *Geology* 31 (9), 737-740.
- Railsback, L.B., 2005. A synthesis of systematic mineralogy. *American Mineralogist* 90 (7), 1033-1041.
- Reeder, S., Taylor, H., Shaw, R.A., Demetriades, A., 2006. Introduction to the chemistry and geochemistry of the elements. In: Tarvainen, W. and de Vos (Eds.), *Geochemical Atlas of Europe. Part 2. Interpretation of Geochemical Maps, Additional Tables, Figures, Maps, and Related Publications*. Geological Survey of Finland, Espoo, pp. 48-429.
- Retallack G.J., 1997. *A Colour Guide to Paleosols*. Wiley, Chichester.
- Retallack, G.J., Germán-Heins J., 1994. Evidence from paleosols for the geological antiquity of rain-forest. *Science* 265 (5171), 499-502.
- Schellenberger, A., Veit, H., 2006. Pedostratigraphy and pedological and geochemical characterization of Las Carreras loess-paleosol sequence, Valle de Tafi, NW-Argentina. *Quaternary Science Reviews* 25, 811-831.
- Schwertmann, U., 1993. Relations between iron oxides, soil color, and soil formation. In: Bigham, J.M., Ciolkosz, E.J., Luxmoore, R.J., *Soil Color*. SSSA Special Publication 31, 51-70.
- Smalley, I., Leach, J.A., 1978. The origin and distribution of the loess in the Danube Basin and associated regions of East-Central Europe- A review. *Sedimentary Geology* 21, 1-26.
- Smalley, I., Krinsley, D.H., 1978. Loess deposits associated with deserts. *Catena* 5, 53-66.
- Smalley, I., O'Hara-Dhand, K., Machalett, B., Jary, Z., Jefferson, I., 2009. Rivers and loess: the significance of long river transportation in the complex event-sequence approach to loess deposit formation. *Quaternary International* 198 (1-2), 7-18.
- Smykatz-Kloss, B., 2003. *Die Lößvorkommen des Pleiser Hügellandes bei Bonn und von Neustadt/Wied sowie der Picardie: Mineralogisch-geochemische und*

-
- geomorphologische Charakterisierung, Verwitterungs-Beeinflussung und Herkunft der Löss. Dissertation, University of Bonn. URL: http://hss.ulb.uni-Bonn.de/diss_online/math_nat_fak/2003/smykatz-kloss_bettina, downloaded at 02.06.2008, URN: urn:nbn:de:hbz:5n-03082.
- Tan, H., Ma, H., Zhang, X., Lu, H., Wang, J., 2006. Typical geochemical elements in loess deposits in the Northeastern Tibetan Plateau and its paleoclimatic implications. *Acta Geologica Sinica*. 80 (1), 110-117.
- Taylor, S.R., McLennan, S.M., 1985. *The Continental Crust: Its Composition and Evolution*. Blackwell, London.
- Taylor, S.R., McLennan, S.M., McCulloch, M.T., 1983. Geochemistry of loess, continental crustal composition and crustal model ages. *Geochimica et Cosmochimica Acta* 47, 1897-1905.
- Újvári, G., Varga, A., Balogh-Brunstad, Z., 2008. Origin, weathering and geochemical composition of loess in southwestern Hungary. *Quaternary Research* 69 (3), 421-437
- Wedepohl, K.H., 1978. *Handbook of Geochemistry*. Springer Verlag, Berlin.
- Yadav, S., Rajamani, V., 2004. Geochemistry of aerosols of northwestern part of India adjoining the Thar Desert. *Geochimica et Cosmochimica Acta* **68 (9)**, 1975-1988.
- Yang, S.Y., Li, C.X., Yang, D.Y., Li, X.S., 2004. Chemical weathering of the loess deposits in the lower Changjiang Valley, China, and paleoclimatic implications. *Quaternary International* 117, 27-34.

Study 4

0.7-Million years of progressive aridization recorded in SE-European loess sequences

Björn Buggle^{1,2*}, Ulrich Hambach³, Martin Kehl⁴, Ludwig Zöller³, Slobodan B. Marković⁵
and Bruno Glaser¹

¹Soil Biogeochemistry, Martin-Luther-University Halle-Wittenberg, von-Seckendorff-Platz 3,
06120 Halle, Germany

²Soil Physics Department, University of Bayreuth, D-95440 Bayreuth, Germany.

³Chair of Geomorphology, University of Bayreuth, D-95440 Bayreuth, Germany

⁴Institute of Geography, University of Cologne, D-50932 Köln, Germany..

⁵Chair of Physical Geography, Faculty of Sciences, University of Novi Sad, Faculty of Sciences, Trg Dositeja Obradovića 3, 21000 Novi Sad, Serbia.

unsubmitted

Abstract

Long, continuous terrestrial records of the Pleistocene climate evolution of Central and SE-Europe are scarce. Multi-proxy records of the weathering and soil formation history from loess-paleosol sequences in the middle and lower Danube Basin document a progressive aridization and/or cooling of this region over the last 700 ka. Corresponding trends are discernible in climate archives in a W-E transect across mid-latitude Eurasia and linked to the uplift of Central-East Asian mountain ranges. Evidence for long-term drying and/or cooling of interglacials are expressed in archives within the current steppe belt. During peak interglacials, environmental conditions have been close to threshold values for the stability of eozones and the findings demonstrate the sensitivity of this region to past and present climate change.

Keywords: Climate change, palaeoclimate, Eurasia, Aridization

Study

In Europe, only few long-term and (quasi-)continuous terrestrial climate archives exist extending over the Late and Mid-Pleistocene. In the temperate climate region, these are essentially pollen records from the Velay region in France (1, 2), comprising the last 450 ka and the pollen records of Tenaghi Phillipon and Ioannina (Greece) for the last ~ 450 and 1,350 ka from the Mediterranean region (3, 4). Since different ecosystems react in a different way to climate change, there is still a need to establish further continental climate records for Europe to study interactions between ecosystems and climate change.

The lowlands of the middle (Pannonian/Carpathian Basin) and lower Danube Basin form the westernmost extension of the Eurasian steppe belt. During the Quaternary, decametres of loess accumulated in these basins, building up plateau-like landforms. It has been demonstrated in several studies that loess-paleosol sequences (LPSS) of this area represent sensitive climate archives, allowing regional and transcontinental correlation of paleoclimate proxies (e.g. 5-10). Two prominent LPSS are the Mircea Voda sequence (Romania, 44°19'15"N, 28°11'21"E) and the Batajnica/Stari Slankamen sequence (Serbia, 44°55'29"N, 20°19'11"E / 45°7'58"N, 20°18'44"E) (see Fig. 4-S1 and Fig. 4-S2 for pictures of the profiles). Previous investigations have shown that both sequences comprise more than 700,000 years of climate history. Hence, these sites can be regarded as key archives for the Quaternary climate development in SE - central Europe (10, 11).

In the study presented, soil formation and weathering history of the Mircea Voda and Batajnica/Stari Slankamen LPSS are reconstructed to gain further insight into the Late and Mid-Pleistocene climate evolution of the SE European steppe region. A multi-proxy approach is applied comprising micromorphological, geochemical and grain size parameters of weathering and soil formation (12).

Fig. 4-1 shows the peak values of these proxies for the interglacial pedocomplexes of the Mircea Voda and Batajnica/Stari Slankamen sites. For loess layers, the minimum values are given. The full record is presented in the supporting material (Fig. 4-S3 and Fig. 4-S4). The micromorphological proxy of soil formation intensity (MPI) is implemented as an index for groundmass development, as determined by microscopic observations of paleosol thin sections (12, Table 4-S1). MPI values for the Mircea Voda site show a significant trend of decreasing soil formation intensity from older to younger interglacial pedocomplexes. Corresponding trends in the micromorphological aspect of Mid- and Late Pleistocene paleosols have been also described by Bronger (13) for the Stari Slankamen site and other sections in the Carpathian Basin, but only applying the Kubiena terminology. The $<5 \mu\text{m}$ fraction as grain size proxy for pedogenesis, and the Chemical Proxy of Alteration (CPA), as proxy for silicate weathering (14), reveal similar trends for the interglacial pedocomplexes (Fig. 4-1). For the glacial loess units, trends in weathering intensity and clay formation are less significant, but still present in the CPA record of Batajnica and Stari Slankamen and in the $<5 \mu\text{m}$ fraction record of Mircea Voda. The sedimentary homogeneity of each LPSS has been proven by Bugge et al. (15). Therefore biasing effects on the applied weathering proxies due to grain size sorting or changes in mineralogical composition can be excluded.

As climatic drivers on silicate weathering and pedogenesis generally both temperature and precipitation have to be considered. In a seasonally dry climate regime, however, as the present day steppe climate of the lower and middle Danube Basin weathering is especially hampered by water deficiency during the periods of dryness, when the wet reactive surface of the minerals is reduced to hydrological inactive soil compartments (16). Hence, presented records of MPI, CPA and $<5 \mu\text{m}$ fraction reflect mainly precipitation but also temperature changes in the SE European steppe region. Consequently, the observed trends in our proxy dataset indicate a progressive aridization and/or cooling of the middle as well as the lower

Danube Basin over the last 600 – 700 ka. The CPA and $<5\mu\text{m}$ records additionally show that spatial climatic trends between both regions are pertained during most interglacials. Today, the Mircea Voda site and the Serbian sites have about the same mean annual temperature ($\sim 11.5\text{ }^{\circ}\text{C}$), but annual precipitation is about 200 - 250 mm lower at the Romanian site ($\sim 430\text{ mm}$, *11*). Except for the S6 pedocomplex (Marine Isotope Stage 17), also during past interglacials (MIS 5, MIS 7, MIS 9, MIS 11, MIS 13 - 15) conditions were dryer in the lower than in the middle Danube Basin as revealed by the pedogenesis proxies.

The U-ratio (i.e. ratio of the 16-44 μm fraction to the 5.5-16 μm particle size fraction) reflects predominantly variations due to sedimentological effects (*17-20*). According to this proxy record (Fig. 4-1), the aridization and/or cooling trend is accompanied by an increase in wind strength. The trend in wind strength is significant for the glacial units and generally more significant for the dryer lower Danube Basin. Only there, the U-ratio indicates a weak increase of wind strength also during the interglacials.

Not only weathering intensity or sedimentological properties of the paleosol units changed, but also trends in the general type of soil development refer to a continuous aridization and cooling. While rubified (Luvic) Cambisols of the older parts ($>\text{MIS } 13$) of the Mircea Voda and Batajnica/Stari Slankamen sections indicate a Mediterranean-like climate, younger paleosols represent fossil stepp. This temporal pattern in soil development (Fig. 4-2) points towards an increasing climate continentality and is typical for loess-paleosol sequences in the middle and lower Danube Basin, such as in Hungary (*13, 21*), Serbia (*6, 13, 21, 22, 23*), Romania (*24*) and Bulgaria (*5, 7*). Furthermore, mineralogical (*22, 23*) and palynological investigations (*25*) on sites and cores in the middle Danube Basin give further evidence for a progressive cooling and aridization of Late and Mid-Pleistocene interglacials.

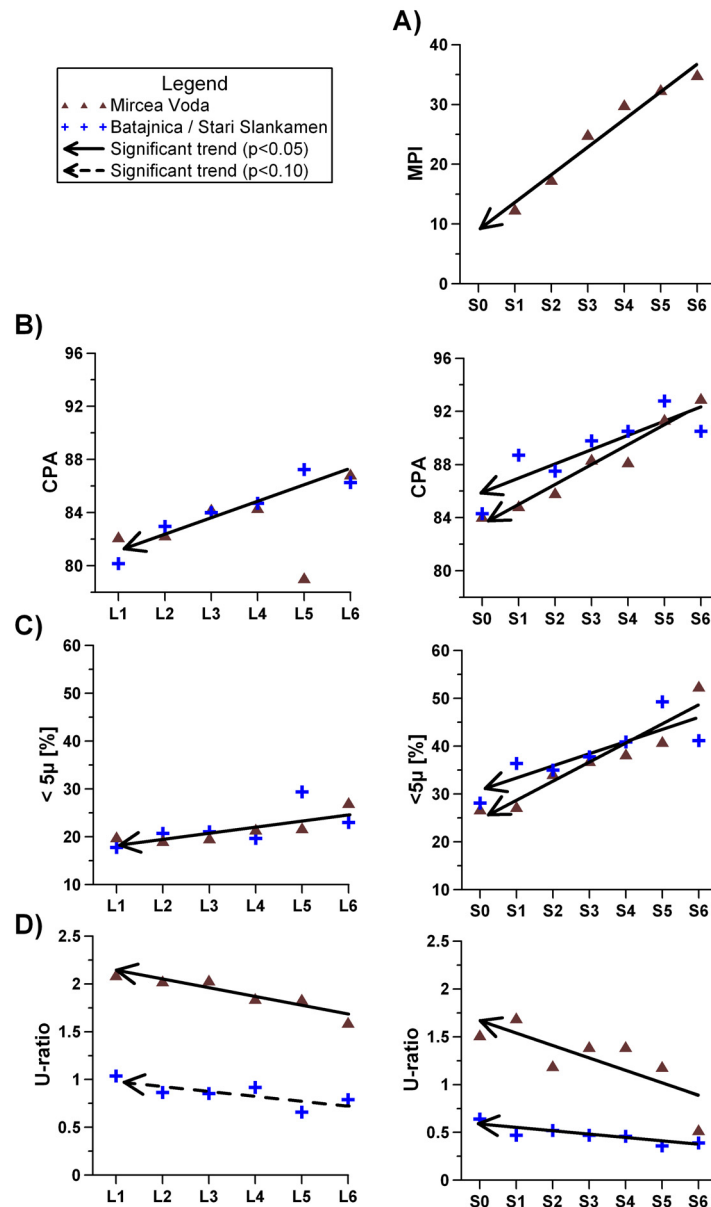


Fig. 4-1. Peak values for pedogenesis, weathering and wind strength proxies for the last six glacial and interglacials preserved in loess-paleosol sequences of the middle (Batajnica/Stari Slankamen site) and lower Danube Basin (Mircea Voda site). For interglacial units (S0-S6), the maximum value of each pedocomplex is shown (the lowest value for the U-ratio) and for glacial units, the lowest value of each loess layer (L1-L6) is presented (the highest value for the U-ratio). The chronostratigraphic placement of the units (11) is given in Fig. 4-S3 and Fig. 4-S4. of the supplementary material) The Micromorphological Proxy of soil formation Intensity (MPI) is a measure for groundmass development of paleosol thin sections (c/f related distribution pattern and b-fabric, 12) and reflects pedogenesis intensity. B) The Chemical Proxy of Alteration (CPA) gives a record of silicate weathering and C) the <5µ fraction is a proxy of pedogenic clay formation. MPI, CPA and the <5µ fraction are sensitive to changes in humidity and/or precipitation, whereas the U-ratio is applied as grain size proxy of wind strength. Significant trends in peak values are indicated by solid arrows ($p < 0.05$) and dashed arrows ($p < 0.1$). The gradual change in peak values of this set of proxies indicates a progressive aridization and/or cooling of today's SE European steppe region.

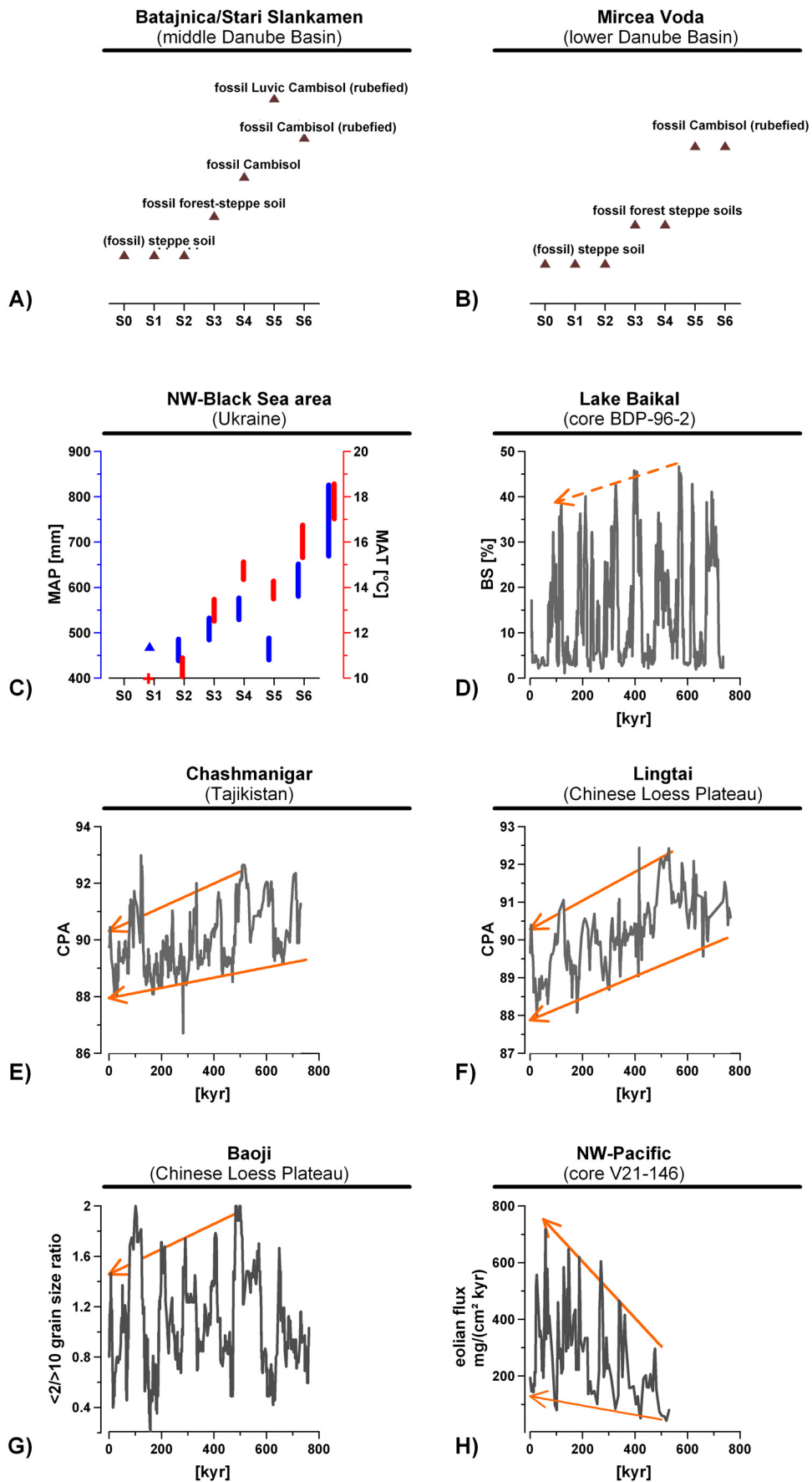


Fig. 4-2. Comparison of climate proxy records from mid-latitude Eurasia over the last six interglacial to glacial cycles. All records indicate aridization and/or a decrease of temperature for interglacials partly also glacials over the last 600-800 ka. A and B) Paleosol succession of the middle and lower Danube Basin as preserved in the loess-paleosol sequence (LPSS) Batajnica/Stari Slankamen (10, 13) and Mircea Voda (see Table 4-S2), respectively; C) Mean annual temperature (MAT) and precipitation (MAP) of the NW Black Sea area, as reconstructed from paleopedologic and environmental magnetic properties of LPSS using a modern analogue approach (44, 45); D) Biogenic Silica content (BS) in Lake Baikal sediments (core BDP 96-2) as proxy of summer temperature (46); E and F) Chemical Proxy of Alteration (CPA) record of the Chashmanigar LPSS (Tajikistan) and Lingtai LPSS (Chinese Loess Plateau) (47). Silicate weathering intensity reflects mainly humidity but also temperature. G) $<2 / >10 \mu$ grain size ratio record of the Baoji LPSS (Chinese loess plateau) reflecting weathering intensity (hence humidity and/or temperature) and wind strength (32); H) Dust flux record in the NW Pacific (core V21-146) as proxy for aridization of eastern Asia (48). Significant trends in peak values are indicated by solid arrows ($p < 0.05$) and dashed arrows ($p < 0.1$). Site-specific deviations are mainly recorded for MIS 17 and MIS 5. For the Chashmanigar, Lingtai and Baoji record, the S1 has been excluded from trend calculation.

As briefly summarized in the “supporting material”(see also Fig. 4-2) the aridization trends reported from the steppe region of SE-Europe can be traced eastwards to interior Eurasia following climate archives along the mid-latitude steppe. Hence, a common trigger seems to be evident. Direct orbital forcing does not account for these trends (see Fig. 4-1). Therefore, other mechanisms are needed causing this feature in central Eurasian climate archives. A mechanism commonly referred to is uplift of the Himalaya-Tibet ensemble and Central Asian mountain ranges (26, 27, 28), which explains the development of B-climates in the Eurasian mid-latitudes, according to modelling results (29, 30). Proxy records of other potential triggers such as a gradual decline in atmospheric CO₂, changes in North Atlantic sea surface hydrography and the global ice volume (see Fig. 4-3) cannot explain observed Mid-Pleistocene aridization and/or cooling trends. Thus, in lack of other plausible mechanisms, we focus on the uplift hypothesis, though late Cenozoic uplift rates are still under debate and regionally highly variable. For the last 800 ka, values range for example from >0.8 km in the SE-Margin of the Tibetan plateau (31), 1 km for the Kunlun Pass area in the Central Tibetan plateau and 1.6 - 4 km for the Central Nepalese Himalaya (32), but also lowering of elevation has been reported for parts of the Tibetan plateau (33) Notwithstanding the controversial discussion concerning the Tibetan plateau, surrounding mountain edges are still growing (33).

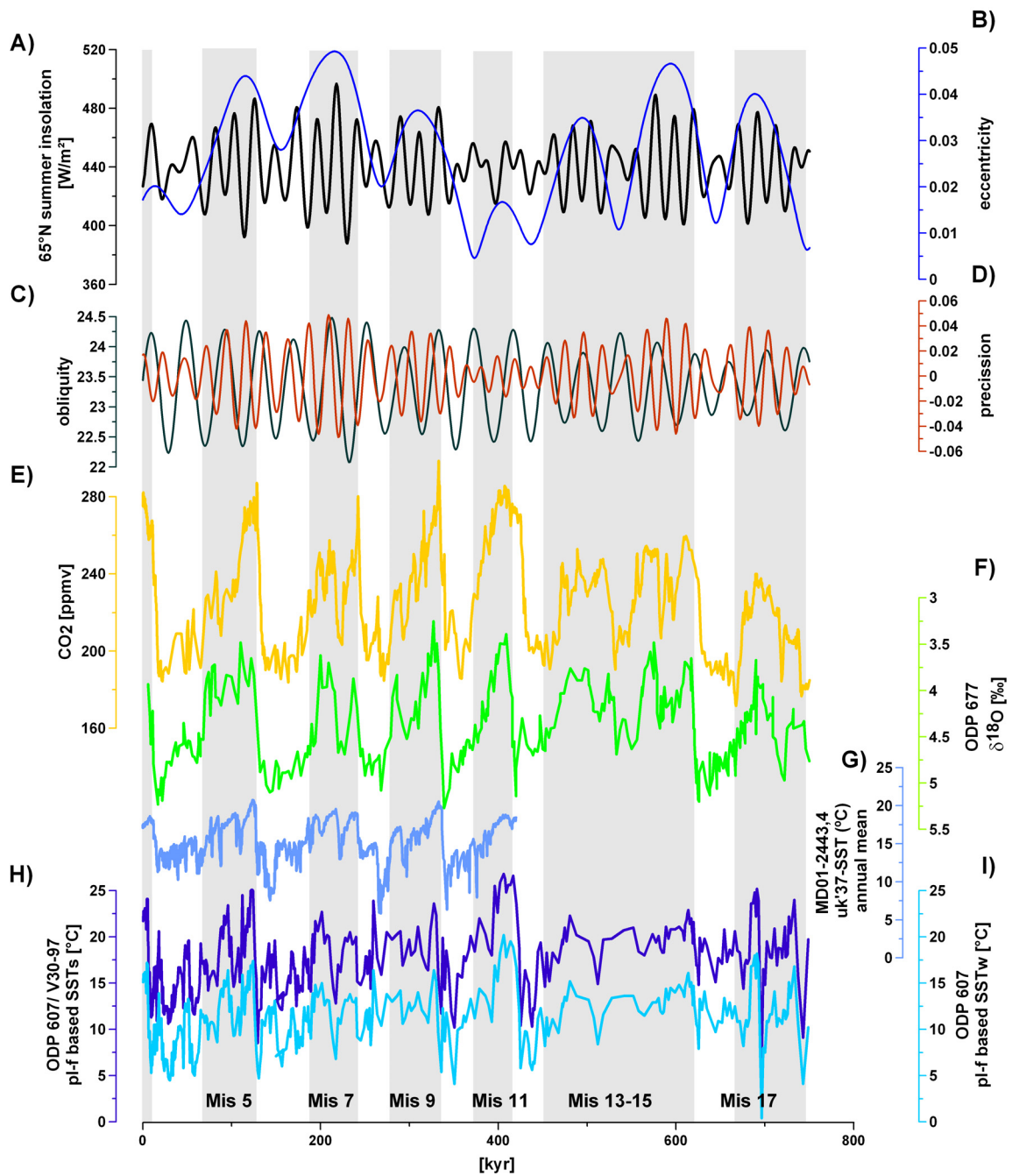


Fig. 4-3. Comparison of proxy records for potential long-term triggers on Eurasian climate during the last 17 marine isotope stages. A-D) The daily insolation at 65°N during the summer solstice, the eccentricity of the Earth's orbit, phasing in obliquity and precession of the Earth (49); E) Atmospheric CO₂ concentration in parts per million by volume (ppmv) (50); F) δ¹⁸O values of benthic foraminifera from ODP-site 677 as proxy of global ice volume (51). G) U₃₇^k based mean annual sea surface temperature (SST) at the Iberian Margin (cores MD01-2443 and MD01-2444; 52); H and I) Changes of the summer and winter sea surface temperature in the North Atlantic (composite record from ODP site 607 and core V30-97, 53). SST estimates are based on species composition of planctonic foraminifera (pl-f). None of these parameters and proxies show trends over the last 600-700 ka that could indicate a trigger for observed gradual aridization and or cooling in mid-latitude Eurasia.

Due to denudation, reported uplift values are somewhat higher than net increase in elevation. Moreover, $\delta^{18}\text{O}$ based approaches of paleoaltimetry suggest for parts of the Tibetan plateau and the Himalayas a hypsometry similar as today, already during the Late Miocene. However, a standard error of about 20% is given for this method, when estimating high altitudes (34). Therefore, Late Cenozoic elevation changes of up to ~ 800 m (Tibetan Plateau) and ~ 1500 m (High Himalayas) cannot be excluded by these findings. Yet, it has been shown by climate models that already such small changes in elevation (10 or 20% of today's altitude) of Himalaya-Tibet orogen and Central Asian mountain ranges have a significant effect on Eurasian climate, also in SE Europe (35, 36). Hence, although the intensity of mountain rise cannot exactly be quantified it seems to be a likely trigger for observed cooling and aridization trends in the Late and Mid-Pleistocene of interior Eurasia and also SE European steppe region (see supporting material for an overview on the climatic implications of the uplift hypothesis).

Following the modelling studies, this trigger should also have an influence on climate in the E Mediterranean and eventually also in temperate central Europe, if it is effective in SE European steppe regions (29, 36). However, available long-term climate records from central Europe such as the Velay Pollen sequence in France (1, 2) or the compilation of loess-paleosol sites from the Rhine valley in Germany (37) do not reveal a comparable trend in interglacial vegetation and paleosol typology. For the Rhine valley, soil development on loess sites always peaked in Luvisols during the past four major interglacials (37). Also from the pollen record of Tenaghi Phillipon and Ioannina corresponding trends have neither been reported in the percentage of temperate tree pollen nor in the relative abundance of individual species (3, 4, 38). At the moment, we cannot provide a definite answer on why clear evidence of a gradual cooling and aridification during the Mid-Pleistocene in these regions is lacking. We propose two explanations. I) Quaternary uplift of alpine orogens in Central and Eastern

Europe could have induced changes in regional atmospheric circulation. Today's SE European steppe region is situated E to SE of the Alps and E to S of the Carpathian Mountains. Blocking of the westerlies by these mountains is an essential factor promoting dryness and a stronger continental influence in the Pannonian and lower Danube Basin. Recalculated uplift intensity for the last 800 ka from published Quaternary uplift rates gives values of up to 420 m for the Carpathian mountains (39, 40) and 560 m for the Northern Calcareous Alps (41). For the time span between two interglacials, this would mean uplift values of ~ 50 and ~ 70 m in average, respectively (42). Up to now, it is not evaluated by modelling studies how strong changes in elevation in this magnitude enhance rain shadow effects on a regional scale. II). Today, the SE European Steppe region is the westernmost extension of the Eurasian steppe belt separating the temperate zone of central Europe and the Mediterranean ecozone of the S and W Balkan Peninsula. We propose that during Pleistocene warm periods, this region was probably always a transitional zone between the temperate, Mediterranean and continental ecozone being highly sensitive for climate change. Such a transitional zone represents a system at the limits of its stability. It is likely to be highly sensitive to climate change. In the case of the Pannonian and lower Danube Basin, cooling and aridification of Pleistocene interglacials is reflected by a change from a Mediterranean ecozone to a steppe ecozone, which is recorded in paleobotanical and paleopedological-geochemical parameters (13, 22, 23, 25). The early Mid-Pleistocene Mediterranean ecozone of this region was probably close to threshold values in its stability in contrast to the peak interglacial ecozones at the Velay site and Rhine area in central Europe, as well as in Tenaghi Phillipon.

Concluding, gradual aridization and cooling of today's SE European steppe region since the late Pleistocene is a regional expression of corresponding trends in interior Eurasia. As general trigger we propose the uplift of Central Asian mountain ranges. In Europe, this trend

is especially expressed in the today's steppe region. We suggest that this is caused by i) a regional amplification of the aridization trend due to Quaternary uplift of Central-East European mountain ranges (Alps, Carpathians) and in particular by ii) the sensitivity of this region in reflecting changing climate parameters, since environmental conditions during peak interglacials have been close to threshold values in the stability of ecozones (Mediterranean vs. continental steppe). The high sensitivity of this region and its ecozones (continental steppe, temperate and Mediterranean zone in transition state) to aridification is an issue of relevance for decision makers with respect to future climate change projections, which predict decreasing summer precipitation for SE Europe (43).

References and Notes

- 1 M. Reille, J.-L. de Beaulieu, H. Svobodova, V. Andrieu-Ponel, C. Goeury, *J. Quat. Sci.* **15** (7),665-685 (2000).
- 2 J.-L. de Beaulieu et al., *Quat. Sci. Rev.* **20**, 1593-1602 (2001).
- 3 P. C. Tzedakis, K. D. Bennett, *Quat. Sci. Rev.* **14**, 967-982 (1995).
- 4 P. C. Tzedakis, H. Hooghiemstra, H. Pälike, *Quat. Sci. Rev.* **25**, 3416-3430 (2006).
- 5 D. Jordanova, N. Petersen, *Geophys. J. Int.* **171**, 1036-1047 (1999).
- 6 S. B. Marković, E. Oches, P. Sümegi, M. Jovanović, T. Gaudenyi, *Quat. Int.* **149**, 80-86 (2006).
- 7 D. Jordanova, J. Hus, R. Geeraerts, *Geophys. J. Int.* **138**, 533-540 (2007).
- 8 P. Antoine et al., *Quat. Int.* **198**, 19-36 (2009).
- 9 M. P. Bokhorst et al., *Quat. Int.* **198**, 113-123 (2009).
- 10 S. B. Marković, et al., *Quat. Int.* **198**, 255-266 (2009).
- 11 B. Buggle et al., *Quat. Int.* **196**, 86-106 (2009).
- 12 Materials and methods are available as supporting material.
- 13 A. Bronger, *Kieler Geographische Schriften* **45** (1976).

- 14 B. Buggle, B. Glaser, U. Hambach, N. Gerasimenko, S. B. Marković, (in press) *Quat. Int.* [doi:10.1016/j.quaint.2010.07.019](https://doi.org/10.1016/j.quaint.2010.07.019).
- 15 B. Buggle et al., *Quat. Sci. Rev.* **27**, 1058-1075 (2008).
- 16 A. F. White, A. E. Blum, *Geochim. Cosmochim. Acta* **59** (9), 1729-1747 (1995).
- 17 J. Vandenberghe, B. S. Huijzer, H. Mùcher, W. Laan, *J. Quat. Sci.* **13** (5), 471-485 (1998).
- 18 J. Vandenberghe, G. Nugteren, *Global Planet. Change* **28**, 1-9 (2001).
- 19 Y. Sun, H. Lu, Z. An, *Palaeogeogr. Paleoclimatol. Palaeoecol.* **241**, 129-138 (2006).
- 20 M. Zech et al., *Geoderma* **143** (3-4), 281-295 (2008).
- 21 A. Bronger, *Quat. Int.* **106-107**, 11-31 (2003).
- 22 N. Kostić, N. Protić, *Catena* **41**, 217-227 (2000).
- 23 S. B. Marković, N. Kostić, E. A. Oches, *Rev. Mex. Cienc. Geol.* **21**, 79-87 (2004).
- 24 C. G. Panaiotu, E. C. Panaiotu, A. Grama, C. Necula, *Phys. Chem. Earth (A)* **26**, 893-898 (2001).
- 25 A. Ronai, *Palaeogeogr., Palaeoclimatol. Palaeoecol.* **8**, 265-285 (1970)
- 26 N. V. Alexeeva, M. A. Erbajeva, *Quat. Int.* **179**, 190-195 (2008).
- 27 C. Deng, J. Shaw, Q. Liu, Y. Pan, R. Zhu, *Earth Planet. Sci. Lett.* **241**, 248-259 (2006).
- 28 Z. Ding, Z. Yu, N. W. Rutter, T. Liu, *Quat. Sci. Rev.* **13**, 39-70 (1994).
- 29 W. F. Ruddiman, J. E. Kutzbach, *J. Geophys. Res.* **94** (D15), 18,409-18,427 (1989).
- 30 A. J., Broccoli, S. Manabe, *J. Clim.* **5**, 1181-1201 (1992).
- 31 Y. Wu et al., *Geomorphology* **36**, 203-216 (2001).
- 32 A. E. Blythe, D. W. Burbank, A. Carter, K. Schmidt, J. Putkonen, *Tectonics* **26**, TC3002 (2007).
- 33 M. Fort, *Palaeogeogr. Palaeoclimatol. Palaeoecol.* **120**, 123-145 (1996).
- 34 D. B. Rowley, R. T. Pierrehumbert, B. C. Currie, *Earth Planet. Sci. Lett.* **188**, 253-268 (2001).
- 35 M. Abe, T. Yasunari, A. Kitoh, *Isl. Arc.* **14**, 378-388 (2005).

-
- 36 D. Jiang, Z. Ding, H. Drange, Y. Gao, *Advances in Atmospheric Sciences* **25** (5), 709-722 (2008).
- 37 W. Schirmer, *Central European Journal of Geosciences* **2** (1), 32-40 (2010).
- 38 P. C. Tzedakis, H. Pälike, K. H. Roucoux, L. de Abreu, *Earth Planet. Sci. Lett.* **277**, 307-317 (2009).
- 39 F. Radulescu, V. Mocanu, V. Nacu, C. Diaconescu, *J. Geodyn.* **22** (1/2), 33-50 (1996).
- 40 D. Necea, W. Fielitz, L. Matenco, *Tectonophysics* **410**, 137-156 (2005).
- 41 M. C. Meyer, R. A. Cliff, C. Spötl, M. Knipping, A. Mangini, *Quat. Sci. Rev.* **28**, 1374-1391 (2009).
- 42 Again these are maximum values for the net increase in elevation above sea level
- 43 J. Räisänen et al., *Clim. Dyn.* **22**, 13-31 (2004).
- 44 A. Tsatskin et al., *Palaeogeogr. Palaeoclimatol., Palaeoecol.* **143**, 111-133 (1998).
- 45 A. Tsatskin et al., *Phys. Chem. Earth (A)* **26** (11-12), 911-916 (2001).
- 46 A. A. Protopenko et al., *Quat. Res.* **55**, 123-132 (2001).
- 47 S. Yang, F. Ding, Z. Ding, *Geochim. Cosmochim. Acta* **70**, 1695-1709 (2006).
- 48 S. A. Hovan, D. K. Rea, *Paleoceanography* **6** (3), 349-370 (1991).
- 49 A. Berger, M. F. Loutre, *Quat. Sci. Rev.* **10**, 297-317 (1991).
- 49 D. Lüthi et al., *Nature* **453**, 379-382 (2008).
- 50 N. J. Shackleton, A. Berger, W. R. Peltier, *Trans. R. Soc. Edinburgh. Earth Sci.* **81**, 251-261 (1990).
- 52 B. Martrat, et al., *Science* **317**, 502-507 (2007).
- 53 W. F. Ruddiman, M. E. Raymo, D. G. Martinson, B. M. Clement, J. Backman, *Paleoceanography* **4**(4), 353-412 (1989).
- 54 We thank Tivadar Gaudenyi, Mladjen Jovanović and Irina Glaser for assistance during fieldwork, Ana Malagodi for support in sample preparation, J. Eidam (University of Greifswald) for XRF analyses, L. Zöller and M. Zech for critical comments and S. Schimmelpfennig for improving language style. This study was financially supported by the German Research Foundation DFG (GL 327/8-2,3).

Supporting Material

a) Supporting Text

S1 Material and Methods

S1.1 Sampling, laboratory procedures

For micromorphological analyses one representative, undisturbed sample was taken per each pedomember horizon of the Mircea Voda section. Due to already available detailed micromorphological investigations and soil descriptions (*S1*, *S2*) no further samples were taken from the Batajnica and Stari Slankamen section. Samples for grain size measurements and geochemical analyses have been taken from all profiles. Younger pedocomplex units (MIS 5, Mis 7, MIS 9) were sampled in higher resolution for geochemistry and texture. At the Batajnica section (Serbia), the three lowermost pedocomplexes are influenced by water-logging. Therefore, samples of the older units were taken from the section Stari Slankamen and a composite loess-paleosol sequence Batajnica/Stari Slankamen was constructed. Further details on sampling strategy are described in a previous study (*S3*). All samples were stored in air-tight plastic bags until drying in the laboratory at 40 °C.

Thin sections of $\geq 2.8 \times 4.8$ cm² were prepared by Th. Beckmann (Schwülper-Lagesbüttel, Germany) according to the procedures given in Beckmann (*S4*). Micromorphological description follows the terminology of Stoops (*S5*). Grain size analysis was performed using a Malvern Mastersizer S analyzer. Sample pretreatment followed the procedure described in Konert and Vandenberghe (*S6*). The >600 µm fraction was removed by wet sieving and prior to laser measurements samples were subjected to ultrasonic treatment for complete

disaggregation. The composition of major and trace elements was analyzed via XRF and presented in Bugge et al. (S3).

Determination of soil colors was performed on soil clods in moist and dry conditions, using the Munsell soil color charts (S7).

The chronostratigraphy of the sites has been already established by Bugge et al. (S8) using pedostratigraphic marker horizons and correlation of characteristic pattern of magnetic susceptibility pattern with the benthic $\delta^{18}\text{O}$ record from ODP 677 as proxy of the global ice volume (S9). The nomenclature of stratigraphic units follows the S-L system applied for Chinese loess-paleosol sequences (e.g. S10, S11).

S1.2 Applied proxies for soil formation and weathering intensity

S1.2.1 Micromorphological proxies – rational

In paleopedologic studies micromorphological investigations have been established as tool to identify pedogenic processes and thus to characterize and classify fossil soils (S1, S12, S13). Micromorphological parameters have also been used to describe the intensity of soil forming processes. Especially the type of b-fabric (birefringence-fabric) has shown up as a valuable proxy in several studies. Starting from unmodified loess or weak unleached paleosols having a calcitic crystalline b-fabric, usually an undifferentiated b-fabric evolves, indicating a carbonate-free groundmass with low to moderate clay content. With increasing intensity of soil formation stipple-speckled, mosaic-speckled and striated b-fabrics usually develop, reflecting higher clay content and mobility of clays due to clay dispersion and orientation in clay domains (S5, S14 - S16). Besides the b-fabric also the c/f related distribution was selected as parameter, which is likely to reflect intensity of pedogenic clay formation. The c/f related distribution describes the relative distribution of coarse and fine fabric units in the groundmass and with increasing (pedogenetically formed) clay content the c/f related

distribution should evolve from a coarse-fabric supported pattern (e.g. coarse monic, close porphyric) to a fine-fabric supported pattern (e.g. open porphyric) (S5). We ranked the different types of c/f related distribution and b-fabric according to their appearance with increasing groundmass development and assigned numerical values to the different ranks. The sum of rank values for the c/f related distribution and b-fabric-type is implemented as micromorphological proxy of soil formation intensity (MPI) (see Table 4-S1).

S1.2.2 Grain size proxies - rational

As direct proxy of the clay content, we apply the <5 µm size fraction, as determined by laser analysis. The <5 µm fraction shows the best correlation (minimum sum of squared residuals) with earlier published results (S1) from pipette analysis for the Stari Slankamen section. The 5 µm cut is slightly below the classically applied 8 µm laser-equivalent to the “pipette-clay” content (S6). It is in between the clay-cut published for the Surduk section in Serbia (<4.6 µm fraction; S17) and the grain size proxy for pedogenic clay published for other loess-paleosol sites in Serbia and Ukraine (<5.5 µm; S18).

While the <5.5 µm fraction is essentially controlled by pedogenesis, the ratio of the 16–44 µm / 5.5-16 µm fraction (so-called U-ratio) reflects predominantly sedimentary processes (S19, S20 and references therein). Hence, in loess-paleosol studies the U-ratio has been commonly applied as proxy for aeolian activity and wind strength (e.g. S21-S23). As such the U-ratio is also implemented in the present study.

S1.2.3 Chemical weathering index – rational

As chemical proxy of silicate weathering, Buggle et al (S24) proposed the molar ratio of $\text{Al}_2\text{O}_3/(\text{Al}_2\text{O}_3 + \text{Na}_2\text{O}) \times 100$ for loess-paleosol sequences. This ratio was initially introduced by Cullers (S25) as CIW and later on by Buggle et al (S24) implemented for loess-paleosol

sequences as Chemical Proxy of Alteration (CPA). In contrast to commonly applied weathering indices such as the Rb/Sr ratio or the Chemical Index of Alteration (CIA, *S26*) it does not involve uncertainties due to dynamics of secondary carbonates.

S2 Results and Discussion

S2.1 Overview on records of Mid-Pleistocene aridization and cooling trends in mid-latitude Eurasia

In the following we give a review on paleoclimate records showing that Mid-Pleistocene aridization / cooling can be traced across mid latitude Eurasia from the SE-European steppe belt to Central Asia. Starting in vicinity of the lower Danube basin, corresponding shifts in soil forming processes and weathering intensity, respectively, can also be found north of the Black Sea Coast in the steppe belt of the southern East European Plain. In Moldova, S-Ukraine and S-Russia, Tsatskin et al. and Velichko et al. (*S27, S28, S29*) found rubified paleosols of MIS 13 - 15 and older on several sites, which they interpreted as soils developed under a Mediterranean climate. Younger paleosols were identified as fossil Chernozems. Using transfer functions of pedological, rock magnetic properties and climate derived from modern analogs, decreases in MAT and MAP from ~ 19 to 10 °C and ~ 800 to ~ 500 mm, respectively were reconstructed for the area, north of the Black Sea Coast (*S27, S28*, see Fig. 4-2). Yet in these studies, no mechanistic explanation is given for the observed climatic evolution. Further to the East, in the mid-latitudes of Asia, corresponding climate patterns could be deduced from archives in Siberia. In Mid- to Late Pleistocene paleosol successions of West Siberia a transition from meadow soils to Chernozem-like soils reflect cooling and/or drying (*S30*). This is also supported by the Pleistocene faunal development of the Baikal region (*S31*) and a weak decrease of biogenic silica content in interglacial periods of the last 600 ka as revealed in core BDP-96-2 and the stacked BDP-96-2 and GC1 record of Lake

Baikal (*S32, S33*, see Fig. 4-2). This decrease cannot be solely explained by astronomical factors, since summer maximum air temperature for Siberia, predicted from energy balance modelling, do not reveal a similar trend (*S34*). However, corresponding trends for cooling and drying are reported from many Central Asian and Chinese loess deposits (e.g. Fig. 4-2) based on the micromorphological soil development intensity (*S35*), geochemical weathering proxies (*S36, S37*), iron mineralogy (*S38*), grain size proxies of weathering or wind strength (*S39, S40*), dust accumulation rates (*S41*) and pollen records (*S42, S43*). Though there are site-specific deviations, mainly recorded for the S6 (negative deviation) and S1 (positive deviation), the general trend preserved in this variety of proxies consistently indicates aridization and/or cooling of interior Eurasia since the early Pleistocene. Also a gradual expansion of C4 vegetation since 850 ka has been reported for Central Asia, which however, has been interpreted in terms of increasing summer precipitation (*S41*). Yet, in light of the available palynological data and the weathering records this trend more likely reflects aridization. Further evidence for cooling, aridization and increasing atmospheric dynamics of interior Eurasia is provided by mass accumulation rate (MAR) records from the northern Pacific (Fig. 4-2) showing increasing dust flux over the last 500 ka.

S2.2 The effect of Himalayan-Tibetan uplift on Eurasian climate – a short overview on the “uplift-theory”

According to modelling results of Ruddiman et al and Broccoli and Manabe (*S44, S45*), the uplift of these mountains has direct impact on atmospheric circulation pattern. It causes a diversion of the westerly circulation, weakening of the westerlies north of the uplift region due to a low level cyclonic flow and an intensified vertical atmospheric motion. Furthermore, due to temperature-snow-albedo feedbacks the uplift areas act as source of cold air masses. Hence, an intensification of the central Asian-Siberian high pressure cell in winter, an

increased subsidence next to the mountain areas in summer, rain shadow effects and the weakening of the westerlies north of the uplift region represent a mechanistic background when explaining aridification of Central Asia by the “uplift-theory”. These models (“mountain” versus “no mountain” run) suggest explicitly for the Northern Black sea region and the Eastern Mediterranean cooler and wetter winters but a more significant decrease of temperature and precipitation in summer time due to a decrease in westerly winds, more intensified northeasterly winds and increased subsidence. Geological observations from the E Mediterranean supporting the validity of this mechanism during the Pliocene are summarized in Ruddiman and Kutzbach (1989, *S44*).

b) Supporting References

- S1 A. Bronger, *Kieler Geographische Schriften* **45** (1976).
- S2 S. B. Marković, et al., *Quat. Int.* **198**, 255-266 (2009).
- S3 B. Buggle et al., *Quat. Sci. Rev.* **27**, 1058-1075 (2008).
- S4 T. Beckmann, *Hohenheimer Bodenkundliche Hefte* **40**, 89-103 (1997).
- S5 G. Stoops, *Guidelines for analysis and description of soil and regolith thin sections* (Soil Science Society of America, Madison, WI, 2003).
- S6 M. Konert, J. Vandenberghe, *Sedimentology* **44**, 523-535 (1997).
- S7 *Munsell color charts* (Munsell Color Company, Baltimore, MD, 1975).
- S8 B. Buggle et al., *Quat. Int.* **196**, 86-106 (2009).
- S9 N. J. Shackleton, A. Berger, W. R. Peltier, *Trans. R. Soc. Edinburgh. Earth Sci.* **81**, 251-261 (1990).
- S10 E. Derbyshire, R. A. Kemp, X. Meng, *J. Geol. Soc. London* **154**, 793-805 (1997).
- S11 J. Chen, J. Junfeng, W. Balsam, Y. Chen, L. Liu, Z.. *Palaeogeogr. Palaeoclimatol. Palaeoecol.* **183**, 287-297 (2002).
- S12 A. Tsatskin et al., *Palaeogeogr. Palaeoclimatol., Palaeoecol.* **143**, 111-133 (1998).
- S13 R. A. Kemp, *Catena* **35**, 179-196 (1999).

- S14 D. Magaldi, M. Tallini, *Catena* **41**, 261-276 (2000).
- S15 N. Günster, A. Skowronek, *Quat. Int.* **78**, 17-32 (2001).
- S16 M. Kehl, M. Frechen, A. Skowronek, *Quat. Int.* (**140-141**), 135-149 (2005).
- S17 P. Antoine et al *Quat. Int.* **198**, 19-36 (2009).
- S18 M. P. Bokhorst et al., *Quat. Int.* **198**, 113-123 (2009).
- S19 J. Vandenberghe, B. S. Huijzer, H. Mücher, W. Laan, *J. Quat. Sci.* **13** (5), 471-485 (1998).
- S20 J. Vandenberghe, H. Lu, D. Sun, J. Van Huissteden, M. Konert, *Palaeogeogr. Paleoclimatol. Palaeoecol.* **204**, 239-255 (2004).
- S21 Vandenberghe, G. Nugteren, *Global Planet. Change* **28**, 1-9 (2001).
- S22 Y. Sun, H. Lu, Z. An, *Palaeogeogr. Paleoclimatol. Palaeoecol.* **241**, 129-138 (2006).
- S23 M. Zech et al., *Geoderma* **143** (3-4), 281-295 (2008).
- S24 B. Buggle, B. Glaser, U. Hambach, N. Gerasimenko, S. B. Marković, *Quat. Int.*, (accepted) [doi:10.1016/j.quaint.2010.07.019](https://doi.org/10.1016/j.quaint.2010.07.019).
- S25 R. L. Cullers, *Lithos* **51**, 181-203 (2000).
- S26 H. W. Nesbitt, G. M. Young, *Nature* **299**, 715-717 (1982).
- S27 A. Tsatskin et al., *Palaeogeogr. Paleoclimatol., Palaeoecol.* **143**, 111-133 (1998).
- S28 A. Tsatskin et al., *Phys. Chem. Earth (A)* **26** (11-12), 911-916 (2001).
- S29 A.A. Velichko et al., *Quat. Int.* **198**, 204-219 (2009).
- S30 V. S. Zykina, V. S. Zykina, *Quat. Int.* **106-107**, 233-243 (2003).
- S31 N. V. Alexeeva, M. A. Erbajeva, *Quat. Int.* **179**, 190-195 (2008).
- S32 D. F. Williams et al., *Science* **278**, 1114-1117 (1997).
- S33 A. A. Protopenko et al., *Quat. Res.* **55**, 123-132 (2001).
- S34 D. A. Short, J. G. Mengel, T. J. Crowley, W. T. Hyde, G. R. North, *Quat. Res.* **25**, 157-173 (1991).
- S35 N. Rutter, Z. Ding, *Quat. Sci. Rev.* **12**, 853-862 (1993).
- S36 N. J. Vidic, K. L. Verosub, M. J. Singer, *Geoph. Monog.* **137**, 231-240 (2003).

- S37 S. Yang, F. Ding, Z. Ding, *Geochim. Cosmochim. Acta* **70**, 1695-1709 (2006).
- S38 C. Deng, J. Shaw, Q. Liu, Y. Pan, R. Zhu, *Earth Planet. Sci. Lett.* **241**, 248-259 (2006).
- S39 Z. Ding, Z. Yu, N. W. Rutter, T. Liu, *Quat. Sci. Rev.* **13**, 39-70 (1994).
- S40 S. L. Yang, Z. L. Ding, *Sedimentology* **51**, 77-93 (2004).
- S41 S. Yang, Z. Ding, *Palaeogeogr. Palaeoclimatol. Palaeoecol.* **235**, 330-339 (2006).
- S42 A. E. Dodonov, *Quat. Sci. Rev.* **14**, 707-720 (1995).
- S43 F. Wu, et al., *Earth Planet. Sci. Lett* **257**, 160-169 (2007).
- S44 F. Ruddiman, J. E. Kutzbach, Forcing of Late Cenozoic northern hemisphere climate by plateau uplift in Southern Asia and the American West. *J. Geophys. Res.* **94** (D15), 18,409-18,427 (1989).
- S45 A. J., Broccoli, S. Manabe, The effects of orography on mid-latitude northern hemisphere dry climates. *J. Clim.* **5**, 1181-1201 (1992).

c) Supporting Tables and Figures

Table 4-S1. Groundmass characteristics of soil thin sections and their ranking following increasing groundmass development intensity with soil formation (carbonate leaching, clay formation, clay translocation). The micromorphological proxy of soil formation (MPI) is obtained from the sum of rank values of c/f related distribution pattern and b-fabric. Intermediate rank values are assigned to transitional groundmass types

| Rank value | c/f related distribution pattern | b-fabric |
|------------|----------------------------------|------------------|
| 0 | Close porphyric | crystallitic |
| 5 | Single spaced porphyric | undifferentiated |
| 10 | Double spaced porphyric | speckled |
| 15 | open porphyric | striated |

Table 4-S2. Summary of paleopedologic characteristics of the pedocomplexes at the Mircea Voda site and soil typological interpretation. The description of micromorphological features follows the terminology proposed by Stoops (S5 2003). The abundance of humous matrix and stains, clay cutans, detritic carbonates in thin sections is described semiquantitatively as follows: absent (No), few (I), frequent (II), very frequent (III). Furthermore, the lowest calcium carbonate values and highest values of clay content are given for each fossil soil horizon. High resolution records for clay content are presented in Fig. 4-S4, and for calcium carbonate given in Bugge et al. (S24). Paleopedologic characteristics and description of the Batajnica/Stari Slankamen site have already been published (S1; S2) and high resolution grain size and carbonate records of the Serbian site are shown in Fig. 4-S3 and Bugge et al. (S24).

| Stratigraphic unit | Field observations | | Micromorphological observations | | | | | Analytical data | | | Soil horizon | Soil typological interpretation | | |
|--------------------|--------------------|--|--------------------------------------|-----------------------------------|------------------------|---------------------|---|-----------------|----------------------|----------------------------|--------------|---------------------------------|-----------------------|-------------------------------------|
| | Thickness [dm] | Munsell color wet/dry | Groundmass | | | | Microstructure | Clay cutans | Secondary carbonates | Min. CaCO ₃ [%] | | | Max. clay content [%] | Max. TOC Content [%] |
| | | | Birefringence fabric | C/f related distribution | Humous matrix & stains | Detritic carbonates | | | | | | | | |
| S0 | 9 | 10YR2/2 // 10 YR5/2 | n.d. | n.d. | n.d. | n.d. | n.d. | n.d. | n.d. | 10 | 26.9 | 1.7 | Ah | Chernozem |
| L1S1 | 5 | 10YR4/4 – 10YR5/4 // 10YR7/3 | Crystallitic b-fabric | Close fine enaolic | III | III | Apedal channel to vughy microstructure | No | II | 17.1 | 28.7 | 0.18 | fAh | weakly developed fossil steppe soil |
| S1 | 15 | 10YR4/4 – 10YR5/4 // 10YR7/3 – 10YR6/3 | Crystallitic b-fabric | Close to single-spaced porphyric | III | III | Weakly separated subangular blocky microstructure; intrapedal channel to spongy microstructure | No | I | 11.7 | 27.4 | 0.35 | fAh | Fossil steppe soil |
| S2S1 | 11 | 10YR6/4 // 10YR8/3 | Crystallitic b-fabric | Close to single-spaced porphyric | III | III | Weakly separated subangular to angular blocky microstructure; intrapedal channel to spongy microstructure | No | I | 9.4 | 27.5 | 0.19 | fAh | Fossil steppe soil |
| S2S2 | 5 | 10YR3/4 – 10YR4/3 // 10YR5/3 – 10YR7/3 | Undifferentiated b-fabric | Close to single-spaced porphyric | III | II | Channel microstructure superimposed on vughy microstructure | No | I | 12.9 | 34.3 | 0.31 | fAh | Fossil steppe soil |
| S2S3 | 5 | 10YR3/3 – 10YR4/4 // 10YR6/3 | Undifferentiated b-fabric | Close to single-spaced porphyric | III | II | Channel microstructure superimposed on vughy microstructure | No | II | 6.7 | 33.1 | 0.34 | fAh | Fossil steppe soil |
| S3 | 10 | 10YR3/4 – 10YR4/3 // 10YR5/4 | Stipple speckled b-fabric | Closed to double-spaced porphyric | III | I | Spongy microstructure | No | No | 3.9 | 37.0 | 0.38 | fABh | Fossil forest steppe soil |
| S4 | 9 | 10YR3/4 – 10YR4/4 // 10YR5/4 – 10YR6/4 | Stipple speckled b-fabric | Single-spaced to open porphyric | II | No | Channel to spongy microstructure | No | II | 4.4 | 38.4 | 0.26 | fABh | Fossil forest steppe soil |
| S5 | 14 | 7.5YR4/6 // 10YR6/4 | Stipple speckled b-fabric | double-spaced to open porphyric | II | II | Moderately separated angular-subangular microstructure; intrapedal channel to vughy microstructure | No | II | 14 | 41 | 0.29 | fBw | Fossil Cambisol |
| S6S1 | 3 | 7.5YR5/6 // 7.5YR6/6 | Stipple speckled – striated b-fabric | Single-spaced to open porphyric | II | I | Weakly separated angular-subangular microstructure; intrapedal channel to vughy microstructure | No | No | 6.0 | 44.4 | 0.14 | fBw | Fossil Cambisol |
| S6S2 | 8 | 7.5YR4/6 // 7.5YR6/4 | Stipple speckled – striated b-fabric | Double-spaced to open porphyric | II | I | Moderately to weakly separated angular microstructure with intrapedal channel to vughy microstructure | No | II | 16.0 | 52.6 | 0.18 | fBw | Fossil Cambisol |

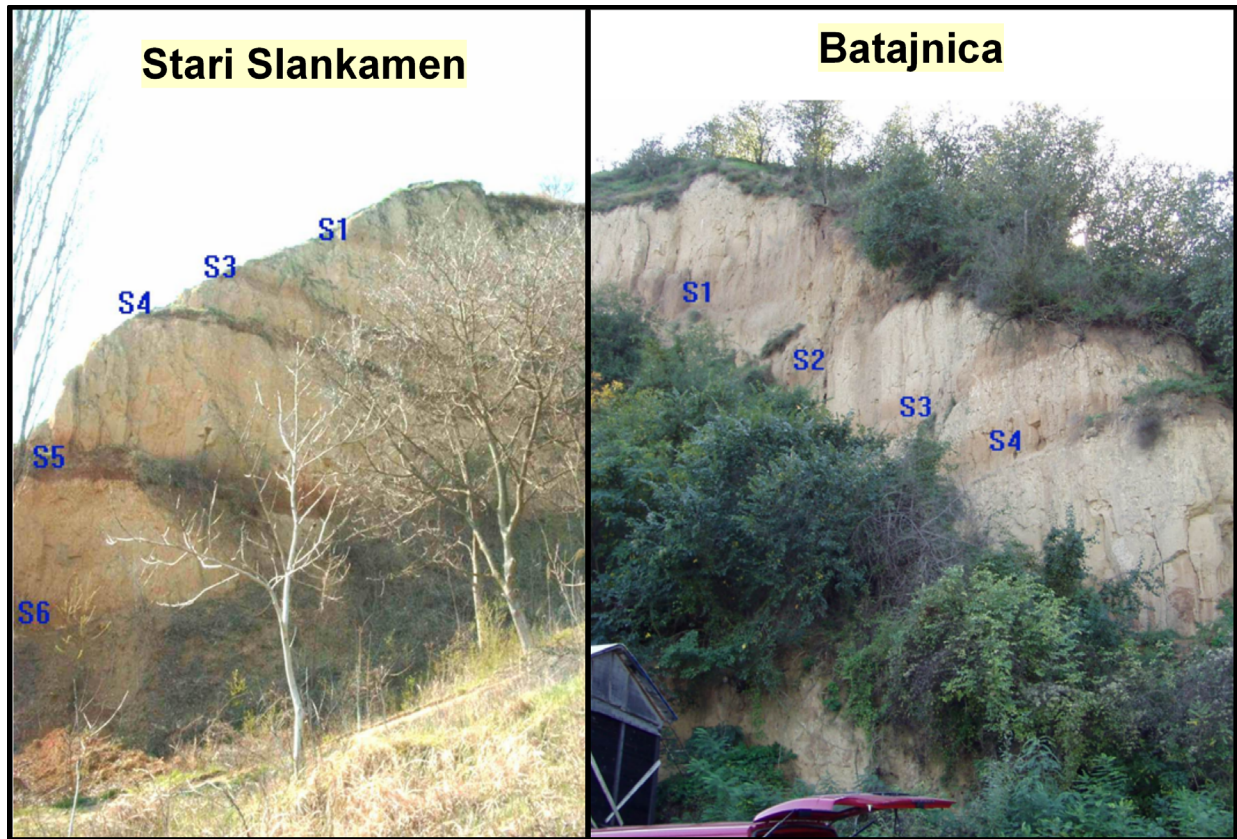


Fig. 4-S1. Picture of Stari Slankamen and Batajnica site (middle Danube Basin, Serbia). Pedostratigraphic units are denoted with S according to the S-L nomenclature for Chinese loess-paleosol sequences. The chronostratigraphic placement of the pedocomplexes is shown in Fig. 4-S3.

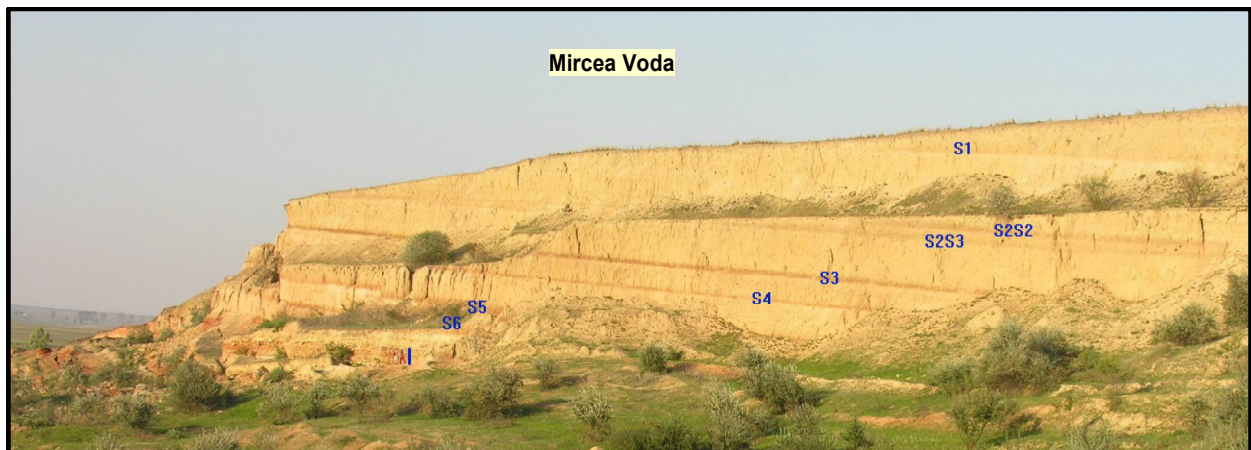


Fig. 4-S2. Picture of the Mircea Voda site (lower Danube Basin, Romania). The vertical blue line indicates the size of a man [~ 1.8 m] at the base of the profile. Pedostratigraphic units are denoted with S according to the S-L nomenclature for Chinese loess-paleosol sequences. The chronostratigraphic placement of the pedocomplexes is shown in Fig. 4-S4.

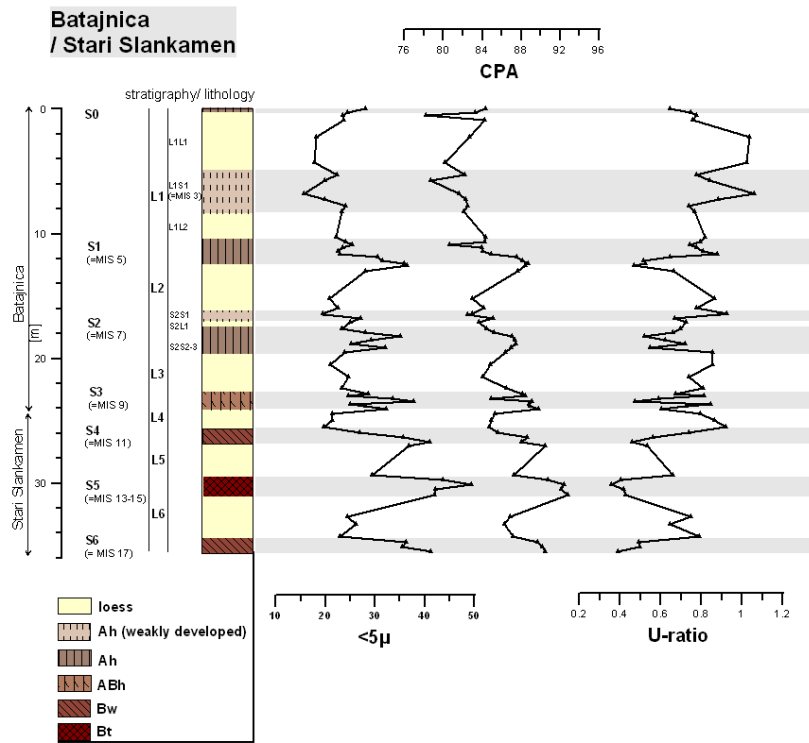


Fig. 4-S3. The $<5\ \mu\text{m}$, CPA and U-ratio record of the composite loess-paleosol sequence Batajnica/Stari Slankamen (middle Danube Basin, Serbia). The CPA record is taken from Buggle et al (S24). The chronostratigraphic placement of the pedocomplexes is based on the work of Buggle et al (S8).

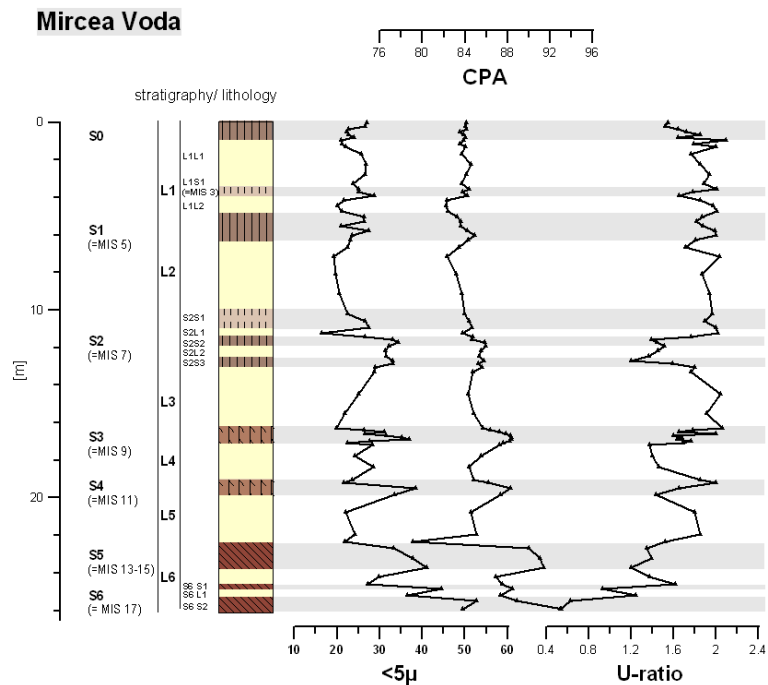


Fig. 4-S4. The $<5\ \mu\text{m}$, CPA and U-ratio record of the composite loess-paleosol sequence Mircea Voda (lower Danube Basin, Serbia). The CPA record is taken from Buggle et al., S24). The chronostratigraphic placement of the pedocomplexes is based on the work of Buggle et al (S8).

Study 5

Iron mineralogical proxies and Quaternary climate change in SE-European loess-paleosol sequences.

Björn Buggle^{1,2*}, Ulrich Hambach³, Karoly Müller², Ludwig Zöller², Slobodan B. Marković⁴
and Bruno Glaser¹

¹Soil Biogeochemistry, Martin-Luther-University Halle-Wittenberg, von-Seckendorff-Platz 3,
06120 Halle, Germany

²Soil Physics Department, University of Bayreuth, D-95440 Bayreuth, Germany.

³Chair of Geomorphology, University of Bayreuth, D-95440 Bayreuth, Germany

⁴Chair of Physical Geography, Faculty of Sciences, University of Novi Sad, Faculty of
Sciences, Trg Dositeja Obradovića 3, 21000 Novi Sad, Serbia.

unsubmitted

*

Corresponding author: Björn Buggle, Phone:+49(0)921-552174

E-mail: Bjoern.Buggle@uni-bayreuth.de

Abstract

The loess-paleosol sequences Batajnica/Stari Slankamen (Serbia) and Mircea Voda (Romania) represent archives for the climate and landscape development of the middle and lower Danube basin during the last 700.000 years. A multi-proxy approach relying on iron mineralogical parameters is applied to decipher Quaternary climate evolution in this region. For detecting changes in the iron mineralogical composition rock magnetic investigations, diffuse reflectance spectroscopy (drs) and Munsell color based proxies are employed. The results show that environmental conditions during mid and early Mid-Pleistocene interglacials were more favourable for hematite formation, suggesting a more oxidizing pedoclimate as in more recent interglacials. This is also reflected in a gradual increase of ARM/SIRM linked to a preferential hematization of coarse grained ferrimagnetica and relates to warmer climate conditions and a more extended estival dry period. At the same time, rock magnetic parameters indicate a preferential destruction of fine grained magnetic particles in older paleosols resulting from seasonal excess moisture. Hence, a straight-forward interpretation of the magnetic susceptibility record in terms of pedogenesis intensity or rainfall seems not appropriate at these profiles.

A progressive cooling and decrease of rainfall during the Mid- and Late Pleistocene is not only evidenced for interglacial pedocomplexes but also for glacial loess layers. This finding is in line with previously published proxy records of silicate weathering and clay formation at these sites and similar trends reported from mid-latitude Eurasia. Relating iron mineralogical proxies to paleopedological characteristics and proxies of silicate weathering, we could additionally reveal a change in the seasonal pattern of the temperature and precipitation regime from a Mediterranean type to a steppe type climate, highlighting the potential of such a multi-proxy approach.

Discussing potential triggers, the inferred trend of cooling, aridification and increasing continentality is best explained by Quaternary uplift of Eurasian mountain belts inducing changes in atmospheric circulation. Regarding the lower and middle Danube Basin, this trend possibly is regionally amplified by the uplift of the Alps and Carpathians (rain shadow effects), providing a driving mechanism for the westward extension of the Eurasian steppe belt into Central and SE-Europe.

Keywords: rock magnetism, diffuse reflectance spectroscopy, hematite, rubification, Pleistocene, loess

1 Introduction

Loess-paleosol sequences (LPSS) comprising several glacial-interglacial cycles are widely spread along the Danube River in Hungary, Serbia, Bulgaria and Romania. Their potential as paleoclimate archives has been proven in previous studies. Pattern of paleoenvironmental proxy records have been correlated across Eurasia to well established climate archives, the loess sites of Central Asia and China, as well as to marine records of the global ice volume (e.g. Jordanova and Petersen, 1999a; Panaiotu et al., 2001; Bronger, 2003; Marković et al., 2006; Jordanova et al., 2007, Buggle et al., 2009; Balescu et al., 2010). Besides the Pollen sequence from the Velay region (France) (Reille et al., 2000; de Beaulieu, 2001), as well as Ioannina and Thenagi Phillipon (Greece) (Tzedakis and Bennett, 1995; Tzedakis et al., 2006), quasi-continuous terrestrial records for the Late and Mid-Pleistocene climate in Europe can only be provided by these archives. Essentially the sites Batajnica and Stari Slankamen (middle Danube - i.e. Carpathian-, Pannonian Basin) and Mircea Voda (lower Danube Basin) have been regarded as key sections comprising at least 700.000 years of climate history (Buggle et al., 2009; Marković et al., 2009; Marković et al., submitted). Hitherto, paleoclimatic research on these sites focused on paleopedological proxies such as micromorphological indicators of soil development intensity, mineralogy of silicates, grain size parameters or geochemical based weathering indices (Kostic and Protic, 2000; Marković et al., 2008; Marković et al., 2009; Buggle et al., 2009; Buggle et al., submitted). These proxy records revealed a gradual decrease of silicate weathering intensity and pedogenic clay formation during the Mid- and Late Pleistocene going along with a change in paleosol typology from fossil (rubified) Luvisols and (rubified) Cambisols to fossil steppe soils. As reviewed in Buggle et al (submitted) similar trends can be traced in mid-latitudinal Eurasia from SE-Europe to the Chinese Loess Plateau, reflecting gradual changes in paleoclimatic

conditions. The observed patterns have been predominantly interpreted in terms of increasing aridification and/or cooling, possibly triggered by Quaternary uplift of Eurasian mountain ranges (Bugge et al., submitted). However, existing data still leave open for discussion whether it is a change in the absolute annual sum of precipitation and/or temperature or rather a change in the seasonal distribution of rainfall. Therefore, the (first) objective of the present study is to provide further evidences helping to elucidate this issue by means of iron mineralogical investigations.

On the one hand, the amount of iron oxides formed during pedogenesis on the one hand reflects soil formation intensity. Therefore, chemical as well as rock magnetic based iron mineralogical proxies such as the dithionite-soluble iron fraction (Fed) (e.g. Guo et al., 1996; Ding et al., 2001) or the bulk magnetic susceptibility (χ) and frequency-dependent susceptibility ($\chi_{fd\%}$) (e.g. Maher and Thompson, 1995; Evans and Heller, 2001; 2003; Avramov et al., 2005) are widely applied as proxies for pedogenesis intensity in loess-paleosol studies. On the other hand, formation and stability of different iron minerals and their grain size fractions depend on (soil-) environmental conditions such as soil water content, redox potential of soil water (Eh), pH, presence of organic ligands, soil temperature and seasonal variations of these parameters (Thompson and Oldfield, 1986; Cornell and Schwertmann, 2003; Orgiera and Compagnucci, 2006). Hence, the assemblage of pedogenic iron minerals can be a sensitive indicator also for changes in amount and seasonal distribution of precipitation. The presence of an intense warm-dry period, for example, promotes formation of hematite and can be reflected in soil color proxies of hematite (Bronger, 1976; Torrent et al., 1983; Kämpf and Schwertmann, 1983; Yaalon, 1997; Vidic et al., 2004). Goethite, in contrast, is the more stable iron species under cooler and wetter conditions or with high humus content such as in steppe soils (Cornell and Schwertmann, 2003). Yet, quantification of hematite and goethite using visually measured soil color proxies, X-ray

diffraction technique and Mössbauer spectrometry is either not very precise or time consuming (Torrent and Barrón, 1993; Post et al., 1993; Ji et al., 2002). Recently transfer functions have been developed allowing a fast and more precise determination of the hematite and goethite content and hematite vs. goethite ratio in loess and paleosols via diffuse reflectance spectroscopy measurements (Ji et al., 2002; Torrent et al., 2007). Furthermore, rock magnetic techniques are frequently applied to gain insight in the assemblage of iron oxides in soils and sediments (e.g. Jordanova and Petersen, 1999a, b; Panaiotu et al., 2001; Liu et al., 2007). They allow for example to identify gleyzation and reductive dissolution of fine grained magnetic oxides characterising periods of excess soil moisture (Thompson and Oldfield, 1986) or help to identify hematization of maghemite, indicative for dry periods with strongly oxidizing conditions (Torrent et al., 2006; 2007). Hence multi-proxy approaches involving rock magnetic and spectroscopic investigations are proposed to infer paleoclimatic information from iron mineralogy (Vidic et al., 2004; Torrent et al., 2007). Here, we apply for the first time such a multi-proxy approach on European loess-paleosol sequences.

Concerning the profiles Mircea Voda, Batajnica and Stari Slankamen, the only existing record relating to iron-mineralogy, is the bulk magnetic susceptibility record presented by Bugge et al. (2009) and Marković et al. (2009, submitted). These authors found an increase in interglacial peak magnetic susceptibility from the modern soil to Marine Isotope Stage (MIS) 9, reflecting enhanced formation of ferrimagnetica with higher intensity of pedogenesis. Bugge et al (2009) hypothesized that the decrease of χ in older paleosols results from dissolution of highly magnetic susceptible particles of superparamagnetic size (SP) ($\sim < 30 \mu\text{m}$) due to increasing excess of rainfall. The evaluation of this hypothesis via more comprehensive rock magnetic analyses is a further objective of the present study.

2 Material and methods

2.1 The sites and sampling

The regional settings of the sites have been described previously (Bugge et al., 2008, 2009). Briefly, the sections Batajnica (44° 55' 29'' N, 20° 19' 11'' E) and Stari Slankamen (45° 7' 58'' N, 20° 18' 44'' E) are situated at the Banks of the River Danube 15 and 45 km upstream of Belgrade in the Serbian part of the Pannonian Basin. The climate of this area can be characterized as Cfb type climate with a mean annual precipitation (MAP) of 683 mm and mean annual temperature (MAT) of 11.9 °C (station Belgrade). Rainfall maximum is in June (90 mm/month) and a second maximum occurs in December (58 mm/month) (Fig. 5-1). According to the definition of Walter (1974), there is a dry period of 1 month (August).

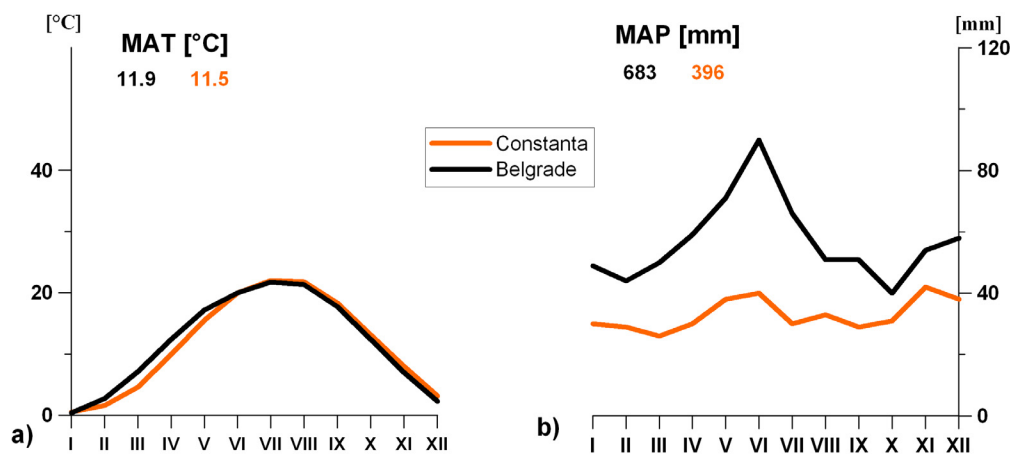


Fig. 5-1. Climatic data (WMO, 1996) of stations Belgrade (Serbia) and Constanta (Romania). a) temperature and b) precipitation.

The Mircea Voda site is located in the Dobrudja plateau about 13 km east of the Danube River in Romania (44° 19' 15'' N, 28° 11' 21'' E). With 11.5 °C MAT but only ~ 400 mm MAP (climate station Constanta) this area is considerably dryer than the Serbian locations (Fig. 5-1). Two rainfall maxima with about the same magnitude occur in June and in November (~40 mm/month). The climate is of Cfa type with a dry period from ~ May to

October and a period of drought from ~ July to September according to Walter's (1974) criteria.

Due to ground water influence at the older part (>MIS 9) of the Batajnica section and a major hiatus in younger part of the Stari Slankamen section, Bugge et al (2009) build a composite LPSS from the MIS 1 to MIS 9 sequence of Batajnica and MIS 10 to MIS 17 sequence of Stari Slankamen. In the following we refer to this composite sequence as "Batajnica/Stari Slankamen" LPSS. Both, the LPSS Batajnica/Stari Slankamen and Mircea Voda comprise more than six major loess-paleosol couples corresponding to glacial interglacial cycles. Paleopedological descriptions of these sites are available in Conea (1969), Bronger (1976), Bronger (2003), Marković et al., (2009) and Bugge et al. (submitted). The chronostratigraphy was established by Bugge et al., (2009) and Marković (2009) and confirmed by Timar et al., (2009), Balescu et al., (2010) and Schmidt et al (2010). The nomenclature of chronostratigraphic units follows the "S-L" system used in Chinese loess-paleosol sequences (see Bugge et al., 2009).

For the present study, we focus on the uppermost six major loess-paleosol couples corresponding to the last 17 MIS. Pedocomplexes were sampled continuously and at least three representative samples were taken from each intercalated loess unit. Details on sampling strategy are described in Bugge et al. (2008, 2009). Samples were stored in air tight plastic bags and dried at 40 °C in the laboratory.

2.2 Rock magnetic proxies: measurement and background

For rock magnetic measurements the dried material was filled into plastic boxes and subsequently compressed and fixed with cotton wool before closing the lid in order to prevent movement of sediment particles during the measurements. The sediment mass served as normalizer. The low field magnetic susceptibility was measured in an AC-field of 300 A/m at

875 Hz using the AGICO KLY-3-Spinner-Kappa-Bridge (AGICO, Brno, Czech Republic) and is given as mass specific susceptibility (χ). The data have been previously published by Buggle et al., (2009). χ reflects concentration of ferrimagnetic minerals and also grain size distribution. Pedogenetically formed fine-grained superparamagnetic (SP) ferrimagnetica (<0.03 μm) have a 2-3 times higher χ than single-domain, pseudosingle-domain (SD, PSD; \sim 0.03-10 μm) and multidomain ferrimagnetica (MD, $>\sim$ 10 μm) (Tang et al., 2003).

The frequency dependence of susceptibility ($\chi_{fd\%}$) is a measure for the relative contribution of SP-ferrimagnetica close to the SP-SD threshold and is generally applied as proxy for the exclusively pedogenetically formed ferrimagnetica (Banerjee, 1994; Liu et al., 2007). The $\chi_{fd\%}$ was determined with a MAGNON Susceptibility Bridge (MAGNON, Dassel, Germany) at AC-fields of 300 A/m at 0.3 and 3 kHz respectively ($\chi_{fd\%} = [\chi(0.3 \text{ kHz}) - \chi(3\text{kHz})] / \chi(0.3 \text{ kHz}) \times 100$ in %). With χ_{fd} we refer to the absolute difference of low to high frequency susceptibility values, reflecting the concentration of SP-ferrimagnetica.

Induced isothermal remanent magnetizations (IRMs) were determined after exposition of the samples to a pulsed field of 2000 and 350 mT (back field) respectively along one spatial axis. Magnetization was produced using a MAGNON PM II pulse magnetiser and measured via an AGICO JR6-spinner magnetometer. The IRM acquired in the 2 T field is regarded as saturation isothermal remanent magnetization (SIRM). As the SP-size fraction is defined by the absence of magnetic remanence under room temperature, IRMs are essentially controlled by the concentration of SD to MD-ferrimagnetica. Furthermore, IRMs depend on the mineralogical composition with ferrimagnetica (magnetite, maghemite) being more easily magnetized than antiferromagnetica (goethite, hematite) (Evans and Heller, 2001). Therefore, the S-ratio ($\text{IRM}_{0.35\text{T}}/\text{SIRM}$) is indicative for the relative abundance of ferrimagnetica to antiferromagnetica and a concentration-independent proxy (Maher 1986, Wang et al., 2006). A proxy for the absolute concentration of antiferromagnetica is the HIRM ($\text{HIRM} = 0.5 \times$

(IRM_{0.35T} +SIRM) (Geiss et al., 2004). As χ is essentially controlled by the concentration of SP-ferrimagnetica and SIRM decreases from the SD to MD fraction, the SIRM/ χ is sensitive for variations in grain size distribution of magnetic minerals, especially the ratio of SD fraction vs. SP fraction (Zhou et al. 1990). As χ_{fd} is a more specific measure for the concentration of SP-ferrimagnetica, we apply the SIRM/ χ_{fd} ratio.

Anhyseretic remanent magnetizations (ARMs) were induced with a 50 μ T static field and 100 mT alternating field (AF) amplitude using a Magnon AFD 300 demagnetiser. The ARM was produced along one spatial axis and remanent magnetization was measured via the AGICO JR6-spinner magnetometer. Similar as the SIRM, the ARM reflects the concentration of remanence carrying magnetic phases. However, the ARM decreases more strongly from the SD to the MD-fraction as the SIRM. Therefore, the ARM/SIRM ratio is a useful concentration-independent proxy for detecting changes in the ratio SD fraction vs. SD-MD fraction (van Velzen and Deckers, 1999; Evans and Heller, 2003). Moreover ARM/ χ and especially ARM/ χ_{fd} is sensitive to variations of the SD vs. SP fraction (Oldfield et al., 2009).

The coercivity of remanence (B_{cr}) gives the intensity of the backfield necessary to remove an acquired SIRM from a sample. Magnetic phases with high coercivity such as antiferromagnetica are regarded as magnetic “hard” and phases with low coercivity such as magnetite and maghemite are regarded as magnetic “soft”. Hence B_{cr} is related to magnetic mineralogy and can be regarded as a concentration-independent proxy for the antiferromagnetica to ferrimagnetica ratio (Evans and Heller, 2003, Wang et al., 2006). Since B_{cr} is highest for the particles of the SD-fraction, lower for the MD-fraction and decreases with increasing contribution of SP-particles, also changes in grain size distribution of magnetic phases can be detected via B_{cr} , if mineralogical composition is constant (Avramov et al., 2006). Furthermore, high B_{cr} values are typical for early stages of pedogenesis due to internal stress in partially maghemitized MD magnetite (van Velzen and Deckers, 1999; Deng

et al., 2006). The B_{cr} was determined by increasing stepwise acquisition of IRM reversely to a prior acquired IRM_{2T} . B_{cr} was then calculated by linear interpolation between the data points (acquired IRM/applied pulse field).

2.3 Soil color proxies

Colors were determined on soil clods in wet and dry conditions, using the Munsell color chart (Munsell, color company, 1975). As proxy for rubification i.e. soil reddening, indicative of hematite, we applied the Rubification Index (RI) proposed by Harden (1982) (see also Vidic et al., 2004) and the Redness Rating (RR) according to Torrent et al. (1980) and Torrent and Barrón (1993). The RI (Eq. 1) translates the increase in redness between a soil or paleosol and its parent material into a numerical value by comparing the changes in hue and chroma. For each increase in hue or chroma between the dry or wet colors of the soil and the parent material, the RI increases by ten points. Due to the uniform color of the „pure“ loess, we followed the approach of Marković et al (2009) and defined a common color value for the parent material i.e. the loess at each site. Thus, it was possible to obtain a continuous rubification record of each pedocomplex, even if the respective loess unit below is pedogenetically overprinted. In contrast to Harden (1982) we allowed also negative values of the RI.

$$RI = 10[(\text{hue } \Delta X_{\text{wet}}) + (\text{chroma } \Delta X_{\text{wet}}) + (\text{hue } \Delta X_{\text{dry}}) + (\text{chroma } \Delta X_{\text{dry}})] \quad (1)$$

with

ΔX_{wet} and ΔX_{dry} : difference in hue and chroma, respectively, between soil and parent material, for Munsell colors wet and dry, respectively.

$$RR = \frac{(10-H) * C}{V}$$

with

C: chroma

V: value

H: YR hue or the R hue minus 10, H= 10 for all Y hues

i.e. 10 for 10YR , 0 for 10 R, 10 for 2.5 Y

(2)

The RR (Eq. 2) was calculated as average from moist and dry Munsell colors. Both, the RI and the RR rely on the positive relation of chroma and the chroma to lightness (i.e. “Munsell value”) ratio, respectively, to the total iron oxide content, as well as the power of hue to discriminate between hematite and goethite (Hurst, 1977).

2.4 Diffuse reflectance spectroscopy, background, measurements and calculations

Up to now there exist essentially two different types of transfer functions for LPSS to assess hematite and goethite contents and hematite/goethite ratios from diffuse reflectance spectra. The approach of Ji et al. (2002) relies on a multiple linear regression analysis of brightness, the violet, blue, green, yellow, orange and red spectra and the hematite and goethite content of loess material. However, it has been recently criticized that the regression functions were derived from loess material spiked with synthetic iron minerals, having reflectance characteristics different from natural hematite (Torrent et al., 2007). Torrent et al (2007) showed that the regression functions of Ji et al. (2002) underestimates hematite concentrations. Hence in the present study, we apply the approach of Torrent et al. (2007), who quantifies goethite and hematite via the band intensity of characteristic absorption bands for these minerals i.e. ~ 425 nm (I425) and ~535 nm(I535). Regression functions between band intensity and the Hematite/(Hematite+Goethite) ratio (Hm/(Hm+Gt)), as determined via differential x-ray diffraction, were derived from 22 samples of Mediterranean Alfisols and

Inceptisols (regression function 1, Eq. 3) and from 83 loess-paleosol samples from the Chinese loess plateau (regression function 2, Eq. 4). Subsequently Torrent et al. (2007) calculated absolute hematite and goethite contents from the Hm/(Hm+Gt) ratio assuming that the dithionite-soluble Fe-fraction (Fe_d) essentially pertains to these two minerals. Results from both regression functions are very similar and Torrent et al (2007) finally adopted the average value. Due to the mentioned drawback of Ji et al.'s (2002) regression functions, we applied the Torrent et al (2007) approach.

$$Y = -0.133 + 2.871 \times X - 1.709 \times X^2 \quad (3)$$

$$Y = (22.2 \times 10^3 I_{535}) / [(8.56 \times 10^3 I_{425}) + (22.2 \times 10^3 I_{535})] \quad (4)$$

with

Y = Hematite/(Hematite+Goethite) ratio

X = $I_{535} / (I_{425} + I_{535})$

Diffuse reflectance spectra were recorded from 350 to 2500 nm using an AgriSpec spectrometer coupled with a Mug-Light A1221000 detector (ASDI Inc, Boulder, Colorado, USA). The sampling interval was 1.4 nm for the spectral region 350-1000 nm and 2 nm for the region >1000 nm. Reflectance intensity was measured relative to a white HALON (sintered polytetrafluorethylene) standard. The spectra were taken from dried, ground sample material to reduce effects of grain size variations on brightness. To quantify band intensities of hematite and goethite from reflectance spectra we followed the procedure given in Scheinost et al, (1998) and Torrent et al., (2007). First, for each sample, the reflectance function was transformed into a remission function applying the Kubelka-Munk theory. Subsequently, the second derivative of the remission function was calculated using a Savitzky-Golay smoothing. A moving window of 30 data points was adopted for the smoothing procedure, because this provided second-derivative spectra with well resolved

absorption bands and low background noise. As index for the band intensities we used the amplitude between the ~415 nm minimum and ~445 nm maximum for goethite and the ~535 nm minimum and ~680 nm maximum for hematite (Scheinost et al., 1998). Hm/(Hm+Gt) ratios were calculated using regression function 1 and 2. Due to similar results, we adopted the average value (Torrent et al., 2007). Only hematite to goethite ratios were calculated and no absolute contents, because the application of Fe_d to estimate the sum of both minerals, possibly leads to erroneous results. The Fe_d fraction is not well defined, depending on mineralogy as well as grain size of iron minerals and treatment temperature and time (van Oorschot and Dekkers, 1999; Varadachari, et al., 2006). Furthermore, Bronger (1976) questions the use of Fe_d as proxy for pedogenic iron minerals in paleosols using examples from the Stari Slankamen section. As Fe_d values do not correspond to weathering and soil formation intensity at this and other sites, postpedogenic alteration affecting the dithionite-solubility of iron oxides has been postulated (Bronger 1976).

3 Results/Discussion

3.1 Concentration related magnetic parameters

All parameters related to concentration of ferrimagnetic grain size fractions (χ_{fd} , ARM, SIRM) show an increase from loess to soil (Fig. 5-2). Hence pedogenic enhancement of low field susceptibility observed in these SE-European LPSS does reflect formation of SP and SD-ferrimagnetica. Besides that, systematic higher HIRMs in paleosols reveal pedogenic formation of antiferromagnetica such as hematite or goethite. The minimum susceptibility values of the loess units at both sites are very similar ($21-28 \cdot 10^{-8} \text{ m}^3/\text{kg}$), not regarding the L5 at Stari Slankamen, where the loess samples are pedogenetically overprinted from the overlying S4 pedocomplex (Bugge et al., 2009). Concentration of individual ferrimagnetic grain size fractions and of antiferromagnetic minerals, however, increases from younger to

older loess units. This trend is well expressed in the χ_{fd} , ARM, SIRM and HIRM record of the Batajnica/ Stari Slankamen section, but less clear in the Mircea Voda section. Such an increasing pedogenic formation of iron minerals is in line with a similar trend in intensity of silicate weathering and pedogenic clay formation, as given with the Chemical Proxy of Alteration (CPA) record and $<5\mu\text{m}$ grain size fraction record by Buggle et al (submitted; see Fig. 5-3). Comparing the maximum values of χ , χ_{fd} , ARM, SIRM and HIRM in each interglacial pedocomplex of the Mircea Voda site (Fig. 5-2), the S0, S1 and S2 acquired similar concentration of antiferromagnetica and ferrimagnetic grain size fractions during pedogenesis. The values in these (fossil) steppe soils (Buggle et al. submitted) are remarkable lower as in the S3, S4 and S5 (fossil forest steppe soils and fossil Cambisols). This is in line with paleopedological and geochemical proxies recording a higher soil development and weathering intensity of older pedocomplexes (Buggle et al., submitted, Fig. 5-3). However, χ decreases from the S3 to the S6. This contrasts the gradual increase of pedogenesis intensity from younger to older pedocomplexes (Buggle et 2009; Buggle et submitted). Our results reveal that the decrease of χ is related to a decline in the content of SP- (see χ_{fd}), SD (see ARM) and SD-MD-ferrimagnetica (see SIRM) from S3 to S6. Ferrimagnetic concentrations in the S6 appear to be as low or even lower as in the (fossil) steppe soils S0-S2. Moreover, a decline in the content of antiferromagnetica from S3 to S6 can be detected in the HIRM record.

In the Batajnica / Stari Slankamen section there is no distinct contrast between the S0, S1, S2 and the S3, S4, S5 (Fig. 5-2). The maximum low field susceptibility, along with the content of the individual ferrimagnetic grain size fractions, increases more gradually from S0 downwards to S3. A subsequent decline is less clear as in Mircea Voda due to high ferrimagnetica contents in S5 and remarkable low values in S4. The former can be related to intensified pedogenesis, since soil formation and weathering proxies also attain maximum

values in the S5 of the Batajnica/Stari Slankamen section (Buggle et al., 2009). The low ferrimagnetica contents of the S4 and also S6, however, contrast the paleopedological characteristics of these units.

Hence at both sections, the records of concentration dependent rock magnetic proxies, including also common proxies of pedogenesis as χ_{fd} , do not always correspond to soil formation intensity. Understanding the reasons behind, is crucial for a meaningful paleoenvironmental interpretation of rock magnetic parameters. Here we introduce a set of mechanisms, which could explain this discrepancy, and evaluate in the following chapters each process by the available datasets and proxies. Generally, the enrichment of ferrimagnetica in (fossil) soils reflects conditions controlling formation and transformation of magnetite and maghemite. In detail, possible explanations of the observed trends are 1) reduced microbial activity and hence reduced formation of ferrimagnetica via biological induced mineralization (extracellular) as well as biological organized mineralization (intracellular) (e.g. Maher, 1998; Evans and Heller, 2001), 2) moisture levels exceeding the optimum conditions for the formation and stability of ferrimagnetica (Buggle et al., 2009), 3) a reduced thermal induced formation of ferrimagnetica due to lower frequency of wild fire (e.g. Thompson and Oldfield, 1986), 4) hematization of maghemite in strongly oxidizing environment (Torrent et al., 2006; 2007), 5) changes in the detrital concentration of ferrimagnetica and 6) dilution of ferrimagnetica by higher carbonate contents (Heller and Liu, 1984). Hypothesis 6 is refused, since we could not find a significant correlation of χ_{fd} and carbonate content (presented in Buggle et al., 2010) for the Mircea Voda ($R^2 = 0.20$) and Batajnica/Stari Slankamen section ($R^2 = 0.41$).

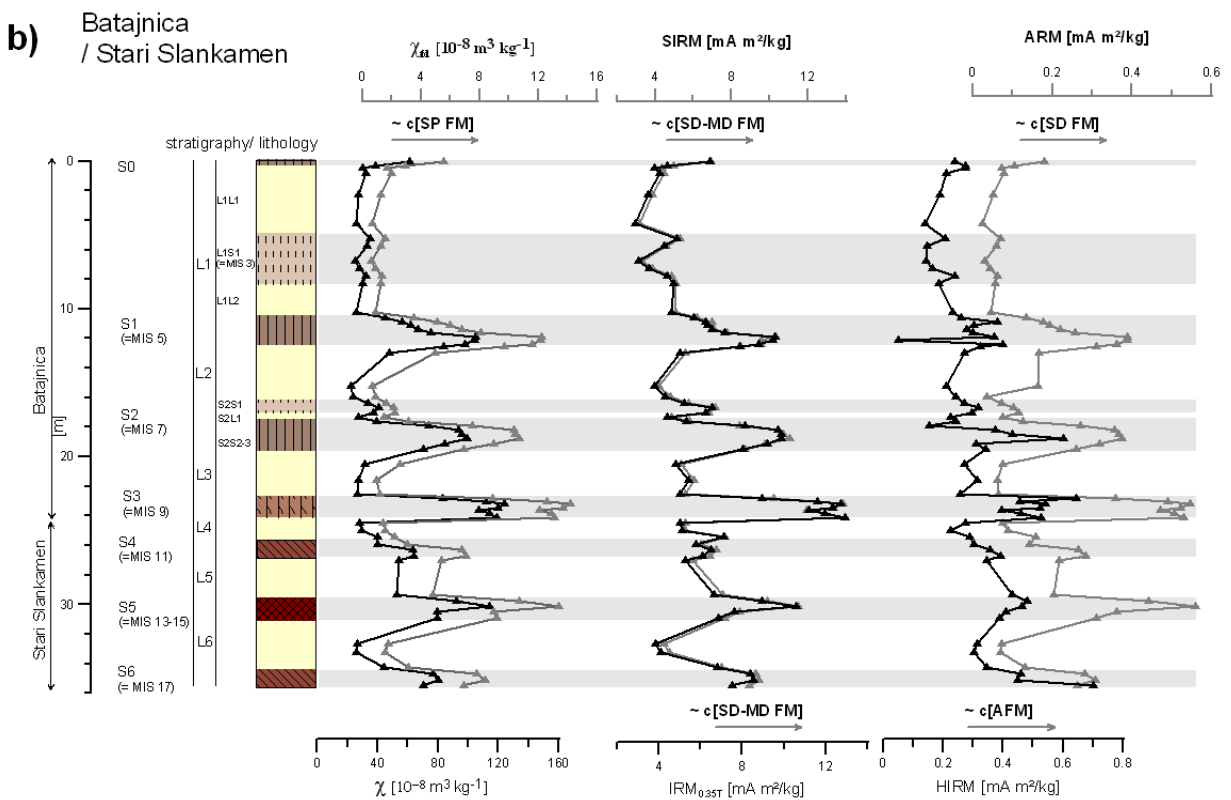
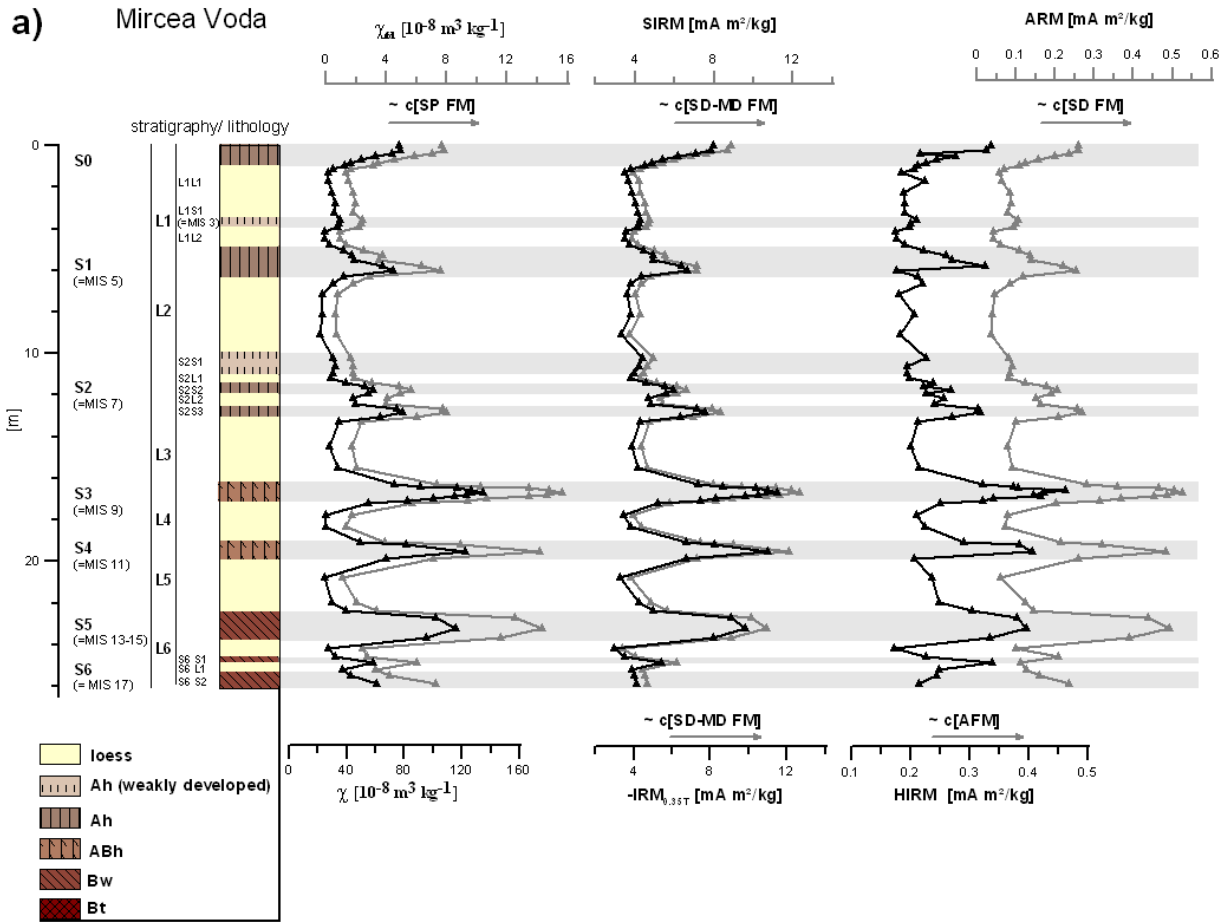


Fig. 5-2,a), b). Depth profiles of χ , χ_{fd} , ARM, $IRM_{0.35T}$, SIRM and HIRM for the Mircea Voda and Batajnica/Stari Slankamen section. The interpretation of these parameters is indicated at the abscises with c[SP FM] referring to the concentration of superparamagnetic ferrimagnetica, c[SD-MD FM] to the concentration of ferrimagnetica in the SD-MD range, c[SD FM] to the concentration of ferrimagnetica in the SD range and c[AFM] to the concentration of antiferromagnetica. The stratigraphy and lithology is given according to Bugge et al., (2009) and Bugge et al. (submitted). Note, that the absence of Ah horizon in units S3, S4, S5 and S6 does not imply erosion but that they could not be identified in the paleopedological investigation of Bugge et al. (submitted). Degradation of organic material rendered field identification of A horizons difficult and sampling resolution for micromorphological analysis was low (Bugge et al. submitted).

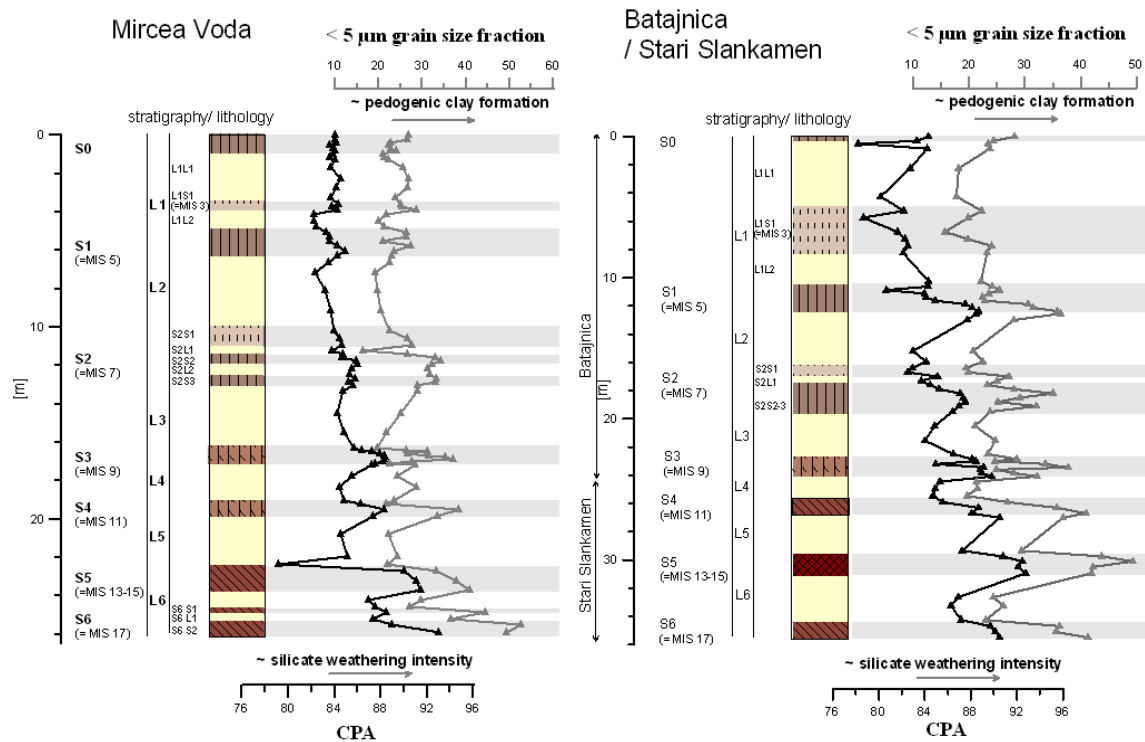


Fig. 5-3. Depth profiles of the $< 5 \mu\text{m}$ grain size fraction as proxy for pedogenic clay formation and of the chemical proxy of alteration (CPA) as proxy for silicate weathering. Data are redrawn from Bugge et al. (submitted).

In order to check for changes in the composition of the detrital ferrimagnetica (hypothesis 4), we use a $\chi_{fd} - \chi$ crossplot to determine background susceptibilities of the loess-paleosol units, since χ_{fd} is a measure for the pedogenetically formed SP-grain size fraction (e.g. Forster et al., 1994; Avramov et al., 2006). The results (Fig. 5-4) show that for both sites loess and paleosol samples plot on a straight line, therefore significant down-profile changes in parent material composition are excluded. The lower background susceptibilities of the Mircea Voda site ($\sim 16.9 \cdot 10^{-8} \text{ m}^3 \text{ kg}^{-1}$ vs. $\sim 19.0 \cdot 10^{-8} \text{ m}^3 \text{ kg}^{-1}$) are probably due to higher dilution by

diamagnetic quartz (Bugge et al., 2008). Parameters sensitive to mineralogy and grain size distribution of magnetic particles may shed light on the validity of the remaining hypotheses.

Besides χ , χ_{fd} , ARM, SIRM also the HIRM, conventionally regarded as proxy for antiferromagnetica, does not correspond to proxies of silicate weathering in some units especially the S3-S6 of Mircea and the S4 and S5 in Stari Slankamen.

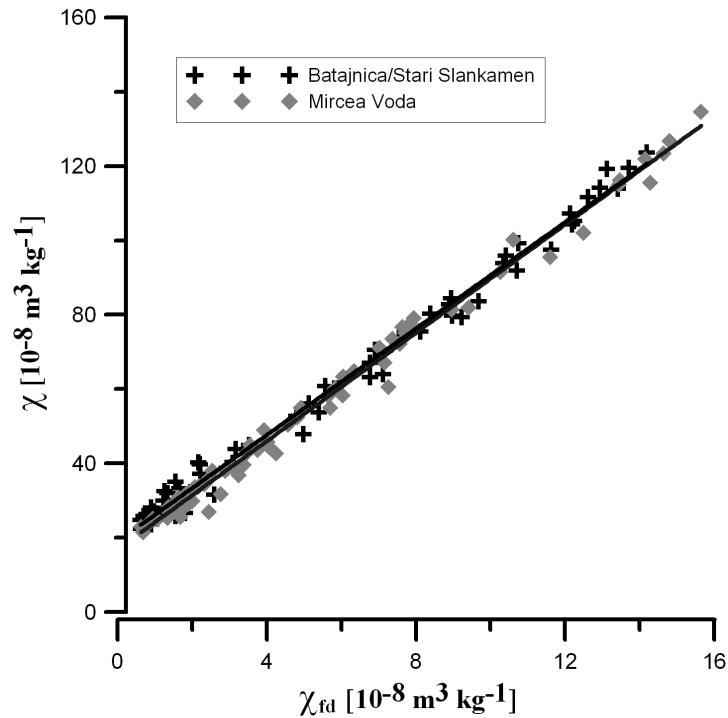


Fig. 5-4. $\chi_{fd} - \chi$ crossplot for loess and paleosol samples of the Mircea Voda and Batajnica/ Stari Slankamen LPSS. χ_{fd} and χ show a significant correlation with $R^2 > 0.99$ for both sections. The regression function for the Mircea Voda site is $Y = 7.3 \times X + 16.9$ and for the Batajnica/Stari Slankamen site $Y = 7.2 \times X + 19.0$. The intercept denotes the background susceptibility i.e. initial susceptibility of the parent material before pedogenesis.

Decreasing goethite and hematite content in units with high silicate weathering intensity appears curious from a paleopedological point of view, since weathering of iron-silicates represent a major source for pedogenic iron oxides (Cornell and Schwertmann, 2003). The discrepancy between the HIRM and the CPA could then indicate that rate of iron release from silicates is not a limiting factor on hematite and goethite formation, possibly due to the presence of a direct non-silicate precursor such as detritical ferrihydrite or magnetite and

maghemite (Cornell and Schwertmann, 2003; Torrent et al., 2006; 2007). Alternatively the validity of HIRM as hematite and goethite proxy might be questioned. Indeed, the decrease in paleosol HIRM from S3 to S6 at Mircea Voda and S4 of Stari Slankamen closely resembles the changes in parameters related to the concentration of ferrimagnetica. Hence, in the Mircea Voda and Batajnica/Stari Slankamen LPSS interaction of the magnetite and maghemite phase in partially oxidized magnetite likely contributes to the HIRM (Liu et al., 2002; Maher, 2004). With increasing thickness of the oxidized rim, internal stresses are reduced possibly explaining HIRM decrease in highly weathered paleosols (Liu et al., 2005). Additionally, the degree of Al-substitution can influence HIRM of antiferromagnetica (Liu and Roberts, 2007), which, however cannot be evaluated with the present dataset.

3.2 Magnetic grain size and mineralogy

Comparing loess and paleosol units, the $\chi_{fd}\%$, ARM/χ_{fd} , $SIRM/\chi_{fd}$ and $ARM/SIRM$ indicate a relative enrichment of SP over SD over MD particles during pedogenesis (Fig. 5-5). This prevalence of SP particles among the pedogenic ferrimagnetica suggests that magnetic enhancement in the paleosols is not primarily controlled by the abundance of magnetosome-forming bacteria, since these produce especially SD ferrimagnetica (Oldfield 2007). A more likely explanation is wild fire induced and pedogenic induced magnetic enhancement or a combination of both. This would result in the formation of SP and also SD ferrimagnetica (Thompson and Oldfield, 1986; Gedye et al., 2000; Evans and Heller, 2003). Lower B_{cr} in paleosols has been commonly observed in European and Chinese loess sections and related to the relative increase in pedogenic formed soft ferrimagnetic phases and the presence of partially oxidized magnetite in loess (Evans and Heller, 2003; Gendler et al., 2006, Wang et al., 2006).

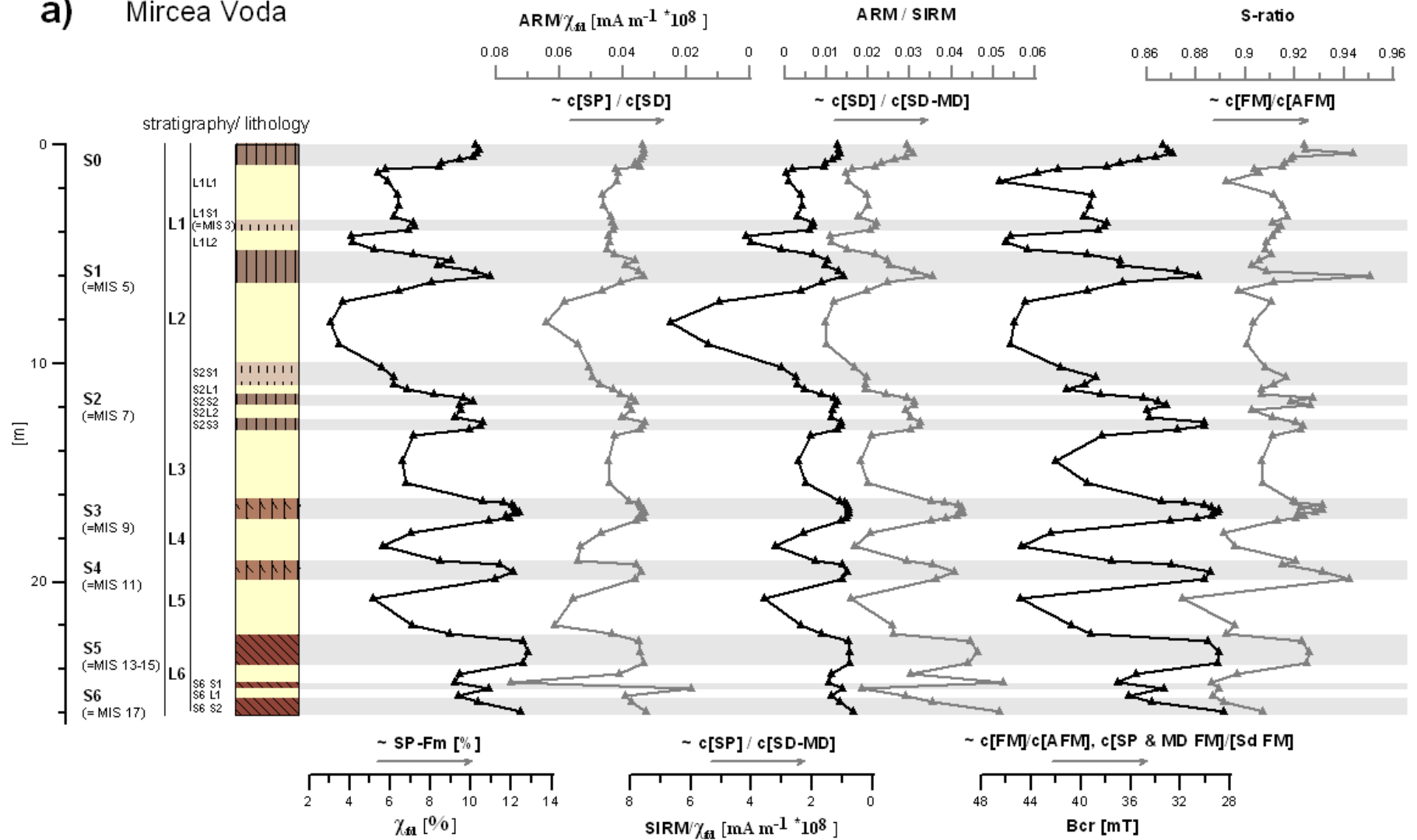
Regarding the loess units of the Mircea Voda section, the ferrimagnetic grain size distribution of the L1 and especially L2 is characterized by the lowest percentage of fine, superparamagnetic particles and highest fraction of coarse-grained MD-particles as indicated by minima in $\chi_{fd\%}$ and ARM/SIRM (Fig. 5-5). This is also true for the Batajnica/Stari Slankamen section (Fig. 5-5). Additionally, high ARM/ χ_{fd} values in the L2 loesses underline that contribution of the pedogenic derived SP-fraction is small in this unit. These findings suggests that climate in MIS 6 has been colder and/or dryer as during formation of the last glacial loess and especially the older loess units L3 to L6. At both sections, elevated $\chi_{fd\%}$ values of the L3 to L6 points to an increase in the SP-fraction. The interpretation in terms of higher moisture levels in older glacial stages would be in line with observed trends in CPA and the $<5 \mu\text{m}$ fraction (Fig. 5-3), from which Buggle et al (submitted) concluded gradual aridification and/or cooling of the glacial intervals over the Mid-Pleistocene. In Mircea Voda, corresponding changes in absolute content of the ferrimagnetic grain size fractions in loess are too subtle to be revealed by the depth profiles of χ_{fd} , SIRM and ARM, not so at the Batajnica/Stari Slankamen LPSS.

As to the paleosols, the relative contribution of SP particles ($\chi_{fd\%}$) in pedocomplexes S3-S6 of Mircea Voda is elevated compared to the (fossil) steppe soil S0-S2 (Fig. 5-5). On a first glance, this seems to correspond to a more intense silicate weathering and pedogenic clay formation, characterizing pedocomplexes S3 to S6 (Buggle et al submitted, Fig. 5-3), However, the increase in weathering and soil formation intensity towards S5 and S6 suggested by the $\chi_{fd\%}$ is less pronounced as one would expect from the CPA and $<5 \mu\text{m}$ record. The $\chi_{fd\%}$ vs. χ_{lf} crossplot (Fig. 5-6) reveals that the relative contribution of SP particles approaches saturation at $\chi_{fd\%}$ values around 12. Saturation of $\chi_{fd\%}$ at values between 10 and 12 is a commonly observed phenomenon in (fossil) soils (e.g. Jordanova and Petersen, 1999b; Liu et al., 2004, Jordanova et al., 2007), suggesting that changes in susceptibility are related

to the concentration of SD and SP particles rather than their relative proportion (Liu et al., 2007). As concentration of all magnetic grain size fractions decrease from the S3 to S6 in Mircea Voda (see Fig. 5-2), the slight increase in $\chi_{fd\%}$ appears to be related to a preferential enrichment of SP particles in course of ferrimagnetica destruction. Therefore hypotheses one and three are less likely. Additionally the steady increase in the ARM/SIRM ratio towards the older paleosols suggests an increase in the SD/MD ratio, which in the context of decreasing ferrimagnetic concentration refers to a preferential destruction of coarse MD-particles. Gallagher et al (1968) and Chen et al., (2005) found that stability of ferrimagnetica against oxidation into hematite increases with smaller grain size. Hence, hematization of ferrimagnetica likely explains the discrepancy between χ , ARM and SIRM and the weathering intensity of the S4-S6 at Mircea Voda. The S-ratio shows a decrease possibly reflecting a higher fraction of hematite in S5 and S6. High S values in S4 and low in S2 do not contradict enhanced hematization in S4 to S6, because the S parameter is not only sensitive for hematite but also for goethite. B_{cr} is also controlled by several iron phases and its decrease from younger to older paleosols follows the trends in $\chi_{fd\%}$. Hence it predominantly reflects changes in the relative content of superparamagnetica (Jordanova et al., 2007).

Regarding the pedocomplexes of the Batajnica/Stari Slankamen LPSS, $\chi_{fd\%}$ of the S1 and S2 is higher as in the respective units of the Mircea Voda section (Fig. 5-5). From the $\chi_{fd\%}$ vs. χ crossplot (Fig. 5-6) it is visible that already in these fossil steppe soils $\chi_{fd\%}$ is close to saturation, whereas at Mircea Voda only pedocomplexes S3 to S6 reach $\chi_{fd\%}$ saturation. This suggests a considerably higher humidity at the Serbian sites favouring the pedogenic production of SP-ferromagnetica during MIS 7 and MIS 9. In the older units, where $\chi_{fd\%}$ is close to saturation at both sites, the rainfall appears to be high enough in the lower Danube Basin so that SP formation is not moisture limited anymore.

a) Mircea Voda



b) Batajnica / Stari Slankamen

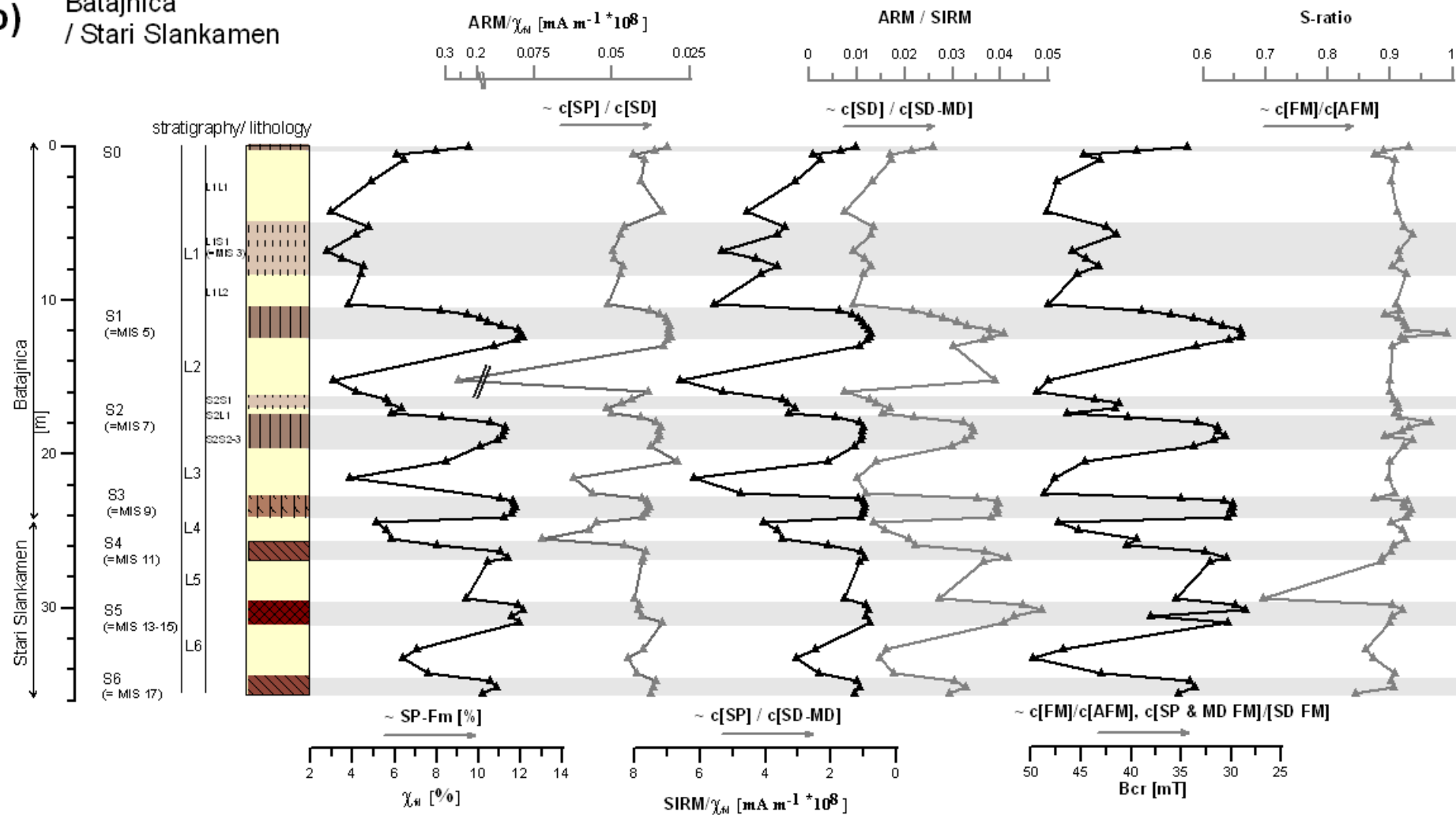


Fig. 5-5. Depth profiles of the concentration-independent magnetic proxies $\chi_{fd}\%$, ARM/χ_{fd} , $SIRM/\chi_{fd}$, $ARM/SIRM$, Bcr and S-ratio for a) the Mircea Voda and b) the Batajnica/ Stari Slankamen section.

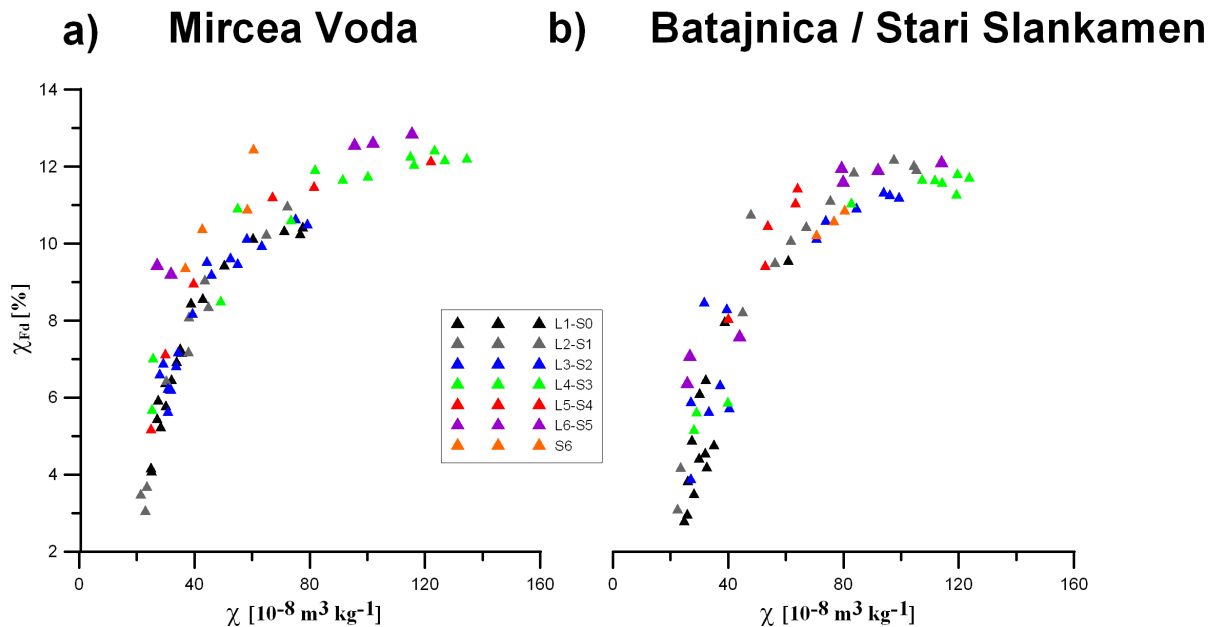


Fig. 5-6. $\chi_{fd}\%$ – χ crossplot for loess and paleosol samples of the a) Mircea Voda and b) Batajnica/ Stari Slankamen LPSS. $\chi_{fd}\%$ approaches saturation in paleosols at values around 12.

Having a closer look on the $\chi_{fd}\%$ depth profile of Batajnica/Stari Slankamen, a somewhat weak increase from the S0 to the S5, interrupted by high $\chi_{fd}\%$ values in the last interglacial pedocomplex S1, could be detected (Fig. 5-5). This change in grain size distribution is also reflected in a decreasing B_{cr} . Furthermore, the relative increase in the superparamagnetic fraction is accompanied by a trend in the ratio of SD over MD ferrimagnetica (see ARM/SIRM). These patterns are similar as in the Mircea Voda profile, so that we infer the same interpretation i.e. preferential removal of MD - ferrimagnetica due to hematization. Correspondingly also the S-ratio tend to decrease from younger to older paleosols, although lower values can be caused by higher goethite contents, too. Compared to Mircea Voda, trends in concentration-dependent and concentration independent parameters are not as clear developed (Fig. 5-5). We relate this to the climatic difference between the sites. Today and likely in past interglacials the Serbian site is characterized by higher annual rainfall values as Mircea Voda (Bugge et al., 2009; submitted). Hence, pedoclimatic threshold values for the

formation and stability of pedogenic ferrimagnetica might have been more easily surpassed in periods with enhanced rainfall. An indication for this is that χ , χ_{fd} and $\chi_{fd\%}$ of the strongly developed pedocomplexes S3 to S5 is lower in the Batajnica/Stari Slankamen LPSS as in the Mircea Voda LPSS (Fig. 5-2, Fig. 5-6), whereas it is the other way round in the fossil steppe soils S1 and S2. This does not contradict the postulated hematization of MD-ferrimagnetica. A pronounced seasonality of rainfall may provide both, strongly oxidizing and reducing conditions. The balance of both controls iron mineralogy directly as well as indirectly via frequency and intensity of fires. All this complicates paleoenvironmental interpretation of individual rock magnetic features at the Batajnica/Stari Slankamen section and additional (iron mineralogical) proxies are necessary to avoid speculative conclusions.

3.3 Diffuse reflectance spectroscopy and soil color proxies for hematite and goethite

The RI and the RR are widely applied Munsell-color based proxies for hematite content in soils and sediments (e.g. Vidic et al., 2004; Marković et al., 2009; Torrent and Barron, 1993). At the Batajnica/Stari Slankamen LPSS as well as at Mircea Voda, both indices reveal that the S5 and S6 offset from younger interglacial pedocomplexes by higher hematite content (Fig. 5-7). In Mircea Voda, hematite maximum is recorded in S6 and in Batajnica/Stari Slankamen in S6 according to the RI and in S5 according to the RR. The RI shows absence of rubification only in the L1, L2, L4 of Batajnica/Stari Slankamen and L2 of Mircea Voda. While there is no trend for the loess units, the RI gradually increases from younger to older paleosols at both sites. In contrast, the RR is zero in L6 and in all units above S5, indicating the absence of hematite in all loess and paleosol units of Mircea Voda and Batajnica/Stari Slankamen younger than MIS 13. The discrepancies between both proxies are related to the different concepts behind. The most essential differences are 1) that the RR relies not only on chroma but on the chroma/lightness ratio to estimate iron oxide content and 2) it is more conservative,

assuming the presence of hematite only if hue is 7.5 YR or redder. By definition hues of 10 YR or 2.5 Y as they prevail in the loess units and the younger pedocomplexes of the studied sites, will result in RR-values of zero. The RI, however, is not restricted to a certain hue range and may therefore be sensitive for already very small amounts of hematite, not sufficient to produce hues of 7.5 YR. But in the 2.5 Y and 10 YR range, changes in goethite content may strongly interfere (Schwertmann, 1993). Nevertheless, the RI appears to be sensitive to changes in lithology and soil development intensity (Fig. 5-7, and Marković et al., 2009).

As a sensitive and more accurate way to determine the presence of hematite we focus on the diffuse reflectance spectroscopy (drs). Accordingly, hematite can be identified in all interglacial paleosols, except in the Batajnica S0 (Fig. 5-7). This underlines that RR is a too conservative estimate of the hematite content. The drs-derived hematite / (hematite + goethite) ratio ($Hm/(Hm+Gt)$) furthermore points to the absence of hematite in most loess layers at both sections, revealing that RI values of 10 in the loess units of Mircea Voda are likely due to goethite and not due to hematite. As loess layers appear to be free of hematite, hematite in paleosols can be regarded to be of pedogenic origin. Therefore, the increase in $Hm/(Hm+Gt)$ from the S0 to the S6 in Mircea Voda and from the S0 to S5 at Batajnica/Stari Slankamen (Fig. 5-7) express a shift to hematite promoting soil forming conditions. Also a significant correlation between the $Hm/(Hm+Gt)$ ratio and ARM/SIRM, SIRM/ $\chi_{fd\%}$ and $\chi_{fd\%}$ is obtained (Fig. 5-8), showing a relative decrease of MD-ferrimagnetica and in turn a relative enrichment of fine grained SP-ferrimagnetica with increasing hematite to goethite proportion. These findings give further support for increasing hematization of ferrimagnetica in older paleosols. The absence of a relationship between ARM/ $\chi_{fd\%}$ and $Hm/(Hm+Gt)$ (Fig. 5-8) indicates that the proportion of SP vs. SD ferrimagnetica is not influenced by hematization, which is in line with the preferential oxidation of the MD-fraction to hematite.

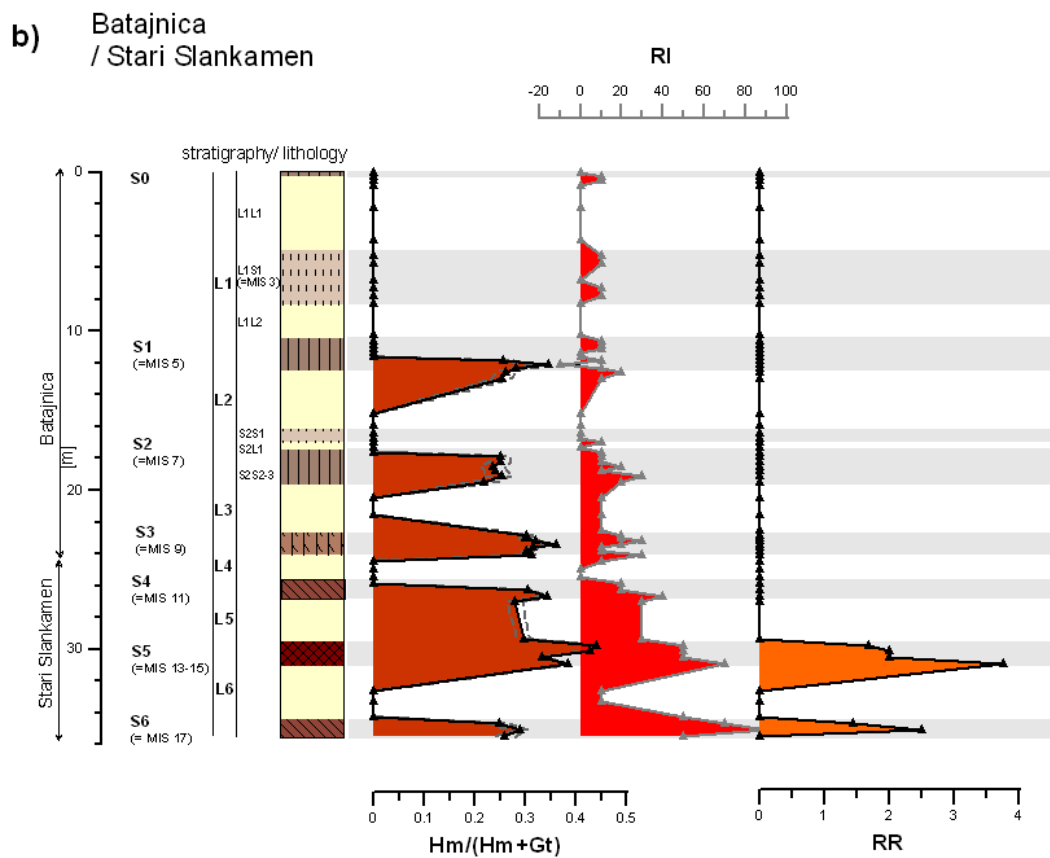
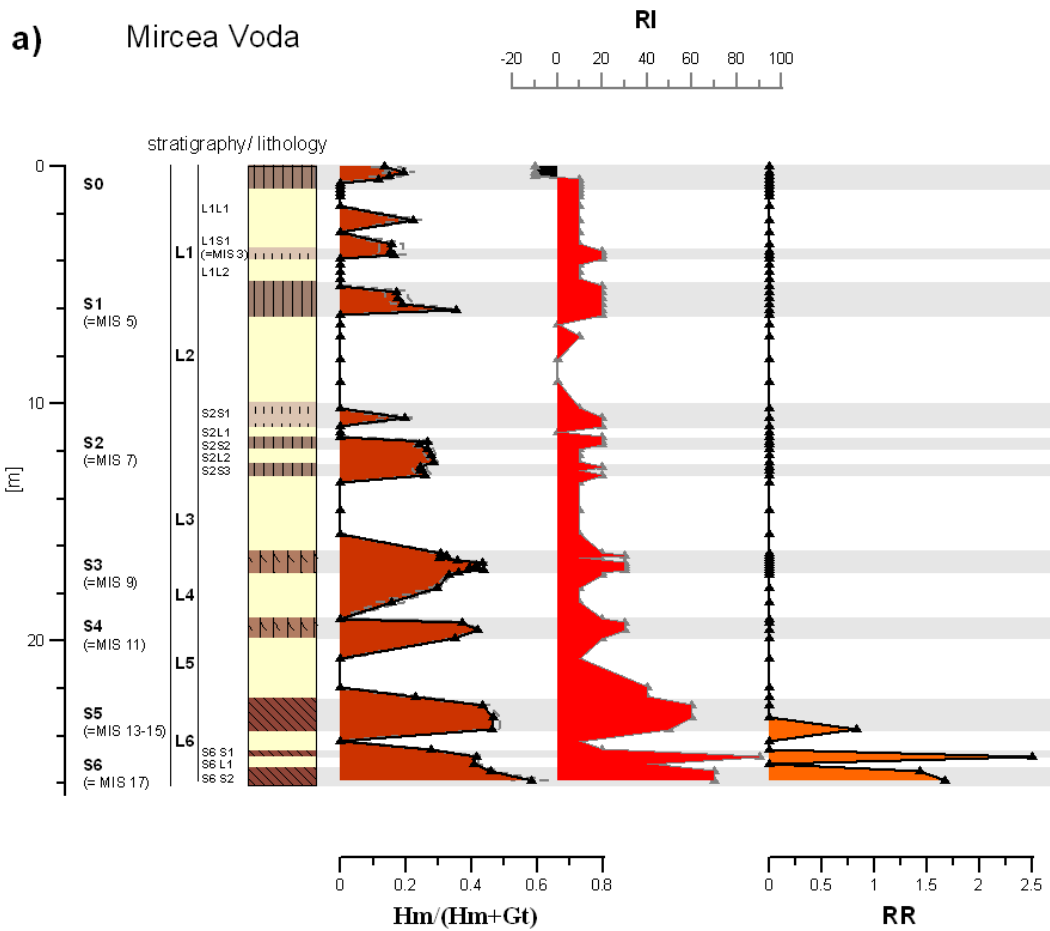


Fig. 5-7, a), b). Depth profiles of the RI (Rubification Index according to Harden 1982) and RR (Redness Rating according to Torrent et al 1980 and Torrent and Barron 1993) and the Hematite/(Hematite + Goethite) ratio (Hm/(Hm+Gt) for the profiles a) Mircea Voda and b) Batajnica/Stari Slankamen. RR and RI are proxies of rubification and soil reddening due to hematite, respectively, and calculated from Munsell colors. Note, negative RI values of the modern soil in Mircea Voda reflect soil darkening due to organic matter. The Hm/(Hm+Gt) was determined via diffuse reflectance spectroscopy following the Torrent et al (2007) approach. The grey dashed lines represent the results using calibration curves derived from Mediterranean soils and a loess-paleosol sequence (Torrent et al., 2007). Hm/(Hm+Gt) depth profiles obtained from both calibration curves are similar, underlining the robustness of the applied transfer functions. Following Torrent et al (2007), we focused on the mean values of both (solid black line) for further interpretation.

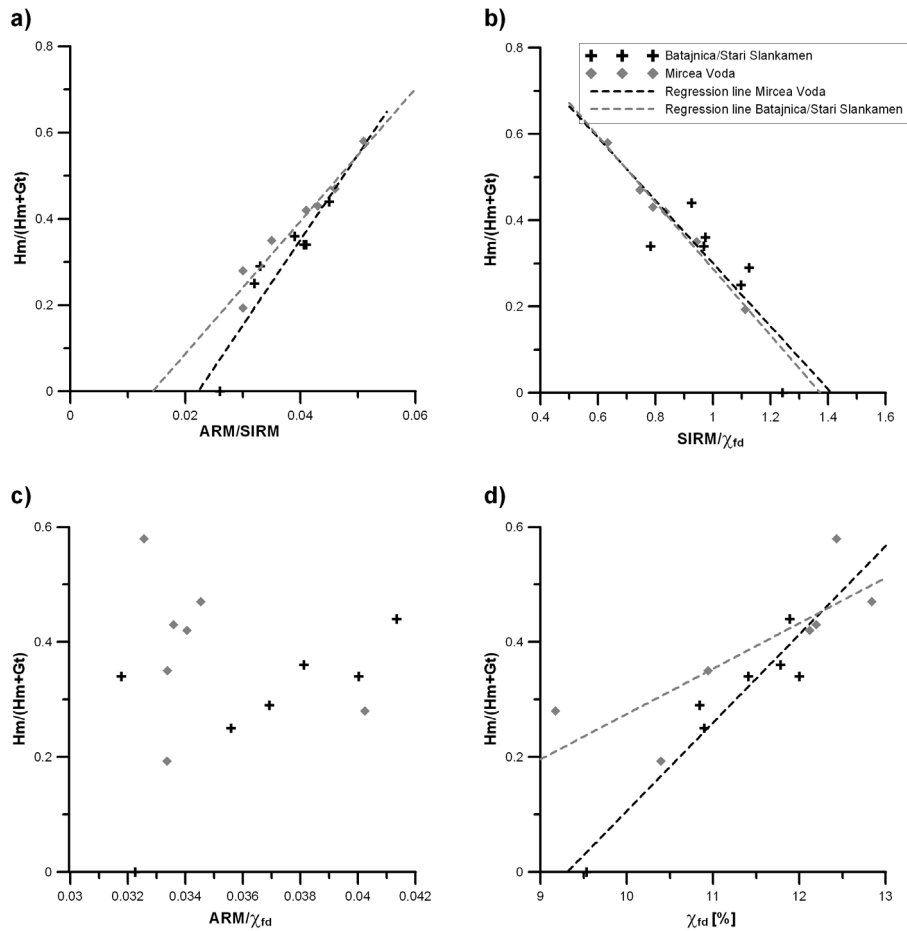


Fig. 5-8. Crossplot of the Hm/(Hm+Gt) ratio vs. rock magnetic proxies of the ferrimagnetic grain size distribution. Only samples with peak Hm/(Hm+Gt) values in interglacial pedocomplexes are shown i.e. peak value of S0, S1, S2 and so on. Significant correlation ($p < 0.05$) were obtained for a) the Hm/(Hm+Gt) vs. ARM/SIRM crossplot ($R^2 = 0.94$ and 0.86 , for Mircea Voda and Batajnica/Stari Slankamen), b) the Hm/(Hm+Gt) vs. SIRM/χ_{fd} crossplot ($R^2 = 0.99$ and 0.61), d) the Hm/(Hm+Gt) vs. χ_{fd} [%] crossplot ($R^2 = 0.67$ and 0.90 , for Mircea Voda and Batajnica/Stari Slankamen). No, significant relation was found between Hm/(Hm+Gt) and ARM/χ_{fd} at both sections.

Exceptions to the gradual increase in Hm/(Hm+Gt) ratios within the paleosols are the S1, showing relatively high hematite proportions at both sections, and the S6 of Stari Slankamen, showing relatively high proportions of goethite. These features are also consistent to changes in the ferrimagnetic grain size distribution, suggesting a more oxidative soil environment in the last interglacial at both sites and less oxidative conditions during MIS 17 at the Serbian site.

Finally it is to note that, from the identified correlations of ferrimagnetic grain size fractions to Hm/(Hm+Gt) (Fig. 5-8) we do not preclude hematite formation directly from ferrihydrite, in contrast to Torrent et al., (2006) and Hao et al., (2009). As ferrihydrite is a common precursor for hematite and goethite, the efficiency of this pathway essentially influences hematite – goethite proportions. Due to the relative low content of magnetite and maghemite in soils compared to hematite and goethite (Torrent et al., 2007), we conclude that hematization of ferrimagnetica should affect Hm/(Hm+Gt) ratios only to a minor degree. Hence, the good correlation of Hm/(Hm+Gt) to rock magnetic grain size proxies suggests that soil environments suitable for hematite production directly from ferrihydrite provide also conditions oxidizing enough to transform ferrimagnetica, especially of the MD-fraction, into hematite.

3.4 Proxies of iron mineralogy vs. silicate weathering – an integrative perspective on Quaternary climate change

The concentration and composition of iron minerals as revealed by various methods such as rock magnetism, soil color or spectroscopy have been established as valuable paleoclimate proxies in loess research (see Section 1). A different approach to assess paleoclimatic information from loess mineralogy or elemental composition is the use of proxies for silicate weathering or pedogenic neoformation of silicates. A review on silicate weathering proxies in

loess research is given in Buggle et al (2010). As iron mineralogy and silicate weathering react in a different way to climate change, it is promising to integrate both approaches to achieve a more comprehensive paleoclimatic interpretation.

The essential fundamentals for this integrated view are the following. Regarding the intensity of silicate weathering, in a seasonally dry climate regime as the steppe or the Mediterranean and subtropical type, especially intensity and duration of moisture supply over the year control weathering intensity. During dry periods the wet reactive surface of the minerals is restricted to hydrological inactive soil compartments and mineral weathering is reduced (White and Blum, 1995). Besides that weathering intensity depends also from temperature during hydrolytic active periods (i.e. seasonality of rainfall) (Brady and Carroll, 1994; White and Blum, 1995). While warm and wet conditions provide the best environment for intense silicate weathering, the formation of hematite is related to warm, but alternating wet (formation of ferrihydrite) and dry (transformation of ferrihydrite to hematite) pedoenvironment (Cornell and Schwertmann, 2003). Furthermore, low winter temperatures in addition to the estival dry period lead to the accumulation of organic material, high contents of which hamper hematite crystallization and favor goethite formation (Cornell and Schwertmann, 2003). Therefore, increasing hematite/goethite ratios can not only be indicative of higher summer temperatures and dryness but also of higher winter temperatures. As shown in the previous Sections rock magnetic parameters do not only allow tracing hematization and pedogenesis intensity, but also periods with excess moisture. Under these aspects, we, in the following, apply the rock magnetic and drs-data of Batajnica/Stari Slankamen and Mircea Voda as well as the silicate weathering records given in Buggle et al (submitted) to infer paleoclimatic changes between individual interglacials and also glacials in the lower and middle Danube Basin over the last 17 MIS. In detail, the paleoclimatic discussion focus on the <math><5\ \mu\text{m}</math> grain size fraction record as proxy of pedogenic clay formation (Buggle et al.,

submitted), the CPA record as proxy for silicate weathering intensity (Buggle et al., 2010, submitted), the Hm/(Hm+Gt) ratio as proxy for hematite vs. goethite promoting conditions, and rock magnetic parameters for the concentration and grain size distribution of ferrimagnetica (χ_{fd} , $\chi_{fd\%}$, ARM, ARM/ χ_{fd} , SIRM, SIRM/ χ_{fd} , ARM/SIRM), allowing to assess hematization and excess soil moisture. The following discussion is based on comparing the peak values of the individual proxies in each interglacial pedocomplex and glacial loess layer respectively (see Fig. 5-9).

3.4.1 Interglacial climate change

The modern soil S0 has been described as steppe soil at Mircea Voda as well as Batajnica. The CPA and $<5 \mu\text{m}$ fraction are slightly higher at the Serbian site, reflecting the more humid conditions, especially the higher amounts of rainfall in early summer (May to July, see Fig. 5-1). In turn, the differences in Hm/(Hm+Gt) ratio between the sites reflect the more pronounced dryness of the Mircea Voda site, promoting hematite formation. In line with more intense summer dryness ARM/SIRM and $\chi_{fd\%}$ are higher and SIRM/ χ_{fd} slightly lower at Batajnica indicating more oxidizing conditions resulting in hematization of especially MD-ferrimagnetica. Though today's precipitation is lower at the Romanian site, the modern soil of Mircea Voda shows higher concentration of ferrimagnetica (χ_{fd} , SIRM and ARM) as its Serbian counterpart. This peculiarity can be best explained by more frequent grassland fires in the relative dry Romanian feather-grass steppe environment promoting formation of SP and possibly also SD ferrimagnetica (Gedye et al., 2000). Hence, the set of proxy data is consistent with the modern climatic trends in the study area highlighting the potential of the approach to reveal past climate change.

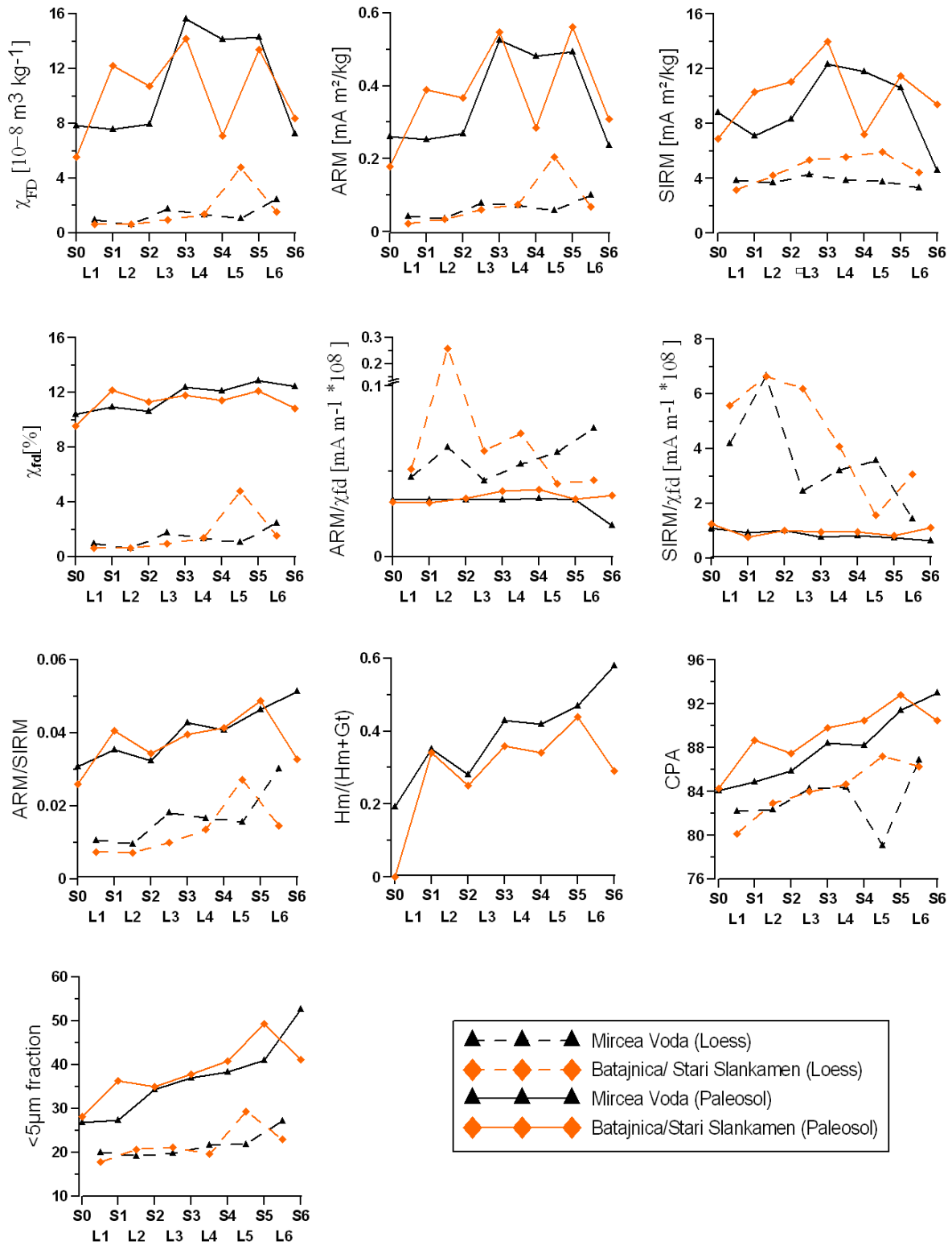


Fig. 5-9. Peak values for selected rock magnetic parameters (this study), the drs-derived Hm/(Hm+Gt) ratio (this study), the CPA (Buggle et al., submitted) and $<5 \mu\text{m}$ fraction (Buggle et al., submitted). For interglacial pedocomplexes the maximum value of each parameter is given and for glacial loess layers the minimum values.

From S0 to S1, increasing hematite to goethite ratios at both sites could indicate more pronounced summer dryness due to higher summer temperature, prolongation of the dry period and/or a decrease of summer precipitation. Also, the proxies of the ferrimagnetic grain size distribution support increasingly oxidizing conditions and hematization. As silicate weathering yields highest rates with rainfall in a warm pedoclimate, enhanced silicate weathering intensity do not support a decline of the early summer precipitation maxima. Also a warmer winter season, favourable for biological activity and decrease of organic matter content, unlikely triggered higher hematite to goethite ratios. The modern soils as well as the S1 and S2 have been identified as (fossil) steppe soils (Buggle et al., submitted), so that a significant change in the presence of organic ligands disturbing hematite crystallization appears not plausible. Moreover, due to mean temperatures of winter months around or slightly above zero, increasing cold season precipitation would not explain enhanced hydrolytic activity i.e. weathering. Concluding, higher summer temperatures eventually accompanied by more pronounced rainfall in spring-to early summer and/or autumn during the last interglacial gives the most reasonable explanation for observed changes in silicate weathering intensity and hematite –goethite proportion. Summer temperatures higher than during the Holocene and stronger seasonality of precipitation are consistent to higher summer sea surface temperature records of the North Atlantic and Mediterranean and climate modelling results for the Northern Hemisphere and have been related to the orbital configuration (Ruddiman et al., 1989; Harrison et al., 1995; Kandiano and Bauch, 2003; Matrat et al., 2007; Leduc et al., 2010). Compared to the Holocene, the Eemian climate optimum is characterized by large values of eccentricity. Furthermore, perihelion occurred during northern summer and tilt of the earth axis was high, resulting in large mid-June insolation values, especially in the Northern Hemisphere (Harrison et al., 1995, Berger et al., 2007, Yin and Berger, 2010). However, environmental implications are not uniform at both

sites, as indicated by the presented proxy data. The shift in CPA, <5 μm fraction and concentration dependent rock magnetic parameters is more pronounced at the Serbian site, suggesting a more intense increase in rainfall in this region. From the Hm/(Hm+Gt) ratio and hematization sensitive rock magnetic parameters (ARM/SIRM and $\chi_{fd\%}$) it appears that not only hydrolytic conditions but also oxidative conditions were more enhanced in the middle Danube Basin. This is tentatively interpreted in terms of more pronounced seasonality in the middle Danube Basin during S1 formation.

From S1 to S2, CPA, <5 μm fraction, χ_{fd} and ARM decrease again at the Batajnica site so that rainfall values during MIS 7 optimum probably have been intermediate between those of the Eemian and the Holocene optimum. In contrast at the Mircea Voda site, weathering and clay formation proxies points to higher non-cold season precipitation as during MIS 5e. Hm/(Hm+Gt), ARM/SIRM and $\chi_{fd\%}$ decrease at both sites, reflecting that summer temperatures or duration of summerly dry period is intermediate between the Holocene conditions and the Eemian. This is consistent to isotope data from the Spannagel Cave in the European Alps revealing cooler conditions and lower equilibrium line altitude of the Alpine glaciation as during the MIS 5e (Spötl et al., 2007). Furthermore, in the long Pollen records from the Massif Central, France, none of the three MIS 7 warm phases show vegetation succession comparable to full interglacial conditions (Reille et al., 2000). Additionally, pollen records from Ioannina, Greece, give evidence of relative cool conditions, which however have been mainly related to the winter season (Roucoux et al., 2008). Also summer sea surface temperatures in the North Atlantic (Ruddiman, 1989; Kandiano, 2003; Matrat et al., 2007), atmospheric CO_2 concentration (Lüthi et al. 2008) and global sea level stands (Antonioli et al., 2004) are lower than during the Holocene, showing that cooler conditions during MIS 7 are not only a regional phenomenon. This contrasts a direct forcing by Northern Hemispheric (NH) mid-June insolation. The insolation peak during MIS 7 was higher as during MIS 5 and

even the highest of the last 500 ka. (Berger et al., 2007). This implies that there is no simple relation between NH-summer insolation and summer temperatures and/or duration of summer dryness in SE-Europe. Finally, it also argues against the “insolation-driven” hypothesis, we presented for the MIS 5. Likely, there are feedback mechanisms, nonlinearities in the coupling of ice sheets – ocean - atmosphere and insolation or other types of forcing that strongly modulate the direct influence of summer insolation on summer temperature (Paillard, 2001). It is intriguing that the insolation maxima in MIS 7 is preceded by the lowest insolation minimum of the last 900 ka caused by low obliquity. Hence, due to a shift from one extreme insolation mode to the other, oceanic heat balance and ice sheet extension possibly did not reach steady state equilibrium to peak insolation before the onset of the next low insolation mode (Dutton et al., 2009). Notwithstanding the reasons for suppressed sea surface temperatures, the good correspondence of the SE-European hematization record to pattern in the North Atlantic sea surface temperature regarding the MIS 1, MIS 5 and MIS 7 peak values suggest a strong North Atlantic influence on SE-European summer temperatures.

From S2 to S3, the Hm/(Hm+Gt) ratio increase to values higher as in younger pedocomplexes. Also values of ARM/SIRM and $\chi_{fd}\%$ are consistent with more intense hematization as during MIS 7. This indicates relative warm summers and/or prolonged summer dryness during MIS 9. The paleopedologic characteristics of the S3 at Mircea Voda (Bugge et al., submitted) and Batajnica/Stari Slankamen (Bronger, 1976; Marković et al., 2009) still indicate steppe or forest-steppe environment and hence high organic matter contents during time of paleosol formation. Therefore, relieve of the organic matter constraints on hematite formation due to higher winter temperatures is less likely. In addition, CPA, $<5 \mu\text{m}$ and all concentration related ferrimagnetic grain size parameters show higher values as in S0, S1 and S2. Regarding increasingly oxidizing summer conditions favouring hematite formation, the strong increase in hydrolytic activity and magnetic enhancement

likely reflects more pronounced rainfall in spring to early summer and/or autumn but not during the high and late summer dry period. In contrast to the CPA and $<5 \mu\text{m}$ record, the enhancement of ARM and especially χ_{fd} from S2 to S3 is less pronounced in Batajnica compared to Mircea Voda. With respect to lower $\chi_{\text{fd}\%}$ and higher $\text{SIRM}/\chi_{\text{fd}}$ and $\text{ARM}/\chi_{\text{fd}}$, this apparently results from high seasonal moisture exceeding optimum conditions for the pedogenic formation and stability of fine magnetic particles. Hence, in line with the silicate weathering intensity, this indicates that that similar as today in MIS 9 the Serbian site experienced more rainfall as the Romanian one. Also in MIS 9, climatic characteristics in the middle and lower Danube Basin, as deduced from the presented rock magnetic, grain size and geochemical records, seem not to be directly related to summer insolation intensity. Peak insolation during MIS 9 was lower as in MIS 7 and MIS 5 (Berger et al., 2007). Also summer sea surface temperatures of the North Atlantic were not higher as during younger interglacials (Ruddiman et al., 1989; Kandiano and Bauch, 2003), suggesting that not only insolation but also sea surface hydrography fails to explain interglacial climate characteristics of the SE-European lowlands. Based on modelling results, Yin and Berger (2010) related higher Northern Hemispheric summer temperatures to the atmospheric CO_2 concentration. However, it is questionable if the relatively high CO_2 partial pressure in the atmosphere is a forcing for or rather a consequence of warmer interglacial conditions. Greenhouse gases presumably amplify astronomically induced climate change (Claussen, 2007; Sirocko, 2007). Nonetheless, this unlikely explains higher temperatures in MIS 9, because initial forcings such as summer insolation as well as duration of the interglacial are not outstanding compared to younger interglacials (Sirocko, 2007). Another potential trigger, the global ice volume, reflected in benthic $\delta\text{-}^{18}\text{O}$ records, attains a minimum for the last 700 ka (Shackleton et al. 1990). Although we cannot exclude atmospheric teleconnections, we doubt whether this signal is translated to mid-latitude Eurasia, if sea surface temperatures do not react. Hence, we

follow the interpretation of Buggle et al. (submitted). They reviewed a trend preserved in a variety of climate proxy records from mid-latitude Eurasia showing higher summer temperatures and more rainfall in MIS 9 and older interglacials compared to the Holocene and MIS 7. Buggle et al. (submitted) proposed that this trend is related to Quaternary uplift of Eurasian mountains. Specifically for the middle and lower Danube Basin, the relevance of Alpine and Carpathian mountain uplift has been highlighted by these authors.

From the S3 to S4, summer temperature and/or duration of the dry period stays essentially unchanged or slightly decreases, as inferred from only subtle decrease in hematite to goethite ratio and rock magnetic proxies sensitive for hematization. The silicate weathering and clay formation record suggests a further increase in rainfall in MIS 11. In contrast, concentration of ferrimagnetite decreases at both sites. The decrease of χ_{fd} , ARM and SIRM is pronounced at Batajnica/Stari Slankamen, but only slightly at Mircea Voda. Due to a slight shift in the relative contribution of SP-particles as indicated by $\chi_{fd\%}$, we relate this to excess moisture. Respective threshold values apparently have been more strongly surpassed in the more humid middle Danube Basin as in the lower Danube Basin. Excess moisture is most easily produced by intensification of rainfall under low temperature conditions i.e. implying low evaporation. This is consistent with only a slight increase of clay formation intensity. Concluding, while summer temperature appears to be on a similar level in MIS 9 and MIS 11, precipitation during the winter half year is higher in MIS 11. In a global context, MIS 11 is the interglacial with the lowest peak summer insolation intensity on the northern hemisphere during the last 700 ka (Berger and Loutre, 1991). However, it is the longest interglacial of this time period. This is also reflected in North Atlantic summer sea surface temperatures attaining maximum values for the Late and Mid-Pleistocene (Kandiano and Bauch, 2003; Matrat et al., 2007, Völker et al., 2010). Apparently summer temperatures in the lower and middle Danube Basin do not respond to high sea surface temperatures of the Nordic Seas, respectively. This is in

line with long-term European pollen records from Greece and the Portuguese margin, which also suggest that the higher summer temperature signal from the North Atlantic does not translate into higher continental summer temperatures during MIS 11. No increase in abundance of Mediterranean taxa and thermophilous tree pollen taxa compared to younger interglacials is recorded in these pollen sequences (Müller and Pross, 2007; Tzedakis et al., 2009). The increase in precipitation reconstructed for the middle and lower Danube Basin loess sections is, however, in line with the tectonic uplift of Eurasian mountain ranges forcing dryness and precipitation in this region as postulated by Bugge et al. (submitted).

From S4 to S5 the Hm/(Hm+Gt) ratio and the ARM/SIRM ratio increase at Mircea and Batajnica/Stari Slankamen. This could indicate a further increase in summer temperature and/or duration of summer dryness in MIS 13 and MIS 15. At both sites, no fossil horizon giving evidence of strong humus accumulation could be identified in the S5 and the paleopedological record as well as magnetic susceptibility pattern do not suggest erosional capping of the A horizon (Bugge et al., 2009; submitted). Furthermore, due to intensity of weathering, clay formation and clay translocation the S5 has been classified as fossil (chromic) Cambisol and Luvisol, respectively (Bronger, 1976; Bugge et al., submitted). In contrast to the fossil steppe soils, factors limiting decomposition of organic material must have been ineffective during MIS 13 and MIS 15. As our results showed that estival dry period became increasingly intense (i.e warmer and or longer) in older interglacials, it is only a rise of winter temperatures to values significantly above zero, which can explain changes in soil typology i.e. enhanced degradation of organic matter during mild winters. Higher winter temperatures could be also a reason for enhanced hematite production in S4 as organic matter hampers hematite formation. The CPA, the <5 µm fraction as well as the micromorphological investigations suggest seasonal increase of rainfall causing stronger weathering and onset of lessivation at the Serbian site. (Bugge et al., submitted). Furthermore, an increase in

pedogenic magnetic particles in S5 compared to the S4 is indicated by the χ_{fd} and ARM and especially pronounced in Serbia. Together with higher values of $\chi_{fd\%}$ and at Stari Slankamen also lower ARM/ χ_{fd} , this suggests a decrease of excess moisture. This is in line with higher temperatures inferred for the “rainy” winter half-year, resulting in seasonally reduced precipitation – evaporation difference (P-E). Concluding, our findings indicate Mediterranean like climate conditions in the lower and middle Danube Basin during MIS 13 and MIS 15. This agrees with soil genetic and rock magnetic studies of loess-paleosol sequences further east on the northern Black Sea Coast (S-Ukraine and Moldova), which proposed that the corresponding pedocomplex Pk4 as well as older paleosols developed under a Mediterranean type of climate (Tsatskin et al., 1998, 2001). As reviewed in Yin and Guo (2008) higher temperatures and more rainfall in MIS 13-15 compared to younger interglacials is a more general phenomenon in terrestrial records from mid-latitude Eurasia. The driving mechanism is still unclear. Insolation maxima are lower as during the last interglacial and the residual ice volume as indicated by benthic $\delta^{18}\text{O}$ records (e.g. Shackleton et al., 1990) is rather high for interglacial conditions. Commonly the outstanding climatic conditions during MIS 13 and MIS 15 are related to a strengthened northern hemispheric summer monsoon (see Guo et al., 1998; Yin and Guo, 2008). However, low atmospheric methane contents have been inferred against stronger monsoonal activity. Instead milder winter conditions caused by intensified Atlantic meridional overturning have been recently proposed (Ziegler et al., 2010). This theory is questioned by comparably low sea surface temperatures recorded in the North Atlantic (Ruddiman et al., 1989). Lower height of Eurasian mountain ranges, might be an alternative explanation for milder winter conditions and higher rainfall amounts in mid-latitude Eurasia (Buggle et al., submitted).

The S6 pedocomplex corresponds to MIS 17 and MIS 19 (Buggle et al., 2009). From the S5 to S6 the Hm/(Hm+Gt) and ARM/SIRM ratio show a pronounced decrease at the

Batajnica/Stari Slankamen site. As this indicates less suitable conditions for hematite formation and hematization of ferrimagnetica, respectively, it might point to lower temperatures and or more summer precipitation i.e. a less pronounced dry period in the middle Danube Basin. As at the same time weathering and clay formation proxies (CPA and $<5 \mu\text{m}$ fraction) decrease, higher amounts of summer rainfall can be excluded. A decrease of temperature, especially in the winter half year would additionally explain the more extensive destruction of pedogenic ferrimagnetica due to excess moisture (higher P-E), which is indicated by lower values of concentration dependent rock magnetic parameters and lower $\chi_{fd\%}$ and slightly higher ARM/χ_{fd} and $SIRM/\chi_{fd}$. Also at the Romanian site the dataset indicates higher values of excess moisture. However, in contrast to the Serbian site weathering, clay formation and hematite formation in the S6 of Mircea Voda is more intense as in the S5. Hence, there are no evidences for substantially lower temperatures during S6 formation in Romania. Instead during MIS 17, soil environmental conditions at Mircea Voda appear to be influenced by a more intense summer dry period promoting hematite formation but also more rainfall in the period autumn till early summer promoting weathering intensity. Hence, climate during formation of S6 was of more Mediterranean character in the lower Danube Basin, while in the middle Danube basin lower temperatures likely reduce intensity of weathering and hematite formation. In the pollen record of Thenagi Phillipon (Tzedakis et al., 2009) the abundance of temperate tree pollen is lower as during younger interglacials. This might indicate that relatively cool conditions, probably during the winter season, prevailed also in the Philippi Basin and surrounding mountains during MIS 17. Whether this is a overregional signal being related to the relative low peak in northern hemispheric winter insolation (Berger and Loutre, 1991) remains speculative, as continental records sensitive for the winter temperature in Eurasia are lacking for this marine isotope stage. Notwithstanding the trigger for cooler winter conditions in SE-Europe during MIS 17 an eventual winter

cooling in the lower Danube Basin was not strong enough to be recorded in the mineralogical, geochemical and paleopedologic characteristics of the corresponding pedocomplex at Mircea Voda. At the present state, however, factors and mechanisms responsible for these regional differences remain unclear.

3.4.2 Glacial climate change

As focus of the present study is the reconstruction of interglacial climate conditions and loess layers have been sampled only in lower resolution, we discuss in the following only general trends in the depth profiles and not individual loess layers. At both sites, concentration dependent rock magnetic parameters show a gradual increase towards older loess units. This trend is more pronounced at the Serbian site and likely indicates higher precipitation especially during summer time and or higher temperature. Buggle et al., (submitted) came to a similar conclusion based on corresponding trends in the weathering intensity. Whether the increase of $\chi_{fd}(\%)$ and ARM/SIRM is related to enhanced formation of SP and SD sized pedogenic ferrimagnetica or to a relative enrichment of these fractions due to preferential hematization of MD-ferrimagnetica cannot be decided from the available data. Though it was not possible to identify hematite in loess via diffuse reflectance spectroscopy, this may not necessarily preclude the surficial hematization of ferrimagnetica. We are not aware of any study evaluating the sensitivity of diffuse reflectance spectroscopy to detect hematite rims on maghemite. Nevertheless, accepting the hematization hypothesis, ARM/SIRM and $\chi_{fd}(\%)$ would suggest higher summer temperatures during the older interglacials. Concluding, stronger magnetic and weathering enhancement possibly refer to an increase in moisture eventually preceding a summer dry period i.e. indicating more rainfall in the early summer months. Also malacological investigations from the Late and Mid-Pleistocene loess layers at the Ruma section (Serbia) revealed more humid environmental conditions in the younger

glacials (Marković et al., 2006). Loess formation is essentially controlled by dryness (Pye, 1995). Pleistocene dust sedimentation rates from the lower Danube Basin give evidence of less intensive dust accumulation during older cold stages (Jordanova and Petersen, 1999a, Buggle et al., 2009). A cold stage climate characterized by cold and possibly dry winter conditions and a summerly dry period, which tends to be shorter but also warmer in the middle and early Mid-Pleistocene, would be in line with observed regional trends in loess sedimentation.

4 Conclusion

1. The combination of rock magnetism, hematite proxies and proxies of silicate weathering and pedogenic clay formation is a promising multi-proxy approach in loess-paleosol studies allowing to assess paleoclimatic conditions during periods of soil formation, even with respect to changes in seasonal patterns.
2. Munsell color based proxies for hematite such as the Rubification Index or the Redness Rating might lead to erroneous conclusions as to the presence of hematite in a loess matrix. Diffuse reflectance spectroscopy provides a valuable alternative.
3. The bulk magnetic susceptibility record of SE-European loess-paleosol profiles reflects a complex interplay of several processes and triggers such as pedogenic magnetic enhancement, fire-induced magnetic enhancement, preferential dissolution of fine-grained ferrimagnetic fractions during periods of excess moisture and preferential hematization of coarse grained ferrimagnetic fractions. With the intensity of the individual processes changing with paleoenvironmental conditions, a straight-forward interpretation of the magnetic susceptibility record in terms of pedogenesis intensity or rainfall seems not appropriate. Also the discrepancy between pedogenesis intensity and magnetic susceptibility values characterizing

pedocomplexes S4 and older appears to be related to both, a seasonal moisture excess and hematization during estival dry periods.

4. The good correlation of the diffuse reflectance spectroscopy derived Hm/(Hm+Gt) ratios and the ARM/SIRM in our data set confirms ARM/SIRM to reflect sensitively hematization of ferrimagnetica.

5. Based on the presented multi-proxy data set, we conclude that interglacial climate in the lower and middle Danube Basin considerably changed over the Pleistocene. A Mediterranean type climate with high summer temperatures and a pronounced estival dry period and mild and wet winters prevailed in interglacials of the early and middle Mid-Pleistocene. decreased In subsequent warm periods (winter-) temperatures as well as precipitation decreased resulting in higher continentality and a steppe type climate. Also regarding the cold stages our results suggest a progressive cooling and aridification trend over the Mid- and Late Pleistocene

6. For most interglacials the reconstructed climate in the lower and middle Danube Basin can not be explained by direct insolation forcing. Also when regarding hydrographic conditions of the North Atlantic and global ice volume it is not possible to entirely resolve the set of triggers forcing Quaternary climate trends in this region. Yet, Pleistocene cooling and aridification is not only found in the SE-European loess belt, but also in other climate archives of mid-latitudinal Eurasia. These climatic trends would be in line with the implications of progressive Eurasian mountain uplift, as proposed by Bugge et al (submitted). Especially Quaternary uplift of the Alps and Carpathians could be of relevance for the aridification trend in the middle and lower Danube Basin due to regional changes in atmospheric circulation and rain shadow effects (see Bugge et al., submitted). Hence, uplift of these mountain ranges appears to be a likely driving mechanism for the westward extension of the Eurasian steppe belt into Central and SE-Europe.

We have clearly to emphasize that this is a tentative explanation as the extend of Quaternary mountain rise is still under discussion. However, it appears warrantable to be addressed as at the present state no other triggers are evident, which could force such a gradual climatic trend over the Pleistocene. Following this idea, the climatic response to insolation forcing, oceanic circulation, atmospheric greenhouse gas concentration and (residual) ice volume appears to be superimposed on this long term trend of cooling, aridification and increasing continentality in the lower and middle Danube Basin. Hence, deviations such as the increase of precipitation and summer temperature from MIS 7 to MIS 5 can be explained.

7. Mineral weathering, transformation and neoformation may not only be controlled by climatic conditions, but also by the time available for soil forming processes (i.e. the duration of an interglacial period). Hence, further studies employing paleovegetation proxies such as pollen, phytoliths, biomarkers and carbon isotopes should be desired to validate and complement the paleoenvironmental picture of Quaternary climate evolution in the lower and middle Danube Basin drawn from paleopedology, element composition (weathering indices) and (iron) mineralogy.

Acknowledgements

We thank Tivadar Gaudenyi, Mladjen Jovanović and Irina Glaser for assistance during fieldwork. This study was financially supported by the German Research Foundation DFG (GL 327/8-2).

References

- Antonioli, F., Bard, E., Potter, E.-K., Silenzi, S., Improta, S., 2004. 215-ka history of sea-level oscillations from marine and continental layers in Argentarola Cave speleothems (Italy). *Global and Planetary Change* 43, 57-78.
- Avramov, V.I., Jordanova, D., Hoffmann, V., Roesler, W., 2006. The role of dust source area and pedogenesis in three loess-paleosol sections from North Bulgaria: A mineral magnetic study. *Studia Geophysica et Geodaetica* 50 (2), 259-282.
- Balescu, S., Lamothe, M., Panaiotu, C., Panaiotu, C., 2010. La Chronologie IRSL des sequences loessiques de l'est de la Roumanie. *Quaternaire* 21 (2), 115-126.
- Banerjee, S.K., 1994. Contributions of fine-particle magnetism to reading the global paleoclimate record. *Journal of Applied Physics* 75 (10). 5925-5930.
- Berger, A., Loutre, M.F., 1991. Insolation values for the climate of the last 10 million years. *Quaternary Science Reviews*, 10, 297-317.
- Berger, A., Loutre, M.F., Kasper, F., Lorenz, S.J., 2007. Insolation during Interglacial. In: Sirocko, F., Claussen, M., Sánchez Goni, M.F., Litt, T (Eds.), *The Climate of Past Interglacials. Development in Quaternary Science* 8, Elsevier, Amsterdam, pp 13-27.
- Brady, P.V., Carroll, S.A., 1994. Direct effects of CO₂ and temperature on silicate weathering: Possible implications for climate control. *Geochimica et Cosmochimica Acta* 58 (8), 1853-1856.
- Bronger A., 1976. Zur quartären Klima – und Landschaftsentwicklung des Karpatenbeckens auf paläopedologischer und bodengeographischer Grundlage. *Kieler Geographische Schriften* 45.
- Bronger A., 2003. Correlation of loess-paleosol sequences in East and Central Asia with SE Central Europe - Towards a continental Quaternary pedostratigraphy and paleoclimatic history. *Quaternary International* 106-107, 11-31.
- Buggle B., Glaser B., Zöller L., Hambach U., Marković S., Glaser I., Gerasimenko N., 2008. Geochemical characterization and origin of Southeastern and Eastern European loesses (Serbia, Romania, Ukraine). *Quaternary Science Reviews* 27, 1058-1075.
- Buggle B., Hambach U., Glaser B., Gerasimenko N., Marković, S.B, Glaser I., Zöller L., 2009. Stratigraphy and spatial and temporal paleoclimatic trends in East European loess paleosol sequences. *Quaternary International* 196, 86-106.
- Buggle, B., Glaser, B., Hambach, U., Gerasimenko, N., Marković, S., 2010. An evaluation of geochemical weathering indices in loess-paleosol studies. *Quaternary International* (in press). Doi. 10.1016/j.quaint.2010.07.019
- Buggle, B., Hambach, U., Kehl, M., Zöller, L. Marković, S.B., Glaser, B., 0.7 Million Years of progressive aridization recorded in SE-European loess sequences. (to be submitted)
- Chen, T., Xu, H., Xie, Q., Chen, J., Ji, J., Lu, H., 2005. Characteristics and genesis of maghemite in Chinese loess and paleosols: Mechanism for magnetic susceptibility enhancement in paleosols. *Earth and Planetary Science Letters* 240, 790-802.
- Claussen, M., 2007. Introduction to climate forcing and climate feedbacks. In: Sirocko, F., Claussen, M., Sánchez Goni, M.F., Litt, T (Eds.), *The Climate of Past Interglacials . Development in Quaternary Science* 8, Elsevier, Amsterdam, pp 3-13.
- Conea, A., 1969. Profils de Loess en Roumanie. *Supplément au Bulletin de l'Association française pour l'étude du Quaternaire*, 127-134.
- Cornell R.M., Schwertmann U. 2003. *The iron oxides*. Wiley-VCH, Weinheim.

- de Beaulieu, J.-L., Andrieu-Ponel, V., Reille, M., Gröger, E., Tzedakis, C., Svobodova, H., 2001. An attempt at correlation between the Velay pollen sequence and the Middle Pleistocene stratigraphy from central Europe. *Quaternary Science Reviews* 20, 1593-1602.
- Deng, C., Shaw, J., Liu, Q., Pan, Y., Zhu, R., 2006. Mineral magnetic variation of the Jingbian loess/paleosol sequence in the northern Loess Plateau of China: Implications for Quaternary development of Asian aridification and cooling. *Earth and Planetary Science Letters* 241, 248-259.
- Ding Z.L., Yang S.L., Sun, J.M., Liu T.S., 2001. Iron geochemistry of loess and red clay deposits in the Chinese Loess Plateau and implications for long-term Asian monsoon evolution in the last 7.0 Ma. *Earth and Planetary Science Letters* 185, 99-109.
- Dutton, A., Bard, E., Antonioli, F., Esat, T.M., Lambeck, K., McCulloch, M.T., 2009. Phasing and amplitude of sea-level and climate change during the penultimate interglacial. *Nature Geoscience* 2, 355-359.
- Evans, M.E., Heller, F., 2001. Magnetism of loess/palaeosol sequences: recent developments. *Earth-Science Reviews* 54, 129-144.
- Evans, M.E., Heller, F., 2003. *Environmental Magnetism – Principles and Applications of Enviromagnetics*. Academic Press, Amsterdam.
- Forster, T., Evans, M.E., Heller, F., 1994. The frequency dependence of low field susceptibility in loess sediments. *Geophysical Journal International* 118, 636-642.
- Gallagher, K.J., Feitknecht, W., Mannweiler, U., 1968. Mechanism of oxidation of magnetite to γ - Fe_2O_3 . *Nature* 217, 1118-1121.
- Gedye, S.J., Jones, R.T., Tinner, W., Ammann, B., Oldfield, F., 2000. The use of mineral magnetism in the reconstruction of fire history: a case study from Lago Origlio, Swiss Alps. *Palaeogeography, Palaeoclimatology, Palaeoecology* 164, 101-110.
- Geiss, C.E., Zanner, C.W., Banerjee, S.K., Joanna, M., 2004. Signature of magnetic enhancement in a loessic soil in Nebraska, United States of America. *Earth and Planetary Science Letters* 228, 355-367.
- Gendler, T.S., Heller, F., Tsatskin, A., Spassov, S., Du Pasquier, J., Faustov, S.S., 2006. Roxolany and Novaya Etuliya - key sections in the western Black Sea loess area: Magnetostratigraphy, rock magnetism, and paleopedology. *Quaternary International* 152-153, 89-104.
- Guo, Z., Liu, T., Guiot, J., Wu, N., Lü, H., Han, J., Liu, J., Gu, Z., 1996. High frequency pulses of East Asian monsoon climate in the last two glaciations: link with the North Atlantic. *Climate dynamics* 12, 701-709.
- Guo, Z., Liu, T., Fedoroff, N., Wei, L., Ding, Z., Wu, N., Lu, H., Jiang, W., An, Z., 1998. Climate extremes in Loess of China coupled with the strength of deep-water formation in the North Atlantic. *Global and Planetary Change* 18, 113-128.
- Hao, Q., Oldfield, F., Bloemendal, J., Torrent, J., Guo, Z., 2009. The record of changing hematite and goethite accumulation over the past 22 Myr on the Chinese Loess Plateau from magnetic measurements and diffuse reflectance spectroscopy. *Journal of Geophysical Research* 114, B12101.
- Harden J.W., 1982. A quantitative index of soil development from field descriptions: Examples from a chronosequence in central California. *Geoderma* 28, 1-28.
- Harrison, S.P., Kutzbach, J.E., Prentice, I.C., Behling, P.J., Sykes, M.T., 1995. The response of Northern Hemisphere extratropical climate and vegetation to orbitally induced changes in insolation during the Last Interglaciation. *Quaternary Research* 43, 174-184.
- Heller, F., Liu, T., 1984. Magnetism of Chinese loess deposits. *Geophysical Journal of the Royal astronomical Society* 77, 125-141.
- Hurst, V.J., 1977. Visual estimation of iron in saprolite. *Geological Society of America Bulletin* 88, 174-176.

- Ji, J., Balsam, W., Chen, J., Liu, L., 2002. Rapid and quantitative measurement of hematite and goethite in the Chinese loess-paleosol sequence by diffuse reflectance spectroscopy. *Clays and Clay Minerals* 50 (2), 208-216.
- Jordanova, D., Petersen, N., 1999a. Palaeoclimatic record from a loess-soil profile in northeastern Bulgaria – II. Correlation with global climatic events during the Pleistocene. *Geophysical Journal International* 138, 533-540.
- Jordanova, D., Petersen, N. 1999b. Palaeoclimatic record from a loess-soil profile in northeastern Bulgaria – I. Rock magnetic properties. *Geophysical Journal International* 138, 520-532.
- Jordanova, D., Hus, J., Geeraerts, R., 2007. Palaeoclimatic implications of the magnetic record from loess/paleosol sequence Viatovo (NE Bulgaria). *Geophysical Journal International* 171, 1036-1047.
- Kämpf, N., Schwertmann, U., 1983. Goethite and hematite in a climosequence in southern Brazil and their application in classification of kaolinitic soils. *Geoderma* 29, 27-39.
- Kandiano, E.S., Bauch, H., 2003. Surface ocean temperatures in the north-east Atlantic during the last 500 000 years: evidence from foraminiferal census data. *Terra Nova* 15, 265-271.
- Kostić N., Protić N., 2000. Pedology and mineralogy of loess profiles at Kapela-Batajnica and Stalać, Serbia. *Catena* 41, 217-227.
- Leduc, G., Schneider, R., Kim, J.-H., Lohmann, G., 2010. Holocene and Eemian sea surface temperature trends as revealed by alkenone and Mg/Ca paleothermometry. *Quaternary Science Reviews* 29, 989-1004.
- Liu, Q., Roberts, A.P., 2007. What do the HIRM and S-ratio really measure in environmental magnetism. *Geochemistry, Geophysics, Geosystems* 8 (9), Q09011.
- Liu, Q., Banerjee, S.K., Jackson, M.J., Zhu, R., Pan, Y., 2002. A new method in mineral magnetism for the separation of weak antiferromagnetic signal from a strong ferrimagnetic background. *Geophysical Research Letters* 29 (12), 1-4.
- Liu, Q., Jackson, M.J., Yu, Y., Chen, F., Deng, C., Zhu, R., 2004. Grain size distribution of pedogenic magnetic particles in Chinese loess/paleosols. *Geophysical Research Letters* 31, L22603.
- Liu, Q., Banerjee, S.K., Jackson, M.J., Deng, C., Pan, Y., Zhu, R., 2005. Inter-profile correlation of the Chinese loess/paleosol sequence during Marine Oxygen Isotope Stage 5 and indications of pedogenesis. *Quaternary Science Reviews* 24, 195-210.
- Liu, Q., Deng, C., Torrent, J., Zhu, R., 2007. Review of recent developments in mineral magnetism of the Chinese loess. *Quaternary Science Reviews* 26, 368-385.
- Lüthi, D., Le Floch, M., Bereiter, B., Blunier, T., Barnola, J.-M., Siegenthaler, U., Raynaud, D., Jouzel, J., Fischer, H., Kawamura, K., Stocker, T.F., 2008. High-resolution carbon dioxide concentration record 650,000-800,000 years before present. *Nature* 453, 379-382.
- Maher, B.A., 1986. Characterisation of soils by mineral magnetic measurements. *Physics of the Earth and Planetary Interiors* 42, 76-92.
- Maher, B.A., 1998. Magnetic properties of modern soils and Quaternary loessic paleosols: paleoclimatic implications. *Palaeogeography, Palaeoclimatology, Palaeoecology* 137, 25-54.
- Maher, B.A., Thompson, R., 1995. Paleorainfall reconstructions from pedogenic magnetic susceptibility variations in the Chinese loess and paleosols. *Quaternary Research* 44, 383-391.
- Maher, B.A., Karloukovski, V.V., Mutch, T.J., 2004. High-field remanence properties of synthetic and natural submicrometre haematites and goethites: significance for environmental contexts. *Earth and Planetary Science Letters* 226, 491-505.
- Marković, S.B., Oches, E., Sümegi, P., Jovanović, M., Gaudenyi, T., 2006. An introduction to the Middle and Upper Pleistocene loess-paleosol sequence at Ruma brickyard, Vojvodina, Serbia. *Quaternary International* 149, 80-86.

- Marković S.B., Bokhorst M.P., Vandenberghe J., McCoy W.D., Oches E.A., Hambach U., Gaudenyi T., Jovanović M., Zöller L., Stevens T., Machalet B., 2008. Late Pleistocene loess-paleosol sequences in the Vojvodina region, north Serbia. *Journal of Quaternary Science* 23, 73-84.
- Marković S.B., Hambach U., Catto N., Jovanović M., Buggle B., Machalet B., Zöller L., Glaser B., Frechen M., 2009. Middle and Late Pleistocene loess sequences at Batajnica, Vojvodina, Serbia. *Quaternary International* 198, 255-266.
- Marković, S.B., Hambach, U., Stevens, T., Kukla, G.J., Heller, F., McCoy, W.D., Oches, E.A., Buggle, B., Machalet, B., Zöller, L. The last million years recorded at the Stari Slankamen loess paleosol sequence: revised chronostratigraphy and longterm environmental trends. (submitted to *Quaternary Science Reviews*)
- Matrat, B., Grimault, J.O., Shackleton, N.J., de Abreu, L., Hutterli, M.A., Stocker, T.F., 2007. Four climate cycles of recurring deep and surface water destabilizations on the Iberian Margin. *Science* 317, 502-507.
- Müller, U.C., Pross, J., 2007. Lesson from the past: present insolation minimum holds potential for glacial inception. *Quaternary Science Reviews* 26, 3025-3029.
- Munsell Color Company, 1975. Munsell color charts. Baltimore, MD.
- Oldfield, F., 2007. Sources of fine-grained magnetic minerals in sediments: a problem revisited. *The Holocene* 17, 1265-1271.
- Orgeira, M.J., Compagnucci, R.H., 2006. Correlation between paleosol-soil magnetic signal and climate. *Earth Planets Space* 58, 1373-1380.
- Oldfield, F., Hao, Q., Bloemendal, J., Gibbs-Eggar, Z., Patil, S., Guo, Z., 2009. Links between bulk sediment particle size and magnetic grain-size: general observations and implications for Chinese loess studies. *Sedimentology* 56, 2091-2106.
- Paillard, D., 2001. Glacial cycles: Toward a new paradigm. *Reviews of Geophysics* 39 (3), 325-346.
- Panaiotu, C. G., Panaiotu, E. C., Grama, A., Necula, C., 2001. Paleoclimatic record from a loess-paleosol profile in Southeastern Romania. *Physics and Chemistry of the Earth (A)* 26, 893-898.
- Post, D.F., Bryant, R.B., Batchily, A.K., Huete, A.R., Levine, S.J., Mays, M.D., Escadafal, R., 1993. Correlations between field and laboratory measurements of soil color. In: Bigham, J.M., Ciolkosz, E.J., Luxmoore, R.J., (Eds.). *Soil Color*. SSSA Special Publications 31, 35-49.
- Pye, K., (1995) The nature, origin and accumulation of loess. *Quaternary Science Reviews* 14, 653-667.
- Reille, M., de Beaulieu, J.-L., Svobodova, H., Andrieu-Ponel, V., Goeury, C., 2000. Pollen analytical biostratigraphy of the last five climatic cycles from a long continental sequence from the Velay region (Massif Central, France). *Journal of Quaternary Science* 15 (7), 665-685.
- Roucoux, K.H., Tzedakis, P.C., Frogley, M.R., Lawson, I.T., Preece, R.C., 2008. Vegetation history of the marine isotope stage 7 interglacial complex at Ioannina, NW Greece. *Quaternary Science Reviews* 27, 1378-1395.
- Ruddiman, W.F., Raymo, M.E., Martinson, D.G., Clement, B.M., Backman, J. 1989. Pleistocene evolution: Northern Hemisphere ice sheets and North Atlantic Ocean. *Paleoceanography* 4 (4), 353-412.
- Scheinost, A.C., Chavernas, A., Barrón, V., Torrent, J., 1998. Use and limitations of second-derivative diffuse reflectance spectroscopy in the visible to near-infrared range to identify and quantify Fe oxide minerals in soils. *Clays and Clay Minerals* 46 (5), 528-536.

- Schmidt, E.D., Machalet, B., Marković, S.B., Tsukamoto, S., Frechen, M., 2010. Luminescence chronology of the upper part of the Stari Slankamen loess sequence (Vojvodina, Serbia). *Quaternary Geochronology* 5 (2-3), 137-142.
- Schwertmann, U., Murad, E., Schulze, D.G., 1982. Is there Holocene reddening (hematite formation) in soils of axeric temperate areas. *Geoderma* 27, 209-223.
- Schwertmann U., 1993. Relations between iron oxides, soil color, and soil formation. In: Bigham, J.M., Ciolkosz, E.J., Luxmoore, R.J., (Eds.). *Soil Color. SSSA Special Publications* 31, 51-70.
- Shackleton, N.J., Berger, A., Peltier, W.R., 1990. An alternative astronomical calibration of the lower Pleistocene timescale based on ODP Site 677. *Transactions of the Royal Society of Edinburgh: Earth Sciences* 81, 251-261.
- Sirocko, F., 2007. Introduction – Paleoclimate Reconstructions and Dating. In: Sirocko, F., Claussen, M., Sánchez Goni, M.F., Litt, T (Eds.), *The Climate of Past Interglacials. Development in Quaternary Science* 8, Elsevier, Amsterdam, pp 47-53.
- Spötl, C., Holzschläger, S., Mangini, A., 2007. The last and penultimate Interglacial as recorded by speleothems from a climatically sensitive high-elevation cave site in the Alps. In: Sirocko, F., Claussen, M., Sánchez Goni, M.F., Litt, T (Eds.), *The Climate of Past Interglacials. Development in Quaternary Science* 8, Elsevier, Amsterdam, pp 471-491.
- Tang, Y., Jia, J., Xie, X., 2003. Records of magnetic properties in Quaternary loess and its paleoclimatic significance: a brief review. *Quaternary International* 108, 33-50.
- Thompson, R., Oldfield, F., 1986. *Environmental Magnetism*. Allen & Unwin Ltd., London.
- Timar, A., Vandenberghe, D., Panaiotu, E.C., Panaiotu, C.G., Necula, C., Cosma, C., van den Haute, P., 2010. Optical dating of Romanian loess using fine-grained quartz. *Quaternary Geochronology* 5 (2-3), 143-148.
- Torrent, J., Barrón, V. 1993. Laboratory measurement of soil color: theory and practice. In: Bigham, J.M., Ciolkosz, E.J., Luxmoore, R.J., (Eds.). *Soil Color. SSSA Special Publications* 31, 21-34.
- Torrent, J., Schwertmann, U., Schulze, D.G., 1980. Iron oxide mineralogy of some soils of two river terrace sequences in Spain. *Geoderma* 23, 191-208.
- Torrent, J., Schwertmann, U., Fechter, H., Alferez, F. 1983. Quantitative relationships between soil color and hematite content. *Soil Science* 136 (6), 354-358.
- Torrent, J., Barrón, V., Liu, Q., 2006. Magnetic enhancement is linked to and precedes hematite formation in aerobic soil. *Geophysical Research Letters* 33, L02401.
- Torrent, J., Liu, Q., Bloemendal, J., Barrón, V., 2007. Magnetic enhancement and iron oxides in the upper Luochuan loess-paleosol sequence, Chinese Loess Plateau. *Soil Science Society of America Journal* 71, 1570-1578.
- Tsatskin, A., Heller, F., Hailwood, E.A., Gendler, T.S., Hus, J., Montgomery, P., Sartori, M., Virina, E.I., 1998. Pedosedimentary division, rock magnetism and chronology of the loess/paleosol sequence at Roxolany (Ukraine). *Palaeogeography, Palaeoclimatology, Palaeoecology* 143, 111-133.
- Tsatskin, A., Heller, F., Gendler, T.S., Virina, E.I., Spassov, S., Du Pasquier, J., Hus, J., Hailwood, E.A., Bagin, V.I., Faustov, S.S., 2001. A new scheme of terrestrial paleoclimate evolution during the last 1.5 Ma in the Western Black Sea Region: Integration of soil studies and loess magnetism. *Physics and Chemistry of the Earth (A)* 26 (11-12), 911-916.
- Tzedakis, P.C., Bennett, K.D., 1995. Interglacial vegetation succession: A view from southern Europe. *Quaternary Science Reviews* 14, 967-982.
- Tzedakis, P.C., Hooghiemstra, H., Pälike, H., 2006. The last 1.35 million years at Tenaghi Philippon: revised chronostratigraphy and long-term vegetation trends. *Quaternary Science Reviews* 25, 3416-3430.

-
- Tzedakis, P.C., Pälike, H., Roucoux, K.H., de Abreu, L., 2009. Atmospheric methane, southern European vegetation and low-mid latitude links on orbital and millennial timescales. *Earth and Planetary Science Letters* 277, 307-317.
- Van Oorschot, I.H.M., Dekkers, M.J., 1999. Dissolution behaviour of fine-grained magnetite and maghemite in the citrate-bicarbonate-dithionite extraction method. *Earth and Planetary Science Letters* 167, 283-295.
- Van Velzen, A.J., Dekkers, M.J., 1999. Low-temperature oxidation of magnetite in loess-paleosol sequences: A correction of rock magnetic parameters. *Studia Geophysica et Geodaetica* 43, 357-375
- Varadachari, C., Goswami, G., Ghosh, K. 2006. Dissolution of iron oxides. *Clay Research* 25, 1-19.
- Vidic N.J., Singer M.J., Verosub K.L., 2004. Duration dependence of magnetic susceptibility enhancement in the Chinese loess-palaeosols of the past 620 ky. *Palaeogeography, Palaeoclimatology, Palaeoecology* 211, 271-288.
- Voelker, A.H.I., Rodrigues, T., Billups, K., Oppo, D., McManus, J., Stein, R., Hefter, J., Grimalt, J.O., 2010. Variations in mid-latitude North Atlantic surface water properties during the mid-Brunhes (Mis9-14) and their implications for the thermohaline circulation. *Climate of the Past* 6, 531-552.
- Walter, H., 1974. *Die Vegetation Osteuropas, Nord- und Zentralasien..* Gustav Fischer Verlag, Stuttgart.
- Wang, X., Lu, H., Xu, H., Deng, C., Cheng, T., Wang, X., 2006. Magnetic properties of loess deposits on the northeastern Qinghai-Tibetan Plateau: palaeoclimatic implications for the Late Pleistocene. *Geophysical Journal International* 167, 1138-1147.
- White A.F., Blum A.E., 1995. Effects of climate on chemical weathering in watersheds. *Geochimica et Cosmochimica Acta* 59 (9), 1729-1747.
- WMO, World Meteorological Organization, 1996. *Climatological Normals (CLINO) for the period 1961-1990.* Secretariat of the World Meteorological Organization, Geneva.
- Yaalon, D.H., 1997, Soils in the Mediterranean region: what makes them different? *Catena* 28, 157-169.
- Yin, Q.Z., Berger, A., 2010. Insolation and CO₂ contribution to the interglacial climate before and after the Mid-Brunhes event. *Nature Geoscience* 3, 243-246.
- Yin, Q.Z., Guo, Z.T., 2008. Strong summer monsoon during the cool MIS-13. *Climate of the Past* 4, 29-34.
- Ziegler, M., Lourens, L.J., Tuenter, E., Reichert, G.-J., 2010. High Arabian Sea productivity conditions during MIS 13 – odd monsoon event or intensified overturning circulation at the end of the Mid-Pleistocene transition. *Climate of the Past* 6, 63-76.
- Zhou, L.P., Oldfield, F., Wintle, A.G., Robinson, S.G., Wang, J.T., 1990. Partly pedogenic origin of magnetic variations in Chinese loess. *Nature* 346, 737-739.

Study 6

Is there a possibility to correct fossil n-alkane data for postsedimentary alteration effects?

Björn Buggle¹, Guido L.B. Wiesenberg², Bruno Glaser¹

¹Soil Physics Department, University of Bayreuth, D-95440 Bayreuth, Germany.

²Agroecosystem Research Department, University of Bayreuth, D-95440 Bayreuth,

Published in

Applied Geochemistry 196, 86-106.

2009

*Corresponding author: Björn Buggle, Phone:+49(0)921-552174

E-mail: Bjoern.Buggle@uni-bayreuth.de

Abstract

The long-chain n-alkane composition of plant material can significantly differ between plant groups e.g. trees and grasses. Due to their relative recalcitrance, they have been employed in paleoecological research as molecular proxies for different types of vegetation. Most of those paleoenvironmental studies rely on the assumption that characteristic molecular fingerprints of plant material are preserved in the fossil organic material without significant alteration. However, there exists evidence that n-alkane distributions may change in course of plant litter degradation. Here, the authors propose and discuss a conceptual approach to the correction of n-alkane patterns in paleosols and terrestrial sediments for postsedimentary alteration effects. This might have potential to improve paleoenvironmental reconstructions derived from these molecular fossils. In soil depth profiles typically a correlation between the OEP (odd over even predominance) and paleoecological valuable long-chain n-alkane ratios (LARs) can be found. Similar relationships have been also obtained from n-alkane records in paleosols. With the OEP serving as proxy of microbial reworking, the correction procedure applies OEP vs. LAR regression functions to correct fossil LARs for degradation effects. The regression functions have been derived from modern soils. The application of the procedure and its significance for paleoecological interpretations is demonstrated on a case study of a loess-paleosol sequence (~ 400 - 700 ka) in Romania. It is shown that changes in the C27/C31 n-alkane ratio at this site are closely related to degradation effects rather than to changes in the paleovegetation (e.g. tree vs. grass abundance). However, it was found that the C29/C31 ratio is a more suitable paleoenvironmental proxy at the Mircea Voda site. The results indicate that there is a future potential to correct fossil n-alkane ratios via the OEP/LAR relationship, however at the moment a general straight forward application of this approach might be critical due to lack of extended and diverse n-alkane records from modern soils. The need of

more systematic n-alkane studies on soil profiles is highlighted to improve knowledge concerning dynamics and actual mechanisms of postsedimentary LAR and OEP changes.

Keywords: biomarker, n-alkanes, lipids, CPI, odd over even predominance, degradation, loess, paleosol

1 Introduction

Long-chain n-alkanes (>C₂₅) with a pronounced dominance of odd over even homologues are essential components of plant cuticular lipids (e.g. Eglinton and Hamilton, 1967). As such they are transferred to the soil surface in course of litterfall, eventually blown or washed into rivers and finally buried in lacustrine or marine sediments. A significant part of leaf-derived lipids will enter the soil organic matter (SOM), which is subsequently either eroded, degraded or buried in situ. If preserved in sedimentary archives, these compounds represent valuable molecular fossils (e.g. Eglinton and Eglinton, 2008). It has been shown that cuticular lipids have a potential for the chemotaxonomical differentiation of plants (e.g. Eglinton et al., 1962; Stevens et al., 1994; Maffei 1996a). However due to inter- and intraspecies variability, their chemotaxonomical value is restricted and mostly allows only a rough differentiation of different plant groups (Borges del Castillo et al., 1967, Schwark et al., 2002). Nevertheless, their relative recalcitrance makes long-chain n-alkanes an especially attractive tool in paleoenvironmental studies. Thus, they are used e.g. to distinguish between tree- or shrub-derived plant material with a predominance of mostly n-C₂₇ or n-C₂₉ and grasses with mostly n-C₃₁ or n-C₃₃ dominance (Cranwell, 1973; Meyers and Ishiwatari, 1993; Maffei et al., 1996a, b; Zhang et al., 2008; Zech et al., 2009b). Hence these compounds are regarded as biomarkers and their ratios (e.g. C₂₇/C₃₁, C₂₉/C₃₁, (C₂₇ + C₂₉)/(C₃₁ + C₃₃)) are applied as proxies for the source determination of fossil organic material e.g. trees (shrubs) vs. grasses (e.g. Schwark et al., 2002; Zhang et al., 2006; Bai et al., 2009; Zech et al., 2009). The motivation of using n-alkanes in studies of fossil soils is – beside their relative recalcitrance – their complementarity to other methods such as pollen studies (Schwark et al., 2002; Zhang et al., 2006). The former should mainly reflect signals of the local, in situ vegetation, whereas the latter can be significantly influenced by long distance transport and tend to give a more

regional signal of paleovegetation (Farrimond and Flanagan, 1996). Furthermore lipid analysis is less time consuming, so that high resolution records can be easily obtained. However, up to now most studies applying the n-alkane biomarker approach rely on the assumption that pattern of long-chain plant derived n-alkanes (pd-n-alkanes) do not change significantly after being incorporated into the sediment or soil organic matter. For a certain time interval, this assumption might be valid in anaerobic and/or acidic environments such as lake sediments or peat profiles. Under these conditions hydrocarbon degradation and microbial activity, respectively, is hampered (Leahy and Colwell, 1990; Meyers and Ishiwatari, 1993). However, even in such environments postsedimentary alteration effects on acyclic, saturated hydrocarbons have been reported (Cranwell, 1981; Meyers, 1997; Xie et al., 2004). These should be even more pronounced in an oxic or eutric environment as in many (paleo-)soils and loess-paleosol sequences, respectively (Moucawi et al., 1981; Diné et al., 1990; Xie et al., 2004a; Bai et al., 2009). As a consequence the recognition of molecular fingerprints and a source apportionment (e.g. tree vs. grass) may become inconclusive (Mazeas et al., 2002).

With the intention of overcoming this problem and to account for possible postsedimentary alteration effects, when interpreting n-alkane records in sedimentary archives, one has to find the answers to the questions:

- 1) How can n-alkane distribution patterns change in the course of postsedimentary alteration?
- 2) How can the extent of postsedimentary alteration be estimated i.e. is there a proxy for n-alkane alteration?

Results and models deriving from lipid analysis of soil depth profiles, mechanistic considerations, as well as incubation experiments provide the background to answer the first

question. Accordingly, one has to be aware of the following effects, when comparing n-alkane patterns of material in different states of decomposition

- a) An enhanced degradation of short-, medium-chain (<C22) pd-n-alkanes as compared to long-chain n-alkanes due to higher solubility and thus bioavailability (Cranwell, 1981; Moucawi et al., 1981; Jambu et al., 1991; Lehtonen and Ketola, 1993; Setti et al., 1993; Marseille et al., 1999; Nguyen Tu et al., 2001).
- b) An increasing contribution of microbially-derived n-alkanes with no pronounced odd over even predominance (OEP). This especially affects n-alkanes of short to medium-chain length (e.g. Cranwell, 1981; Almendros et al., 1996; Huang et al., 1997). However, higher molecular homologues of microbial origin have also been found (Jones and Young, 1970; Albro, 1976; Weete, 1976; Grimalt et al., 1987 and references therein; Jambu et al., 1991; Huang et al., 1996).
- c) An enhanced degradation of the more abundant compounds (“kinetic effect”, Marseille et al., 1999; see also Wiesenberg et al., 2004 and references herein).

For the application of n-alkane records in paleoenvironmental studies (e.g. differentiation of grassland vs. woodland) the relative distribution of long-chain homologues with odd carbon numbers (n-C27, n-C29, n-C31, n-C33) is especially promising (e.g. Zhang et al., 2006; Zech et al., 2008, 2009b). Therefore, degradation effects on short- and medium-chain n-alkanes would not concern such paleoecological interpretation (Jansen et al., 2008). Furthermore a simple first order kinetic of degradation (“kinetic effect”) would only affect the absolute abundance of n-alkane homologues but not n-alkane ratios. However, with decreasing abundance, any contamination by long-chain md-n-alkanes (**m**icrobial **d**erived n-alkanes i.e. n-alkanes synthesized by microorganisms or formed by microbial transformation of other, non n-alkane lipids) becomes more significant. The result is a loss or bias of the paleoecological information provided by the pd-n-alkane pattern in (fossil) soils and sediments (Freeman and

Colarusso, 2001; Huang et al., 1996; Wiesenberg et al., 2008a; Eckmeier and Wiesenberg, 2009; Zech et al., 2010). Hence the focus of this study is to develop a procedure to correct fossil long-chain n-alkane ratios (LARs, e.g. C27/C31, C27/C29, C29/C31) for such postsedimentary alteration effects. Alteration here refers to biodegradation of n-alkanes as well as the contribution of md-n-alkanes. As a potential indicator for alteration intensity measures of the odd over even predominance in n-alkane distributions will be considered such as the OEP or the Carbon Preference Index CPI (e.g. Bray and Evans, 1961; Hoefs et al., 2002; Zhang et al., 2006). This kind of index is generally accepted as an indicator of biodegradation, contribution of md- hydrocarbons and maturity of hydrocarbons (Cranwell 1981; Rieley et al., 1991; Freeman and Colarusso, 2001; Xie et al., 2002, 2004a, b; Zhou et al., 2007; Wiesenberg et al., 2008b). Accordingly, several n-alkane records of soil depth profiles show a decrease of the CPI with depth, indicating increasing alteration (in the previously mentioned sense) (e.g. Huang et al., 1996; Celerier et al., 2009; Jansen and Nierop, 2009). Besides these trends of the CPI, the records of Huang et al. (1996) indicate furthermore a systematic change in characteristic ratios of long-chain (n-C27, n-C29, n-C31, n-C33) n-alkanes. The LAR records go along with shifts of the CPI in the depth profile and approach unity. Yet, such detailed studies on changes of LARs (e.g. C27/C29, C27/C31, C29/C27) in soil depth profiles are rare. In Fig. 6-1 the authors' previously unpublished data on previous investigations are presented. These document a similar relation between the OEP and LARs, are presented

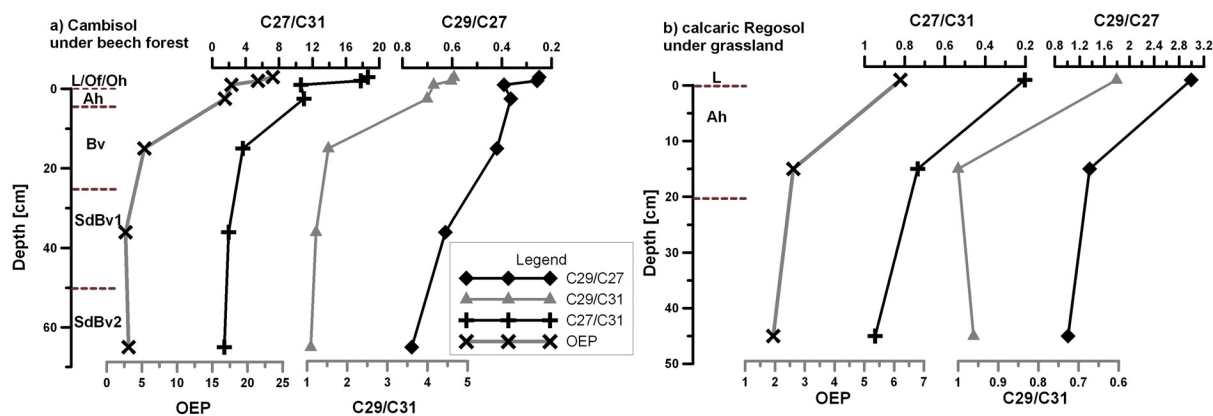


Fig. 6-1. Soil depth profiles of OEP and C27/C31, C29/C31, C29/C27 n-alkane ratios a) for a eutric Cambisol (IUSS Working Group WRB, 2006) under beech forest. The site and the studied soil has been previously described in Rumpel et al. (2004); b) for a calcareous Regosol (IUSS Working Group WRB, 2006) under grassland sampled at the Titel loess plateau 25 km east of Novi Sad (Serbia). All profiles show a decrease of the OEP with soil depth and a concomitant approach of long-chain n-alkane ratios towards unity.

Studies on loess-paleosol sequences reveal such trends not only for modern soils, but also in paleosols (Xie et al., 2004a; Zhang et al., 2006; Zech et al., 2008). On the one hand, these correlations between OEP and LARs suggest that the variations in LARs are mainly caused by postsedimentary alteration effects (degradation of pd-lipids, contribution of long-chain md-n-alkanes), rather than by changes in paleovegetation (Zech et al., 2008). On the other hand, it indicates a possibility to setup a correction for these alteration effects in (paleo-)soil depth profiles by using correlation functions between LARs and the OEP or CPI of long-chain n-alkanes.

In the following the principle and details of the proposed correction procedure will be explained its potential and limits discussed. This is done exemplarily for an n-alkane record of the loess-paleosol section Mircea Voda (Romania). Comprising Marine Isotope stages 11-17, this currently represents the oldest published n-alkane record in European loess-paleosol sequences, to the authors' knowledge.

2 Material and Methods

2.1 Sampling, sample preparation and analytical methods

The loess-paleosol sequence Mircea Voda (44°19'15''N, 28° 11'21'' E) is located on the Dobrudja loess-plateau (Romania) between the Danube River and the Black Sea coast. The aeolian sediments at this site are about 30 m thick and contain more than six interglacial pedocomplexes. The actual vegetation at this site is a steppe grassland. The modern soil is a 120 cm thick calcic Chernozem (IUSS Working Group WRB, 2006). For more detailed information on this site, its geographical setting and the chronostratigraphy, see to Bugge et al. (2008a, 2009). For the present study, the fossil pedocomplexes S4, S5 and S6 were sampled, as well as the intercalated loess units L5 and L6, for n-alkane analysis. These pedocomplexes correspond to Marine Isotope Stages 11, 13-15 and 17-19, respectively (Bugge et al., 2009). The paleosols were sampled continuously in 10-50 cm intervals according to horizontation and thickness of the paleosol, whereas about three representative samples were taken from each individual loess layer. The modern soil was sampled continuously in 15 cm intervals (i.e. eight samples).

The samples were dried at 40 °C and then stored at room temperature until lipid extraction.

The extraction and purification of the n-alkane fraction followed the procedure of Zech and Glaser (2008). Free lipids were extracted with methanol/toluol (7/3) using Soxhlet apparatus. The extraction was performed on 100 g of sample material for 24 h. The extracts were subsequently concentrated via rotary evaporation, and then saponified for 10 min with 0.5 M NaOH in methanol at 100 °C in order to hydrolyze esters. By liquid-liquid extraction with hexane, a low-polarity fraction was separated, containing the n-alkanes, from a high-polarity fraction (e.g. fatty acids, alcohols) with higher affinity to methanol. The low-polarity fraction was then purified via column chromatography with Al oxide and silica gel (each 5 %

deactivated) as stationary phases and hexane/toluol (85/15) as eluent. After concentrating the hydrocarbon fraction, n-alkanes were separated on a HP 6890 GC and quantified with a flame ionization detector (FID). As internal standards and recovery standard 5α -androstanone and hexatriacontane (n-C36) were used. The odd over even predominance (OEP) was quantified according to the formula proposed by Hoefs et al. (2002) (Eq. 1).

$$OEP = \frac{nC27 + nC29 + nC31 + nC33}{nC26 + nC28 + nC30 + nC32} \quad (1)$$

2.2 The approach to correct n-alkane patterns for alteration effects

2.2.1 Principles and assumptions

The approach to derive a correction function for n-alkane patterns relies on the application of the OEP or CPI as a proxy for (bio-)degradation and microbial reworking, respectively. Since both parameters reflect the odd over even predominance of n-alkane homologues, consider the OEP is considered in the following text. Findings would be similar, when using the CPI (for the formula for the CPI see for example Zhang et al., 2006).

In several soil profiles (see Section 1) a direct or inverse relationship between the OEP record and LARs such as $C31/(C27 + C31)$, $C29/(C27 + C29)$ and $C31/(C27 + C31)$ is documented. These relationships suggest that odd over even predominance and LARs tend towards unity with soil depth. Such a general loss of predominance is in accordance with the hypothesis of increasing biodegradation (kinetic effect) combined with increasing input of mid-n-alkanes with postsedimentary alteration (Huang et al., 1996, Marseille et al., 1999, Freeman and Colarusso, 2001 Zech et al., 2009b). The basic idea of the approach is to use this relationship, which can be obtained from modern soils, to setup a correction for the alteration effects in

paleosols. The general concept of the correction procedure is illustrated in a schematic cross-plot of a LAR vs. OEP (Fig. 6-2): calculating the correlation coefficient and the respective regression function, one can obtain a measure for the covariation of a specific LAR and the OEP in a soil depth profile. This regression line in the following is regarded as “alteration line” and it is proposed that this line describes the change of LARs with increasing alteration intensity. For each LAR of interest ($C27/(C31 + C27)$, $C27/(C29 + C27)$, etc.) and each kind of predominance e.g. C31 over C27 and vice versa C27 over C31, one has to set up a separate alteration line by studying the n-alkane distribution in suitable soil depth profiles. Suitable in this sense means that a) the soil is not significantly disturbed by (bio-) turbation, plowing and n-alkane patterns are not significantly biased by input of hydrocarbons from fossil fuel combustion, b) there was no major change in vegetation during soil development causing a shift of the alkane patterns in the soil depth profile, c) the soil depth profile shows the n-alkane dominance of interest e.g. grassland soils to derive degradation lines for a C31 over C27 dominance or forest soils for a C27 over C31 dominance, and d) soil profiles have a substrate similar to each other and also to the paleosols under study for reasons of comparability.

Due to changes in vegetation, organic matter in a paleosol might initially have a different n-alkane composition than the organic matter of the modern soil. Assuming that the slope of the alteration lines for the respective LARs is similar in modern and fossil soils the alteration line of the paleosol (“fossil alteration line”) can be obtained by a graphical solution i.e. via parallel displacement of the alteration line of the modern soil to the position of the fossil soil in the LAR–OEP cross-plot (Fig. 6-2). Then the corrected LAR value of the paleosol can be determined by drawing the “fossil alteration line” back to the OEP value of the reference sample. In this approach the uppermost (least degraded) sample of the modern topsoil as

reference. From this sample the vegetation type under which its alkane pattern developed should be known best.

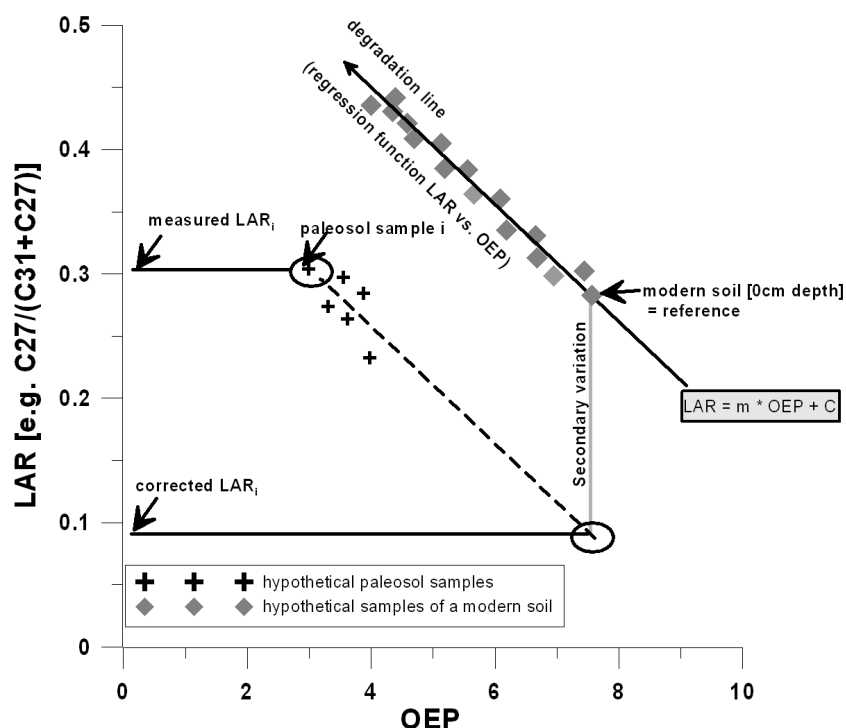


Fig. 6-2. Schematic sketch illustrating the approach to correct fossil LARs (as for example the $C_{27}/(C_{27}+C_{31})$ ratio) for degradation effects. Gray points represent hypothetical samples of a depth profile of a modern soil with C_{31} over C_{27} predominance. Black crosses represent hypothetical samples of a paleosol. The regression line of the OEP – used as a proxy for microbial reworking – versus LAR for the modern soil, is proposed to describe postsedimentary alteration effects on LARs and is therefore regarded as “alteration line”. Assuming that the slope m of the alteration line for the paleosol samples is similar to the modern soil, it is possible to reconstruct corrected LARs for a sample by parallel displacement of the alteration line. As a corrected LAR we regard the hypothetical LAR of a “paleo-sample” with the same intensity of microbial reworking (i.e. same OEP) as the modern topsoil. The distance of the parallel displacement is regarded as secondary variation with respect to the alteration line of the modern soil. It is proposed that these secondary variations reflect variations in initial LAR (here $C_{27}/(C_{27}+C_{31})$) of the fossil organic matter, indicating changes in the paleovegetation. Accordingly, samples plotting on the same alteration line would derive from material with similar initial LAR. For samples with inverse LAR predominance (e.g. C_{27} over C_{31}) a separate alteration line has to be determined in a similar way.

All samples plotting on the fossil alteration line would evolve from the same initial n-alkane pattern. If the fossil alteration line is identical with that of the modern soil, this would indicate that initial (pd-) n-alkane patterns of paleosol and soil were similar. Initial in this sense refers to the same state of low alteration intensity as in modern topsoils. If the intercept of the fossil degradation line is different from the modern one, the distance of parallel displacement could

be regarded as secondary variation around the modern degradation line. These secondary variations reflect the differences in the initial LARs of fossil soil organic matter relative to the modern soil and are the parameter of interest when studying for example the relative change in the contribution of tree-derived n-alkanes in the geological record.

In the approach presented, here, a simple linear regression function is proposed, since this gives the best fits in the OEP-LARs datasets presented in the following Sections.

2.2.2 The mathematical procedure

The graphical reconstruction of corrected LAR values can also be expressed mathematically. Using a linear regression function (Eq. 2) the corrected LAR values of a paleosample can be calculated from the slope of the regression line according to (Eq. 3).

$$LAR_0 = m_0 \times OEP_0 + C_0 \quad (2)$$

with m is the slope of the regression line; C is the intercept of the regression line; 0 is the index for the modern soil

$$LAR_{f, corr} = LAR_{f, msd} + m_0 \times \Delta OEP \quad (3)$$

With f is the index for fossil soils; msd is the index for measured values; $corr$ is the index for corrected values

$$\Delta OEP = OEP_{\text{uppermost sample of modern topsoil}} - OEP_{f, msd} \quad (4)$$

3 Results and discussion

3.1 The alteration lines of $C27/(C31 + C27)$, $C27/(C29 + C27)$, $C31/(C27 + C31)$ for the profile Mircea Voda

Raw data of all identified n-alkane homologues in the modern soil of Mircea Voda and in the studied paleosol and loess samples are reported in the Appendix (Table 6-A1, Table 6-A2). In the following, the focus is only on selected ratios.

In Fig. 6-3 the depth profiles are presented of the OEP as well as LARs of the n-C27, n-C29 and n-C31 homologues in the modern soil of the Mircea Voda site. In the upper 50 cm of the modern soil (section A), any kind of predominances i.e. the OEP, as well as the C31 over C27, the C31 over C29 and C29 over C27 dominance decrease with depth. This feature is in line with the data of Huang et al. (1996) and the authors' findings in other soil profiles (see Fig. 6-1) and indicates that these changes in LARs are probably controlled by postsedimentary alteration effects on the pd-lipids. However in section B (below about 50 cm depth), OEP values increase again, suggesting a lower degree of alteration for the long-chain n-alkanes. In parallel also the $C27/(C31 + C27)$, $C27/(C27 + C29)$ and $C29/(C31 + C29)$ ratios increase again. This atypical depth profile in section B is related to better preservation of n-alkanes probably caused by one or several of the following factors: 1) higher dust accumulation rates during soil formation and faster burial of the organic material, 2) cooler and more arid conditions hampering microbial reworking (referring to both input of md-n-alkanes as well as biodegradation of pd-n-alkanes), possibly during the early Holocene or Younger Dryas (Tomescu, 2000; Bai et al., 2009). However, also a change in the initial pd-n-alkane patterns cannot be excluded. Therefore, in the first approach (variant A) only the uppermost three values were used and in a second approach (variant B) all values of the modern soil were used to obtain alteration lines. Since there is no reversal of the predominances in the soil profile, it was not necessary to sample other modern soils for

setting up alteration lines for reverse predominances e.g. C27 over C31, C29 over C31 and C27 over C29.

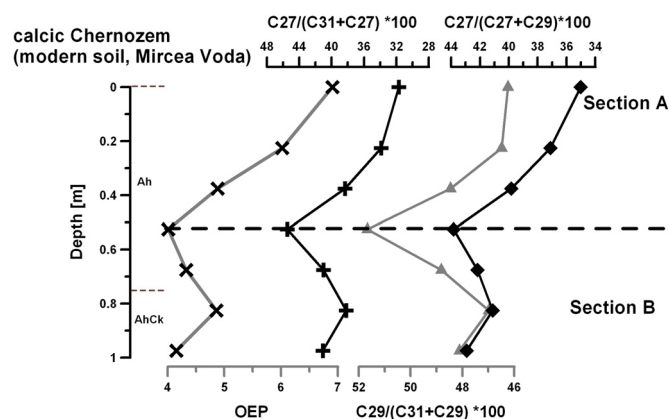


Fig. 6-3. Depth profile of the OEP and selected LARs for the modern soil of the Mircea Voda site. Section A (about the upper 50 cm) shows a decrease of the OEP and an increase of the LARs with depth. In section B this is vice versa.

In both variants, high correlation coefficients were obtained between the LARs and the OEP (see Fig. 6-4) in the modern soil, using linear fits. Except for the $C29/(C29 + C31)$ ratio such relationships were also found in the paleosol samples (Fig. 6-4). Probably this ratio is more strongly controlled by changes in the alkane patterns of the paleovegetation so that the OEP- $C29/(C29 + C31)$ relationship in the fossil samples is masked by more pronounced secondary variations.

The slopes of the OEP vs. LAR regression functions for the first 50 cm of the modern soil, the whole modern soil and the paleosols are in a similar range. Accepting the OEP as an alteration proxy, these findings underline the validity of the LAR correction approach. However, the slope of the regression function for the $C27/(C27 + C31)$ ratio of the whole modern soil (variant B) differs remarkably from that of the top 50 cm and the loess-paleosol samples (-4.15 vs. -3.33 and -3.11). This indicates that the regression function deriving only from section A of the modern soil is more suitable to describe the influence of postsedimentary alteration on the $C27/(C27 + C31)$ ratio. The higher slope obtained from variant B may be caused by contributions of n-alkanes with different initial, pd-n-alkane signatures in the

deeper and older part of the modern soil (section B). Hence, this feature is probably related to a change of vegetation during soil development (section B vs. section A). Thus, for the correction of the paleosol n-alkane ratios, the regression line from the uppermost 50 cm of the modern soil is applied, where a decrease of predominances indicates an alteration controlled change of long-chain n-alkane patterns.

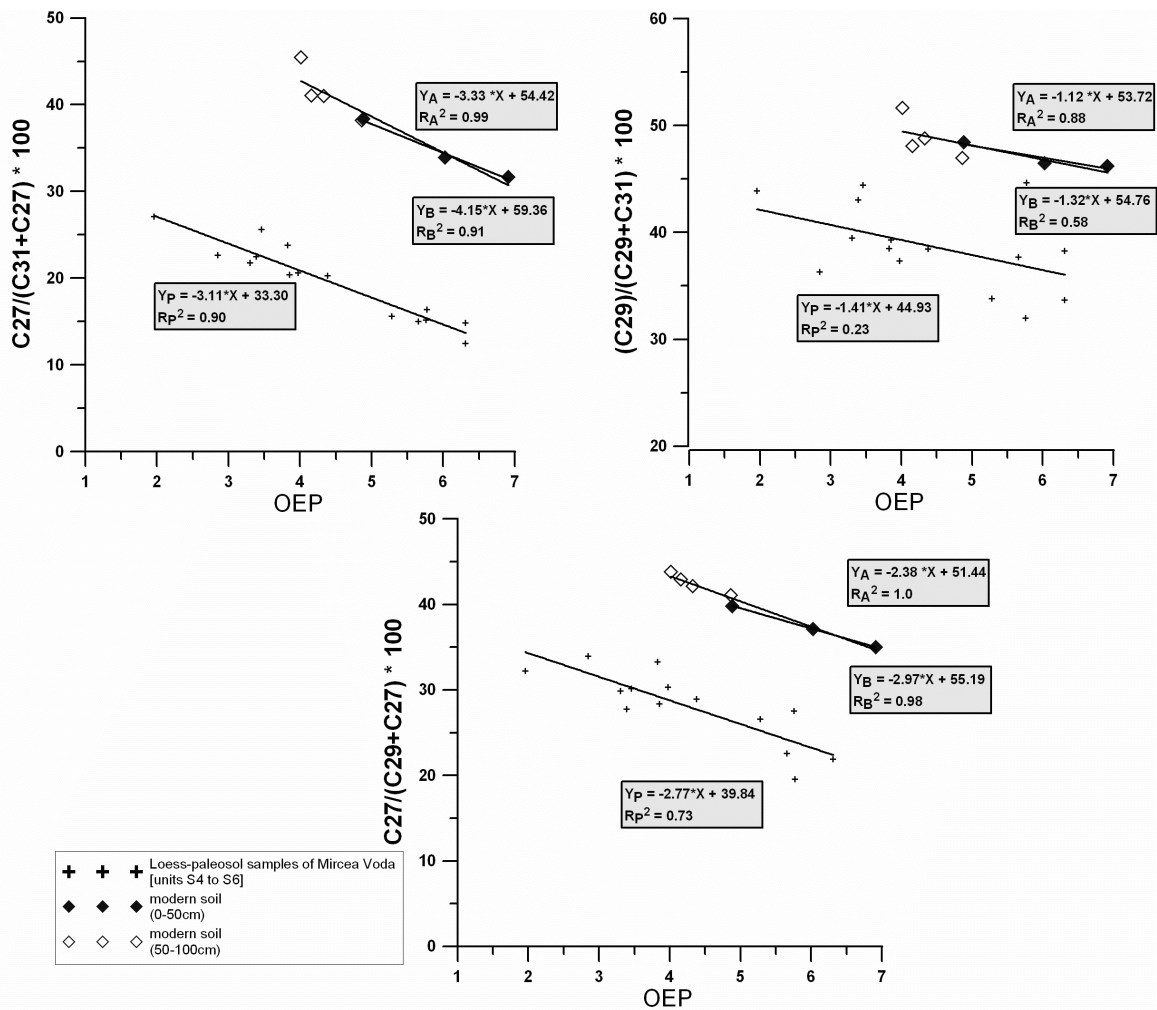


Fig. 6-4. Cross-plot of selected LARs vs. OEP for the modern soil and the loess-paleosol units S4 to S6 of the Mircea Voda site. The regression function and correlation coefficients for the OEP vs. LAR relationships are given for the upper 50 cm of the modern soil (index A), the whole modern soil (0-100cm; index B) and the loess-paleosol samples (index P).

3.2 Corrected vs. uncorrected values

Similar to the modern soil, the OEP record of the fossil soils S4 and S5 shows a decrease of the values with increasing soil depth, reflecting an increase of the alteration intensity (Fig. 6-

5). In the lower parts of a (fossil) soil, organic material was exposed for a longer time to enhanced microbial activity, until the onset of burial by loess under glacial or stadial conditions hampered microbial reworking. Correspondingly, the highest alteration intensity of the S4 pedocomplex is recorded at the base of the paleosol, whereas in the underlying loess layer L5 the OEP is better preserved due to higher burial rates and reduced intensity of microbial reworking during cold climate conditions (Xie et al., 2004a, b). Higher odd over even predominances in loess and lower OEP values in paleosols have also been recognized as characteristic features in several other loess-paleosol sequences (Xie et al., 2004a; Liu and Huang, 2005; Zhang et al., 2006). The S5 is the strongest pedocomplex of the Mircea Voda profile and formed during two warm, interglacial periods (MIS 13 and MIS 15) under Mediterranean-like climate conditions (Bugge et al., 2008b, 2009). Also in this unit, n-alkane alteration as indicated by the OEP, increases with soil depth but extends deeper than pedogenesis (in sense of mineral transformation) into the loess (unit L6). The lowest OEP is even recorded within the loess just below the S5 pedocomplex. No clear patterns of the OEP can be observed in the S6 pedocomplex.

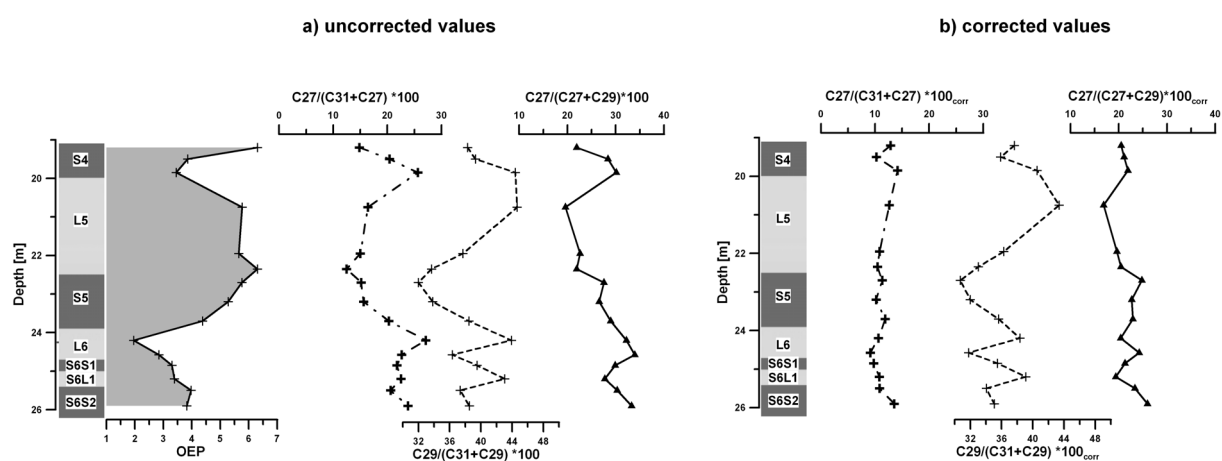


Fig. 6-5. OEP and LAR depth profiles for the loess-paleosol units S4 - S6 of the Mircea Voda site. a) Uncorrected LAR ratios, b) LAR ratios corrected for degradation effects. The stratigraphy of the loess-paleosol sequence is described in more detail in Bugge et al., (2009). Depth values are referred to the top of the whole sequence (S0 - S6).

As already revealed from the correlation coefficients of LARs with OEP, most of the fluctuations of the $C_{27}/(C_{31} + C_{27})$ and $C_{27}/(C_{27} + C_{29})$ ratio can be inversely related to the changes in the OEP, herewith showing typical patterns of a soil depth profile. It is generally accepted that the odd over even predominance either expressed as OEP or CPI is an indicator for the intensity of microbial or thermal degradation (Johnson and Calder, 1973; Freeman and Colarusso 2001; Xie et al., 2002, 2004a, b; Wiesenberg et al., 2008b, 2009). However, studies on fresh, terrestrial plant material also report on pronounced variations of the odd over even predominance not only between but also within different species (Borges del Castillo, 1967; Maffei, 1996a, b; Liu and Huang, 2005; Sachse et al., 2006). Therefore, the question arises, whether the trends of the OEP with depth in the modern soil and also in the fossil soils are indeed related to postsedimentary alteration or rather to changes in the paleovegetation. To answer this question, the ratio of long-chain n-alkanes ($\geq n-C_{25}$) vs. short- to medium-chain length n-alkanes ($< n-C_{25}$) was compared with the OEP. Short to medium chain length n-alkanes are predominantly derived from microorganisms (Weete 1976; Albro 1976) or thermal degradation of organic material (Wiesenberg et al., 2009). Since n-alkane degradation in soils is essentially mediated by microorganisms, a stronger alteration intensity of pd-n-alkanes should be also reflected in this chain length ratio (Xie et al., 2003). Indeed in the modern soil and also in most loess and paleosol units the depth profile of the $Alk_{>C_{25}}/Alk_{<C_{25}}$ ratio is similar to the OEP record (Fig. 6-6). Lower $Alk_{>C_{25}}/Alk_{<C_{25}}$ ratio with decreasing OEP are related to an increase in the absolute abundance of short-chain homologues mainly in the range of C16-C18 going along with decreasing concentrations of long-chain homologues (see Appendix for absolute n-alkane contents). This suggests that the OEP in the sample set is mainly controlled by the intensity of alteration rather than by changes in paleovegetation. Therefore observed patterns and trends in the $C_{27}/(C_{31} + C_{27})$ and $C_{27}/(C_{27} + C_{29})$ ratios are also likely controlled by postsedimentary alteration rather than by changes in

paleovegetation, since they are covarying with the OEP. It has to be noted that the OEP values in the fossil soils are in a similar range to those in the modern soil, suggesting that alteration of the n-alkane pattern is limited after burial of the soils.

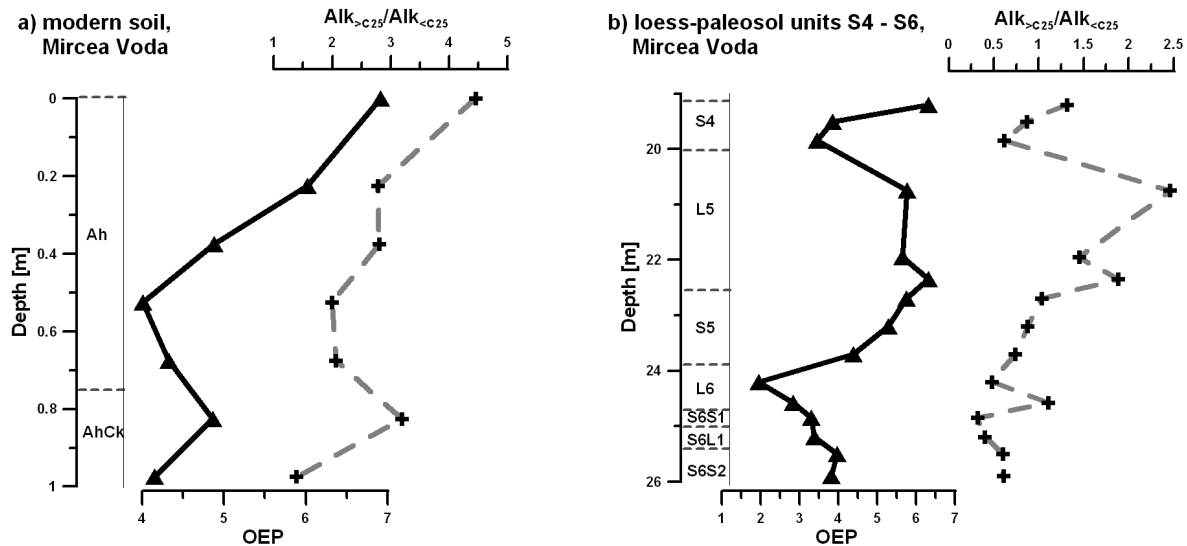


Fig. 6-6. Comparison of the OEP and $Alk_{>C25}/Alk_{<C25}$ ratio in the depth profiles of the modern soil of the Mircea Voda section and the loess-paleosol units S4 - S6.

In the paleosols, the corrected ratios of $C27/(C27 + C29)$ and especially $C27/(C31 + C27)$ show only weak secondary variations as they are strongly correlated with the alteration proxy OEP. In contrast, the uncorrected $C29/(C31 + C29)$ record exhibits several patterns, which do not correspond to changes in the OEP. Pronounced secondary variations are also revealed from the corrected $C29/(C31 + C29)$ ratio. According to the proposed model, such secondary variation is indicative of variations in the n-alkane distribution of the paleovegetation. Following the classical interpretation of C29 vs. C31 as proxy for tree vs. grass vegetation (e.g. Zhang et al., 2006), these secondary variations and the corrected $C29/(C31 + C29)$ ratio, respectively, would suggest a higher contribution of trees during periods of loess accumulation. This is in accordance with the findings from a loess-paleosol sequence in the Carpathian Basin by Zech et al. (2009a, 2010), who also intended to take account for degradation effects in the interpretation of n-alkane data. However, a thorough interpretation

of the Mircea Voda LARs record in terms of paleovegetation needs a survey of n-alkane patterns of the potential local vegetation, an evaluation of the climatic influence on plant LARs and an evaluation of the results by other bioproxies. Such detailed (paleo-)ecological investigations are, however, beyond the scope of this study, but they are topic of the authors' ongoing and future research regarding climate and vegetation history of the middle and lower Danube basin.

3.3 Discussing the assumptions – limits and potential of the correction approach

The approach to correct fossil LARs for postsedimentary alteration effects is essentially based on three assumptions:

- a) The OEP reflects degradation intensity of pd-lipids and a contribution by md-n-alkanes. Thus it can be used as a proxy of postsedimentary alteration.
- b) Postsedimentary alteration reduces any kind of predominances in long-chain n-alkane pattern due to microbial reworking.
- c) The alteration line obtained from modern soil profiles is valid for paleosols.

Assumption a) has been already evaluated in Section 3.2. Since OEP values may differ strongly between different types of vegetation (e.g. Sachse et al., 2006), it is recommended to evaluate this assumption by comparison to other proxies of organic matter degradation or microbial reworking (e.g. the $ALK_{>25}/ALK_{<25}$ ratio). At best, this evaluation is done for every loess-paleosol sequence under study.

Assumption b) the decrease of the odd over even predominance with intensity of biodegradation is a commonly observed phenomenon for lipids in plant tissues, soils and sediments. Hence, the CPI and OEP values of n-alkanes are generally regarded as indicators for degradation (Cranwell 1981; Rieley et al., 1991; Freeman and Colarusso, 2001; Xie et al.,

2002, 2004a, b; Zhou et al., 2007). Several studies on soil profiles have found not only decreasing OEP with soil depth but also a decrease of LARs towards unity (see Section 1). Marseille et al. (1999) explained such a decrease of predominances from O layers to A horizons by a simple kinetic degradation effect. Also other authors refer to preferential degradation, when explaining loss of predominances in n-alkane records from soils and sediments (Nishimura and Baker, 1986; Xie et al., 2004a; Jansen and Nierop, 2009; Zech et al., 2010). Following most models for soil organic matter degradation, a first order kinetic can be assumed for lipid decomposition (Wiesenberg et al., 2004). However such a reaction would only affect the absolute abundance of individual homologues but not their ratios. Therefore, input from md-n-alkanes (as defined in Section 1) is commonly discussed, when explaining loss of preferences with degradation intensity (Huang et al., 1996; Freeman and Colarusso, 2001; Xie et al., 2004a). This “contamination” of the pd-n-alkane distribution becomes more significant with intensity of degradation i.e. reduced absolute abundances of the plant derived homologues. Hence, at least in the studied profiles, microbial reworking is probably the most significant process of postsedimentary LAR alteration. Also n-alkane pattern of the peaty gley and acid brown earth soil studied by Huang et al. (1996) would be in line with this effect and support assumption b. Some incubation experiments suggest that also the chain length of n-alkane homologues might be an important factor controlling degradation rates (Moucawi et al., 1981; Setti et al. 1993). However at the Mircea Voda site C27/C31, C27/C29 and C29/C31 ratios increase with soil depth and decreasing OEP, respectively. Hence, it is concluded that at least for this profile preferred degradation of shorter homologues is not an issue of significance. Yet, for the approach it is basically not important to know the actual mechanisms of n-alkane degradation and microbial reworking, respectively, in a soil profile. In any case the regression function between the OEP (proxy for degradation and microbial reworking, respectively) and LAR should describe alteration

effects empirically and can be used for appropriate corrections. This also includes effects of thermal degradation, which will, similar as microbial reworking, result in a decrease of the odd over even predominance (Wiesenberg et al., 2009). However, with such different processes of postsedimentary alteration slopes of the regression lines are likely to change. Hence it is proposed to setup separate regression functions for thermally altered soils by studying material of different thermal maturity.

However, it has to be emphasized that uncertainties in the degradation model increase (e.g. linear vs. exponential slope; alteration lines of different initial LARs approach each other when LARs approach 50% and OEP is close to unity (predominances are absent or weak). In this case, a reconstruction of initial LARs should be considered critically.

Assumption c) even though in this study the slope for the OEP - LAR regression lines in the modern soil and paleosols is in a similar range (Fig. 6-4.), this is not necessarily true for other profiles. Differences between the reconstructed and the real slope of the alteration line would cause a systematic over- or underestimation of the true LAR values. Those LAR trends which extend over major parts of the depth profile and, which show up only in the corrected values, should especially be discussed critically. A possible way to minimize such artifacts might be to choose those modern soils for setting up an alteration line, which have similar properties like the investigated fossil soils. Similar in this sense refers to soil type, as well as general physical and chemical soil parameters (grain size distribution, pH, Eh, etc). Taking a modern topsoil as reference and not fresh plant material furthermore avoids problems in collecting representative samples of certain types of vegetation, since n-alkane patterns of plant leaves may vary seasonally and with growing stage (Herbin and Robins, 1969; Wiesenberg and Schwark, 2006; Krimm, 2005). In addition, it is proposed that the regression function be based only on data of the mineral horizon and not of the litter layer. n-Alkane degradation in the litter layers may also depend on the structure of the litter and accessibility of different

types of litter (e.g. needles vs. leaves) to microorganisms. For this reason, the recently proposed degradation lines of Zech et al. (2010), which rely on LAR-OEP relationships deriving from litter layers and the respective A-horizons, seem less appropriate to correct n-alkane ratios of fossil mineral soils.

Unfortunately, studies of n-alkanes in mineral soils comprising whole soil depth profiles and not just the uppermost cm of the A horizon are very scarce. Besides the presented datasets from the modern Chernozem of the Mircea Voda site and the dystric Cambisol under beech forest from the Steigerwald-forest (Germany, see Fig. 6-1) a suitable dataset for setting up LAR-OEP regression functions was only found in the study of Huang et al. (1996). The slopes of the respective regression functions (Table 6-1) show remarkable differences between the Chernozem and the Cambisols, but also between same soil types developed under different vegetation with different n-alkane predominances (Cambisol under beech forest vs. Cambisol under grassland). These results underline that the slope of the alteration line for a C31 over C27 predominance for example, cannot be obtained from the slope for the C27 over C31 vs. OEP regression line by simply changing the sign. As long as there are no extensive systematic studies on n-alkane patterns in soil depth profiles, no proper evaluation of the influence of soil properties on the alteration line is possible. However, the presented dataset supports the advice to derive the alteration line of fossil soils from a modern soil with similar characteristics. The case example from the Mircea Voda site indicates that there might be a future potential to correct fossil n-alkane ratios via the OEP/LAR relationship. However, there is a lack of data from modern soils and therefore a lack of understanding of the detailed mechanisms of changing n-alkane patterns with soil depth and alteration. Therefore, a widespread straight forward application of the proposed correction procedure might be critical at the present state of knowledge. Future systematic studies on soils and paleosol in loess

plateaus should help (and are necessary) to decipher effects of pedogenic processes or environmental factors on the OEP-LAR relationship.

Table 6-1. Slopes of LAR - OEP regression lines for the calcic Chernozem of the Mircea Voda site (this study), a dystric Cambisol in the Steigerwald forest (Germany) developed under beech vegetation (this study and Rumpel et al., 2004) and an acid brown earth under grassland pasture (U.K., Huang et al., 1996). The regression line only includes data of the mineral soil horizons and not of the litter layers. Also deeper parts of the profiles, in which a shift in LAR ratios and OEP indicates changes in biomass source (different type of vegetation during soil development), were not included in the regression line.

| | C27/(C27+C31) | C29/(C29+C31) | C27/(C27+C29) |
|--|----------------------|----------------------|----------------------|
| Calcic Chernozem (this study) | -3.33 | -1.12 | -2.38 |
| Cambisol (this study & Rumpel et al., 2004) | 1.61 | 1.74 | 0.67 |
| Acid brown earth (Huang et al., 1996) | -3.74 | -2.47 | -3.7 |

4 Conclusion

n-alkane ratios from fossil organic matter as preserved for example in paleosols may represent valuable proxies for paleovegetation types (e.g. tree vs. grass). However, the original n-alkane ratios may be altered due to microbial reworking. The presented data from soil depth profiles suggest that this results in a general decrease of predominances. This is most likely due to input of md-n-alkanes with low OEP combined with a decreasing abundance of pd-lipids (“kinetic effect”). The lack of systematic studies on soil depth profiles has to be admitted, resulting in limited knowledge concerning controlling mechanisms on n-alkane alteration and especially their dynamics and significance in soils and terrestrial sediments (e.g. loess). Hence, a straight forward application of the proposed correction to soils different from those investigated in this study is critical, at the present state of knowledge. Nevertheless, for the following reasons it is concluded that the proposed correction procedure has a potential to improve paleoecological interpretations of fossil n-alkane records in paleosols, in the future.

1) Every postsedimentary alteration of LARs induced by microbial reworking should be reflected in a correlation between the degradation proxies OEP or CPI and single LARs. Thus, regardless of the mechanism causing LAR alteration, the regression line LAR vs. OEP or CPI (“degradation line”) should empirically describe the change of LARs with increasing alteration intensity.

2) There exists uncertainty when applying the slope of an “alteration line”, which derives from a modern soil, to paleosol samples. However, the proposed empirical approach represents an objective and traceable procedure to quantify alteration effects. In contrast, a qualitative estimation would require knowledge or assumptions on the processes of LAR alteration. Due to a lack of suitable studies on LAR/OEP relationships in modern soils it is recommended to present in any case corrected as well as the uncorrected LARs. This allows a rediscussion of the data, if new datasets are available.

3). The suitability of the OEP as proxy of degradation and microbial reworking, respectively, can and should be independently evaluated by comparison to the ratio of short vs. long-chain n-alkanes or other proxies for intensity of microbial reworking and SOM degradation, respectively. Such an evaluation is crucial and strongly recommended for each fossil n-alkane record in order to exclude that the OEP record is really reflecting changes in paleovegetation and not degradation intensity.

4) Accepting the OEP as an alteration proxy, the secondary variations of LARs around the OEP-LAR regression (i.e. degradation-) line can be determined. Thereafter, it is possible to isolate the initial (i.e. plant-derived) changes in n-alkane patterns from artifacts due to postsedimentary alteration. Such an approach may be not only promising in loess-paleosol sequences, but also in other kinds of sediments.

The case study concerning the n-alkane record from a 400 to 700 ka old loess-paleosol sequence in Romania revealed that changes in C₂₇/C₃₁ n-alkane ratio are closely related to

postsedimentary alteration effects, rather than to changes in the paleovegetation (e.g. tree vs. grass abundance). The findings highlight that it is essential to consider such alteration effects, when interpreting n-alkane patterns as biological fingerprints. The proposed correction procedure is regarded as a first conceptual approach to account for this problem. Fig. 6-7 gives a short guideline for the practical application of the approach. Clearly, the need of more systematic, highly resolved studies on soil depth profiles need to be addressed to evaluate the presented empirical correction functions and to test whether they can be transferred to other sites, (paleo-) soil types and environmental conditions.

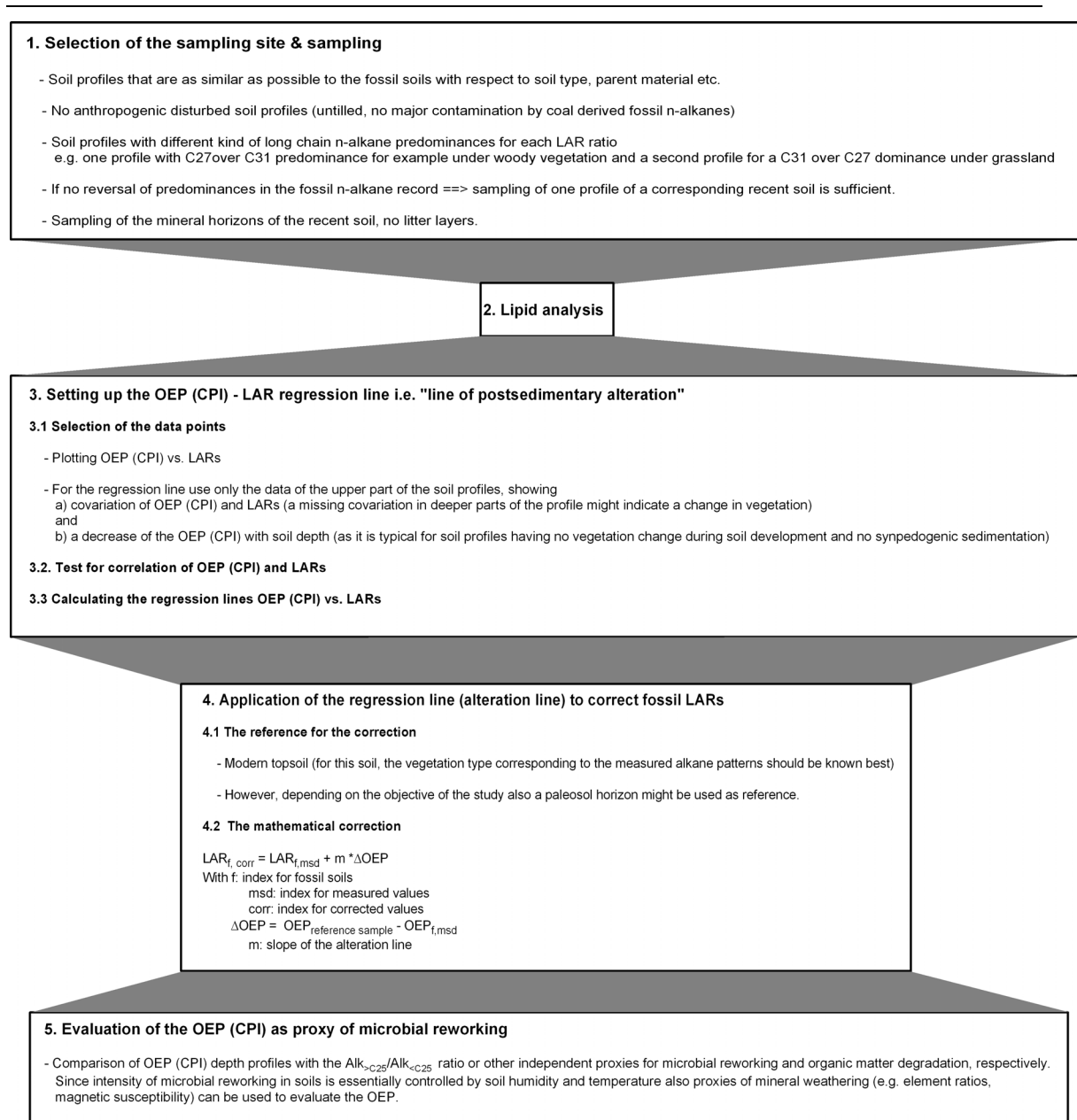


Fig. 6-7. Guidelines for the application of the n-alkane correction procedure.

Acknowledgements.

We thank the German Research Foundation for financial support (DFG GL 327/8-2) and acknowledge the logistic support of our sampling campaign, provided by U. Hambach (University of Bayreuth) and I. Glaser. We also wish to express our gratitude to C. Rumpel for doing the lipid analysis on the Steigerwald-soil. Furthermore we are especially grateful to

Dr. M. Zech and other members of the Chair of Soil Physics, University of Bayreuth, as well as two anonymous reviewers for critical and constructive discussions and comments.

References

- Albro, P.W., 1976. Bacterial waxes. In: Kolattukudy, P.E. (Ed.), *Chemistry and Biochemistry of Natural Waxes*, Elsevier, New York, pp. 419-445.
- Almendros, G., Sanz, J., Velasco, F., 1996. Signatures of lipid assemblages in soils under continental mediterranean forests. *Eur. J. Soil. Sci.* 47, 183-196.
- Bai, Y., Fang, X., Nie, J., Wang, Y., Wu, F., 2009. A preliminary reconstruction of the paleoecological and paleoclimatic history of the Chinese loess Plateau from the application of biomarkers. *Palaeogeog. Paleoclim. Paleoecol.* 271, 161-169.
- Borges del Castillo, J., Brooks, C.J.W., Cambie, R.C., Eglinton, G., Hamilton, R.J., Pellitt, P., 1967. The taxonomic distribution of some hydrocarbons in gymnosperms. *Phytochemistry* 6, 391-398.
- Bray, E.E., Evans, E.D., 1961. Distribution of n-paraffins as a clue to recognition of source beds. *Geochim. Cosmochim. Acta* 22, 2-15.
- Buggle, B., Glaser, B., Zöller, L., Hambach, U., Marković, S., Glaser, I., Gerasimenko, N., 2008a. Geochemical characterization and origin of Southeastern and Eastern European loesses (Serbia, Romania, Ukraine). *Quatern. Sci. Rev.* 27, 1058-1075.
- Buggle, B., Hambach, U., Glaser, B., Gerasimenko, N., Marković, S.B, Glaser, I., Zöller, L., 2009. Stratigraphy and spatial and temporal paleoclimatic trends in East European loess paleosol sequences. *Quatern. Internat.*, 196, 86-106.
- Buggle, B., Hambach, U., Glaser, B., Marković, S., Glaser, I., Zöller, L., 2008b. Long-term paleoclimate records in SE-Europe – the loess paleosol sequences Batajnica/ Stari Slankamen (Serbia) and Mircea Voda (Romania). *Abhandlungen der Geologischen Bundesanstalt* 62, 15-19.
- Celerier, J., Rodier, C., Favetta, P., Lemee, L., Amles, A., 2009. Depth-related variations in organic matter at the molecular level in a loamy soil: reference data for a long-term experiment devoted to the carbon sequestration research field. *Eur. J. Soil. Sci.* 60, 33-43.
- Cranwell, P.A., 1973. Chain-length distribution of n-alkanes from lake sediments in relation to post-glacial environmental change. *Freshwater. Biol.* 3, 259-265.
- Cranwell, P.A., 1981. Diagenesis of free and bound lipids in terrestrial detritus deposited in a lacustrine sediment. *Org. Geochem.* 3, 79-89.
- Dinel, H., Schnitzer, M., Mehuys, G.R., 1990. Soil lipids: origin, nature, content, decomposition and effect on soil physical properties. In: Bollag, J.M., Stotzky, G. (Eds.), *Soil Biochemistry*. Marcel Dekker, pp. 387-429.
- Eckmeier, E., Wiesenberg, G.L.B., 2009. Short-chain n-alkanes (C₁₆₋₂₀) in ancient soils are useful molecular markers for prehistoric biomass burning. *J. Archaeol. Sci.* 36, 1590-1596.
- Eglinton, G., Hamilton, R.J., 1967. Leaf epicuticular waxes. *Science* 156, 1322-1335.
- Eglinton, G., Hamilton, R.J., Raphael, R.A., Gonzalez, A.G., 1962. Hydrocarbon constituents of the wax coatings of plant leaves: a taxonomic survey. *Nature* 193, 739-742.
- Eglinton, T.I., Eglinton, G., 2008. Molecular proxies for paleoclimatology. *Earth Planet Sci. Lett.* 275, 1-16.

- Farrimond, P., Flanagan, R.L., 1996. Lipid stratigraphy of a Flandrian peat bed (Northumberland, UK): comparison with the pollen record. *The Holocene* 6, 69-74.
- Freeman, K.H., Colarusso, L.A., 2001. Molecular and isotopic records of C4 grassland expansion in the late Miocene. *Geochim. Cosmochim. Acta* 65, 1439-1454.
- Grimalt, J.O., Torras, E., Albaigès, J., 1987. Bacterial reworking of sedimentary lipids during sample storage. *Advances Org. Geochem.* 13, 741-746.
- Herbin, G.A., Robins, P.A., 1969. Patterns of variation and development in leaf wax alkanes. *Phytochemistry* 35, 1985-1998.
- Hoefs, M.J.L., Rijpstra, W.I.C., Sinnighe Damsté, J.S., 2002. The influence of oxic degradation on the sedimentary biomarker record I: evidence from Madeira Abyssal Plain turbidites. *Geochim. Cosmochim. Acta* 66, 2719-2735.
- Huang, Y., Bol, R., Harkness, D.D., Ineson, P., Eglinton, G., 1996. Post-glacial variations in distributions, ^{13}C and ^{14}C contents of aliphatic hydrocarbons and bulk organic matter in three types of British acid upland soils. *Org. Geochem.* 24, 273-287.
- Huang, Y., Eglinton, G., Ineson, P., Latter, P.M., Bol, R., Harkness, D.D., 1997. Absence of carbon isotope fractionation of individual n-alkanes in a 23-year field decomposition experiment with *Calluna vulgaris*. *Org. Geochem.* 26, 497-501.
- IUSS Working Group WRB, 2006. World Reference Base for Soil Resources 2006. FAO, Rome.
- Jambu, P., Amblès, A., Diné, H., Secouet, B., 1991. Incorporation of natural hydrocarbons from plant residues into an hydromorphic humic podzol following afforestation and fertilization. *J. Soil. Sci.* 42, 629-636.
- Jansen, B., Nierop, K.G.J., 2009. Methyl ketones in high altitude Ecuadorian Andosols confirm excellent conservation of plant-specific n-alkane patterns. *Org. Geochem.* 40, 61-69.
- Jansen, B., Haussmann, N.S., Tonneijck, F.H., Verstraten, J.B., de Voegt, P., 2008. Characteristic straight-chain lipid ratios as a quick method to assess past forest-páramo transitions in the Ecuadorian Andes. *Palaeogeog. Paleoclim. Paleoecol.* 262, 129-139.
- Johnson, R.W., Calder, J.A., 1973. Early diagenesis of fatty acids and hydrocarbons in a salt marsh environment. *Geochim. Cosmochim. Acta* 37, 1943-1955.
- Jones, J.G., Young, B.V., 1970. Major paraffin constituents of microbial cells with particular references to *Chromatium* sp. *Arch. Mikrobiol.* 70, 82-88.
- Krimm, U., 2005. Untersuchungen zur Interaktion epiphyller Bakterien mit Blattoberflächen und Veränderungen in der Phyllosphäre während der Vegetationsperiode. Dissertation Thesis, Rheinische Friedrich-Wilhelms-Universität Bonn.
- Leahy, J.G., Colwell, R.R., 1990. Microbial degradation of hydrocarbons in the environment. *Microbiol. Rev.* 54, 305-315.
- Lehtonen, K., Ketola, M., 1993. Solvent-extractable lipids of sphagnum, carex, bryales and carex-bryales peats: content and compositional features vs peat humification. *Org. Geochem.* 20, 363-380.
- Liu, W., Huang, Y., 2005. Compound specific D/H ratios and molecular distributions of higher plant leaf waxes as novel paleoenvironmental indicators in the Chinese loess plateau. *Org. Geochem.* 36, 851-860.
- Maffei, M., 1996a. Chemotaxonomic significance of leaf wax n-alkanes in the Umbelliferae, Cruciferae and Leguminosae (Subf. Papilionoideae). *Biochem. Syst. Ecol.* 24, 531-545.
- Maffei, M., 1996b. Chemotaxonomic significance of leaf wax alkanes in the gramineae. *Biochem. Syst. Ecol.* 24, 53-64.

- Marseille, F., Disnar, J.R., Guillet, B., Noack, Y., 1999. n-Alkanes and free fatty acids in humus and A1 horizons of soils under beech, spruce and grass in the Massif-Central (Mont-Lozère), France. *Eur. J. Soil. Sci.* 50, 433-441.
- Mazeas, L., Budzinski, H., Raymond, N., 2002. Absence of stable carbon isotope fractionation of saturated and polycyclic aromatic hydrocarbons during aerobic bacterial biodegradation. *Org. Geochem.* 33, 1259-1272.
- Meyers, P.A., 1997. Organic geochemical proxies of paleoceanographic, paleolimnologic and paleoclimatic processes. *Org. Geochem.* 27, 213-250.
- Meyers, P.A., Ishiwatari, R., 1993. Lacustrine organic geochemistry – an overview of indicators of organic matter sources and diagenesis in lake sediments. *Org. Geochem.* 20, 867-900.
- Moucawi, J., Fustec, E., Jambu, P., 1981. Biooxidation of added and natural hydrocarbons in soils: effect of iron. *Soil Biol. Biochem.* 13, 335-342.
- Nguyen Tu, T. T., Derenne, S., Largeau, C., Mariotti, A., Bocherens, H., 2001. Evolution of the chemical composition of Ginkgo biloba external and internal leaf lipids through senescence and litter formation. *Org. Geochem.* 32, 45-55.
- Nishimura, M., Baker, E.W., 1986. Possible origin of n-alkanes with a remarkable even-to-odd predominance in recent marine sediments. *Geochim. Cosmochim. Acta* 30, 299-303.
- Rieley, G., Collier, R.J., Jones, D.M., Eglinton, G., 1991. The biogeochemistry of Ellesmere Lake, U.K. - I: source correlation of leaf wax inputs to the sedimentary lipid record. *Org. Geochem.* 17, 901-912.
- Rumpel, C., Seraphin, A., Goebel, M.-O., Wiesenberg, G., Gonzales-Vila, F., Bachmann, J., Schwark, L., Michaelis, W., Mariotti, A., Kögel-Knabner, I., 2004. Alkyl C and hydrophobicity in B and C horizons of an acid forest soil. *J. Plant Nutr. Soil Sci.* 167, 685-693.
- Sachse, D., Radke, J., Gleixner, G., 2006. δD values of individual n-alkanes from terrestrial plants along a climatic gradient. Implications for the sedimentary biomarker record. *Org. Geochem.* 37, 469-483.
- Schwark, L., Zink, K., Lechtenbeck, J., 2002. Reconstruction of postglacial to early Holocene vegetation history in terrestrial Central Europe via cuticular lipid biomarkers and pollen records from lake sediments. *Geology* 30, 463-466.
- Setti, L., Lanzarini, G., Pifferi, P.G., Spagna, G., 1993. Further research into the aerobic degradation of n-alkanes in a heavy oil by a pure culture of *A. pseudomonas* sp.. *Chemosphere* 26, 1151-1157.
- Stevens, J.F., Hart, H., Bolck, A., Zwaving, J.H., Malingré, T.M., 1994. Epicuticular wax composition of some European sedum species. *Phytochemistry* 35, 389-399.
- Tomescu, A.M.F., 2000. Evaluation of Holocene pollen records from the Romanian plain. *Rev. Paleobot. Palyno.* 109, 219-233.
- Weete, J.D., 1976. Algal and fungal waxes. In: Kolattukudy, P.E. (Ed.), *Chemistry and Biochemistry of Natural Waxes*, Elsevier, New York, pp. 349-418.
- Wiesenberg, G.L.B., Schwark, L., 2006. Molecular differentiation between numerous C₃- and C₄-crops. *Org. Geochem.* 37, 1973-1982.
- Wiesenberg, G.L.B., Lehndorff, E., Schwark, L., 2009. Thermal degradation of rye and maize straw: Lipid pattern changes as a function of temperature. *Org. Geochem.* 40, 167-174.
- Wiesenberg, G.L.B., Schwarzbauer, J., Schmidt, M.W.I., Schwark, L., 2004. Source and turnover of organic matter in agricultural soils derived from n-alkane/n-carboxylic acid compositions and C-isotope signatures. *Org. Geochem.* 35, 1371-1393.

- Wiesenberg, G.L.B., Schwarzbauer, J., Schmidt, M.W.I., Schwark, L., 2008a. Plant and soil lipid modification under elevated atmospheric CO₂ conditions: II. Stable carbon isotopic values ($\delta^{13}\text{C}$) and turnover. *Org. Geochem.* 38, 103-117.
- Wiesenberg, G.L.B., Schmidt, M.W.I., Schwark, L., 2008b. Plant and soil lipid modifications under elevated atmospheric CO₂ conditions: I. Lipid distribution patterns. *Org. Geochem.* 38, 91-102.
- Xie, S., Guo, J., Huang, J., Chen, G., Wang, H., Farrimond, P., 2004a. Restricted utility of $\delta^{13}\text{C}$ of bulk organic matter as a record of paleovegetation in some loess-paleosol sequences in the Chinese Loess Plateau. *Quaternary Res.* 62, 86-93.
- Xie, S., Lai, X., Yi, Y., Gu, Y., Liu, Y., Wang, X., Liu, G., Liang, B., 2003. Molecular fossils in a Pleistocene river terrace in southern China related to paleoclimate variation. *Org. Geochem.* 34, 789-797.
- Xie, S., Nott, C.J., Avseis, L.A., Maddy, D., Chambers, F.M., Evershed, R.P., 2004b. Molecular and isotopic stratigraphy in an ombrotrophic mire for paleoclimate reconstruction. *Geochim. Cosmochim. Acta* 68, 2849-2862.
- Xie, S., Wang, Z., Wang, H., Chen, F., An, C., 2002. The occurrence of a grassy vegetation over the Chinese Loess Plateau since the last interglacial: the molecular fossil record. *Sci. China Ser. D*, 45, 53-62.
- Zech, M., Glaser, B., 2008. Improved compound-specific delta C-13 analysis of n-alkanes for application in palaeoenvironmental studies. *Rapid Commun. Mass. Spectrom.* 22, 135-142.
- Zech, M., Buggle, B., Glaser, B., 2009. Should alkane biomarker results be corrected for degradation effects when reconstructing vegetation changes? *Geophysical research abstracts* 11, EGU2009-11386.
- Zech, M., Buggle, B., Leiber, K., Marković, S., Glaser, B., Hambach, U., Huwe, B., Stevens, T., Sümege, P., Wiesenberg, G., Zöller, L., 2010. Reconstructing Quaternary vegetation history in the Carpathian Basin, SE Europe, using n-alkane biomarkers as molecular fossils: problems and possible solutions, potential and limitations. *Quaternary Science Journal* 58 (2), 148-155..
- Zech, M., Buggle, B., Marković, S.B., Lucic, T., Stevens, T., Gaudenyi, T., Jovanovic, M., Huwe, B., Zöller, L., 2008. First alkane biomarker results for the reconstruction of the vegetation history of the Carpathian Basin (SE-Europe). *Abhandlungen der Geologischen Bundesanstalt* 62, 123-127.
- Zech, M., Zech, R., Morras, H., Moretti, L., Glaser, B., Zech, W., 2009a. Late Quaternary environmental changes in Misiones, subtropical NE Argentina, deduced from multiproxy geochemical analyses in a palaeosol-sediment sequence. *Quatern. Internat.* 196, 121-136.
- Zech, W., Zech, M., Zech, R., Peinemann, N., Morras, H.J.M., Moretti, L., Ogle, N., Kalim, R.M., Fuchs, M., Schad, P., Glaser, B., 2009b. Late Quaternary palaeosol records from subtropical (38°S) to tropical (16°S) South America and palaeoclimatic implications. *Quatern. Internat.* 196, 107-120.
- Zhang, H., Yang, M., Zhang, W., Lei, G., Chang, F., Pu, Y., Fan, H., 2008. Molecular fossil and paleovegetation records of paleosol S4 and adjacent loess layers in the Luochuan loess section, NW China. *Sci. China Ser. B*, 51, 321-330.
- Zhang, Z., Zhao, M., Eglinton, G., Lu, H., Huang, C.-Y., 2006. Leaf wax lipids as paleovegetational and paleoenvironmental proxies for the Chinese Loess Plateau over the last 170 kyr. *Quatern. Sci. Rev.* 25, 575-594.
- Zhou, W., Song, S., Burr, G., Jull, A.J.T., Lu, X., Yu, H., Cheng, P., 2007. Is there a time transgressive Holocene optimum in the East Asian monsoon area. *Radiocarbon* 49, 865-875.

Appendix

Table 6-A1. Concentration of n-alkane homologues in the modern soil of the Mircea Voda site.

| Modern soil - Mircea Voda | Sample depth [m] | C15 [µg/g] | C16 [µg/g] | C17 [µg/g] | C18 [µg/g] | C19 [µg/g] | C20 [µg/g] | C21 [µg/g] | C22 [µg/g] | C23 [µg/g] | C24 [µg/g] | C25 [µg/g] | C26 [µg/g] | C27 [µg/g] | C28 [µg/g] | C29 [µg/g] | C30 [µg/g] | C31 [µg/g] | C32 [µg/g] | C33 [µg/g] |
|---------------------------|------------------|------------|------------|------------|------------|------------|------------|------------|------------|------------|------------|------------|------------|------------|------------|------------|------------|------------|------------|------------|
| | 0 | 0.033 | 0.090 | 0.106 | 0.071 | 0.054 | 0.039 | 0.045 | 0.026 | 0.053 | 0.037 | 0.145 | 0.068 | 0.336 | 0.122 | 0.623 | 0.060 | 0.724 | 0.044 | 0.347 |
| | 0.225 | 0.027 | 0.080 | 0.079 | 0.073 | 0.048 | 0.042 | 0.044 | 0.029 | 0.046 | 0.034 | 0.103 | 0.047 | 0.199 | 0.079 | 0.336 | 0.033 | 0.387 | 0.024 | 0.185 |
| | 0.375 | 0.031 | 0.102 | 0.094 | 0.083 | 0.049 | 0.040 | 0.038 | 0.026 | 0.044 | 0.036 | 0.115 | 0.066 | 0.237 | 0.111 | 0.358 | 0.034 | 0.380 | 0.029 | 0.196 |
| | 0.525 | 0.034 | 0.092 | 0.094 | 0.091 | 0.061 | 0.048 | 0.046 | 0.027 | 0.047 | 0.034 | 0.108 | 0.068 | 0.207 | 0.095 | 0.265 | 0.025 | 0.248 | 0.019 | 0.110 |
| | 0.675 | 0.021 | 0.079 | 0.086 | 0.077 | 0.052 | 0.045 | 0.040 | 0.027 | 0.039 | 0.028 | 0.089 | 0.055 | 0.169 | 0.078 | 0.231 | 0.022 | 0.243 | 0.019 | 0.111 |
| | 0.825 | 0.016 | 0.057 | 0.068 | 0.068 | 0.047 | 0.038 | 0.038 | 0.021 | 0.038 | 0.026 | 0.102 | 0.065 | 0.213 | 0.089 | 0.305 | 0.028 | 0.344 | 0.029 | 0.159 |
| | 0.975 | 0.012 | 0.054 | 0.058 | 0.063 | 0.043 | 0.037 | 0.033 | 0.018 | 0.029 | 0.019 | 0.049 | 0.032 | 0.085 | 0.035 | 0.113 | 0.012 | 0.121 | 0.010 | 0.050 |

Table 6-A2. Concentration of n-alkane homologues in the loess-paleosol units S4 – S6 of the Mircea Voda site.

| Loess-Paleosol samples - Mircea Voda | Sample depth [m] | C15 [µg/g] | C16 [µg/g] | C17 [µg/g] | C18 [µg/g] | C19 [µg/g] | C20 [µg/g] | C21 [µg/g] | C22 [µg/g] | C23 [µg/g] | C24 [µg/g] | C25 [µg/g] | C26 [µg/g] | C27 [µg/g] | C28 [µg/g] | C29 [µg/g] | C30 [µg/g] | C31 [µg/g] | C32 [µg/g] | C33 [µg/g] |
|--------------------------------------|------------------|------------|------------|------------|------------|------------|------------|------------|------------|------------|------------|------------|------------|------------|------------|------------|------------|------------|------------|------------|
| (units S4 to S6) | 19.2 | 0.015 | 0.054 | 0.064 | 0.058 | 0.042 | 0.029 | 0.032 | 0.015 | 0.024 | 0.013 | 0.016 | 0.020 | 0.032 | 0.014 | 0.112 | 0.015 | 0.181 | 0.011 | 0.052 |
| | 19.5 | 0.027 | 0.083 | 0.107 | 0.086 | 0.053 | 0.062 | 0.048 | 0.023 | 0.026 | 0.018 | 0.022 | 0.032 | 0.040 | 0.028 | 0.101 | 0.017 | 0.156 | 0.013 | 0.052 |
| | 19.85 | 0.023 | 0.069 | 0.103 | 0.087 | 0.061 | 0.054 | 0.039 | 0.022 | 0.029 | 0.019 | 0.017 | 0.027 | 0.032 | 0.018 | 0.073 | 0.011 | 0.092 | 0.011 | 0.033 |
| | 20.75 | 0.015 | 0.044 | 0.049 | 0.046 | 0.034 | 0.027 | 0.031 | 0.014 | 0.028 | 0.017 | 0.030 | 0.038 | 0.050 | 0.025 | 0.205 | 0.026 | 0.254 | 0.018 | 0.105 |
| | 21.95 | 0.008 | 0.037 | 0.064 | 0.099 | 0.060 | 0.052 | 0.043 | 0.028 | 0.033 | 0.022 | 0.026 | 0.030 | 0.046 | 0.021 | 0.158 | 0.031 | 0.260 | 0.012 | 0.064 |
| | 22.35 | 0.014 | 0.045 | 0.048 | 0.046 | 0.032 | 0.026 | 0.031 | 0.012 | 0.025 | 0.011 | 0.013 | 0.026 | 0.033 | 0.014 | 0.118 | 0.019 | 0.232 | 0.014 | 0.079 |
| | 22.7 | 0.020 | 0.074 | 0.097 | 0.069 | 0.052 | 0.034 | 0.033 | 0.013 | 0.020 | 0.012 | 0.014 | 0.019 | 0.033 | 0.019 | 0.086 | 0.015 | 0.182 | 0.010 | 0.059 |
| | 23.2 | 0.026 | 0.089 | 0.111 | 0.067 | 0.045 | 0.040 | 0.027 | 0.009 | 0.014 | 0.009 | 0.013 | 0.016 | 0.028 | 0.016 | 0.078 | 0.016 | 0.152 | 0.011 | 0.053 |
| | 23.7 | 0.032 | 0.092 | 0.097 | 0.071 | 0.046 | 0.022 | 0.023 | 0.008 | 0.014 | 0.009 | 0.013 | 0.020 | 0.027 | 0.015 | 0.066 | 0.012 | 0.106 | 0.007 | 0.040 |
| | 24.2 | 0.014 | 0.050 | 0.069 | 0.066 | 0.043 | 0.038 | 0.036 | 0.017 | 0.027 | 0.017 | 0.011 | 0.029 | 0.016 | 0.013 | 0.033 | 0.009 | 0.043 | 0.006 | 0.020 |
| | 24.575 | 0.011 | 0.019 | 0.030 | 0.018 | 0.026 | 0.021 | 0.029 | 0.017 | 0.024 | 0.016 | 0.031 | 0.019 | 0.019 | 0.011 | 0.037 | 0.012 | 0.065 | 0.010 | 0.028 |
| | 24.85 | 0.019 | 0.074 | 0.116 | 0.096 | 0.065 | 0.057 | 0.047 | 0.029 | 0.031 | 0.020 | 0.011 | 0.017 | 0.015 | 0.007 | 0.036 | 0.008 | 0.054 | 0.006 | 0.023 |
| | 25.2 | 0.016 | 0.058 | 0.076 | 0.068 | 0.045 | 0.040 | 0.035 | 0.014 | 0.019 | 0.011 | 0.007 | 0.014 | 0.013 | 0.005 | 0.035 | 0.007 | 0.046 | 0.007 | 0.018 |
| | 25.5 | 0.013 | 0.046 | 0.057 | 0.050 | 0.036 | 0.027 | 0.025 | 0.011 | 0.016 | 0.007 | 0.005 | 0.015 | 0.016 | 0.005 | 0.036 | 0.006 | 0.060 | 0.007 | 0.023 |
| 25.9 | 0.016 | 0.059 | 0.091 | 0.066 | 0.054 | 0.035 | 0.031 | 0.014 | 0.019 | 0.012 | 0.011 | 0.017 | 0.025 | 0.012 | 0.050 | 0.010 | 0.079 | 0.009 | 0.029 | |

Study 7

Effect of leaf litter degradation and seasonality on D/H isotope ratios of n-alkane biomarkers

Michael Zech^{1,2*}, Nikolai Pedentchouk³, Björn Buggle², Katharina Leiber², Karsten Kalbitz⁴, Slobodan Marković⁵ and Bruno Glaser^{2,6}

¹Chair of Geomorphology, University of Bayreuth, D-95440 Bayreuth, Germany.

²Soil Physics Department, University of Bayreuth, D-95440 Bayreuth, Germany.

³School of Environmental Sciences, University of East Anglia, Norwich:NR4 7TJ, United Kingdom.

⁴Earth Surface Science, Institute for Biodiversity and Ecosystem Dynamics, University of Amsterdam, Nieuwe Achtergracht 166, 1018 WV Amsterdam, The Netherlands

⁵Chair of Physical Geography, University of Novi Sad, Trg Dositeja Obradovića 3, 21000 Novi Sad, Serbia

⁶Department of Terrestrial Biogeochemistry, Martin-Luther University Halle-Wittenberg, Weidenplan 14, D-06120 Halle, Germany

Geochimica Cosmochimica Acta

Submitted

*Corresponding author: Michael Zech, Phone:+49(0)921-552172
E-mail: michael_zech@gmx.de

Abstract

During the last decade, compound-specific hydrogen isotope analysis of plant leaf-wax and sedimentary *n*-alkyl lipids has become a promising tool for paleohydrological reconstructions. However, with the exception of several previous studies, there is a lack of knowledge regarding possible effects of early diagenesis on the δD values of *n*-alkanes. We therefore investigated the *n*-alkane patterns and δD values of long-chain *n*-alkanes from three different C3 higher plant species (*Acer pseudoplatanus L.*, *Fagus sylvatica L.* and *Sorbus aucuparia L.*) that have been degraded in a field leaf litterbag experiment for 27 months.

We found that after an initial increase of long-chain *n*-alkane amounts (up to ~50%), decomposition took place with mean turnover times of 11.7 months. Intermittently, the amounts of mid-chain *n*-alkanes increased significantly during periods of highest mass losses. Furthermore, initially high odd-over-even predominance declined and long-chain *n*-alkane ratios like $n\text{-C}_{31}/\text{C}_{27}$ and $n\text{-C}_{31}/\text{C}_{29}$ started to converge to the value of 1. While bulk leaf litter became systematically D-enriched especially during summer seasons (by ~8‰ on average over 27 months), the δD values of long-chain *n*-alkanes reveal no systematic overall shifts, but seasonal variations of up to 25‰ (*Fagus*, $n\text{-C}_{27}$, average ~13‰).

These findings suggest that a microbial *n*-alkane pool sensitive to seasonal variations of soil water δD rapidly builds up. We propose a conceptual model that accounts for the decomposition of plant-derived *n*-alkanes and the build-up of microbial *n*-alkanes. By this model, the measured *n*-alkane δD results can be explained. Since microbial ‘contamination’ is not necessarily discernible from *n*-alkane concentration patterns alone, care may have to be taken not to over-interpret δD values of sedimentary *n*-alkanes. Furthermore, since leaf-water is generally D-enriched compared to soil and lake waters, soil and water microbial *n*-alkane pools may help explain why soil and sediment *n*-alkanes are D-depleted compared to leaves.

Keywords: *n*-alkanes, hydrogen isotopes, leaf litter, soil, degradation, diagenesis, fractionation, seasonality, paleohydrology proxy.

1 Introduction

During the last decade compound-specific hydrogen isotope ratios (δD) of plant-derived *n*-alkanes in sediments and soils have become a popular paleoclimate proxy for reconstructing δD values of paleoprecipitation and for determining paleoaridity (Huang et al., 2004; Sachse et al., 2004; Xie et al., 2004; Liu and Huang, 2005; Pagani et al., 2006; Mügler et al., 2008; Zech et al., 2010b). This boom is based on several factors:

The isotopic composition of meteoric water (δD and $\delta^{18}\text{O}$) was found to depend on climate parameters such as temperature, continentality and precipitation amount (Craig, 1961; Dansgaard, 1964).

Albeit with a biosynthetic fractionation factor, plant photosynthetic products have the potential to record climate signals because their δD values are related to the source water δD values (Sternberg, 1988; Sessions et al., 1999; Sauer et al., 2001; Sachse et al., 2004).

n-Alkanes are considered to be relatively stable against degradation (Lichtfouse et al., 1998) and alkyl hydrogen atoms are less prone to exchange reactions in comparison with other biomarkers in geologically young, thermally immature sediments (Sessions et al., 2004; Pedentchouk et al., 2006; Dawson et al., 2007).

n-Alkanes originate from specific organisms and hence have the potential to serve as biomarkers (molecular fossils). For instance, long-chain *n*-alkanes with odd-over-even predominance (OEP) originate from terrestrial plant leaf waxes (Eglington and Hamilton, 1967; Kolattukudy, 1976), whereas short- and mid-chain *n*-alkanes in lacustrine sediments often serve as aquatic biomarkers (Ficken et al., 2000; Zech et al., 2009b; Aichner et al., 2010).

The methodological improvements allowed the online-coupling of gas chromatographs via a pyrolysis oven to isotope ratio mass spectrometers (GC-Py-IRMS) (Burgoyne and Hayes, 1998; Hilkert et al., 1999).

For a more detailed review about hydrogen isotopes (D/H) in sedimentary organic matter the reader is referred to Schimmelmann et al. (2006).

Several recent studies have identified various potential problems with interpretation of the δD values of sedimentary *n*-alkanes. First, several authors reported large interspecies δD differences under the same climatic conditions (Liu et al., 2006; Smith and Freeman, 2006; Hou et al., 2007; Feakins and Sessions, 2010). These results provide evidence that care must be taken when interpreting the δD values in the absence of knowledge about vegetation history. Second, within one plant species, variations among different *n*-alkanes were found to be up to 50‰. Furthermore, pronounced seasonal δD leaf-wax *n*-alkane shifts with up to 40‰ were reported (Pedentchouk et al., 2008; Sachse et al., 2009), which can be attributed to short turnover times and suggests that δD values of leaf litter being deposited on soils or in sediments only reflect the climatic conditions of the last weeks before leaf senescence. Third, the limited δD data from plant-soil/sediment systems (Chikaraishi and Naraoka, 2006; Sachse et al., 2006) indicate that long-chain *n*-alkanes of soils and sediments are depleted (by up to -57‰) compared to the fresh plant-derived *n*-alkanes. This finding can only be partly explained with the above mentioned seasonality effect and suggests that soil/sediment organic matter (SOM) formation may cause isotopic alterations, which have not yet been considered when reconstruction paleoclimatic and – hydrologic conditions. Hence, detailed biodegradation and reworking experiments are needed to clarify possible isotopic modifications in plant-soil systems.

In this study we aim to address this open question by presenting and discussing the *n*-alkane concentration patterns and compound-specific δD values of different leaf litter species, which have been decomposed in a field litterbag experiment for 27 months.

2 Material and methods

2.1 Litterbag experiment and samples

The site for the decomposition experiment and further details on the design of the litterbag experiment have been described in detail in separate publications (Gerstberger et al., 2004; Don and Kalbitz, 2005; Kalbitz et al., 2006). In brief, it is located in the Fichtelgebirge (Northeast Bavaria, Germany; 50°08'35''N, 11°52'10''E) and was covered by *Picea abies* for about 160 years. Elevation is 780 m a.s.l. and soil development has resulted in a sandy loam to loamy Albic Rustic Podzol (Wrb, 2006). The climate in the area is characterized by 1100 mm mean annual precipitation, a mean annual temperature of around 5 °C and a persistent snow cover during the winter season. δD values of the throughfall range from about -87‰ in the winter to -18‰ in the summer.

The litterbag experiment started in June 2001. Air-dried senescent foliage litter from 5 different species, including the three broad-leaf species *Acer pseudoplatanus L.*, *Fagus sylvatica L.* and *Sorbus aucuparia L.* were exposed in the field for 1, 3, 5, 9, 12, 16, 21 and 27 months. The litter from coniferous species *Picea abies L. (Karst.)* and *Pinus sylvestris L.* was not included in this study due to significantly lower *n*-alkane concentrations, making accurate compound-specific δD measurements impossible. The leaf litter was packed in bags made from nylon mesh and deposited on the forest floor simulating leaf litter accumulation. In order to account for the spatial variability of the decomposition processes, 12 plots (replications) were established at two neighbouring sites, resulting in 24 subsamples for each plant species at each harvesting time. The litterbags were completely covered by naturally fallen leaf litter after 1.5 years. At the end of each collection, leaf litter was cleaned manually to remove fungal hyphae, roots, shoots and insects. After drying and grinding, subsamples were combined for *n*-alkane and δD analyses. Together with the fresh non-degraded leaves, the here presented sample batch comprises 27 mixed samples in total.

Kalbitz *et al.* (2006) found that mass loss over the 27 months ranged from 26% (*Fagus*) to 58% (*Sorbus*). Estimating the relative contribution of cellulose and lignin and correcting for mass losses, they additionally observed a total cellulose decomposition ranging from 51% (*Fagus*) to 86% (*Sorbus*), whereas the total lignin decomposition reached only up to 11% (*Sorbus*) (Table 7-1).

Table 7-1. Mass loss of different leaf litter species (*Acer*, *Fagus* and *Sorbus*), relative depletion of cellulose and total cellulose decomposition, relative enrichment of lignin and total lignin decomposition (from Kalbitz *et al.* (2006)) and relative depletion of total *n*-alkanes ($\Sigma(n\text{-C}_{20}$ to $n\text{-C}_{35}$) and total *n*-alkane decomposition after 27 months of leaf litter degradation.

| Litter/property | <i>Acer</i> | | <i>Fagus</i> | | <i>Sorbus</i> | |
|--|-------------|----------------|--------------|------------|---------------|------------|
| | Fresh | Decomposed | Fresh | Decomposed | Fresh | Decomposed |
| Mass loss (%) | 0 | 43.5 | 0 | 26.0 | 0 | 57.7 |
| Cellulose ^a | 16.6 | 11.4 | 18.9 | 12.6 | 24.0 | 7.9 |
| Total cellulose decomposition (%) | 0 | 61.2 | 0 | 50.7 | 0 | 86.1 |
| Lignin ^b | 11.0 | 25.3 | 20.2 | 27.2 | 16.0 | 33.5 |
| Total lignin decomposition (%) | 0 | 0 ^c | 0 | 0.4 | 0 | 11.4 |
| $\Sigma(n\text{-C}_{20}\text{-}n\text{-C}_{35})$ ($\mu\text{g/g}$) | 228 | 85 | 371 | 85 | 398 | 125 |
| Total <i>n</i> -alkane decomposition (%) | 0 | 79.0 | 0 | 83.0 | 0 | 86.7 |

^avan Soest procedure: acid-detergent fibre - acid-detergent lignin: % of dry weight.

^bvan Soest procedure: acid-detergent lignin: % of dry weight.

^cindeed, a 30% accumulation was observed, which can be attributed to methodological shortcomings of the applied procedure

2.2 Analytical procedures

2.2.1 n-Alkane quantification

n-Alkanes from the leaf litter samples were prepared according to a slightly modified procedure described by Zech and Glaser (2008) in the Laboratory of the Department of Soil Physics, University of Bayreuth, Germany. Briefly, the procedure involves extraction of lipids with methanol/toluene (7/3) using an accelerated solvent extractor (ASE 200, Dionex, Germering, Germany) and purification of *n*-alkanes on silica/aluminium oxide (both 5% deactivated) columns with hexane/toluene (85/15) as eluent. 20 μg of 5 α -androstane and 40 μg

hexatriacontane ($n\text{-C}_{36}$) were added as internal and recovery standards, respectively. Quantification of the n -alkanes was performed on an HP 6890 gas chromatograph equipped with a flame ionization detector (FID). Note that sample A3 (*Acer*, 5 months) revealed inexplicable anomalies in the n -alkane pattern as well as in the δD values and was therefore excluded from further data evaluation and illustration. Turnover times (T) (mean residence times) for n -alkane decomposition were calculated based on a first-order kinetic model according to Eq. 1,

$$T = -\frac{1}{k} \quad (1)$$

where k is the decomposition rate, which is calculated according to Eq. 2.

$$k = \frac{\ln(\text{amount alkane}(t_2) - \text{amount alkane}(t_1))}{t_2 - t_1} \quad (2)$$

Data points for month 0 were excluded for the determination of the turnover times in order to account for the time lag of microbial activity.

2.2.2 Compound-specific δD analysis

δD values of $n\text{-C}_{27}$, $n\text{-C}_{29}$, and $n\text{-C}_{31}$ alkanes recovered from the leaf litter samples were determined in the Stable Isotope Laboratory at the University of East Anglia, UK using a Thermo Scientific Delta V Advantage isotope ratio mass spectrometer interfaced to a Thermo Scientific Trace GC Isolink. Individual n -alkanes were separated using an Agilent J&W DB-5 column (30 m x 0.25 mm x 0.25 μ film thickness). The GC oven was programmed from 50 °C (1 min) at 20 °C/min to 150 °C (0 min), then at 6 °C/min to 300 °C (5 min). Pyrolysis conversion of organic hydrogen to H_2 was achieved at 1420 °C. Hydrogen isotopic composition of n -alkanes is expressed relative to Vienna Standard Mean Ocean Water (VSMOW) based on an in-house reference gas adjusted daily using a squalane standard obtained from A. Schimmelmann, Indiana

University, USA. The margin of error for sample *n*-alkane δD measurements was no greater than $\pm 5\%$.

2.2.3 Bulk δD analysis

Bulk δD values of the leaf litter samples were determined in the Laboratory of Isotope Biogeochemistry of the Bayreuth Center of Ecology and Environmental Research (University of Bayreuth, Germany). For the thermal conversion, a TC/EA oven (HEKAtech, Wegberg, Germany) was coupled via a ConFlo III Interface (Thermo Fisher Scientific, Bremen, Germany) with a Delta V Plus isotope ratio mass spectrometer (Thermo Fisher Scientific). The standard deviation of bulk δD analyses is typically less than $\pm 2\%$. All δD values are expressed in per mil (‰) relative to the Vienna Standard Mean Ocean Water (VSMOW) based on an in-house reference gas (H_2 from Rießner-Gase GmbH, 96215 Lichtenfels, Germany, purity 6.0), which was calibrated using standards obtained from IAEA (VSMOW2, SLAP2 and IAEA-CH-7).

3 Results

3.1 *n*-Alkane concentrations, absolute *n*-alkane masses and *n*-alkane patterns

Kalbitz et al. (2006) found that mass losses over 27 months range from 26% (*Fagus*) to 58% (*Sorbus*). Fig. 7-1. illustrates that after starting the field experiment in June 2001, the most prominent mass losses occurred during autumn 2001 and autumn 2002, whereas no or less significant mass losses took place in March and June 2002 and for September 2003.

The *n*-alkane concentration patterns of the three investigated leaf litter species reveal high abundances of long-chain *n*-alkanes in the range from *n*-C₂₅ to *n*-C₃₁ with a strong odd-over-even predominance (OEP, Fig. 7-2), which is typical for leaf-wax *n*-alkanes. *Acer* leaf litter is dominated by *n*-C₂₇ and *n*-C₂₉, *Fagus* leaf litter strongly by *n*-C₂₇ and *Sorbus* leaf litter by *n*-C₂₉ and smaller amounts of *n*-C₃₁. Although the concentrations of these long-chain *n*-alkanes vary

substantially among the different leaf litter species, both Fig. 7-1 and Fig. 7-2 show that their concentrations decreased significantly after 27 months (on average from 154 to 37 $\mu\text{g/g}$ litter). This indicates that *n*-alkanes were more rapidly decomposed compared to other plant-derived organic compounds such as lignin and cellulose (Table 7-1). Kalbitz et al. (2006) reported that leaf litter lignin had on average almost doubled its concentration in the organic matter after 27 months. In this study, mean turnover times for long-chain *n*-alkanes range from 9.3 to 14.5 months (Table 7-2).

Interestingly, except for *n*-C₂₇ of *Fagus*, the *n*-alkane concentrations as well as the absolute *n*-alkane amount (referenced against the initial absolute *n*-alkane mass) (Fig. 7-1) did not decrease immediately when leaf litter degradation started. Instead, in July and September 2001, absolute *n*-alkane amount in the leaf litterbags increased by up to ~50% (*Acer n*-C₂₇ and *Sorbus n*-C₃₁). One may try explaining these findings by involving leaf litter sampling inhomogeneity. However, given the fact that each sample is a mixture of 24 subsamples from the field and based on the observation of the overall steady trends (except for *Fagus*, September 2001), our results suggest that there occurred either an *in situ* production or an additional input of long-chain *n*-alkanes from an external source during the first months. Only in the spring 2002, after 9 months of leaf litter degradation, concentrations of all long-chain *n*-alkanes started to decrease dramatically and also amounts fell considerably below the initial values until October 2002. After the rate of decrease slowed down in winter 2002/2003 (Fig. 7-1), decomposition accelerated again during summer 2003 and by September 2003 on average 85% of the *n*-alkanes were decomposed. Leaf litter degradation was also accompanied by commonly observed changes of *n*-alkane patterns. Originally high OEPs were levelled out (Fig. 7-1) and long-chain *n*-alkane ratios like *n*-C₃₁/*n*-C₂₇ and *n*-C₃₁/*n*-C₂₉ (Fig. 7-1) were converging to the value 1. This observation was recently used in order to suggest and apply models that account for degradation effects when reconstructing vegetation changes using long-chain *n*-alkane ratios in soils and

sediments (Zech et al., 2009a; Buggle et al., 2010; Zech et al., 2010a). Strikingly, the mid-chain n-alkanes ($\Sigma(n\text{-C}_{20}$ to $n\text{-C}_{24}$)), which are present not only in higher plant leaf-waxes but are known to be produced by microbial organisms (Jones, 1969; Grimalt et al., 1988; Ladygina et al., 2006), reveal different degradation patterns in comparison with the long-chain n-alkanes.

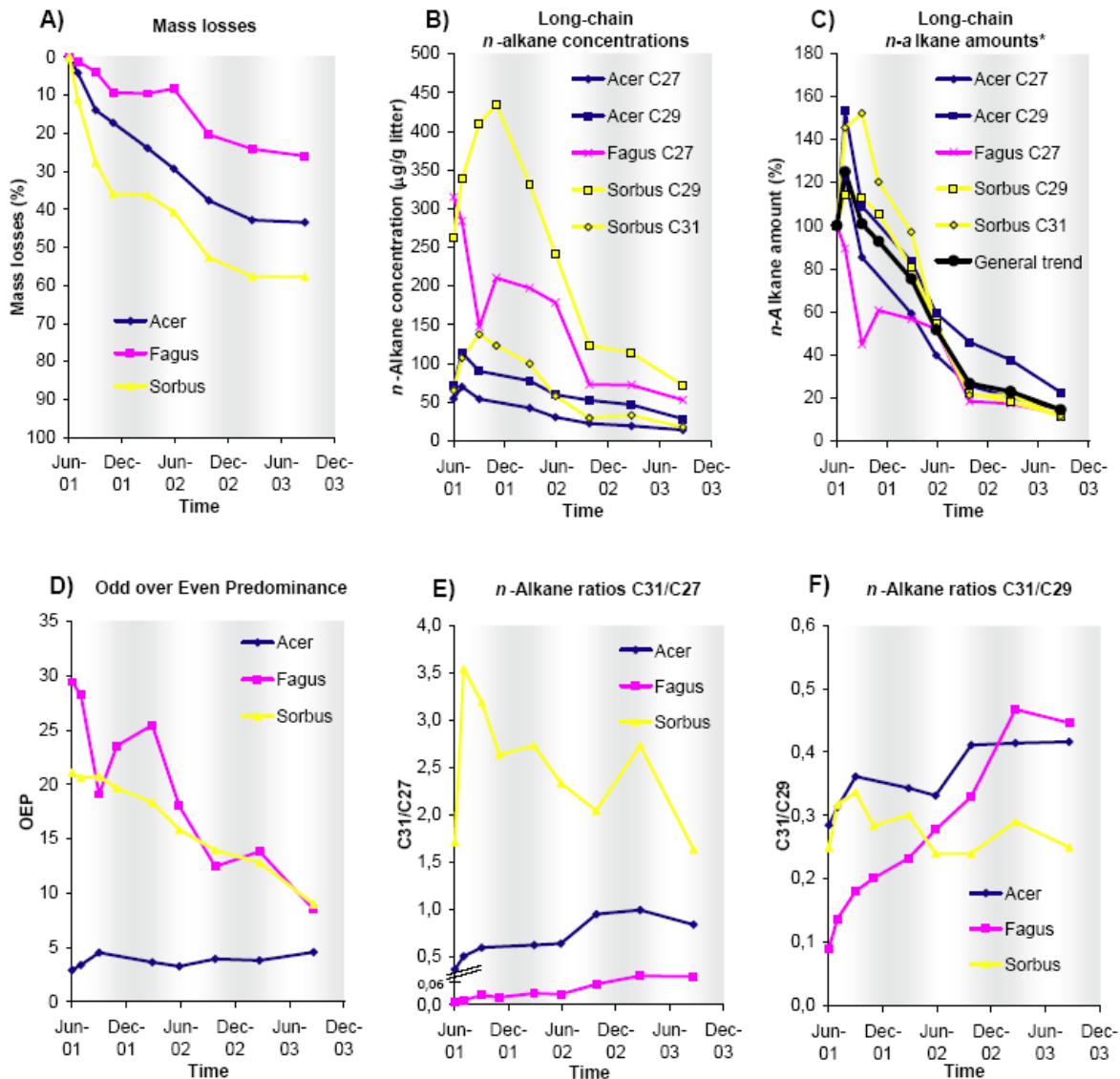


Fig. 7-1. Mass losses a) from Kalbitz et al. (2006) and long-chain n-alkane characteristics for three different leaf litter species (*Acer*, *Fagus* and *Sorbus*) during 27 months of leaf litter degradation in a field experiment. b) n-Alkane concentrations, c) n-alkane amounts, d) odd-over-even predominance and e), f) n-alkane ratios. Bright background indicates summer, dark one winter. *Referenced against the initial amount (month 0 = 100%).

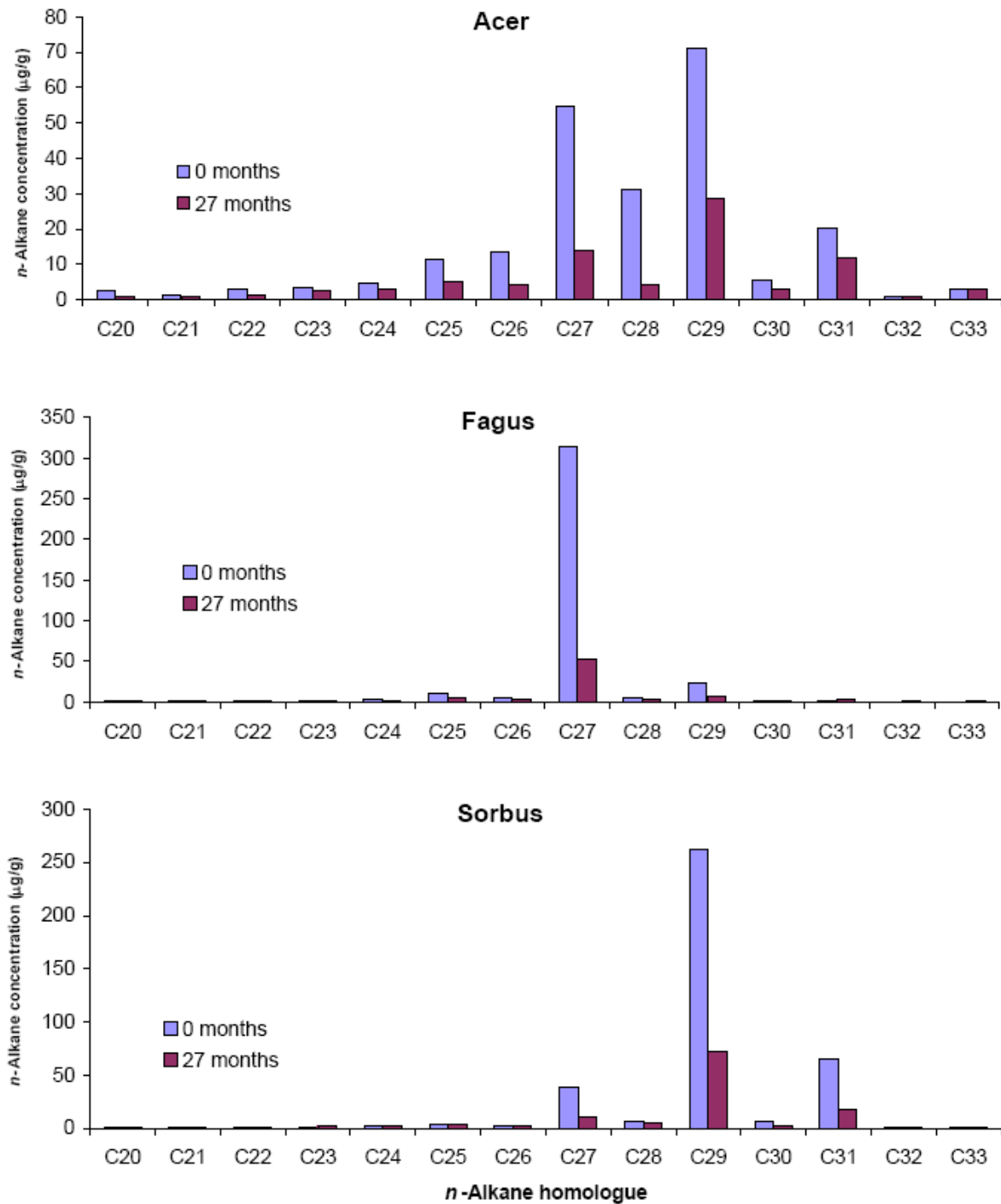


Fig. 7-2. n-Alkane concentration patterns of three different leaf litter species (*Acer*, *Fagus* and *Sorbus*) before (0 months) and after (27 months) leaf litter degradation in a field experiment.

Firstly, they occur in lower concentrations (Fig. 7-2 and Fig. 7-3) and show much less decrease during 27 months of leaf litter degradation (from 6.1 to 4.9 µg/g litter and mean turnover time of 34.1 months; Table 7-2).

Table 7-2. Rates of decomposition, coefficients of correlation for a first order decay and turnover times for mid- and long-chain n-alkanes of three leaf litter species (*Acer*, *Fagus* and *Sorbus*) during 27 months of leaf litter degradation.

| | <i>Acer</i> | | | <i>Fagus</i> | | <i>Sorbus</i> | | | Mean | |
|----------------|-----------------------------|---------------------------|---------------------------|-----------------------------|---------------------------|-----------------------------|---------------------------|---------------------------|-----------------------------|--------------------------------------|
| | $\Sigma(n-C_{20}-n-C_{24})$ | <i>n</i> -C ₂₇ | <i>n</i> -C ₂₉ | $\Sigma(n-C_{20}-n-C_{24})$ | <i>n</i> -C ₂₇ | $\Sigma(n-C_{20}-n-C_{24})$ | <i>n</i> -C ₂₉ | <i>n</i> -C ₃₁ | $\Sigma(n-C_{20}-n-C_{24})$ | $\Sigma(n-C_{27},n-C_{29},n-C_{31})$ |
| k | -0,030 | -0,082 | -0,069 | -0,013 | -0,073 | -0,045 | -0,099 | -0,108 | -0,029 | -0,086 |
| R ² | 0,61 | 0,98 | 0,98 | 0,23 | 0,85 | 0,77 | 0,95 | 0,95 | 0,64 | 0,97 |
| T (months) | 33,1 | 12,2 | 14,5 | 80,0 | 13,8 | 22,1 | 10,1 | 9,3 | 34,1 | 11,7 |

k = decomposition rate; R² = coefficient of correlation for a first order kinetics decay, T = turnover time in months

Secondly, the trends are often reversed when compared to the long-chain n-alkanes. While in spring and summer 2002 the long-chain n-alkanes were decomposed fastest and their decrease also accelerated again in summer 2003, the mid-chain n-alkane amounts were increasing during these periods (Fig. 7-3). Hence, we suggest that the increase in mid-chain n-alkanes concentrations and amounts may be the result of soil microbial activity, whereas the long-chain n-alkanes increasingly represent a mixed pool of decomposing plant-derived n-alkanes and *in situ* produced microbial n-alkanes or externally introduced n-alkanes. Further evidence for questioning the long established belief that long-chain n-alkanes in soils predominantly derive from plants comes from the D/H isotopic signature of the individual long-chain n-alkanes.

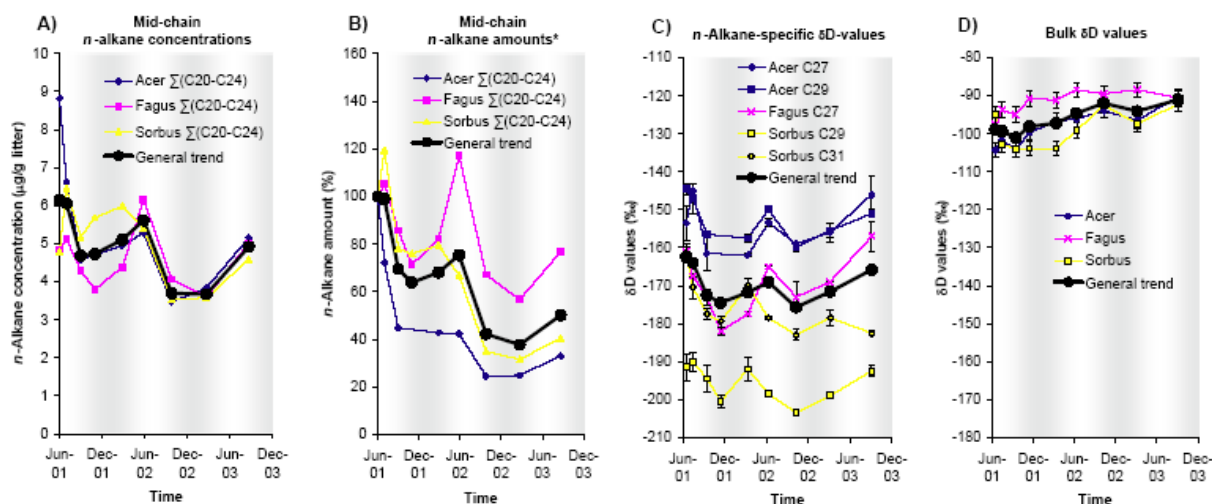


Fig. 7-3. a) Mid-chain n-alkane concentrations ($\Sigma(n-C_{20}$ to $n-C_{24})$), b) mid-chain n-alkane amounts ($\Sigma(n-C_{20}$ to $n-C_{24})$), c) compound-specific δD -values of the most abundant individual n-alkanes and d) bulk δD -values for three different leaf litter species (*Acer*, *Fagus* and *Sorbus*) during 27 months of leaf litter degradation in a field experiment. Bright background indicates summer, dark one winter. *Referenced against the initial amount (month 0 = 100%).

3.2 Compound-specific δD values of individual n-alkanes

Fig. 7-3 illustrates that bulk organic matter experienced systematic δD enrichment during leaf litter degradation especially in the summers 2002 and summer 2003 (on average from -99 to -91‰). This can be caused by the preferential removal of relatively D-depleted organic compounds, and/or by the exchange of organically bound hydrogen atoms in organic compounds with reactive functional groups, such as carboxyl and hydroxyl groups (Schimmelmann et al., 2006) with D-enriched soil water.

The long-chain alkanes $n\text{-C}_{27}$, $n\text{-C}_{29}$, and $n\text{-C}_{31}$ in the broad-leaf litter species are significantly depleted in deuterium compared to bulk organic matter, with δD values of *Acer* n-alkanes ranging from -145 to -162‰, *Fagus* from -157 to -182‰ and *Sorbus* from -162 to -204‰ (Fig. 7-3). While bulk δD values show no seasonal variations, δD values of all 5 analysed individual n-alkanes reveal systematic variations, which are strikingly similar to those of mid-chain n-alkane concentrations and amounts (Fig. 7-3). On average, n-alkanes become depleted by about 12‰ from June to November 2001. In March and June 2002, when mid-chain n-alkanes indicate *in situ* production of microbial n-alkanes (Fig. 7-3), mean δD values increase by about 5‰ but become more negative again in October (about 6‰). In contrast, March and September 2003 are characterised by D-enrichment (about 10‰), which is once again accompanied by an increase of the mid-chain n-alkanes. Similar to the n-alkane concentration and amount patterns mentioned above, the seasonal patterns in the δD values of the n-alkanes also suggest that the long-chain n-alkanes do not explicitly derive from the degrading leaf litter. Even though the overall absolute and relative concentrations of long-chain n-alkanes steadily decrease during the experiment (Fig. 7-1), the trend may conceal not only the periodic contributions in the spring/summer months, but also a gradual build-up of n-alkanes from another source. We argue that there is an additional n-alkane source, which is sensitive to the seasonal δD variations of the precipitation ranging from about -87‰ in the winter to -18‰ in the summer.

4 Discussion

4.1 Absence of D/H exchange reaction and negligible fractionation during biodegradation

Temporal shifts of bulk organic matter δD values during leaf litter decomposition and diagenesis can be explained by the preferential removal of isotopically different labile organic compounds. Furthermore, organically bound hydrogen atoms present in certain functional groups (e.g. in carboxyl and hydroxyl groups) are prone to hydrogen exchange reactions with surrounding water (Schimmelmann et al., 2006). While these processes may account for the observed bulk δD shifts in our litterbag experiment, they are unlikely to explain the observed δD variations of individual n-alkanes (Fig. 7-3). It is generally accepted that even over geological timescales post-depositional processes do not significantly affect δD values of sedimentary n-alkanes (Yang and Huang, 2003; Sessions et al., 2004; Pedentchouk et al., 2006; Dawson et al., 2007).

Another possible process, which has to be considered when searching for explanations for our n-alkane δD litterbag results is fractionation due to biodegradation. Pond et al. (2002) have shown in a biodegradation study of crude oil that due to preferential decomposition of D-depleted n-alkanes, remaining short-chain n-alkanes became D-enriched by up to ~25%. However, the authors also reported that the D/H composition of long-chain n-alkanes was relatively stable. Although we cannot completely rule out a minor effect of biodegradation on our n-alkane δD results, fractionation cannot explain the seasonal variations, which we found during leaf litter degradation.

4.2 Possible sources of the new long-chain n-alkanes

In our litterbag experiment, neither the initial increase of long-chain n-alkanes (Fig. 7-1) nor the intermittent increase of mid-chain n-alkanes (Fig. 7-3) nor the δD variations of individual n-alkanes (Fig. 7-3) can be explained solely by the decomposition of plant-derived leaf-wax n-

alkanes in the litter. Therefore, we argue that a significant pool of additional n-alkanes started to affect the amount of leaf litter n-alkanes shortly after the experiment was set up. Both the quantitative role and the D/H composition of this additional pool seem to depend on the season. Recently, significant seasonal δD shifts of up to $\sim 40\text{‰}$ were reported for leaf-wax n-alkanes (Pedentchouk et al., 2008; Sachse et al., 2009). Furthermore, it is well known that abrasion from leaf-surfaces produces aerosols reflecting the leaf-wax lipid composition (Rogge et al., 1993; Simoneit, 2005; Andreou and Rapsomanikis, 2009). Consequently, the deposition of these aerosols on forest soils and our litterbags may partly account for the observed increases of n-alkane amounts (Fig. 7-1) and the seasonal pattern of n-alkane specific δD values (Fig. 7-3). However, the additional input of higher plant leaf-wax lipids by aerosols can neither explain sufficiently the mid-chain n-alkane increases (Fig. 7-3) nor the systematic trends of OEPs and n-alkane ratios (Fig. 7-1) in our samples.

Many bacteria produce n-alkane distribution patterns ranging from C11 to C35 often without any OEP (Ladygina et al., 2006). By this, n-alkanes from bacterial and higher plant-leaf waxes can be distinguished. The n-alkane patterns of many fungi (e.g. *Aspergillus sp.*) resemble those of the bacteria. For instance, Jones (1969) and Weete (1972) reported on many soil microorganisms having no OEP and n-alkane patterns maximising in the range from n-C₂₇ to n-C₃₁. Last but not least, Grimalt et al. (1988) found that the wet storage of sediment samples produced mid-chain n-alkanes with no OEP. Distinguishing between these two sources is possible because many bacteria produce n-alkane distribution patterns ranging from C11 to C35 often without any OEP (Ladygina et al., 2006). Hence we hypothesize that a microbial n-alkane pool in our leaf litter samples could be responsible for the observed increases of mid- and long-chain n-alkane amounts, the declining OEPs and the seasonal δD variations.

n-Alkanes mainly of bacterial origin were also detected in throughfall and stem water, presumably occurring especially in colloidal dispersion (Colina-Tejada et al., 1996). In the

present study, it is not possible to exclude such a contribution from canopy bacteria. However, in comparison with in situ microbial activity in soil and the litter layer, this appears as a minor source.

4.3 Modelling leaf litter *n*-alkane decay and built-up of a microbial *n*-alkane pool – explaining the seasonality of the *n*-alkane δ D results

While it is argued that the plant leaf-wax *n*-alkanes in the litter have not undergone any significant isotopic shift during biodegradation (Section 4.1), the postulated soil microbial *n*-alkane pool (Section 4.2) is not only variable in its amount over time due to its built-up and simultaneous decomposition, but also susceptible to variations in δ D of precipitation and soil water, because soil microorganisms incorporate this isotopic signature during biosynthesis.

In the following, a conceptual model is set up assessing the effects of the decay of leaf-wax *n*-alkanes, the built-up of a microbial *n*-alkane pool and changes in the total *n*-alkane pool (Fig. 7-4). Accordingly, the decay of plant derived *n*-alkanes starts with a two-month time lag; the decomposition rate is decreasing in winter months and increasing in summer months. δ D values of the plant-derived *n*-alkanes remain constant at -160‰ over the period of leaf litter degradation. It is assumed that there is an increase in the amount of microbial *n*-alkanes during the first several months as well as during the following spring and early summer, when plenty of easily degradable organic compounds from fresh leaf litter are available. Slight decreases are assumed for the winter months and the year 2003 because of lower temperatures and less favourable substrate conditions. Furthermore, the contribution of newly synthesized *n*-alkanes versus ‘old’ microbial *n*-alkanes is estimated based on expected microbial activity, which is low in the winter, high in the spring/summer and gradually decreases from year to year (Fig. 7-4). δ D values of newly synthesized *n*-alkanes are calculated by presuming a D-depletion of approximately -160‰ during biosynthesis (Sachse et al., 2006) relative to δ D of the source water

(Fig. 7-4). δD values of total microbial *n*-alkanes were calculated from newly synthesized and ‘old’ *n*-alkanes using a mass balance equation. Finally, the total *n*-alkane δD values were determined by summing up the total microbial and the plant-derived *n*-alkanes using a mass balance equation.

δD values resulting from this conceptual model for the litterbag experiment show the same seasonal trends as the measured δD values. Also amplitudes of δD variations are very similar (Fig. 7-4). The only outlier is September 2003, where more positive measured δD values can be possibly explained by the 2003 European heat wave. This finding provides support for the idea that leaf litter decomposition is accompanied by a simultaneous build-up of a microbial *n*-alkane pool, which can cause seasonal variations of long-chain *n*-alkane δD values of up to 25‰ in the case of *n*-C₂₇ in *Fagus* litter (average value 13‰).

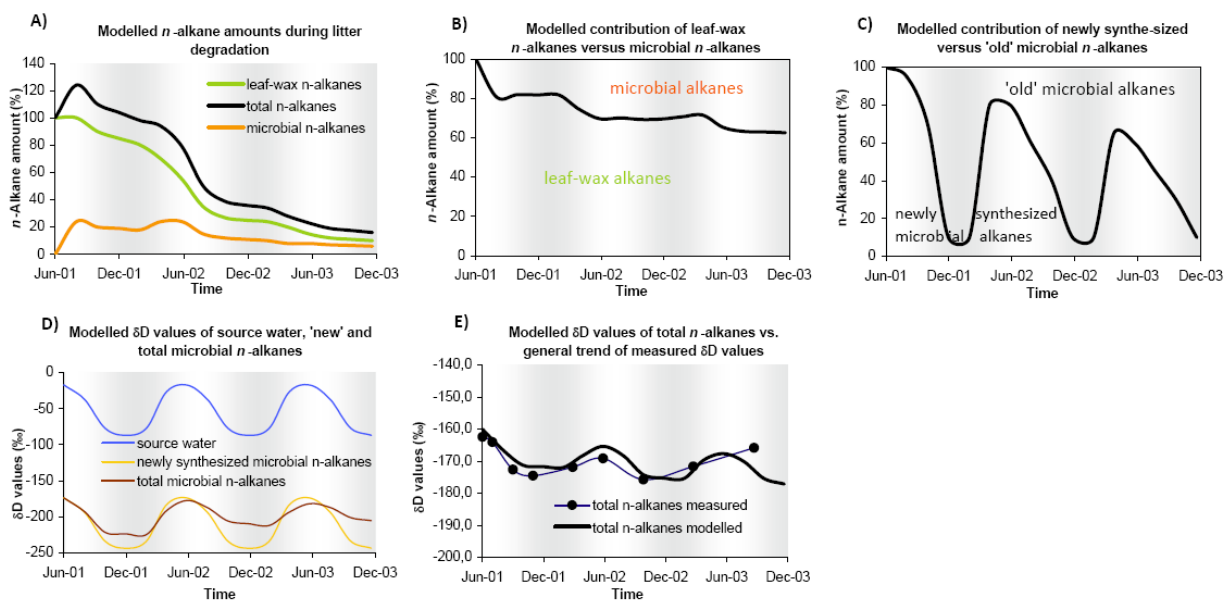


Fig. 7-4. a) and b) Modelled total, plant and microbial *n*-alkane amounts, c) modelled contribution of newly synthesized microbial *n*-alkanes versus ‘old’ ones, d) modelled δD values for source water, newly synthesized and total microbial *n*-alkanes and e) comparison of modelled total *n*-alkane δD values with mean measured δD values. Bright background indicates summer, dark one winter.

4.4 Implications for turnover-times, origin of long-chain *n*-alkanes in soils/sediments and δD values of *n*-alkanes as paleoclimate proxy.

Seasonal δD variations of leaf-wax *n*-alkanes have already been reported (Pedentchouk et al., 2008; Sachse et al., 2009). The authors concluded that *n*-alkanes in plant leaf waxes have very short turnover times (within weeks). For comparison, we calculated mean *n*-alkane turnover times for leaf litter decomposition of around 11.7 months (Table 7-2) and assumed for our model the microbial *n*-alkane pool to be renewed by 60% to 80% within 2 months during summer seasons. Nevertheless, we are aware that under steady-state conditions in soils, where more *n*-alkanes are protected against degradation e.g. in microaggregates, turnover times will be much longer. For instance, Wiesenberg et al. (2004) reported turnover times of *n*-alkanes in cropped soils ranging from 35 to 60 years.

Sachse et al. (2009) furthermore concluded from their results that the isotopic signal reaching soils and sediments represents only the last weeks before leaf senescence. Since D-enrichment by evapotranspiration in soil and leaf-water is less pronounced in autumn compared to summer, the δD values of *n*-alkanes in leaf litter are more negative than in fresh leaves. The strong influence of D-enrichment in leaf-water due to transpiration on δD values of plant waxes was recently also demonstrated by Feakins and Sessions (2010). Accordingly, this finding can partly explain the significant D-depletion of up to 94‰ (average 55‰) observed by Chikaraishi and Naraoka (2006) for the transition from fresh leaves to soils. However, it can not explain the progressive depletion from leaf litter to mold and finally soil. The δD results from our litterbag experiment support the idea that microbial reworking during leaf litter degradation is responsible for this depletion, because soil microorganisms use soil water as source, whereas plants incorporate D-enriched leaf-water. Further studies should explore the extent of seasonal variations in δD values of *n*-alkanes in microbially active topsoils.

The *n*-alkane concentration pattern (Fig. 7-2), the discussion about microbial *n*-alkane sources (Section 4.2) and the model explaining the seasonal δD variations (Section 4.3.) have shown that even when *n*-alkane patterns still look very characteristic for leaf-waxes, significant amounts of *n*-alkanes can be contributed by microorganisms. Furthermore, microorganisms typically reveal high abundances of mid-chain *n*-alkanes and are also able to produce short-chain *n*-alkanes. Hence, virtually all *n*-alkanes which are used as biomarkers for terrestrial or aquatic plants in paleoclimate studies of lake sediments can potentially be influenced by early degradation as well as by eroded or leached soil organic matter. Firstly, this may help explaining *n*-alkane pattern differences between lacustrine sediments and dominant vegetation in the catchment as for instance described by Sachse et al. (2006). Secondly, these soil microbial *n*-alkane pools have more negative δD values than terrestrial plants (leaf-water D-enrichment) and at the same time can be supposed to have more positive δD values (soil water enrichment) than aquatic plants except for semi-arid and arid ecosystems like Tibetan Plateau (Mügler et al., 2008). Our results suggest that paleoclimate studies using δD values as a proxy for paleohydrology should consider not only paleovegetation history (Liu et al., 2006; Smith and Freeman, 2006; Feakins and Sessions, 2010), but also potential contribution of organic compounds from microbial biomass with different δD signature.

5 Conclusions

Aiming at contributing to the discussion whether *n*-alkane biomarkers and especially the paleoclimate proxy δD of long-chain *n*-alkanes is affected by early diagenesis/decomposition, we investigated three different broad-leaf litter species, which have been degraded in the field for 27 months. From our results and the discussion we draw several conclusions:

- Concentrations and amounts of plant leaf-wax *n*-alkanes are decreasing rapidly during leaf litter decomposition (~85% in 27 months, mean turnover time around 11.7 months).

-
- Leaf litter degradation is accompanied by characteristic changes of the *n*-alkane patterns, namely the decrease of originally high OEPs and the convergence of long-chain *n*-alkane ratios to the value 1. This should be taken into account when trying to reconstruct vegetation changes based on *n*-alkane patterns (Zech et al., 2009a).
 - Changing *n*-alkane patterns, initial long-chain *n*-alkane increases and intermittent mid-chain *n*-alkane increases indicate that a microbial *n*-alkane pool is rapidly build up and starts to overprint the original *n*-alkane patterns of decomposing leaf litter.
 - The build-up of a microbial *n*-alkane pool, which is susceptible to δD variations of source water, can cause seasonal δD variations in decomposing leaf litter of up to 25‰ (*Fagus*, *n*-C₂₇, average 13‰). A respective conceptual model is proposed and supports this idea.
 - The build-up of a microbial *n*-alkane pool can be made responsible for the observed shift in δD values from fresh leaf litter to soil and sediments. This should be kept in mind when applying the *n*-alkane δD paleoclimate proxy to terrestrial paleosols.
 - Similarly, unless SOM erosion/leaching and early leaf litter degradation can be excluded, also δD values of long-chain *n*-alkanes in lacustrine sediments are likely to reflect a mixed plant and microbial signal rather than a solely plant leaf-wax signal. Short- and mid-chain *n*-alkanes are not exclusive biomarkers for aquatic plants either, but can be produced by soil microorganisms, too. Therefore care must be taken when interpreting δD values of sedimentary *n*-alkanes.

Acknowledgements

We would like to thank A. Mergner and M. Tuthorn (University of Bayreuth, Germany) for support during laboratory work and all members of PAST research group from BayCEER, University of Bayreuth, for intensive discussions. Our work also greatly profited from generous logistic support provided by Prof. B. Huwe (University of Bayreuth), Prof. L. Zöllner (University

of Bayreuth) and Prof. Z. Svirčev (University of Novi Sad, Serbia). We are also very grateful to Prof. G. Gebauer and his team (University of Bayreuth) for conducting the TC/EA-IRMS measurements, to C. Bogner (University of Bayreuth) for providing isotope data of precipitation from Waldstein locality and to Dr. J. Lüers (University of Bayreuth) for providing climate data from the Fichtelgebirge. The study was partly funded by the German Research Foundation (DFG: ZE 844/1-1) and RCUK Fellowship to N. Pedentchouk. M. Zech also greatly acknowledges the support given by the Alexander von Humboldt-Foundation.

References

- Aichner B., Herzschuh U., and Wilkes H. (2010) Influence of aquatic macrophytes on the stable carbon isotopic signatures of sedimentary organic matter in lakes on the Tibetan Plateau. *Organic Geochemistry* **41**(7), 706-718.
- Andreou G. and Rapsomanikis S. (2009) Origins of n-alkanes, carbonyl compounds and molecular biomarkers in atmospheric fine and coarse particles of Athens, Greece. *Science of Total Environment* **407**, 5750-5760.
- Buggle B., Wiesenberg G., and Glaser B. (2010) Is there a possibility to correct fossil n-alkane data for postsedimentary alteration effects? *Applied Geochemistry* **25**(7), 947-957.
- Burgoyne T. and Hayes J. M. (1998) Quantitative production of H₂ by pyrolysis of gas chromatographic effluents. *Analytical Chemistry* **70**, 5136-5141.
- Chikaraishi Y. and Naraoka H. (2006) Carbon and hydrogen isotope variation of plant biomarkers in a plant–soil system. *Chemical Geology* **231**, 190-202.
- Colina-Tejada A., Amlès A., and Jambu P. (1996) Nature and origin of soluble lipids shed into the soil by rainwater leaching a forest cover of *Pinus maritima* sp. *European Journal of Soil Science* **47**, 637-643.
- Craig H. (1961) Isotopic variations in meteoric waters. *Science* **133**, 1702-1703.
- Dansgaard P. (1964) Stable isotopes in precipitation. *Tellus* **16**, 436-468.
- Dawson D., Grice K., Alexander R., and Edwards D. (2007) The effect of source and maturity on the stable isotopic compositions of individual hydrocarbons in sediments and crude oils from the Vulcan Sub-basin, Timor Sea, Northern Australia. *Organic Geochemistry* **38**, 1015-1038.
- Don A. and Kalbitz K. (2005) Amounts and degradability of dissolved organic carbon from foliar litter at different decomposition stages. *Soil Biology and Biochemistry* **37**, 2171-2179.
- Eglinton G. and Hamilton R. (1967) Leaf epicuticular waxes. *Science* **156**, 1322-1334.
- Feakins S. and Sessions A. (2010) Controls on the D/H ratios of plant leaf waxes in an arid ecosystem. *Geochimica et Cosmochimica Acta* **74**, 2128-2141.
- Ficken K. J., Li B., Swain D. L., and Eglinton G. (2000) An n-alkane proxy for the sedimentary input of submerged/floating freshwater aquatic macrophytes. *Organic Geochemistry* **31**, 745-749.
- Gerstberger P., Foken T., and Kalbitz K. (2004) The Lehstenbach and Steinkreuz catchments in NE Bavaria, Germany. In *Biogeochemistry of Forested Catchments in a Changing*

- Environment: a German Case Study* (ed. E. Matzner), pp. 15-44. Ecological Studies 172, Springer.
- Grimalt J., Torras E., and Albaiges J. (1988) Bacterial reworking of sedimentary lipids during sample storage. *Organic Geochemistry* **13**, 741-746.
- Hilkert A., Douthitt C., Schlüter H., and Brand W. (1999) Isotope ratio monitoring gas chromatography/mass spectrometry of D/H by high temperature conversion isotope ratio mass spectrometry. *Rapid Communications in Mass Spectrometry* **13**, 1226-1230.
- Hou J., D'Andrea W., MacDonald D., and Huang Y. (2007) Hydrogen isotopic variability in leaf waxes among terrestrial and aquatic plants around Blood Pond, Massachusetts (USA). *Organic Geochemistry* **38**, 977-984.
- Huang Y., Shuman B., Wang Y., and Webb III T. (2004) Hydrogen isotope ratios of individual lipids in lake sediments as novel tracers of climatic and environmental change: a surface sediment test. *Journal of Paleolimnology* **31**, 363-375.
- Jones J. G. (1969) Studies on Lipids of Soil Micro-organisms with Particular Reference to Hydrocarbons. *J. gen. Microbiol.* **59**, 145-152.
- Kalbitz K., Kaiser K., Bargholz J., and Dardenne P. (2006) Lignin degradation controls the production of dissolved organic matter in decomposing foliar litter. *European Journal of Soil Science* **57**, 504-516.
- Kolattukudy P. E. (1976) Biochemistry of plant waxes. In *Chemistry and Biochemistry of Natural Waxes* (ed. P. E. Kolattukudy), pp. 290-349. Elsevier.
- Ladygina N., Dedyukhina E., and Vainshtein M. (2006) A review on microbial synthesis of hydrocarbons. *Process Biochemistry* **41**, 1001-1014.
- Lichtfouse E., Chenu C., Baudin F., Leblond C., Silva M., Behar F., Derenne S., Largeau C., Wehrung P., and Albrecht P. (1998) A novel pathway of soil organic matter formation by selective preservation of resistant straight-chain biopolymers: chemical and isotope evidence. *Organic Geochemistry* **28**(6), 411-415.
- Liu W. and Huang Y. (2005) Compound specific D/H ratios and molecular distributions of higher plant leaf waxes as novel paleoenvironmental indicators in the Chinese Loess Plateau. *Organic Geochemistry* **36**, 851-860.
- Liu W., Yang H., and Li L. (2006) Hydrogen isotopic compositions of n-alkanes from terrestrial plants correlate with their ecological life forms. *Oecologia* **150**, 330-338.
- Mügler I., Sachse D., Werner M., Xu B., Wu G., Yao T., and Gleixner G. (2008) Effect of lake evaporation on δD values of lacustrine n-alkanes: A comparison of Nam Co (Tibetan Plateau) and Holzmaar (Germany). *Organic Geochemistry* **39**, 711-729.
- Pagani M., Pedentchouk N., Huber M., Sluijs A., Schouten S., Brinkhuis H., Damste J. S. S., Dickens G., and Expedition 302 Scientists. (2006) Arctic hydrology during global warming at the Palaeocene/Eocene thermal maximum. *Nature* **442**, 671-675.
- Pedentchouk N., Freeman K. H., and Harris N. (2006) Different response of δD values of n-alkanes, isoprenoids, and kerogen during thermal maturation. *Geochimica et Cosmochimica Acta* **70**, 2063-2072.
- Pedentchouk N., Sumner W., Tipple B., and Pagani M. (2008) $\delta^{13}C$ and δD compositions of n-alkanes from modern angiosperms and conifers: An experimental set up in central Washington State, USA. *Organic Geochemistry* **39**, 1066-1071.
- Pond K., Huang Y., Wang Y., and Kulpa C. (2002) Hydrogen Isotopic Composition of Individual n-Alkanes as an Intrinsic Tracer for Bioremediation and Source Identification of Petroleum Contamination. *Environmental Science & Technology* **36**, 724-728.
- Rogge W., Hildemann L., Mazurek M. A., Cass G., and Simoneit B. R. T. (1993) Sources of fine organic aerosol. 4. Particulate abrasion products from leaf surfaces of urban plants. *Environmental Science & Technology* **27**, 2700-2711.

- Sachse D., Kahmen A., and Gleixner G. (2009) Significant seasonal variation in the hydrogen isotopic composition of leaf-wax lipids for two deciduous tree ecosystems (*Fagus sylvatica* and *Acer pseudoplatanus*). *Organic Geochemistry* **40**, 732-742.
- Sachse D., Radke J., and Gleixner G. (2004) Hydrogen isotope ratios of recent lacustrine sedimentary n-alkanes record modern climate variability. *Geochimica et Cosmochimica Acta* **68**(23), 4877-4889.
- Sachse D., Radke J., and Gleixner G. (2006) δD values of individual n-alkanes from terrestrial plants along a climatic gradient – Implications for the sedimentary biomarker record. *Organic Geochemistry* **37**, 469-483.
- Sauer P. E., Eglinton T., Hayes J. M., Schimmelmann A., and Sessions A. (2001) Compound-specific D/H ratios of lipid biomarkers from sediments as a proxy for environmental and climatic conditions. *Geochimica et Cosmochimica Acta* **65**(2), 213-222.
- Schimmelmann A., Sessions A., and Mastalerz M. (2006) Hydrogen Isotopic (D/H) Composition of Organic Matter During Diagenesis and Thermal Maturation. *Annual Review of Earth and Planetary Sciences* **34**, 501-533.
- Sessions A., Burgoyne T., Schimmelmann A., and Hayes J. M. (1999) Fractionation of hydrogen isotopes in lipid biosynthesis. *Organic Geochemistry* **30**, 1193-1200.
- Sessions A., Sylva S., Summons R. E., and Hayes J. M. (2004) Isotopic exchange of carbon-bound hydrogen over geologic timescales. *Geochimica et Cosmochimica Acta* **68**(7), 1545-1559.
- Simoneit B. R. T. (2005) A review of current applications of mass spectrometry for biomarker/molecular tracer elucidations. *Mass Spectrometry Reviews* **24**, 719-765.
- Smith F. and Freeman K. H. (2006) Influence of physiology and climate on δD of leaf wax n-alkanes from C_3 and C_4 grasses. *Geochimica et Cosmochimica Acta* **70**, 1172-1187.
- Sternberg L. (1988) D/H Ratios of environmental water recorded by D/H ratios of plant lipids. *Nature* **333**, 59-61.
- Weete J. (1972) Aliphatic hydrocarbons of the fungi. *Phytochemistry* **11**, 1201-1205.
- Wiesenberg G. L. B., Schwarzbauer J., Schmidt M. W. I., and Schwark L. (2004) Source and turnover of organic matter in agricultural soils derived from n-alkane/n-carboxylic acid compositions and C-isotope signatures. *Organic Geochemistry* **35**, 1371-1393.
- WRB. (2006) World reference base for soil resources 2006 - A framework for international classification, correlation and communication. FAO.
- Xie S., Nott C. J., Avsejs L. A., Maddy D., Chambers F. M., and Evershed R. P. (2004) Molecular and isotopic stratigraphy in an ombrotrophic mire for paleoclimate reconstruction. *Geochimica et Cosmochimica Acta* **68**(13), 2849-2862.
- Yang H. and Huang Y. (2003) Preservation of lipid hydrogen isotope ratios in Miocene lacustrine sediments and plant fossils at Clarkia, northern Idaho, USA. *Organic Geochemistry* **34**, 413-423.
- Zech M., Andreev A., Zech R., Müller S., Hambach U., Frechen M., and Zech W. (2010a) Quaternary vegetation changes derived from a loess-like permafrost palaeosol sequence in northeast Siberia using alkane biomarker and pollen analyses. *Boreas* **39**, 540-550.
- Zech M., Buggle B., Leiber K., Marković S., Glaser B., Hambach U., Huwe B., Stevens T., Sümegei P., Wiesenberg G., and Zöller L. (2009a) Reconstructing Quaternary vegetation history in the Carpathian Basin, SE Europe, using n-alkane biomarkers as molecular fossils: problems and possible solutions, potential and limitations. *Eiszeitalter und Gegenwart - Quaternary Science Journal* **85**(2), 150-157.
- Zech M. and Glaser B. (2008) Improved compound-specific $\delta^{13}C$ analysis of n-alkanes for application in palaeoenvironmental studies. *Rapid Communications in Mass Spectrometry* **22**, 135-142.

- Zech M., Zech R., Morrás H., Moretti L., Glaser B., and Zech W. (2009b) Late Quaternary environmental changes in Misiones, subtropical NE Argentina, deduced from multi-proxy geochemical analyses in a palaeosol-sediment sequence. *Quaternary International* **196**, 121-136.
- Zech R., Huang Y., Zech M., Tarozo R., and Zech W. (2010b) Permafrost carbon dynamics control atmospheric CO₂ over glacial-interglacial cycles. *Nature* submitted.

List of Publications

a) peer-reviewed journals

- Buggle, B.**, Glaser, B., Hambach, U., Gerasimenko, N., Marković, S., 2010. An evaluation of geochemical weathering indices in loess-paleosol studies. *Quaternary International* (in press). Doi: 10.1016/j.quaint.2010.07.019
- Buggle B.**, Wiesenberg G., Glaser B., 2010. Is there a possibility to correct fossil n-alkane data for postsedimentary alteration effects? *Applied Geochemistry* 25 (7), 947-957.
- Schatz, A.-K., Zech, M., **Buggle, B.**, Gulyás, S., Hambach, U., Marković, S., Sümegi, P., Scholten, T., 2010. The late Quaternary loess record of Tokaj, Hungary: Reconstructing palaeoenvironment, vegetation and climate using stable C and N isotopes and biomarkers. *Quaternary International* (in press). Doi:10.1016/j.quaint.2010.10.009
- Buggle B.**, Hambach U., Glaser B., Gerasimenko N., Marković, S.B, Glaser I., Zöller L., 2009. Stratigraphy and spatial and temporal paleoclimatic trends in East European loess paleosol sequences. *Quaternary International* 196, 86-106.
- Marković S.B., Hambach U., Catto N., Jovanović M., **Buggle B.**, Machalett B., Zöller L., Glaser B., Frechen M., 2009. Middle and Late Pleistocene loess sequences at Batajnica, Vojvodina, Serbia. *Quaternary International* 198, 255-266.
- Buggle B.**, Glaser B., Zöller L., Hambach U., Marković S., Glaser I., Gerasimenko N., 2008. Geochemical characterization and origin of Southeastern and Eastern European loesses (Serbia, Romania, Ukraine). *Quaternary Science Reviews* 27, 1058-1075.

b) non-peer-reviewed journals and conference proceedings

- Buggle, B.**, Gerasimenko, N., Hambach, U., Glaser, B., Zöller, L., 2009. Insights into the Mid- and Late Pleistocene paleoenvironment of the Ukraine – the loess-paleosol sequence Stry Kaydaky. In: Gajin, S. (Ed.), *International Conference on Loess Research (2009; Novi Sad) – Abstract Book*. p.120, University of Novi Sad, Faculty of Sciences, Novi Sad (Serbia).
- Buggle, B.**, Glaser, B., 2009. Correction procedure for the degradation effect on n-alkane ratios. Gajin, S. (Ed.), *International Conference on Loess Research (2009; Novi Sad) – Abstract Book*. pp.143-145, University of Novi Sad, Faculty of Sciences, Novi Sad (Serbia).
- Buggle, B.**, Glaser, B., Zöller, L., Hambach, U., Marković, S.B., 2009. Paleoclimatic trends in Southeastern Europe: Evidence from soil color and geochemical records in loess paleosol sequences. Gajin, S. (Ed.), *International Conference on Loess Research (2009; Novi Sad) – Abstract Book*. pp.130-131, University of Novi Sad, Faculty of Sciences, Novi Sad (Serbia).
- Buggle, B.**, Glaser, B., Zöller, L., Hambach, U., Marković, S.B., Gerasimenko, N., 2009. The loess deposits of the Danube and Dnieper area and their geochemical characteristics. Gajin, S. (Ed.), *International Conference on Loess Research (2009; Novi Sad) – Abstract Book*. pp.134-135, University of Novi Sad, Faculty of Sciences, Novi Sad (Serbia).
- Buggle, B.**, Zech, M., Glaser, B., 2009. n-Alkanes as molecular fossils and biomarkers in loess-paleosol sequences – a review. In: Gajin, S. (Ed.), *International Conference on*

- Loess Research (2009; Novi Sad) – Abstract Book. p.24, University of Novi Sad, Faculty of Sciences, Novi Sad (Serbia).
- Buggle, B.,** Zech, M., Gerasimenko, S., Marković, S., Hambach, U., Glaser, B., 2009. 600.000 years of Quaternary landscape history in Southeastern Europe: A lipid biomarker perspective. *Geophysical Research Abstracts* 11, EGU2009-8191.
- Buggle, B.,** Zech, M., Gerasimenko, N., Marković, S., Hambach, U., Glaser, B., 2009. Lipid biomarker records in SE-European loess paleosol sequences. What do they tell us about 600.000 years of landscape history? In: IMOG 2009 Scientific Committee (Eds.), *The 24th international Meeting on Organic Geochemistry (2009, Bremen) – Book of Abstracts*. p.147, University of Bremen – MARUM, Germany.
- Buggle, B.,** Zech, M., Gerasimenko, N., Marković, S.B., Hambach, U., Glaser, B., Zöller, L., 2009. 600 kyr of Quaternary landscape history in SE Europe – What do molecular fossils (n-alkanes) tell us?. Gajin, S. (Ed.), *International Conference on Loess Research (2009; Novi Sad) – Abstract Book*. pp.146-147, University of Novi Sad, Faculty of Sciences, Novi Sad (Serbia).
- Marković, S.B., Hambach, U., Stevens, T., Machalett, B., Kukla, G.J., Oches, E.A., McCoy, W.D., **Buggle, B.,** Gavrilo, M.B., Gavrilo, M.M., Basarin, B., Zöller, L., 2009. The last million years recorded at the loess – palaeosol sequences in the Vojvodina Region, Serbia. In: Gajin, S. (Ed.), *International Conference on Loess Research (2009; Novi Sad) – Abstract Book*. p.26, University of Novi Sad, Faculty of Sciences, Novi Sad (Serbia).
- Schatz, A.K., Zech, M., **Buggle, B.,** Hambach, U., Marković, S.B., Sümegi, P., Scholten, T., Zöller, L., 2009. Trees or no trees at Tokaj, Hungary – First n-alkane biomarker results. Gajin, S. (Ed.), *International Conference on Loess Research (2009; Novi Sad) – Abstract Book*. p.128, University of Novi Sad, Faculty of Sciences, Novi Sad (Serbia).
- Zech, M., **Buggle, B.,** Glaser, B., 2009. Endmember Modelling: A proposal to account for degradation effects on n-alkane biomarkers when reconstructing Quaternary Vegetation Changes. Gajin, S. (Ed.), *International Conference on Loess Research (2009; Novi Sad) – Abstract Book*. p.132, University of Novi Sad, Faculty of Sciences, Novi Sad (Serbia).
- Zech, M., **Buggle, B.,** Glaser, B., 2009. Reconstructing Quaternary vegetation changes using n-alkanes as biomarkers: a proposal to account for degradation effects. In: IMOG 2009 Scientific Committee (Eds.), *The 24th international Meeting on Organic Geochemistry (2009, Bremen) – Book of Abstracts*. p.555, University of Bremen – MARUM, Germany.
- Zech, M., **Buggle, B.,** Glaser, B., 2009. Should alkane biomarker results be corrected for degradation effects when reconstructing vegetation changes. *Geophysical Research Abstracts* 11, EGU2009-11386.
- Zech, M., **Buggle, B.,** Marković, S., Hambach, U., Stevens, T., Zöller, L., 2009. Multi-proxy analytical characterization and palaeoclimatic interpretation of the Crvenca loess-palaeosol sequence, Serbia. *Geophysical Research Abstracts* 11, EGU2009-11426.
- Buggle, B.,** Glaser B., Zöller, L., Hambach, U., Marković, Glaser, I., Gerasimenko N., 2008. Origin of loess in the (Middle/Lower) Danube Basin (and Dnieper Area). In: Reitner, J.M., Fiebig, M.C., Neugebauer-Maresch, C., Pacher, M., Winiwarter, V. (Eds.), *Veränderter Lebensraum- Gestern, Heute und Morgen. Abhandlungen der Geologischen Bundesanstalt* (62), 11-14.
- Buggle, B.,** Glaser, B., Zöller, L., Hambach, U., Marković, S., Glaser, I., Gerasimenko, N., 2008. The loesses of the Danube and Dnieper area – a geochemical based provenance study. In: Zech, W., Röhringer, I., Ni, A. (Eds.), *Climate Change and Landscape Evolution in the Central Asian Mountains and the Surrounding Basins: Past, Present*

- and Future - International Symposium in Memory of the 80th Anniversary of the German-Russian Alay/Pamir -Expedition in 1928 (2008; Tashkent and Dushanbe).. Volume of Abstracts, pp. 39-49.
- Buggle, B.**, Hambach, U., Glaser, B., Marković, S.B., Glaser, I., Zöller, L., 2008. Long-Term Paleoclimate Records in SE-Europe – The loess paleosol sequences Batajnica / Stari Slankamen (Serbia) and Mircea Voda (Romania). In: Reitner, J.M., Fiebig, M.C., Neugebauer-Maresch, C., Pacher, M., Winiwarter, V. (Eds.), *Veränderter Lebensraum- Gestern, Heute und Morgen. Abhandlungen der Geologischen Bundesanstalt* (62), 15-19.
- Buggle, B.**, Hambach, U., Glaser, B., Marković, S., Glaser, I., Zöller, L., 2008. Deriving paleoclimatic information from loess-paleosol sequences applying a soil color index of pedogenesis and a new geochemical proxy of the silicate weathering intensity. In: Zech, W., Röhringer, I., Ni, A. (Eds.), *Climate Change and Landscape Evolution in the Central Asian Mountains and the Surrounding Basins: Past, Present and Future - International Symposium in Memory of the 80th Anniversary of the German-Russian Alay/Pamir -Expedition in 1928 (2008; Tashkent and Dushanbe). Volume of Abstracts*, pp. 39-49, Academy of Sciences Republik of Uzbekistan, Tashkent.
- Hambach, U. Marković, S.B., **Buggle, B.**, Gaudenyi, T., Jovanovic, M., Machalet, B., Frechen, M., Rolf, C., Zöller, L., 2008. Vojvodinian loess-paleosol sequences as archive of repeated Pleistocene paleoclimatic changes.- *Geo2008 – Resources and Risks in the Earth System, Schriftenreihe der Deutschen Gesellschaft für Geowissenschaften* 60, 203.
- Marković, S.B., Hambach, U., Machalet, B., Stevens, T., Kukla, G.J., Smalley I.J., Oches, E.A., McCoy, W.D., Zöller, L., **Buggle, B.**, Jovanovic, M., O'Hara Dhand, K., Gaudenyi, T., Frechen, M., 2008. Danube Loess Stratigraphy: Serbian Viewpoint. In: Reitner, J.M., Fiebig, M.C., Neugebauer-Maresch, C., Pacher, M., Winiwarter, V. (Eds.), *Veränderter Lebensraum- Gestern, Heute und Morgen. Abhandlungen der Geologischen Bundesanstalt* (62); 201—202.
- Zech, M., **Buggle, B.**, Marković, S., Lucic, T., Stevens, T., Gaudenyi, T., Jovanovic, M., Huwe, B., Zöller, L., 2008. First Alkane Biomarker Results for the Reconstruction of the Vegetation History of the Carpathian Basin (SE Europe). In :Reitner, J.M., Fiebig, M.C., Neugebauer-Maresch, C., Pacher, M., Winiwarter, V. (Eds.), *Veränderter Lebensraum- Gestern, Heute und Morgen. Abhandlungen der Geologischen Bundesanstalt* (62); 123-127.
- Buggle, B.**, Glaser, B., Hambach, U., Zöller, L., Gerasimenko, N., Glaser, I., Marković, S.B., 2007. Löss-Paläoböden Sequenzen an Donau und Dnieper – Klimaarchive der letzten 700.000 Jahre. *Mitteilungen der Deutschen Bodenkundlichen Gesellschaft* 110 (2), 439-440.

Acknowledgements/Danksagung

Ich danke allen, die mir während meiner Doktorandenzeit freundschaftlich und fachlich zur Seite standen. Mein besonderer Dank richtet sich an:

Prof. Dr. Bruno Glaser, der mir mit diesem Promotionsthema den Weg in die Wissenschaft eröffnete. Ganz besonders schätze ich, dass er mir die Möglichkeit zur kritischen Diskussion eigener Ideen bot, und auch den nötigen Freiraum und das Vertrauen diese im Rahmen des DFG Projektes “DFG GL 327/8-2,3“ umzusetzen. Auch für die frühe und intensive Einführung in die nationale und internationale Wissenschaftsgemeinde im Rahmen von Tagungsteilnahmen möchte ich mich bedanken. Ich habe dadurch viel Erfahrung, aber auch Partner und Freunde gewonnen. Mein Dank richtet sich auch an die Familie von Prof. Glaser (Irina, Boris, Richard) für die freundschaftliche Aufnahme während der Probennahme im „wilden Osten“ und auch während der Bayreuther Zeit.

Prof. Ludwig Zöller. Sein allzeit offenes Ohr, sein Witz und die tiefgehenden Fachgespräche mit nahezu unerschöpflichem Detailwissen gewürzt stellten eine wertvolle Bereicherung dar.

Dr. Ulrich Hambach, für sein intensives persönliches Engagement. Die fundierten wissenschaftlichen Diskurse und die vertrauensvolle, herzliche Atmosphäre waren prägend. Nicht zuletzt bleibt auch der „Fahrspaß“ auf den Straßen Serbiens und Rumäniens in guter Erinnerung.

Prof. Huwe, für die Bereitstellung von Arbeitsplatz und Labor um an seinem Lehrstuhl diese Promotion durchzuführen. Sein aktive Interesse an Themen jenseits der Bodenphysik verdient anerkennend Erwähnung.

Dr. Michael Zech, der mir nicht nur als Wissenschaftler mit Rat und Tat zur Seite stand, sondern mich auch als Freund während der Doktorandenzeit begleitet hat, und dies auch bei zahlreichen, erlebnisreichen Feldaufenthalten. Er war nicht nur bei der Probennahme am Seil eine Sicherung.

Dr. Hans von Suchodoletz für die angenehme (Arbeits-)atmosphäre während seiner Bayreuther Zeit, den gemeinsamen „long nights of science“ und den unterhaltsamen Feierabenden

Dr. Guido Wiesenberg für immer spannende Diskussionen zum Thema Lipide und Dr. Markus Fuchs für allzeit kritische und hilfreiche Kommentare und zukunftsweisende Anregungen und Perspektiven.

Prof. Dr. Slobodan Marković und Prof. Natalia Gerasimenko für die Begleitung bei Feldarbeiten in Serbien beziehungsweise in der Ukraine. Prof. Marković öffnete das Tor zum „land of opportunities“ Danke für die freundschaftliche und fruchtbare Zusammenarbeit.

PD. Dr. Martin Kehl, für die Einführung in die Mikromorphologie und die Geduld am Mikroskop.

Ich danke auch allen weiteren Kooperations-Partnern und Freunden im In- und Ausland, die mich während der Doktorandenzeit gastfreundlich aufgenommen haben und mich tatkräftig unterstützten. Insbesondere seien hier erwähnt die Mitarbeiter der „Bodenwissenschaften“ der Universität Bonn als auch die Mitarbeitern der Geographie der Universität Novi Sad namentlich Tivadar Gaudenyi, Mladjen Jovanovic, Biljana Basarin nebst Ehemann und Djordje Vasiljevic.

Herzlichsten Dank gebührt den Mitarbeitern (ob diplomiert oder nicht), Hilfskräften und Ehemaligen des früheren Lehrstuhls Bodenkunde, des Lehrstuhls Bodenphysik und des Lehrstuhls Geomorphologie für die inspirierende Arbeitsatmosphäre, die Hilfsbereitschaft und

die schöne Zeit, die ich in diesem Kreis erfahren durfte. Ihr wart mehr als nur Kollegen! Folkert Bauer, Janne Benesch, Jago Birk, Christina Broesike, Michaela Dippold, Manfred Fischer, Janine Franke, Markus Fuchs, Steffen Heinrich, Diana Henniger, Marco Lara, Katharina Leiber, Mareike Ließ, Sebastian Kreutzer, Anna Kühnel, Sebastian Kreutzer, Karoly Müller, Ines Röhringer, Poldi Sauheidl, Andrea Schmitt, Gisela Wiedemann, Michael Zech, Ihnen und den anderen Dank dafür. Außerdem sei hier noch für die kleineren und auch mal etwas größeren Hilfen im Labor Dank an Iris Schmiedinger, Angelika Mergner und Tanja Gonter ausgesprochen. Auch die Hilfe von Ana Malagodi bei der Probenaufbereitung soll nicht unerwähnt bleiben. Nicht zuletzt gebührt Frau Gabriele Wittke Dank für die große und kleine Hilfe im Dschungel der Verwaltung.

Besten Dank gilt meinen Brüdern und ihren Familien, sowie meinen Freunden, ganz besonders Rainer Nerlinger, Dominik Siebers, Achim Reinhardt und Sven Fahrner für die gemeinsamen Pausen zum „Wiederaufladen der Akkus“.

Von Herzen, bin ich besonders meinen Eltern Kirsten und Lothar Buggle dankbar, die mich immer mit all Ihren Kräften und Ihrer Liebe unterstützt haben. Sie legten den Grundstein zu meiner persönlichen und beruflichen Entwicklung. Alles was ich bis jetzt erreicht habe und noch erreichen werde, wäre nicht ohne meine Eltern möglich gewesen. Vielen Dank für Alles.

Zu guter Letzt möchte ich natürlich noch einer Person danken, die vor etwas über ein Jahr in mein Leben getreten ist, meine Freundin Sonja. Es war für Dich sicher nicht immer leicht mit Einem der soviel Zeit mit seiner Schreibtischlampe verbringt (☺). Nichtsdestotrotz bist Du zu mir gestanden, bist mein Licht geworden, hast mir Rückhalt gegeben und mich für den Endspurt beflügelt. Herzlichen Dank für Alles! - Der Flug geht weiter mit gemeinsamem Ziel.

Declaration/Erklärung

Hiermit erkläre ich, dass ich diese Arbeit selbständig verfasst und keine anderen als die angegebenen Quellen und Hilfsmittel verwendet habe. Ich erkläre ferner, dass ich an keiner anderen Hochschule als an der Universität Bayreuth ein Promotionsverfahren begonnen habe.

Björn Buggle

Bayreuth, Februar 2011